

Multi-Axis Point Absorber Wave Energy Converters



Daniel Richardson

**This dissertation is submitted for the degree of Doctor of
Philosophy**

May 2019

Department of Engineering

Declaration

This thesis has not been submitted in support of an application for another degree at this or any other university. It is the result of my own work and includes nothing that is the outcome of work done in collaboration except where specifically indicated. Many of the ideas in this thesis were the product of discussion with my supervisor Professor George Aggidis.

Excerpts of this thesis have been published in the following conference manuscript.

D. Richardson and G. Aggidis, “The Economics of Multi-Axis Point Absorber Wave Energy Converters,” in *Proceedings of the ASME 2013 32nd International Conference on Ocean, Offshore and Arctic Engineering*, Nantes, 2013.

Daniel Richardson

Lancaster University, UK

Abstract

A multi-axis point absorber wave energy converter (MA-PAWEC) can be defined as a point absorber wave energy converter that absorbs energy from multiple modes of body motion using a power-take-off (PTO) system operating in multiple degrees of freedom. There is a lack of knowledge around whether MA-PAWECs could produce a lower cost of energy compared to the most common point absorber type, the heaving device. This research seeks to address this gap.

A generic spherical MA-PAWEC with PTO on the heave and surge axes is assessed on an energy absorption and cost of energy basis relative to an equivalent heaving device. Linear theory was used to model the energy absorption under motion and power constraints. For heave+surge MA-PAWECs the results suggest that for low power constraints (relative to wave climate) and large available excursions then surge as the primary axis with heave as a secondary axis may be the most cost effective option. If the power constraint is large and excursions are tightly limited heave should be the primary axis with surge a secondary axis.

By selecting axes that are best suited for different wave types a MA-PAWEC can absorb energy more consistently. This gives better utilisation of grid connection infrastructure: a MA-PAWEC with the same rated grid connection as a single axis equivalent can deliver significantly more energy. A MA-PAWEC should have its PTO system sized with the sum of the individual axes PTO limits higher than the rated device output.

The relative cost-of-energy for the MA-PAWEC vs. the heave device under the modelling conditions considered here suggests that MA-PAWECs have the potential to be both significantly better and significantly worse than the incumbent heave devices. MA-PAWECs are therefore not a clear-cut advancement over heave devices, but the performance upside justifies further research in to this device type.

Acknowledgements

I would like to thank my supervisor, Professor George Aggidis, whose patience and guidance has been invaluable throughout this work, and the late Dr Andy McCabe who was always ready to discuss a problem.

A huge note of appreciation to Daphné who has supported me throughout this endeavour with sacrifices of her own.

This work was funded by EPSRC Supergen Marine III.

Contents

Table of Figures	8
Table of Tables	12
Notation.....	13
Glossary of Acronyms	15
1 Introduction.....	16
1.1 Motivation.....	16
1.2 Defining a MA-PAWEC.....	17
1.3 A Brief History of Wave Energy	18
1.4 Aims and Objectives	20
1.5 Thesis Layout.....	21
2 Literature Review.....	22
2.1 The Nature of the Resource	22
2.1.1 Wave Generation.....	22
2.1.2 Energy in a Wave.....	23
2.1.3 Mathematical Representation.....	24
2.1.4 Model Validity	27
2.1.5 Wave Spectrums	28
2.1.6 The Resource.....	31
2.2 Wave Energy Absorption.....	33
2.2.1 Benefits of Wave Energy	33
2.2.2 The Engineering Challenge.....	34
2.2.3 Classification of Wave Energy Converters	34
2.2.4 Hydrodynamics	45
2.2.5 Geometry.....	54
2.2.6 Power Take Off Methods.....	55
2.2.7 Mooring.....	57
2.3 Conclusions.....	59
3 Initial Multi-Axis Considerations	61
3.1 The Prevalence of the Single Axis Device.....	61
3.2 Which Modes and PTO Axes?.....	62
3.2.1 Modes and Axes.....	63
3.2.2 Geometry.....	66

3.2.3	Axis Selection	67
3.3	Resonance	69
3.4	PTO Considerations	69
3.5	Arrays.....	70
3.6	Conclusions.....	71
4	Relative Energy Output under Motion Constraints.....	73
4.1	Generic Device.....	73
4.2	Unconstrained Optimum Performance.....	76
4.3	Global Weighted Constraint - Optimum Performance.....	77
4.3.1	Relative Capture Widths under a Global Weighted Constraint	80
4.3.2	Comparative Energy Production under a Global Weighted Constraint	83
4.4	Independent Constraints – Optimum Performance	88
4.4.1	Relative Capture Widths under Independent Constraints	89
4.4.2	Comparative Energy Production under Independent Constraints	91
4.5	Conclusions.....	94
5	Relative Energy Output under Power Constraints	96
5.1	Power Absorbed under Optimum Motion Control.....	96
5.2	Optimum Power Absorption under Power Constraints.....	100
5.3	Optimum Power Absorption under Motion and Power Constraints	103
5.4	Energy Production under Motion and Power Constraints.....	108
5.5	Conclusions.....	124
6	Economics of MA-PAWECs	126
6.1	WEC Economics	126
6.2	Cost Estimation.....	128
6.2.1	Performance Characteristics.....	129
6.2.2	Capital Costs (CAPEX)	130
6.2.3	Operating Costs (OPEX).....	135
6.3	Levelised Cost of Energy	135
6.4	Conclusions.....	139
7	Conclusions.....	140
7.1	Recommendations for Further Work	142
	References.....	143
	Appendices.....	153
A.1	Appendix 1 – WAMIT	153

A.2	Appendix 2 – Relative Capture Widths under Global Weighted Motion Constraints and Independent Motion Constraints	159
A.2.1	Wave Amplitude Ratio (A/a) 0.025 radii of device	159
A.2.2	Wave Amplitude Ratio (A/a) 0.125 radii of device	162
A.2.3	Wave Amplitude Ratio (A/a) 0.225 radii of device	165
A.2.4	Wave Amplitude Ratio (A/a) 0.325 radii of device	168
A.2.5	Wave Amplitude Ratio (A/a) 0.425 radii of device	171
A.2.6	Wave Amplitude Ratio (A/a) 0.525 radii of device	174
A.2.7	Wave Amplitude Ratio (A/a) 0.625 radii of device	177

Table of Figures

Figure 1: Degrees of freedom for a floating body.....	18
Figure 2: Orbital motions of water particles in a wave in deep water and at the shore [31]....	23
Figure 3: Graph showing ranges of validity for different wave theories (from [32]). In contrast to Table 1, in this graph depth is denoted by d rather than h	28
Figure 4: Regular (top) and irregular (bottom) waves.	29
Figure 5: Bretschneider spectrum with a spectral peak of 0.1579 Hz (period of 6.3339 s) and H_s of 0.5 m.	30
Figure 6: Quarterly rose diagrams for peak period at the Wavehub test site [34].	31
Figure 7: Global wave resource atlas [36].	32
Figure 8: UK wave power resource [41].....	33
Figure 9: The Pelamis attenuating WEC [58].....	37
Figure 10: Artist’s impression of a row of Salter’s ducks acting as a terminating WEC [59].	37
Figure 11: The PowerBuoy point absorber WEC from Ocean Power Technologies [65].	38
Figure 12: WaveSub by Marine Power Systems, a submerged body MA-PAWEC [66].	39
Figure 13: Categories for mode of operation of WECs (from [18]).	40
Figure 14: (Top) A shoreline oscillating water column WEC [68], (Bottom) A floating oscillating water column WEC [18].....	40
Figure 15: The WaveDragon overtopping WEC [70].....	41
Figure 16: Submerged pressure differential WECs. Left: AWS point absorbers [73]. Right: Bombora line absorber [74].	42
Figure 17: The Corpower heaving buoy WEC [75].....	43
Figure 18: Submerged oscillating body WECs. Left: the CETO device from Carnegie Wave [79]. Right: a multi-axis device from 40SouthEnergy [78].	44
Figure 19: The Oyster bottom mounted surging WEC [80].	44
Figure 20: 2D radiation patterns of a symmetrical WEC from [81]. (a) Incident wave. (b) The radiated wave when the device is moving in heave. (c) The radiated wave when the device is moving in pitch or surge. (d) The superposition of (a), (b) and (c) and represents 100% absorption of the incident wave.	46
Figure 21: Radiated wave pattern of a heaving axisymmetric point absorber. From [81]. The straight lines are the incident waves. The circular lines are the radiated waves.	46
Figure 22: Submerged sphere array configurations.	53
Figure 23: Evolution of the SEAREV concept, taken from [105].	55
Figure 24: PTO process from wave to grid with different technologies. Adapted from [28] to include mechanical path.....	56
Figure 25: Mooring configurations investigated by Fitzgerald and Bergdahl [113].....	59
Figure 26: Generic device configurations. (a) Heave PAWEC. (b) Surge PAWEC. (c) Multi-Axis PAWEC (MA-PAWEC).....	74
Figure 27: Plot of maximum RCW for an axisymmetric device oscillating in heave, surge, and combined heave and surge.	76
Figure 28: Relative Capture Widths (RCW) of a heaving PAWEC with a $0.5a$ motion constraint.....	81
Figure 29: Relative Capture Widths (RCW) of a surging PAWEC with a $0.5a$ motion constraint.....	81

Figure 30: Relative Capture Widths (RCWs) of a heaving and surging MA-PAWEC under a global motion constraint with a constraint of $0.5a$ on each axis.	82
Figure 31: RCW for an amplitude ratio (A/a) of 0.125 at a motion constraint of $0.5a$ in the three configurations heave only, surge only, and heave+surge.....	82
Figure 32: Energy Production (EP) of the three devices in a set of waves based on Table 2 with each axis at different motion constraints. The single mode device outputs are shown by the extreme edges of the surface. Contour shading to help show 3D curvature.	85
Figure 33: Energy Production (EP) of the single axis devices (extreme edges of surfaces in Figure 32) and an equal axis constraint configuration i.e. the diagonal slice from the origin of Figure 32.	86
Figure 34: Relative Energy Production (EP), indexed to the heave device EP value, of four different sizes of device with the radius ranging from 2m to 5m.	88
Figure 35: RCW of a heave+surge MA-PAWEC with independent constraints of $0.5a$ on each axis.	90
Figure 36: RCW for an amplitude ratio (A/a) of 0.125 at a motion constraint of $0.5a$ in the three configurations heave only, surge only, and heave+surge (both global and independent constraint curves shown).....	90
Figure 37: Energy Production (EP) of the three devices in a wave climate based on Table 2 with each axis at different independent motion constraints. The single mode device outputs are shown by the extreme edges of the surface. Contour shading to help show 3D curvature.	91
Figure 38: Energy production at different motion constraints for the heave, surge and heave+surge configurations. Motion constraints are equal for each axis. Both independent and global weighted constraint curves are shown.....	92
Figure 39: Percentage difference in energy production of the independent motion constraint heave+surge configurations vs. the global weighted heave+surge constraint, heave only and surge only. Equal motion constraints on each axis.	93
Figure 40: Percentage difference between the energy production under independent motion constraints and global weighted constraints.....	93
Figure 41: Average absorbed power in Heave with unconstrained motion for an axisymmetric point absorber with optimal motion.	98
Figure 42: Average absorbed power in Surge with unconstrained motion for an axisymmetric point absorber with optimal motion.	98
Figure 43: Average absorbed power in Heave+Surge with unconstrained motion for an axisymmetric point absorber with optimal motion.	99
Figure 44: Wavehub seastate frequency of occurrence. Sea states represented by significant wave heights and zero crossing periods.	99
Figure 45: Absorbed average power for an unconstrained axisymmetric point absorber with optimal motion in heave with a 340 kW power constraint.	101
Figure 46: Absorbed average power for an unconstrained axisymmetric point absorber with optimal motion in surge with a 340 kW power constraint.	101
Figure 47: Absorbed average power for an unconstrained axisymmetric point absorber with optimal motion in heave+surge with a combined 340 kW global power constraint.	102
Figure 48: Absorbed average power for an unconstrained axisymmetric point absorber with optimal motion in heave+surge with a 340 kW independent power constraint on each axis (680 kW combined power constraint).....	102
Figure 49: Power absorption matrix of the semi-submerged spherical PAWEC in heave with $0.5a$ motion constraint.....	104

Figure 50: Power absorption matrix of the semi-submerged spherical PAWEC in heave with 0.5a motion constraint and a 340 kW power constraint.....	104
Figure 51: Power absorption matrix of the semi-submerged spherical PAWEC in surge with 0.5a motion constraint.....	105
Figure 52: Power absorption matrix of the semi-submerged spherical PAWEC in surge with 0.5a motion constraint and a 340 kW power constraint.....	105
Figure 53: Power absorption matrix of the semi-submerged spherical PAWEC in heave+surge with independent 0.5a motion constraints.....	106
Figure 54: Power absorption matrix of the semi-submerged spherical PAWEC in heave+surge with independent 0.5a motion constraints and a global power constraint of 340 kW.	106
Figure 55: Power absorption matrix of the semi-submerged spherical PAWEC in heave+surge with independent 0.5a motion constraints and a global power constraint of 680 kW.	107
Figure 56: Power absorption matrix of the semi-submerged spherical PAWEC in heave+surge with independent 0.5a motion constraints and independent power constraints of 340 kW on each axis.....	107
Figure 57: Energy production in Heave under motion and power constraints. Power constraints are represented by the power constraint ratio (P_c/P_{wc}) and are scaled per number of axes.	110
Figure 58: Energy production in Surge under motion and power constraints. Power constraints are represented by the power constraint ratio (P_c/P_{wc}) and are scaled per number of axes. ...	110
Figure 59: Energy production in Heave+Surge under motion and global power constraints. Power constraints are represented by the power constraint ratio (P_c/P_{wc}) and are scaled per number of axes.....	111
Figure 60: Energy production in Heave+Surge under motion and independent power constraints. Power constraints are represented by the power constraint ratio (P_c/P_{wc}) and are scaled per number of axes.....	111
Figure 61: Energy production under power and motion constraints with a power constraint $0.5P_{wc}$	113
Figure 62: Energy production under power and motion constraints with a power constraint $1P_{wc}$	113
Figure 63: Energy production under power and motion constraints with a power constraint $1.5P_{wc}$	114
Figure 64: Energy production under power and motion constraints with a power constraint $2P_{wc}$	114
Figure 65: Energy production under power and motion constraints with a power constraint $2.5P_{wc}$	115
Figure 66: Energy production under power and motion constraints with a power constraint $3P_{wc}$	115
Figure 67: Energy production under power and motion constraints with a power constraint $3.5P_{wc}$	116
Figure 68: Energy production under power and motion constraints with a power constraint $4P_{wc}$	116
Figure 69: Energy production under motion constraints for the three configurations heave, surge and heave+surge. No Power constraints.....	117
Figure 70: The effect of the power constraint on energy production for heave, surge and heave+surge configurations under motion constraints 0.5a.	118

Figure 71: The effect of the power constraint on energy production for heave, surge and heave+surge configurations under motion constraints 0.4a.	118
Figure 72: The effect of the power constraint on energy production for heave, surge and heave+surge configurations under motion constraints 0.3a.	119
Figure 73: The effect of the power constraint on energy production for heave, surge and heave+surge configurations under motion constraints 0.2a.	119
Figure 74: The effect of the power constraint on energy production for heave, surge and heave+surge configurations under motion constraints 0.1a.	120
Figure 75: Percentage of time heave configuration was operating at maximum power capacity.	122
Figure 76: Percentage of time surge configuration was operating at maximum power capacity.	122
Figure 77: Percentage of time heave+surge configuration was operating at maximum power capacity with a global power constraint.	123
Figure 78: Percentage of time heave+surge configuration was operating at maximum power capacity with independent power constraints.	123
Figure 79: Economic matrix for a WEC	127
Figure 80: Example cost breakdowns for WECs. (a) Capital cost breakdown. (b) Project cost breakdown. [22]	131
Figure 81: Relationship between PTO weighting and relative LCOE.	138
Figure 82: Flow diagram showing the process of running WAMIT with input and output files (adapted from [133]).	154
Figure 83: Format of output file for added mass and damping coefficients.	157
Figure 84: Format of output file for exciting force coefficients.	158

Table of Tables

Table 1: Formulae for various wave properties under linear theory (formulae from [17]).....	26
Table 2: Frequency table for the Wavehub test site plotting frequency of sea state occurrence in bins of significant wave height (H_s) and zero crossing period (T_z) [121]......	84
Table 3: Upper and lower bounds of the scaling factors relating the performance of the MA-PAWEC with that of the heave device.....	129
Table 4: CAPEX scale factors for a MA-PAWEC device relative to a heave device.	136
Table 5: Relative LCOE matrix for the upper and lower bounds of the performance and CAPEX scaling factors.	137
Table 6: Relative LCOE matrix for Structure weighting of 10%, PTO of 66%	137
Table 7: Relative LCOE matrix for PTO weighting of 10%, Structure of 66%	138
Table 8: Values of the exponent k for the non-dimensional damping coefficient.	155
Table 9: Input parameters for hemisphere WAMIT run.	157

Notation

Unless otherwise specified:

Notation	Description
*	Denotes the conjugate transpose
A	Incident wave amplitude (m)
$A(\omega)$	Frequency dependent added mass
a	Radius of device (m)
AEP	Annual Energy Production (J)
$B(\omega)$	Frequency dependent damping coefficient
B_{ij}	Frequency dependent damping coefficient for modes i,j
\bar{B}_{ij}	Frequency dependent non-dimensional damping coefficient for modes i,j
\mathbf{B}	Frequency dependent damping matrix
C	Buoyancy coefficient
c	Celerity or phase velocity (m/s)
c_g	Group velocity (m/s)
C_{sf}	Capital cost scaling factor
d	Water depth (m)
E_w	Energy per unit width of wave (J/m)
e	Euler's number ~ 2.71828
E_k	Kinetic Energy per unit width of wave (J/m)
E_p	Potential Energy per unit width of wave (J/m)
EP	Energy Production (J)
F_{ext}	External force
F_f	Frequency dependent wave induced force component
F_H	Hydrostatic forces
F_R	Radiated forces
\mathbb{F}_R	Complex coefficient for radiated force
F_S	Exciting forces
F_T	Total force
f_j	Frequency of occurrence of sea state j
f_{ij}	Frequency of occurrence of wave with period i , height j
g	Acceleration due to gravity (9.80665m/s ² to 5dp)
H	Wave height (m)
H_s	Significant wave height (m)
\mathbf{I}	Identity matrix
h	Water depth (m)
i	Imaginary number $\sqrt{-1}$
i	Subscript index notation
j	Subscript index notation
K	PTO stiffness (N/m)
k	Wavenumber (m ⁻¹)
L	Capture width of a device (m)
L_{opt}	Optimum capture width of a device (m)
m	Mass (kg)

N	Number of degrees of freedom
P	Mean power absorbed by device (W)
P_c	Power constraint (W)
P_{ij}	Power absorbed from a wave with period i , height j
P_j	Converted useful power from sea state j (W)
P_{opt}	Optimum mean power absorption (W)
P_{sf}	Performance scaling factor
P_w	Power per unit width of wave front (W/m)
P_{wc}	Power of wave climate incident across the width of the device (W)
Re	Denotes the real part of a complex variable
S	Cross-sectional area at the unperturbed free surface (m ²)
$S(T)$	Spectral density (m ² /Hz)
T	Wave period (s)
T_p	Peak period (s)
T_s	Significant wave period (s)
T_z	Zero-upcrossing period (s)
t	Time (s)
U	Complex N -vector describing the velocity of the body
U_{opt}	Complex N -vector describing optimum velocity (m/s)
u	Horizontal velocity component (m/s)
w	Vertical velocity component (m/s)
X	Displacement in the arbitrary X direction (m)
\dot{X}	First derivative w.r.t. time of X (m/s)
\ddot{X}	Second derivative w.r.t. time of X (m/s ²)
X_i	Complex exciting force coefficient in mode i
\hat{X}_i	Complex exciting force coefficient in mode i for a unit amplitude wave
\bar{X}_i	Non-dimensional exciting force coefficient in mode i
\mathbb{X}	Complex N -vector describing exciting force
$\hat{\mathbb{X}}$	Complex N -vector describing exciting force for a unit amplitude wave
\mathbb{X}_{inc}	Complex coefficient for exciting force due to incident waves
\mathbb{X}_{diff}	Complex coefficient for exciting force due to diffracted waves
x	Displacement in the Cartesian x direction (m)
z	Displacement in the Cartesian z direction (m)
α	Proportion of device radius
β	Wave heading (degrees) relative to device
η	Free surface displacement (m)
λ	Wavelength (m)
ζ	Complex constant
π	Pi
ρ	Density (kg/m ³)
ω	Angular frequency (s ⁻¹)
μ	Lagrange multiplier
γ_i	Velocity constraint in each degree of freedom i
Γ	$N \times N$ diagonal velocity constraint matrix with elements γ_i

Glossary of Acronyms

Acronym	Description
AEP	Annual Energy Production
AWS	Archimedes Wave Swing
BEM	Boundary Element Method
CAPEX	Capital expenditure/cost
CWR	Capture Width Ratio
DECC	Department of Energy and Climate Change
DNV	Det Norske Veritas – an offshore standards body
DOF	Degree of freedom
EOM	Equation of motion
EP	Energy Production
EPSRC	Engineering and Physical Sciences Research Council
GHG	Greenhouse gas(es)
IEA-OES	International Energy Agency – Ocean Energy Systems
LCOE	Levelised cost of energy
LCOE _{REL}	Relative levelised cost of energy
LUREG	Lancaster University Renewable Energy Group
MA-PAWEC	Multi-axis Point absorber wave energy converter
OPEX	Operational expenditure/cost
OWC	Oscillating water column
OWSC	Oscillating wave surge converter
PAWEC	Point absorber wave energy converter
SPAWEC	Single point absorber wave energy converter
PTO	Power-take-off
R&D	Research and Development
RCW	Relative Capture Width
SWL	Still water level
WEC	Wave Energy Converter
WSW	West South-West

1 Introduction

This introductory chapter begins by setting out the motivations for research in to ocean waves as a renewable energy source before going on to introduce the concept of a multi-axis point absorber wave energy converter (WEC) which will be the central theme of this thesis. A brief history of the wave energy industry is then presented to provide context and is important for understanding the development of WECs. This is followed by a statement of the aims and objectives of this research along with a description of the layout of this thesis.

1.1 Motivation

In response to climate change and energy security concerns demand for renewable energy is increasing globally. The Paris Agreement of 2015 [1] to combat climate change resulted in many countries vowing to lower greenhouse gas (GHG) emissions and invest in a sustainable low carbon future. Worldwide investment in renewables now exceeds that for fossil fuels in a trend that is set to continue [2] [3]. The UK and EU have pledged to at least an 80% reduction in emissions from 1990 levels by 2050 with a large proportion of these reductions coming from replacing fossil fuels with renewable energy sources [4] [5] [6] [7]. For the UK, with its energetic wave climate, wave energy can play a significant part in the renewable energy mix. Many other countries could also exploit the wave energy on their shores with an estimated 2 TW of wave power available worldwide [8]. However, so far the industry has failed to develop as quickly as predicted with two of the UKs most advanced wave energy device companies going in to administration in 2014 [9] and 2015 [10]. In 2013 the UK Department of Energy and Climate Change (DECC) estimated 200-300 MW of wave energy could be installed in UK waters by 2020 [11]. By 2018 only 11.3 MW of wave energy capacity had been installed in all of Europe, with just 2.9 MW in the water, the remaining 8.4 MW having been decommissioned. Only one device was installed in the UK in 2018 and this was rated at 5.2 kW [12]. These installed values are orders of magnitude lower than estimates and insignificant relative to the scale of UK generation capacity (103.6 GW as of 2018 [13]). For comparison, 3.7 MW of new tidal stream capacity and 11.7 GW of new wind capacity was installed in Europe in 2018 [12] [14].

This disappointing progress can be traced back to the high cost of placing energy generating equipment in the marine environment. The wave energy industry must find ways to lower the

cost of energy in order to compete not only with fossil fuels but nuclear and other renewable technologies too. It is estimated that the cost of wave energy must be reduced by 50-75% by 2025 (from 2012 levels) in order to compete with offshore wind [15]. This thesis is intended to be a step along that path towards competitively priced wave energy.

1.2 Defining a MA-PAWEC

It will be convenient for the remainder of this thesis to reduce the cumbersome ‘Multi-Axis Point Absorber Wave Energy Converter’ to the acronym MA-PAWEC. This differentiates the concept as a subset of the more generally used acronym PAWEC (Point Absorber Wave Energy Converter). The definition of a point absorber WEC will be covered in Chapter 2, p38.

To the authors knowledge the acronym MA-PAWEC is introduced in this thesis (and derived paper). There is precedent in existing literature for the terms multi-axis, multi-mode and multi-DOF (Degree of Freedom) applied to point absorbers with the term ‘quasi point absorber’ sometimes used to refer to point absorbers that are not axisymmetric or that operate in modes other than vertically [16]. There has been little explicit work carried out on multi-axis WECs in the past and so it is necessary to specify a robust definition of the term MA-PAWEC in order to provide clarity on the boundaries of this work.

Rigid body motion can be described fully using six degrees of freedom; three translational and three rotational. These modes of motion are denoted as surge, sway, heave, roll, pitch and yaw respectively. They correspond to translation along and rotation about the x, y, z axes of the Cartesian coordinate system centred on the body (Figure 1). The body motion and coordinate system shown in Figure 1 was adopted by wave energy developers from the existing offshore hydrodynamic literature, upon which much of the wave energy industry theory is based. By convention, the wave train is in the direction of the positive x axis for head-on waves.

Within this thesis the definition of a MA-PAWEC is rooted in the PTO system of the PAWEC which absorbs energy from the body motions. The intent behind a multi-axis device is to absorb energy from more than one of the six modes of motion of a rigid body as described in Figure 1 and to do so with a PTO system operating in more than one degree of freedom. A multi-axis PTO system would absorb energy along either multiple translational axes, rotation about multiple axes, or a combination of translational and rotational movements. It is important here to note the difference between absorbing energy from multiple modes of

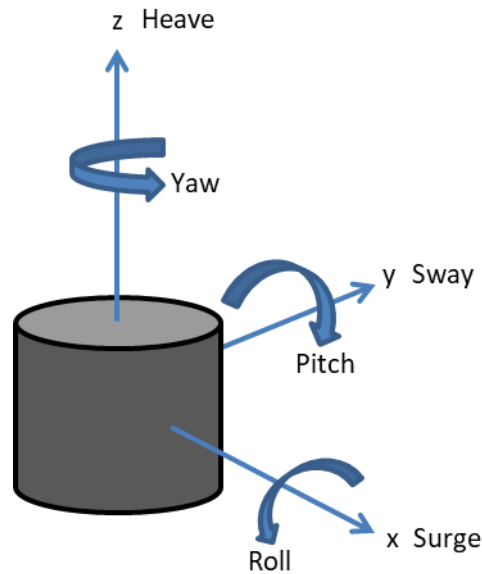


Figure 1: Degrees of freedom for a floating body.

motion of the body, and absorbing energy from multiple degrees of freedom of the PTO. A translational PTO operating on a 45 degree axis between the heave and surge axes would be able to absorb energy from both the heave and surge mode of the WEC body motions, but because it is only operating in a single degree of freedom it would not be classed as a multi-axis device under the definition used here.

The definition of a MA-PAWEC within this thesis going forward is taken as:

- A point absorber wave energy converter that absorbs energy from multiple modes of body motion using a power-take-off system operating in multiple degrees of freedom.

1.3 A Brief History of Wave Energy

To date the wave energy industry has not converged on a preferred design to exploit the wave resource. This is in contrast to the wind industry that has predominantly settled on the horizontal axis three-bladed design which can now be seen across the globe, both onshore and off. Of the many wave energy converter ideas put forward since the 1970s, when commercial scale wave power began attracting serious attention, only a handful have reached commercial or pre-commercial scale deployment. To put this into context, what follows is a brief history of the wave energy industry.

The earliest wave energy patent dates back to 1799 in France [17], however modern wave energy can be considered to start with Yoshio Masuda in the 1940s in Japan. His work began with the development of a navigation buoy powered by what is now known as a floating oscillating water column (OWC) wave energy converter (WEC) [18]. In the 1970s the oil crisis prompted governments to plan alternative energy arrangements and a paper by Stephen Salter of the University of Edinburgh published in the journal 'Nature' in 1974 brought attention, and consequently funding, to wave energy research [19]. At the same time Christopher Cockerell's experiments on a contouring raft were published in New Scientist. In 1975 the UK Department of Energy started a research programme into various methods of extracting wave energy and as development of ocean energy has continued other countries have started their own programmes. The early work was primarily done in the UK, Japan, Norway, US, Sweden and France [18].

In the UK, in 1978, there was a crisis of confidence in wave energy as early research indicated a high electricity cost of 20-50p/kWh. Within a year the cost estimates were down to 5-15p/kWh [20] but unfortunately for the industry the subsequent resolution of the oil crisis led to a decline in government funding in the early 1980s. The most notable achievements over the subsequent few years were the installation of several OWCs. Research activity picked up again in the early 1990s with the European Commission including wave energy in an R&D programme of renewable energies [18]. More recently still in 2001, the International Energy Agency (IEA) established an 'Implementing agreement on Ocean Energy Systems (IEA-OES)' [21]. The aim of these programmes is to facilitate and coordinate ocean energy R&D to enable commercialisation of the technology. For the present day, in the UK, wave energy is now receiving Government incentives for commercialisation of the technology via additional tariffs for renewable energy and financing for development [22]. Similar incentive schemes are present in other countries. The UK has also invested in developing expertise in the wave energy industry with the EPSRC Supergen initiative to fund research in to marine energy [23] and which has funded this work.

Over the course of this history there have been a great variety of ideas put forward. The oft quoted statistic is from McCormick which states that by 1981 there were over one thousand patented wave energy conversion techniques in Japan, North America, Western Europe and the UK [17]. The US Department of Energy [24] lists 145 different WEC concepts currently in development around the world and this number is not exhaustive. Earlier designs tended to be on a very large scale (MW to GW) as a result of the motivation from the Government to produce large amounts of power and make a meaningful contribution towards the national grid. As the Government funding began to dry up, focus shifted towards smaller devices of the order of kW and MW.

Throughout this forty year period, and particularly in the latter half, after the demise of large-scale Government funded projects, there has been an overwhelming trend towards smaller devices utilising the heave response (vertical translation motion). There are many excellent reasons for choosing this configuration which will be discussed later in the thesis. In general however, it is possible to extract larger amounts of energy by utilising both the heave and surge forces of the wave. This can be achieved with multiple PTO axes or by careful design of a single PTO axis.

For a more detailed history and overview of wave energy the reader is referred to Cruz (ed.) [25], Salter [20], Falcao [18] and the IEA ocean energy reports [26].

1.4 Aims and Objectives

What history has showed is that the power from the many wave energy converters already proposed has proved too expensive to compete with other renewables and fossil fuels. Perhaps this cannot be said with certainty of the more recent devices as wave energy projects take years to develop and realise their full potential. However, the lack of design convergence suggests an opportunity to create improved WEC performance through novel configurations. As there are no obvious outstanding configurations it increases the probability that new designs could meet or exceed existing ones.

Aims

As a step on the path towards competitively priced wave energy, this thesis explores the concept of MA-PAWECs and in particular whether they could offer a more attractive development route for the industry. The aims of this research are:

1. To understand the design considerations inherent in developing multi-axis point absorber wave energy converters.
2. To identify if multi-axis point absorber wave energy converters could potentially offer a lower cost of energy than existing single axis devices, and thus be a more attractive development route for the industry.

Objectives

To meet these aims the following research objectives were selected:

1. Identify the criteria for selecting modes and axes for a MA-PAWEC and what is relevant to this choice.
2. Model the hydrodynamic performance of a generic MA-PAWEC against equivalent single axis devices.
3. Model the energy output of a generic MA-PAWEC compared to equivalent single axis devices and the implications of this on PTO choices.
4. Estimate if MA-PAWECs could generate electricity at a lower cost than the most popular PAWEC configuration today; the heaving buoy.

With the increasing demand for renewable energy and the ready availability of ocean waves as a resource, the potential for MA-PAWEC devices to decrease the cost of wave energy is something that should be researched. The current lack of knowledge of how beneficial (if at all) a multi-axis PAWEC could be over the conventional single-axis PAWEC, and the associated potential for a lower cost of energy, is the primary motivation for this research.

1.5 Thesis Layout

Chapter 2 is a literature review of the subject of wave energy, first addressing the nature of the resource and then the engineering challenge of how energy can be extracted from it. Chapter 3 is an initial discussion of some of the factors associated with MA-PAWECs and how they affect the design decisions when embarking on investigating multi-axis PTO on a point absorber. Chapter 4 assesses the hydrodynamic performance of a MA-PAWEC against single axis devices under motion constraints. Chapter 5 assesses the hydrodynamic performance of a MA-PAWEC against single axis devices under both motion and power constraints. Chapter 6 conducts an economic analysis to gain an idea of whether MA-PAWECs can be expected to deliver a lower cost of energy than heaving buoys. Chapter 7 draws overall conclusions from the work.

2 Literature Review

Chapter 2 comprises a review of existing literature relevant to MA-PAWECs. Although there is little explicit work on MA-PAWECs much of the existing work on point absorbers can be applied to the concept. During the period of writing this thesis (2011-2018) there has been an increase in the development of multi-axis devices including the launch of a new device for sea testing [27]. This is encouraging evidence that MA-PAWECs are a promising avenue of research.

As it is of fundamental importance to understand the resource you are trying to exploit, the chapter begins by examining the nature of the wave resource covering the available wave theories and resource characterisation. The engineering challenge of extracting energy from waves is then covered looking at types of device, hydrodynamics, geometry and power take off systems. For a general review of the wave energy industry the reader is referred to [28].

2.1 The Nature of the Resource

2.1.1 Wave Generation

There are many different kinds of waves present in the oceans including wind, tidal, internal, inertial and capillary [29]. Those of interest to wave energy developers are wind generated surface waves which are a product of the wind acting on the surface of the sea through pressure and shear stresses. As such, wave energy can be thought of as third generation solar energy; solar insolation heats the Earth creating thermal gradients which produce wind that create waves when blowing over a body of water. In each transition from solar to wind to waves there is an increase in the power intensity (W/m^2) [17]. Thus, although the total energies of solar and wind are far larger than wave, the energy in waves is presented to us in a much denser form. High energy densities are desirable as they allow small structures to collect large quantities of energy (if they are well designed!) making the energy generation potentially more cost effective.

As a product of wind, waves share the inherent variability of that resource. However, waves can travel for thousands of miles with very little energy dissipated and in this way the ocean acts as an integrator of wind energy, absorbing energy from the wind over a long fetch and delivering it to a coastline. We differentiate between locally produced waves and those that

have travelled from their generation zone as ‘wind waves’ and ‘swell’ respectively. With knowledge of the weather patterns over the ocean fetch, swell waves at the WEC site can be predicted with good accuracy days in advance. Waves therefore have the advantage of being a more predictable source of energy than wind and solar.

2.1.2 Energy in a Wave

Waves are an energy transport phenomenon. Within a wave, energy is transferred by the orbital motion of the water particles (Figure 2). The radius of the orbit at the surface represents the amplitude of the wave, with motion decreasing exponentially with depth. Therefore below a depth of half a wavelength (λ), the water motion due to the wave can be considered negligible and in fact 95% of the energy is contained within a depth of one quarter wavelength. When the wave travels into water of depth less than half a wavelength the circular motion of the water becomes elliptical. Energy is lost through friction with the seabed and the wave slows, its wavelength decreases and it will eventually break, dissipating more energy [30]. In deep water ($>\lambda/2$) the energy is dissipated through viscous losses. As the viscosity of water is low these losses are small. Waves of period greater than nine seconds can travel long distances with little attenuation [30]. Shorter period waves dissipate much of their energy soon after leaving the generation area. White caps are the main source of dissipation – short waves lose energy on the crest of long waves [30].

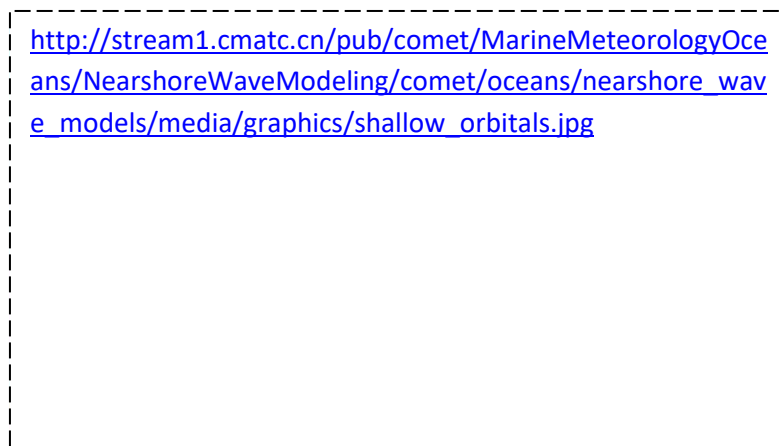


Figure 2: Orbital motions of water particles in a wave in deep water and at the shore [31].

A surface water wave represents an exchange between kinetic and potential energy as it propagates. The waves of interest as a renewable energy source have a wavelength longer than 1 m so that the surface tension of the water can be neglected and gravity is the dominant

restoring force [30]. The total energy in a wave is the sum of the potential and kinetic energies. Energy per unit width of a wave front is given by the equation [17]:

$$E_w = E_p + E_k = \frac{\rho g H^2 \lambda}{8},$$

Equation 1

where E_p is potential energy per unit width, E_k is kinetic energy per unit width, ρ is density of the water, g acceleration due to gravity, H is wave height and λ is wavelength. A deep water sinusoidal wave is composed of equal parts potential and kinetic energy. Potential energy is represented by the wave height while kinetic energy is the motion of the water particles. The wave power, or energy flux, of a unit width of wave is given by [17]:

$$P_w = \frac{\rho g H^2 c_g}{8},$$

Equation 2

where the group velocity, c_g , is given by [17]:

$$c_g = \frac{c}{2} \left[1 + \frac{2kh}{\sinh(2kh)} \right]$$

Equation 3

With the deep and shallow water approximations respectively [17]:

$$c_g = \frac{c}{2}$$

$$c_g = c$$

Equation 4

In these equations h refers to the water depth and k is the wavenumber $k = 2\pi/\lambda$ in radians per metre. What arises from these equations is that in deep water the energy travels at half the speed of the wave. The result of this is that in a wave-group (a number of waves of slightly different wavelengths travelling together) waves will appear at the back of the group and disappear at the front.

2.1.3 Mathematical Representation

Like many natural phenomena, surface gravity waves cannot be exactly described by any yet known mathematical theory. Instead there are multiple theories that approximate the behaviour of waves to a greater or lesser degree of accuracy under certain circumstances.

Linear waves

Linear wave theory (or Airy wave theory) is the simplest mathematical model of waves. In deep water this model assumes a sinusoidal profile to the surface displacement with an incompressible, irrotational and inviscid fluid. Linear theory is most accurate at describing waves with small surface displacements and so can be comfortably used with swell waves in deep water where $\lambda/H > 50$ [30]. For example, for a wave of wavelength 200 m, linear theory is remarkably accurate up to a wave height of 4 m. Accuracy of linear theory decreases with steeper waves as non-linear effects increase and the wave profile deviates further from the smooth sinusoidal wave assumption.

Linear waves have the property of superposition; waves of different heights and wavelengths can be superimposed to create other wave profiles [30]. The advantage of this superposition is the ability to analyse the WEC response to the individual wave components within a sea state and then superimpose these responses to get the resulting motion within the sea state. Table 1 shows the linear formulae for various wave properties under linear theory. The deep and shallow water approximations are also included.

The water particle velocity equations in Table 1 show that surface particle velocity increases as depth decreases. The point at which the maximum horizontal velocity exceeds the phase velocity is referred to as the break point. After this point the wave spills and energy is lost to turbulence.

Non-linear waves

While the sinusoidal profile of the linear wave is a good representation of a swell wave in deep water with a low H/λ ratio (steepness), it is not a good model for steeper waves or those in shallow water. Non-linear wave profiles tend to have narrower crests and broad troughs. As a wave moves in to shallow water it starts to be affected by the sea floor and its profile changes to having a narrow crest and wide trough. In order to better model waves that do not follow the linear profile, non-linear models have been developed.

One such higher order wave model is Stoke's series model. The accuracy of the model can be improved by adding successive terms in the series. The first order theory is simply a linear wave, the profile of which is given by the free surface equation in Table 1. Stoke's second

Property		Deep Water Approximation	Transitional	Shallow Water Approximation
Validity		$h/\lambda > 1/2$	-	$h/\lambda < 1/20$
Free Surface Displacement (m)		$\eta = \frac{H}{2} \cos\left(\frac{2\pi x}{\lambda} - \frac{2\pi t}{T}\right)$		N/A
Period (s)		$T = \sqrt{\frac{2\pi\lambda}{g}}$	$T = 2\pi \left[\frac{2\pi g}{\lambda} \tanh\left(\frac{2\pi h}{\lambda}\right) \right]^{-\frac{1}{2}}$	$T = \frac{\lambda}{\sqrt{gh}}$
Wavelength (m)		$\lambda = \frac{gT^2}{2\pi}$	$\lambda = \frac{gT^2}{2\pi} \tanh\left(\frac{2\pi h}{\lambda}\right)$	$\lambda = \sqrt{gh}T$
Phase Velocity (m/s)		$c = \frac{gT}{2\pi}$	$c = \frac{\lambda}{T} = \frac{gT}{2\pi} \tanh\left(\frac{2\pi h}{\lambda}\right)$	$c = \sqrt{gh}$
Group Velocity (m/s)		$c_g = \frac{c}{2}$	$c_g = \frac{c}{2} \left(1 + \frac{2kh}{\sinh(2kh)}\right)$	$c_g = c$
Water Particle Velocity (m/s)	Horizontal	$u = \frac{\pi H}{T} e^{kz} \cos(kx - \omega t)$	$u = \frac{\pi H}{T} \frac{\cosh[k(z+h)]}{\sinh(kh)} \cos(kx - \omega t)$	$u = \frac{H}{2} \frac{\sqrt{g}}{h} \cos(kx - \omega t)$
	Vertical	$w = \frac{\pi H}{T} e^{kz} \sin(kx - \omega t)$	$w = \frac{\pi H}{T} \frac{\sinh[k(z+h)]}{\sinh(kh)} \sin(kx - \omega t)$	$w = \frac{\pi H}{T} \frac{z+h}{h} \sin(kx - \omega t)$

Table 1: Formulae for various wave properties under linear theory (formulae from [17]).

order theory for deep water includes a second term which is a correction to the linear profile and is given by [17]:

$$\eta = \frac{H}{2} \cos(kx - \omega t) + \frac{3}{16} \frac{H^2}{k^2 h^3} \cos[2(kx - \omega t)]$$

Equation 5

The corrections slightly flatten the trough and sharpen the crest. The expressions for celerity and wavelength are the same as those for linear theory. The horizontal water particle velocity according to Stoke's second order theory for deep water is [17]:

$$u = \frac{\omega H}{2kh} \cos(kx - \omega t) + \frac{3}{16} \frac{\omega H^2}{k^3 h^4} \cos[2(kx - \omega t)]$$

Equation 6

A feature of Stoke's second order theory is that it predicts the mass transport convection velocity of the waves; the orbital motions of the water particles have a net translation in the direction of wave travel. This is known as 'Stoke's Drift'.

As depth decreases and wave steepness increases the wave profile changes drastically from its linear sinusoidal form. The crest becomes narrower and higher while the trough becomes broader and flatter until such time as the wave breaks. For long waves in shallow water ($h/\lambda < 0.04$ [30]) the cnoidal wave theory has been developed of which the solitary wave theory is a limiting case [30]. The solitary wave is a shallow water wave of infinite length and period i.e. as its name suggests, a solitary wave is a one-time event. Theoretically the free surface of the solitary wave is entirely above the still water level (SWL). Solitary wave theory results compare well with observations of long waves in shallow water.

While non-linear wave models can be more accurate, in 'deep water' with swell waves the difference between the higher order wave models and linear wave models is small. As a deep water assumption is made for the modelling in this thesis and non-linear wave models are computationally more demanding than linear wave models, the modelling in this thesis assumes linear waves.

2.1.4 Model Validity

It is important when choosing which wave model to use to consider their ranges of validity. Linear theory is most suitable for low amplitude long waves in deep or intermediate depth water. The Stokes higher order models have a greater range of validity including steeper waves and shallower water. Cnoidal theory is useful for waves in shallow water while the solitary wave best represents a breaking wave. These ranges of validity can be described in visual form as in Figure 3. Other than shoreline devices, WECs will normally be situated in intermediate or deep water away from the shallow surf zone so the cnoidal shallow water wave theories will not apply.



Figure 3: Graph showing ranges of validity for different wave theories (from [32]). In contrast to Table 1, in this graph depth is denoted by d rather than h .

2.1.5 Wave Spectrums

The wave theories discussed in the previous section describe monochromatic waves i.e. regular waves with specified heights and periods. Obviously a sea state is usually not monochromatic but is composed of irregular waves of varying heights and periods. Regular wave patterns can be superimposed on each other to create irregular wave patterns. Figure 4 shows the difference between a monochromatic regular wave and the superimposed composition of many regular wave components to create irregular waves.

Irregular or random seas can be described using statistical parameters. The two most common measurable properties of water waves are height and period, and common parameters to describe irregular sea states are the significant wave height (H_s) and significant period (T_s). Significant wave height is the average height of the highest one third of waves. The significant wave period is the average period of the highest third of waves. These parameters correspond to what was visually observed by mariners taking the early wave records. As smaller waves tended to go unnoticed, the average wave parameters recorded tended to represent the average of the highest one third of the waves present.

Sea states can be represented as a spectrum of waves with the parameters height and period. The spectral density $S(T)$ describes the occurrence of waves of particular frequency for a sea

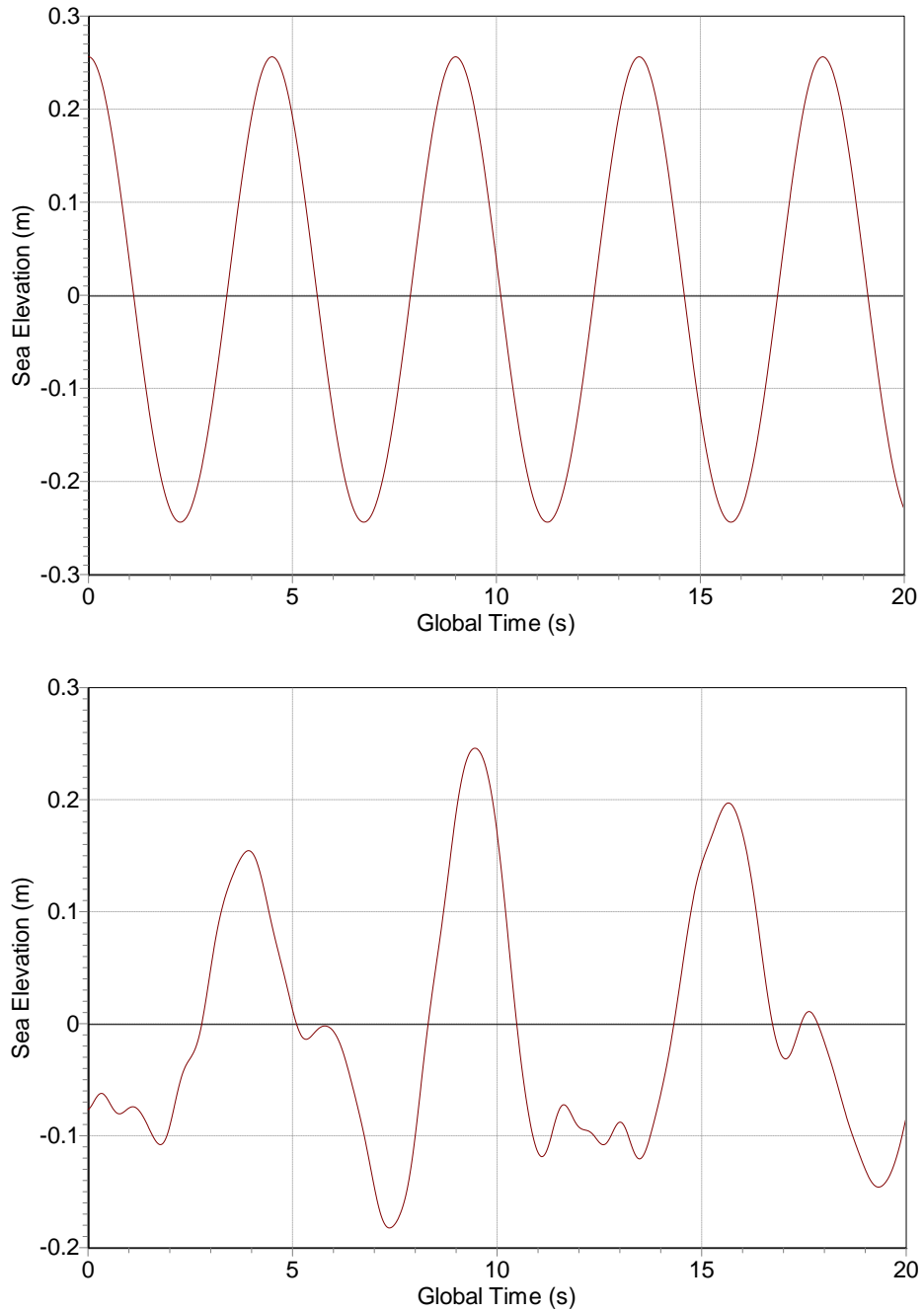


Figure 4: Regular (top) and irregular (bottom) waves.

state. For fully developed seas a generic equation to describe the spectral density is [30]:

$$S(T) = AT^m e^{-BT^n}$$

Equation 7

Here A and B are coefficients that depend on statistical wave properties which in turn depend on the associated wind. If measured data is available the exponent coefficients m and n can be found from curve fitting of the data. One of the most common spectrums is the Bretschneider

spectrum for fully developed seas for which $m = 3$ and $n = 4$. An example of a Bretschneider spectrum is shown in Figure 5.

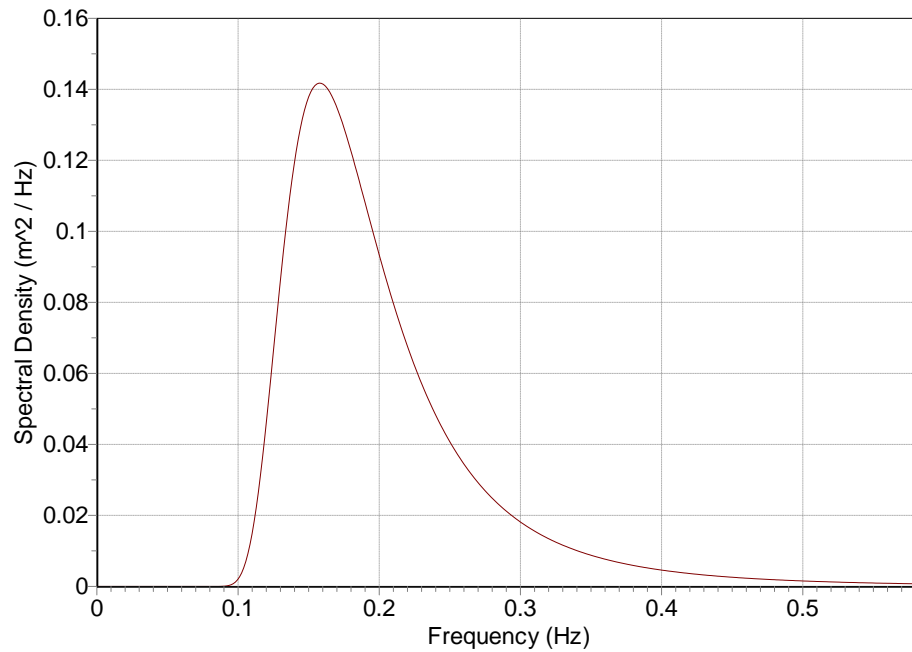


Figure 5: Bretschneider spectrum with a spectral peak of 0.1579 Hz (period of 6.3339 s) and H_s of 0.5 m.

The peak period (T_p) of a spectrum is the period that yields the peak value in the spectral density function and represents the wave period where the energy in a wind-generated sea is at a maximum. This is of obvious interest to wave energy developers as it is where most of the energy in a sea is. It is expressed as [30]:

$$T_p = \left(\frac{5}{4B}\right)^{\frac{1}{4}}$$

Equation 8

The significant wave period (T_s) can be expressed as [30]:

$$T_s = \left(\frac{4}{5}\right)^{\frac{1}{4}} T_p$$

Equation 9

The directionality of the waves can play an important part in the functioning of a device if the mode of operation is directionally dependent. Many sites will have a dominant wave direction from which most of the energy is delivered but the extent of this directionality will vary between different sites due to bottom effects, fetch length in each direction and weather patterns. The directionality of the wave climate at a site can be displayed on rose diagrams.

The example rose diagrams in Figure 6 are for the Wavehub [33] test site situated 16 km off the coast of Cornwall on the south west tip of the UK and so is on the eastern edge of the Atlantic ocean. The rose diagrams are plotted for the peak period parameter. It is obvious that the dominant direction is due west, but there is spreading towards WSW which becomes more significant during the summer. What is also evident from the rose diagrams is the seasonal variation of the wave climate at this site that a WEC must operate in.

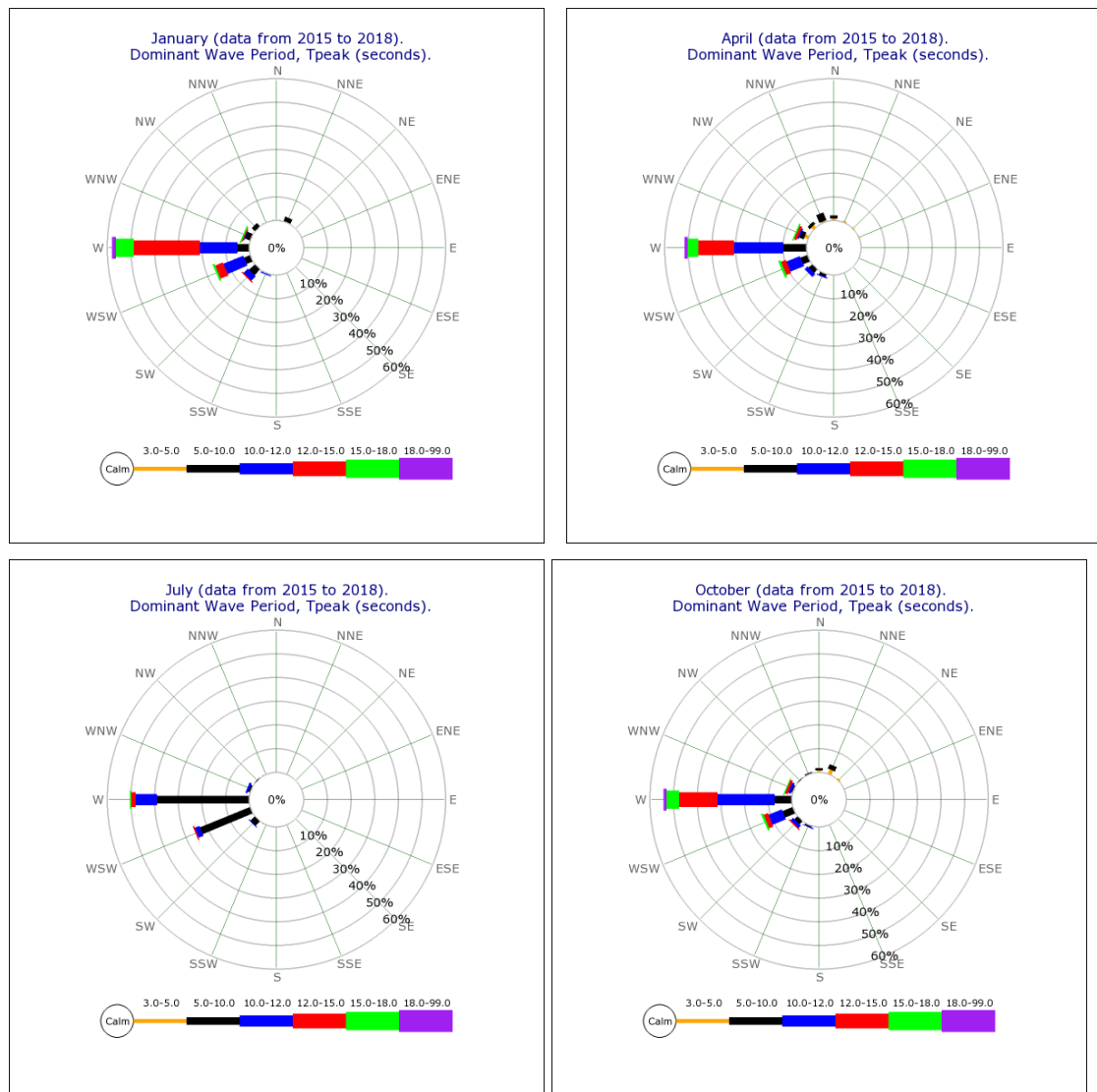


Figure 6: Quarterly rose diagrams for peak period at the Wavehub test site [34].

2.1.6 The Resource

There is an estimated worldwide resource of 2 TW of wave power [35]. The ideal wave climate for generating electricity would be a single consistent frequency of wave that a device

could be optimised for. In reality the wave conditions at a particular location will vary with weather (both locally and along the fetch) over time periods as short as a matter of minutes. This variability over several time scales complicates the design process of a WEC which is trying to maximise energy generation (subject to other design considerations). The wave power available at a particular site is normally expressed as ‘average power per unit length of wave crest’. Typically wave energy developers consider a good offshore location to have a value between 20-70 kW/m (annual average) [17]. This level of energy is mostly found in moderate to high latitudes as shown below on the global wave power atlas in Figure 7. Seasonal variation is generally larger in the northern hemisphere than the southern and therefore the south coasts of South America, Africa and Australia are potentially promising wave energy sites.

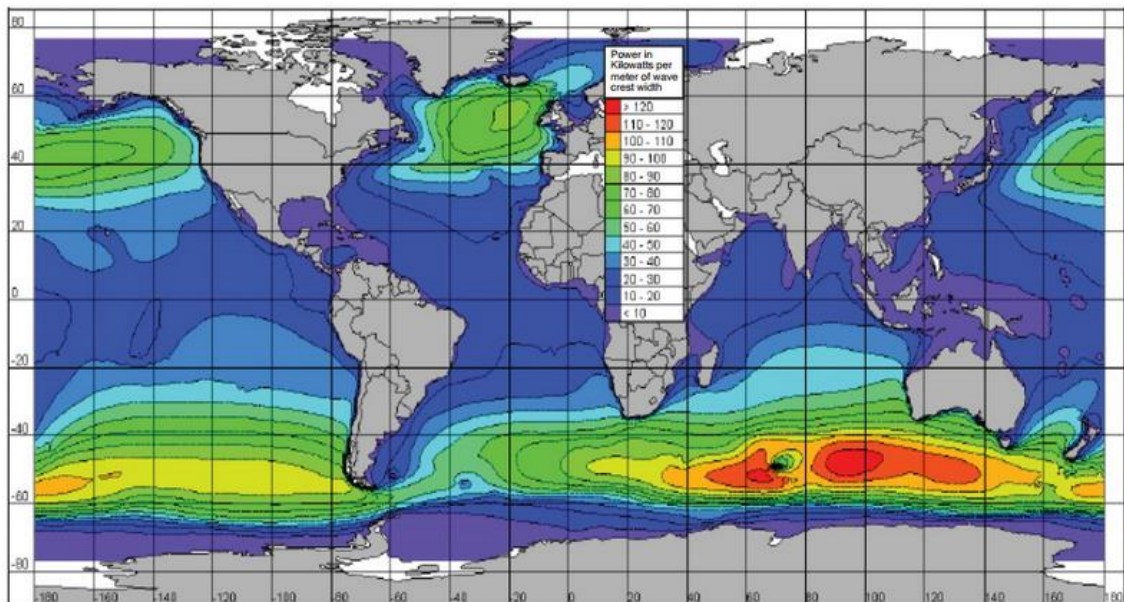


Figure 7: Global wave resource atlas [36].

Being located at a moderate latitude on the eastern coast of the Atlantic gives the UK abundant wave energy as can be seen in Figure 8. Around the UK there is estimated to be 7-10 GW of wave power that can realistically be harnessed [37]. However, although the UK has abundant wave energy, it also has a high range of power. WECs must withstand the colossal power and forces of Atlantic storm waves. Around the coast of Western Europe there is average wave power levels of 30-70 kW/m [38] but with extreme levels of 2 MW/m [39]. This variability can be seen in the seasonal variation between the rose diagrams of Figure 6 in the previous section. Wave resource knowledge is therefore vital to inform a WEC design for survival and energy generation. For European sites the WERATLAS [40] provides high quality results from wind-wave modelling validated by wave measurements where available.

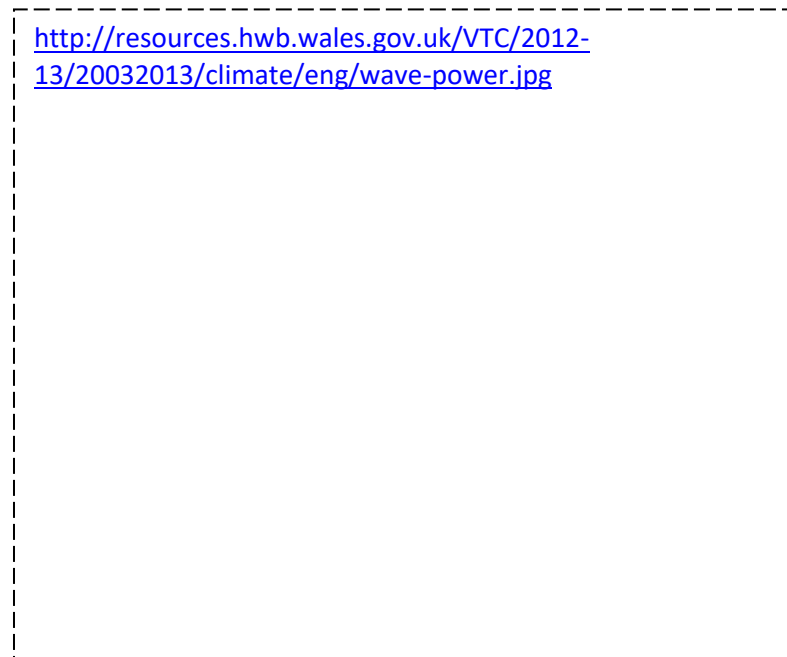


Figure 8: UK wave power resource [41].

WERATLAS contains detailed wave climate and wave energy statistics at 85 points off the Atlantic and Mediterranean coasts and is a useful tool for initial wave energy planning in Europe.

As waves propagate to shore they are modified by bottom effects (refraction, diffraction, bottom friction, wave breaking) and sheltering due to land (headlands and islands). Wave energy resource characterisation for nearshore/shallow water (<50 m) has only been done at specific sites. Portugal has one such nearshore wave atlas called ONDATLAS [42] which covers 500km of roughly straight Portuguese coastline with a bottom profile exhibiting little change over long stretches.

2.2 Wave Energy Absorption

2.2.1 Benefits of Wave Energy

As covered in 2.1.1 wave energy has a higher energy density than wind or solar. Solar energy intensity is 0.1-0.3 kW/m² [43] whereas wave energy has a much higher energy flow of about 2.3 kW/m² for a vertical plane at the water surface [44]. It is therefore a more energy dense source of renewable energy. Waves can cross an ocean with little loss of energy and so with a

long fetch and knowledge of the weather patterns over it, wave resource can also be reliably predicted days in advance. There is limited negative environmental impact [35] with offshore devices generally having the lowest impact. In the UK there is a positive correlation between seasonal electricity demand and wave energy thus wave energy could be a very useful addition to renewable energy sources if we could engineer a device to produce electricity (or another appropriate energy vector) for a competitive price.

2.2.2 The Engineering Challenge

Conventional energy generation engineering traditionally uses high angular velocities with low torque and a regular motion. Waves present an irregular motion of low frequency (~0.1 Hz) and very high forces that must somehow be converted in to electricity of sufficient quality to be acceptable to the grid. There could be variations of this such as producing desalinated water, or powering a micro-grid with less stringent power quality requirements, however most devices to date have been designed with the aim of grid quality power. A successful WEC will accomplish this at a reasonable price which will be determined by the capital & operation costs vs. the revenue from the generated energy. The capital & operation costs will largely be driven by survivability whilst the revenue will be driven by device efficiency: a WEC must survive the worst day of the year and be efficient on the calmest. The offshore operating environment could range from waves as small as 1 kW/m crest width to storm waves with several MW/m crest width. In offshore locations wave direction can be highly variable. The saltwater will corrode materials and biomass will accumulate on any available surface, potentially adding tonnes of additional mass to the device along with increasing drag.

These are the challenges a WEC must overcome and the difficulty of meeting these challenges can be seen in the slow growth of the wave energy industry over the past 40 years.

2.2.3 Classification of Wave Energy Converters

There are a number of ways to classify wave energy converters based on location, dimensions and mode of operation. However, no classification system is perfect and as such there are devices that cannot be easily put in to any particular category. The point absorber category is one example of blurred lines; it is not clear when a point absorber may become classed as a terminator. Semantics aside, the classification system is a convenient structure to outline the principal configurations that have been developed.

Classification by Location

Location refers to the position of the device with respect to water depth and coastline. The three categories are Onshore, Nearshore and Offshore.

Onshore

These devices are mounted on the shoreline, either on the coast itself or in a breakwater. They have the benefit of being easily accessible for maintenance and for grid connection. The shallow water also protects them from extreme conditions by attenuating the waves. The level of this protection is obviously dependent on the local bathymetry. This attenuation can also be a disadvantage as it leads to lower wave powers than deeper water. Again, this is dependent on the site bathymetry; the attenuation due to shallow water can be compensated for by a natural focusing of the waves by the sea bed onto the site. Much like glass refracts a light wave, so the change in depth of water can bend a water wave [17]. An underwater ridge can focus the waves approaching perpendicular to it, much like a bay will spread the waves. Tidal range can also present problems. Due to the dependence on site characteristics, shoreline devices tend to be designed for a specific site and therefore may not be suitable for mass production [28]. This type of WEC could be useful for Island communities as a replacement for expensive diesel generators. Examples of onshore devices are the Islay OWC (Oscillating Water Column) in Scotland, developed by Wavegen [43], the Pico OWC in the Azores [45] and the Mutriku breakwater OWC in Spain [46]. They also typically have the largest visual and environmental impact due to the location on land and by reducing the natural coastline habitat.

Nearshore

Nearshore usually refers to the water depth in which the WEC is located rather than proximity to a coastline. There is a lack of consensus [28] surrounding the term ‘shallow water’ for the nearshore definition but it is suggested to be less than a quarter of the wavelength by Duckers [37]. The boundary obviously then depends on the wave travelling across it; short waves will have a shallower nearshore boundary than long waves. Devices in this zone are often attached to the seabed as it provides a suitable foundation for the device to react against and the depth does not make it prohibitively expensive. To reduce costs further it is possible to piggyback a wave energy converter system onto an offshore wind turbine structure, subject to structural loading constraints. There are devices in development to take advantage of this synergy and commercialise this technology [47] [48] [49]. It would have the added advantage of being able to share power infrastructure such as offshore substations and transmission lines, although these would need to be capable of carrying the additional load. Similar to the shoreline

devices, nearshore devices will suffer from reduced wave power due to attenuation by the sea bed. However, it can be argued that the protection the device has from extreme conditions along with the lower directional spread of the waves outweigh the reduction in wave power [50]. The attenuation can also be used to the WEC's advantage. For example, Oyster, a coupled Pitch and Surge nearshore device, benefits from the elliptical motion of the water created by the shallower water [51]. Careful site surveys to identify bottom effects are still required for nearshore devices to accurately predict wave climate. Depending on how close to land the device is located it may benefit from easier grid connection, low visual impact and low environmental impact. Maintenance is more challenging than shoreline devices but some nearshore devices compensate for this by locating some of their PTO onshore. For example, Oyster pumps high pressure sea water onshore to drive a Pelton wheel [52].

Offshore

Offshore devices are located in deep water, which, if following the shallow water definition for the nearshore zone, must begin at depths greater than one quarter wavelength. Other definitions are a depth exceeding $1/3$ wavelength [44] or greater than 40 m [37]. Without bottom effects the wave climate offshore is more energetic and the visual impact is low, or none at all if sited far enough from land. However, the more energetic deep water waves may necessitate a stronger WEC and careful design of the moorings to withstand the largest storm waves. Despite the more extreme conditions in deep water making the device more structurally expensive Korde [53] has argued that the greater amount of energy available in deep water could still make it more structurally efficient (MWh/ton) than nearshore devices. Maintenance can be difficult in the offshore location if it is heavily dependent on weather windows with a high transit time to site and transmission costs may be higher for offshore sites as it will be further from a grid connection. Having an expanse of sea surrounding the device rather than being backed on to or near a shore can increase the directional spread of the waves for the WEC. Offshore typically has the lowest environmental impact.

By Principal Dimension

A WEC can be classified based on the principal dimension of the device with the three classes of device called attenuators, terminators and point absorbers [54].

Attenuator

Attenuators lie perpendicular to the wave crest (parallel with wave direction) and absorb energy from the wave as it passes down its length. They have a length much greater than their

width. The best known example of this class is the Pelamis sea snake (Figure 9), developed by Pelamis Wave Power [55]. It consists of four floating cylinders connected together at their ends by hydraulic pumps. As the wave passes along Pelamis, the different sections rise and fall and the relative motion between the cylinders is used to extract power (Pelamis also extracts energy from the wave with side-to-side motion through clever control of its hydraulic pumps and is thus a multi-axis device [56]). Attenuators typically align themselves with the incident wave direction by rotating around their mooring. Due to their shape this weather-vaning can be achieved passively. From a hydrodynamic perspective an attenuator can be thought of as the special case of a closely spaced line of point absorbers [57].



Figure 9: The Pelamis attenuating WEC [58].

Terminator

Terminators lie parallel to the wave crest (perpendicular to wave direction). These devices typically have a width much greater than their length. The Salter Duck, developed by Stephen Salter at the University of Edinburgh and the subject of his article in ‘Nature’ in 1974 [19] is a good example of a terminator (Figure 10). Because of its large width, a terminator can be approximated to 2D, and is therefore suitable for testing in narrow wave tanks. All shoreline



Figure 10: Artist’s impression of a row of Salter’s ducks acting as a terminating WEC [59].

devices are effectively terminators as the waves do not pass them; they are terminated (or partially reflected). Similar to the attenuators, incident wave direction typically is important. It can be more difficult to manoeuvre a terminator as it may not have a natural inclination to face the waves. A better strategy may be careful site selection to limit directional spread and a device design that can efficiently absorb waves from a wide angle. An example of a multi-axis terminator is the Bristol Cylinder, developed in the 1980's by Evans [60]. This submerged cylinder can achieve close to 100% efficiency (2D), and under tank testing in a wide tank achieved capture widths exceeding the device dimensions. The same concept was more recently investigated by Heikkinen et al. [61].

Point Absorber

Point absorber wave energy converters (PAWECs or SPAWECs for 'Single...') have small dimensions relative to the wavelengths they are expected to operate in. There are different values for defining what 'small' means. It can range from $1/20^{\text{th}}$ of a wavelength up to $1/3^{\text{rd}}$. Due to their small size it is often assumed that direction is not important for these devices. This is only true for axisymmetric devices and where the heave response is the only concern. The surge of the waves will apply an oscillating horizontal force in the direction of wave travel and if the device is asymmetric then this force will vary with wave direction and should be accounted for. An example of a directionally sensitive point absorber is the Solo Duck [62]. Originally designed as a terminator, with many individual Ducks located on a flexible spine, the Solo Duck is a point absorber equivalent; a single Duck. The PowerBuoy (Figure 11) is an example of an axisymmetric PAWEC [63]. It is a cylindrical buoy that operates in heave by reacting against a submerged damper plate. The majority of PAWECs are similar to the PowerBuoy in that they are axisymmetric and operate in heave. However, some point absorbers have been designed to operate in pitch, surge, yaw, roll or a combination of these, such as the Pelican, at LUREG (Lancaster University Renewable Energy Group) [64]. Due to their lower capital cost and other perceived hydrodynamic benefits PAWECs became the

https://www.oceanpowertechnologies.com/uploads/196342a6a6849b6f6e2d39a21cd61b5d_0_thumb.jpg

Figure 11: The PowerBuoy point absorber WEC from Ocean Power Technologies [65].

preferred option once the Government funding for large projects began to dry up. Point absorbers are small and modular allowing for gradual expansion and development of capacity rather than risking a lot of capital with a single large machine.

MA-PAWECs can be considered a subset of the point absorber WEC category. As was defined in section 1.2 a MA-PAWEC point absorber absorbs energy from multiple modes of body motion using a power-take-off system operating in multiple degrees of freedom. A recent example of a MA-PAWEC that has reached a ¼ size prototype stage for sea testing (as of 2018) is the WaveSub developed by Marine Power Systems [27], shown in Figure 12.



Figure 12: WaveSub by Marine Power Systems, a submerged body MA-PAWEC [66].

Classification by Mode of Operation

Further differentiation between devices is based on how the device operates to capture the wave energy. This is essentially a description of how the device provides a reaction against the force of the wave to generate energy. Falcao [18] divides the type of WEC operation in to three main categories with subcategories associated with each. These are shown in the diagram of Figure 13. Point absorbers generally come under the oscillating body category but there are examples of small floating oscillating water columns that can be counted as point absorbers [67].

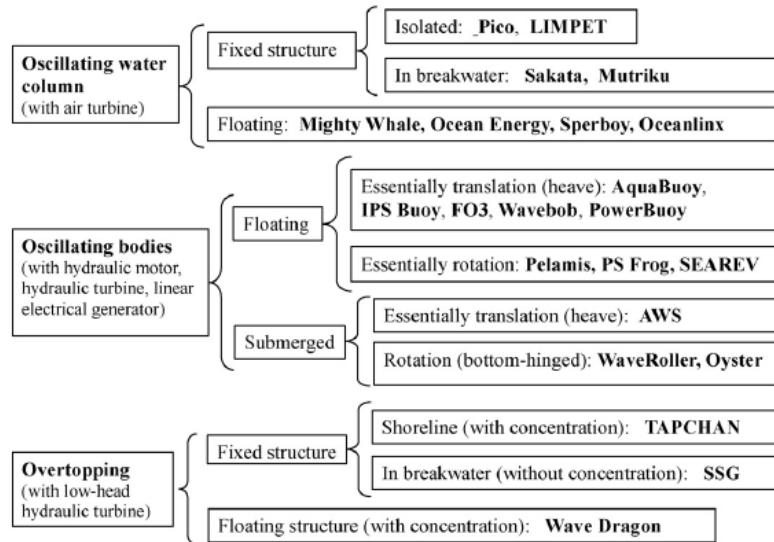


Figure 13: Categories for mode of operation of WECs (from [18]).

Oscillating Water Column (OWC)

An OWC uses an air/water interface within a chamber to act as a piston (see Figure 14). The

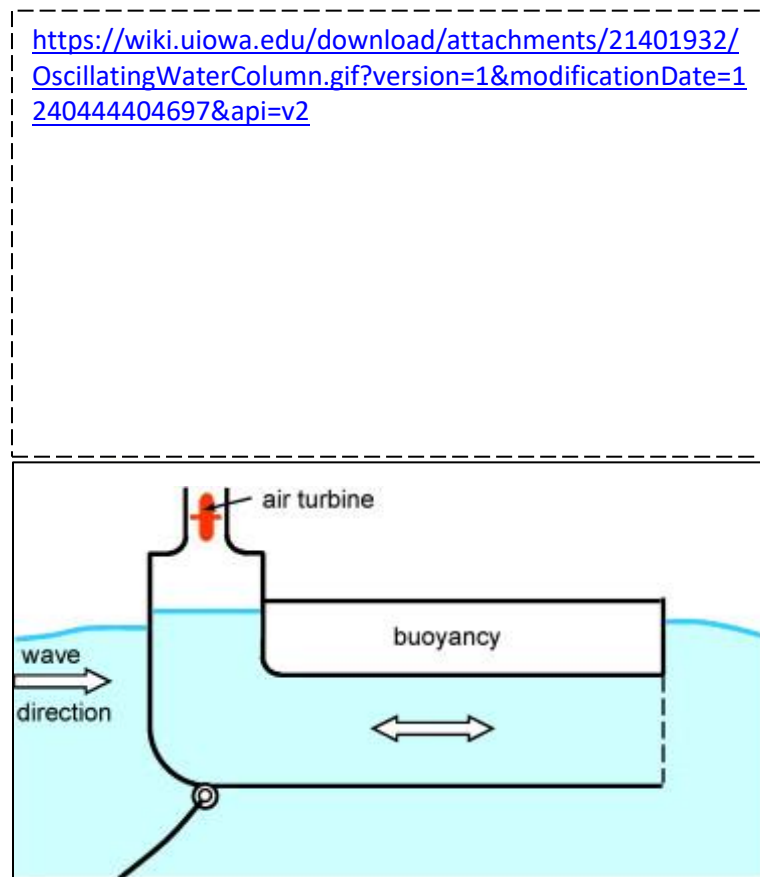


Figure 14: (Top) A shoreline oscillating water column WEC [68], (Bottom) A floating oscillating water column WEC [18].

chamber is open at the bottom to the sea below the water line and at the top to the atmosphere via a turbine for power extraction. As waves impinge on the device the column of water inside the chamber rises and falls due to the open chamber bottom. This oscillating column of water within the chamber pressurises and de-pressurises the air above it, alternately pushing air out and drawing it back in to the chamber. The oscillating airflow passes through the turbine at the chamber top to generate power. Unless flow rectification is used the turbine configuration must be able to cope with oscillating air flows. Typically this is achieved with a Wells turbine, which rotates in the same direction regardless of the direction of fluid flow. The advantages of the OWC are its simplicity and robustness. It can be built into the shoreline as at Islay [43] or as a floating point absorber like the Backward Bent Duct Buoy [67]. Single OWCs cannot have multi-axis PTO applied to them as they use a single air/water interface to capture energy. However, multiple OWCs used together on the same WEC could be used to achieve a multi-axis device e.g. by positioning an OWC at either end of a pitching and heaving buoy.

Overtopping device

Overtopping devices consist of a reservoir raised above the waterline which is filled by the incident waves flowing up a ramp (see Figure 15). The water is then released back to the sea through low-head turbines, for example Kaplan turbines. These devices can be located onshore as with Tapchan [18] or floating as with WaveDragon [69]. WaveDragon uses a pair of curved reflectors to focus the waves onto its central ramp.



Figure 15: The WaveDragon overtopping WEC [70].

Oscillating Bodies

This is the broadest category of WEC and consists of one or more oscillating bodies either submerged or floating. The wave action applies a force to the body which is reacted against using either the sea bed, another floating body, a damping plate or inertial mass. The category

is divided here in to Submerged Pressure Differential, Floating Bodies, Submerged Bodies, and Bottom Mounted Surge Collectors.

Submerged Pressure Differential

Submerged pressure differential devices operate using the difference in pressure between the crests and troughs of waves passing overhead. The Archimedes Wave Swing (AWS) [71] and Bombora [72] are examples of such devices. The AWS is a submerged point absorber (see Figure 16) consisting of an air filled vertical cylinder fixed to the sea bed with a moveable second cylinder (closed at the top end) fitting over it. These two parts form a chamber of air, whose volume can change depending on the applied pressure to the upper moveable cylinder. As a wave crest passes above the device the increased hydrostatic pressure presses against the moveable cylinder and compresses the air within. Once the crest has passed, the pressure from the water is reduced and the air expands again. Power is extracted using linear generators from the motion between the two cylinders. The Bombora [72] is a line absorber (attenuator) utilising the pressure differential to move air between chambers driving an air turbine in the process. Being submerged, pressure differential WECs are away from the slamming forces on the surface experienced by floating WECs and there is very little visual impact. Conversely, maintenance can be difficult. These devices are usually point or line absorbers and as these devices use the seabed as the reaction point they are typically located nearshore.



Figure 16: Submerged pressure differential WECs. Left: AWS point absorbers [73]. Right: Bombora line absorber [74].

Floating Oscillating Bodies

Floating bodies operate at the surface and are therefore exposed to maximum wave energy. An example of a point absorber floating body WEC is the Corpower heaving buoy [75] shown in Figure 17. The buoy drives a mechanical power-take-off (PTO) system deriving the reaction force from the seabed. The Pelamis [55] (see Figure 9) is an example of a line absorbing floating body WEC and it uses the phase difference between floating cylinders to provide the reaction force. The PowerBuoy [63] of Figure 11 is another floating oscillating body point absorber and uses a damping plate for its buoy to react against. Power is captured

from the relative movement. The Wello Penguin [76] instead uses a rotating mass inside its hull to provide a reaction against the wave induced roll, pitch and yaw of the device.

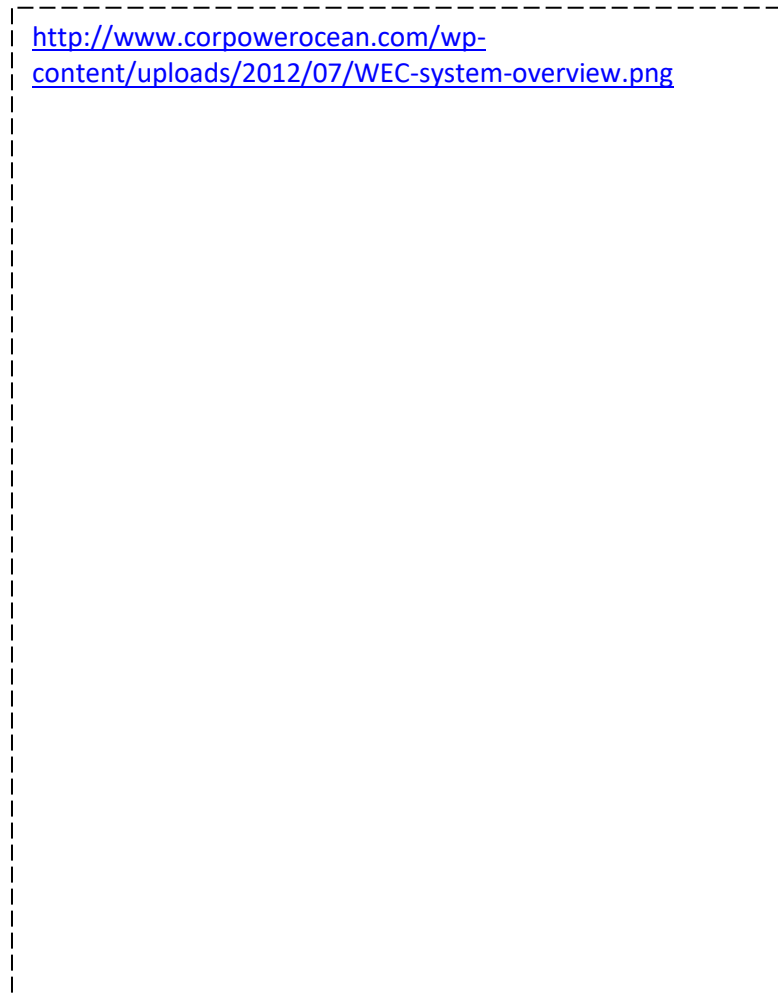


Figure 17: The Corpower heaving buoy WEC [75]

Submerged Oscillating Bodies

Submerged oscillating bodies operate beneath the surface and are therefore not exposed to potentially damaging breaking waves and slamming forces. Examples of submerged oscillating body WECs are the point absorbers CETO from Carnegie Wave Energy [77] and the multi-axis device from 40SouthEnergy [78], both shown in Figure 18. The CETO buoy drives a hydraulic PTO that pressurises water for desalination and power generation. Earlier versions pumped the water onshore but later designs incorporated energy generation equipment at sea. The multi-axis device from 40SouthEnergy uses the relative motion between two submerged bodies. The four mechanical PTO mechanisms allow it to absorb energy from the relative motion between the bodies in multiple modes.

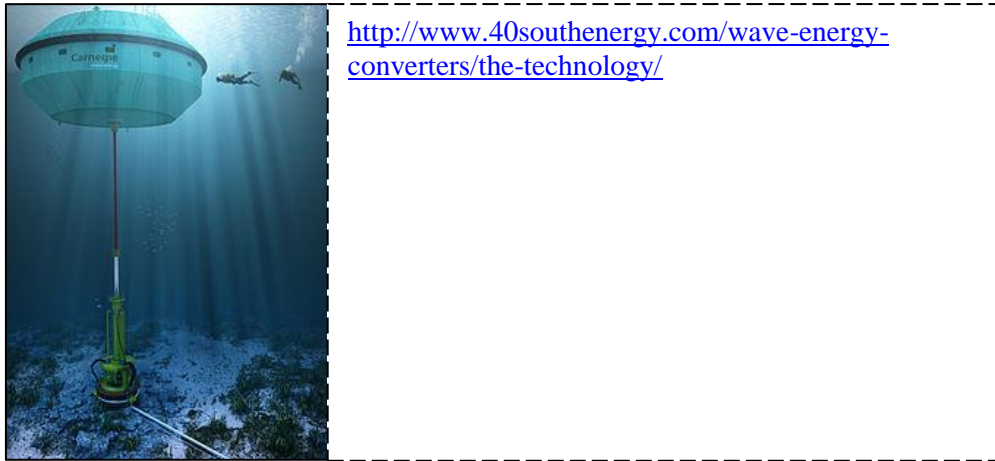


Figure 18: Submerged oscillating body WECs. Left: the CETO device from Carnegie Wave [79]. Right: a multi-axis device from 40SouthEnergy [78].

Bottom-mounted surging collector

The bottom-mounted surge collector generally consists of a vertical plate, hinged on the lower end (usually to the sea bed, possibly on a structure elevated above the sea bed) and aligned perpendicular to the wave direction, thus acting as a terminator (although if the dimensions are small enough it could be considered a single point absorber). The surge action of the waves causes the plate to oscillate back and forth. An example of this type of device is the Aquamarine Oyster [52] shown in Figure 19.

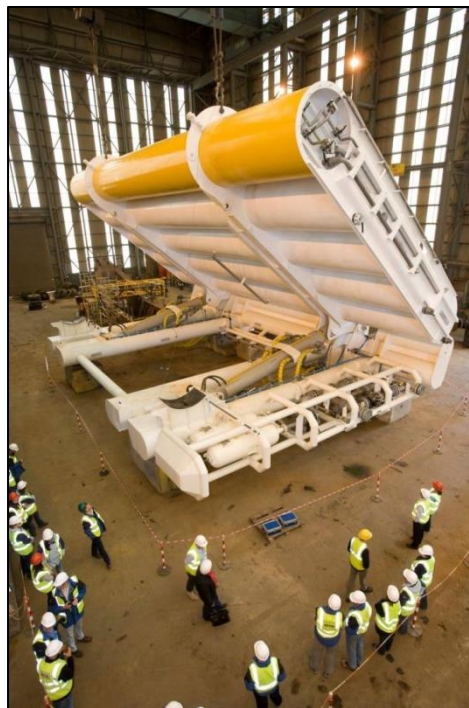


Figure 19: The Oyster bottom mounted surging WEC [80].

2.2.4 Hydrodynamics

The hydrodynamic process of wave energy absorption is theoretically complex with diffraction and radiation phenomena, but the basic premise behind wave energy devices is that a good wave absorber must be a good wave maker [81]. The generated wave must interfere destructively with the incident wave to absorb power and there will be an optimum oscillation amplitude that a WEC must achieve in order to maximise absorbed energy. Due to losses (e.g. friction, flow separation) the optimum amplitude for 'converted useful energy' is lower than the theoretical optimum [81] and for most of the time the optimum amplitude will not be reached because of design limits of the WEC. Only in small waves would a WEC be able to oscillate at the optimum amplitude to generate the required wave radiation pattern to interfere optimally with the incident wave field. The radiation pattern generated by a WEC is determined by its motion and geometry. A 2D example is shown in Figure 20. Under 2D conditions 50% absorption is the maximum possible if there is only a symmetrical radiated wave or anti-symmetrical radiated wave [82] [83] [84] [85]. By combining a symmetrical and anti-symmetrical radiated wave 100% absorption can be achieved. Motion in the heave mode generates a symmetrical waveform while pitch and surge motions generate anti-symmetrical waveforms. In three dimensions the radiated wave will also spread sideways. The 3D radiated wave pattern of a heaving axisymmetric point absorber is shown in Figure 21. Through the phenomenon of using the radiated wave to focus waves on to the PAWEC it is possible to absorb energy from a length of wave front greater than its own width [85] [83] [84] [86].

It is possible to create optimum waveforms using a single mode of motion by modifying the geometry of the WEC. The Salter Duck achieves this by being non-symmetrical; when it moves it only generates a radiated wave in one direction to interfere with the incident wave field. Budal and Falnes [81] suggested that a line absorber like Salter's Duck is probably a better method to maximise energy absorption from the waves but that point absorbers, while less effective, may capture energy at a lower cost i.e. a line of point absorbers instead of Ducks.

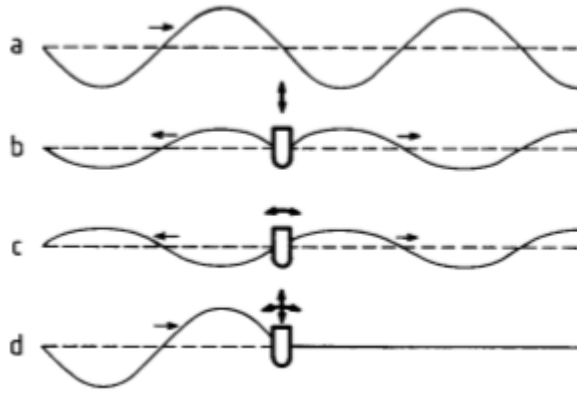


Figure 20: 2D radiation patterns of a symmetrical WEC from [81]. (a) Incident wave. (b) The radiated wave when the device is moving in heave. (c) The radiated wave when the device is moving in pitch or surge. (d) The superposition of (a), (b) and (c) and represents 100% absorption of the incident wave.

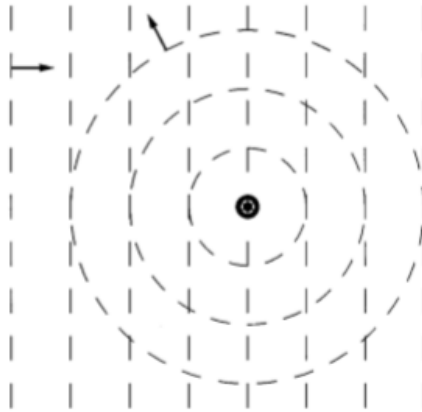


Figure 21: Radiated wave pattern of a heaving axisymmetric point absorber. From [81]. The straight lines are the incident waves. The circular lines are the radiated waves.

Equation of Motion

The equation of motion of a body describes the response of that body to applied forces. In the case of a WEC the applied forces will be from the surrounding fluid and any external forces, for example from a PTO or mooring system. Following that of Thomas [87], the equation of motion (EOM) for a floating body in a single translational direction of motion (X) is given by [87]:

$$m\ddot{X} = F_T(t) + F_{ext}(X, \dot{X}, t),$$

Equation 10

where m is the mass of the body, $X(t)$ is the time-varying displacement, $F_T(t)$ is the time varying total fluid induced force made up of components $F_f(t)$, and $F_{ext}(X, \dot{X}, t)$ represents any external forces. Linear theory can be used with good accuracy to predict kinematic properties of waves that have a height to wavelength ratio (H/λ) less than $1/50$ [17]. Under linear assumptions (deep water, small amplitudes, irrotational, incompressible and inviscid fluid) the fluid induced force $F_f(t)$, can be approximated by [87]:

$$F_f(t) = F_S(t) + F_R(t) + F_H(t),$$

Equation 11

where $F_S(t)$ are the exciting forces, $F_R(t)$ are the radiated forces, and $F_H(t)$ are the hydrostatic forces. The hydrostatic forces are independent of the incident wave under linear theory whereas the exciting and radiated forces are associated with the body response to the incident wave and are frequency dependent. A complex representation of the body motion can be employed to make it more convenient to handle. It can be assumed that the motion of a body in a single mode can be written in complex form as [87]:

$$X(t) = Re\{\xi e^{-i\omega t}\},$$

Equation 12

where Re denotes the real part of the complex number and ξ is a complex constant corresponding to the magnitude and phase of oscillation. The exciting force can now be written in similar form [87]:

$$F_S(t) = Re\{\mathbb{X}e^{-i\omega t}\},$$

Equation 13

where \mathbb{X} is a complex constant which can be considered as being made of two parts [87]:

$$\mathbb{X} = \mathbb{X}_{inc} + \mathbb{X}_{diff},$$

Equation 14

which represent the effect of the incident and diffracted waves respectively. \mathbb{X}_{inc} can be found by integrating the incident wave pressure over the wetted surface of the body. \mathbb{X}_{diff} is more complicated to find as it requires knowledge of the pressure field over the entire wetted surface. Analytical solutions are limited to simple cases and so it is normally found numerically.

The radiation force (force due to the generation of a radiated wave) can be written as [87]:

$$F_R(t) = -\{A(\omega)\ddot{X} + B(\omega)\dot{X}\},$$

Equation 15

or in complex form as [87]:

$$F_R(t) = Re\{\mathbb{F}_R e^{-i\omega t}\},$$

$$\mathbb{F}_R = [\omega^2 A(\omega) + i\omega B(\omega)]\xi,$$

Equation 16

where $A(\omega)$ is the frequency dependent added mass coefficient, and $B(\omega)$ is the frequency dependent damping coefficient. Assuming the displacement X is in heave, the hydrostatic force is due to buoyancy and is given by [87]:

$$F_H(t) = -CX(t) = -Re\{C\xi e^{-i\omega t}\},$$

Equation 17

where C is the buoyancy coefficient. The EOM (Equation 10) can be written with these components substituted in as [87]:

$$(m + A)\ddot{X} + B\dot{X} + CX = Re\{\mathbb{X}e^{-i\omega t}\} + F_{ext}(X, \dot{X}, t)$$

Equation 18

This can apply to multiple modes by replacing the coefficients with the appropriate vector or matrix arrays. The external force is often specified as a linear spring and damping term to keep the equation in a linear form. In reality the mooring and PTO may have highly non-linear characteristics. This form of the EOM is suitable for a frequency analysis for regular wave components. If the assumption of regular wave components is not satisfied, an alternative form of EOM for a single mode of motion suitable for irregular wave fields is [87]:

$$(m + A_\infty)\ddot{X} + \int_0^t K(t - \tau)\dot{X}(\tau)d\tau + CX = F_S(t) + F_{ext}(X, \dot{X}, t)$$

Equation 19

Here A_∞ is a constant related to added mass and $K(t - \tau)$ is the impulse response function related to the radiation damping. However this time domain approach is not used in this work.

To find the coefficients for the equation of motion of a WEC a developer typically uses tank test models or numerical models. Modelling is essential to the development of a WEC device as the ocean is a very expensive environment to work in. Tank tests provide a cheaper

alternative and it is not difficult to scale up experimental results on device models because the viscous drag effects are normally insignificant for wave power devices (even down to scale 1:150) [88]. The viscous losses will depend on the device geometry and motion. Bluff bodies with small motions will have little drag while sharp edges with large motions will have significant drag.

There are various numerical modelling techniques that are used to model WECs. The most common form is linear theory which assumes small amplitudes of waves and body motions, along with an irrotational, inviscid and incompressible fluid. The frequency dependent hydrodynamic coefficients can be found using a boundary element method (BEM). These techniques are all well-established from ship hydrodynamics and there are a number of proprietary software packages for it e.g. WAMIT [89], ANSYS -Aqwa [90]. When analysing a point absorber it may be small enough that diffraction effects can be neglected [57]. The diffraction can only give a subtractive force [91] and so this assumption will increase the resulting coefficients. This is called the ‘point absorber approximation’.

The main disadvantage with linear numerical modelling according to Falcao [18] is not being able to take account of viscous effects (large eddy turbulence) and not being able to accurately model large amplitude water oscillations (non-linear waves). These non-linear effects are known to be important from the shipping and offshore industry. When modelling a WEC there are multiple sources of non-linearity to consider;

- Non-linear exciting force from non-linear waves
- Non-linear damping from PTO and viscous effects
- Non-linear spring

More sophisticated numerical methods include direct numerical simulation, large eddy simulation, Reynolds Averages Navier-Stokes equations, and detached eddy simulations [92] and these can to some extent account for the non-linear effects.

Optimal Hydrodynamic Absorption

The mean hydrodynamic power absorbed by a body (from all six modes) in a monochromatic linear wave is given by [93] [91]:

$$P = \frac{1}{2} \text{Re}\{\mathbb{X}^* \mathbf{U}\} - \frac{1}{2} \mathbf{U}^* \mathbf{B} \mathbf{U},$$

Equation 20

or alternatively [91] :

$$P = \frac{1}{8} \mathbb{X}^* \mathbf{B}^{-1} \mathbb{X} - \frac{1}{2} \left(\mathbf{U} - \frac{1}{2} \mathbf{B}^{-1} \mathbb{X} \right)^* \mathbf{B} \left(\mathbf{U} - \frac{1}{2} \mathbf{B}^{-1} \mathbb{X} \right),$$

Equation 21

where \mathbf{U} is the velocity vector, \mathbb{X} and \mathbf{B} are the exciting force vector and damping matrix respectively, and * denotes the conjugate transpose. It is therefore obvious that the maximum value of P occurs when the velocity is such that the second term is zero. Therefore the optimum mean power absorption is [91]:

$$P_{opt} = \frac{1}{8} \mathbb{X}^* \mathbf{B}^{-1} \mathbb{X}$$

Equation 22

For an axisymmetric point absorber this optimum power equation reduces to a form that remarkably depends only on wavelength. The capture width (L) of a device is the width of wave front equivalent to the energy absorbed by the device and is a useful measure of the performance of a WEC. It is found by dividing the Power absorbed (P) by the incident power across the width of the device, $= P/P_w$. It is a well-known result from linear theory that the optimum capture width of an axisymmetric point absorber with arbitrary geometry operating in heave is [86] [84] [83] [85]:

$$L_{opt} = \frac{\lambda}{2\pi}$$

Equation 23

For the anti-symmetric modes (surge, sway, roll, pitch) motion the optimum capture width depends on the angle of incidence (β) of the wave on the device [94]:

$$L_{opt} = \frac{\lambda}{\pi} \cos^2 \beta$$

Equation 24

As they are derived from linear theory both of these equations are frequency dependent and require unconstrained motion. In high waves or long period waves the necessary amplitudes for a point absorber to generate the required wave may exceed the dimensions of the device resulting in it leaving the water and hence certainly not remaining in the small displacement assumption of the linear regime. Upper bounds for the power absorption of point absorbers have been formulated using a volume approach for heaving, surging and pitching point absorbers [57]. This work restricted the motion of the point absorber to reduce viscous losses

with the conclusion that heave significantly outperformed surge and pitch in longer waves and that the surge mode is much more efficient than pitch for the same available volume stroke [57]. For a heaving small body the maximum power it can absorb depends linearly on its volume [57]. Todalshaug [57] concluded that the upper bound under heave has a weaker decay with wave period than the upper bounds for surge and pitch. Thus as the body gets smaller (or waves larger) heave becomes more attractive. Therefore for small devices (i.e. point absorbers) the recommendation is for heave, possibly in combination with surge. For larger buoys the surge mode becomes more favourable [57].

Optimum power absorption of a point absorber (or system of point absorbers) under a global constraint was originally developed by Evans [95] and then expanded to a global weighted constraint by Pizer [62] [96]. Pizer examined a motion constrained two, three and six DOF PTO for a Solo Duck which showed that device bandwidths and energy absorption from oblique waves could be improved by additional PTO axes [62]. It is however not certain that multi-axis PTO will always absorb more energy than a single axis equivalent. Due to the increasing amount of energy with longer periods of waves, in a broad bandwidth sea, resonance in one degree of freedom can yield greater average power than dual resonance in two degrees of freedom at a lower frequency [97]. Movement along a slope is an efficient single axis method of generation [20] but development of sloped devices remains a challenge.

Babarit [98] summarises the performance of many of the most prominent WECs that have been proposed to date in terms of their capture width ratio (CWR). The sheer number of devices that have been developed dictates that this database cannot be exhaustive, but the statistical results for the groupings of WECs does suggest some general conclusions that are relevant to the industry as a whole. The CWR figures vary widely within each category of WEC (based on operating principle) but it suggests which operating principle typically offers higher CWR. The most hydrodynamically efficient category is the bottom fixed Oscillating Wave Surge Converter (OWSC). Floating OWSCs and overtopping devices appear least efficient. Heaving devices and OWCs are in the middle. As is noted in the paper, this ranking only refers to hydrodynamic performance, without reference to the cost of energy from the device.

Control

In order for a WEC to achieve the optimal absorption it must carefully control its motion [99]. To be an efficient absorber, the oscillating body should oscillate near the frequency of the

incident waves (i.e. at resonance) [18]. Resonance (and therefore maximum absorbed energy) occurs when the body velocity is in phase with the excitation force [86]. Phase control is the process of controlling the body velocity so it is in phase with the exciting force. Problems associated with frequency matching for a point absorber are [18];

- Small point absorbers (of the order of 10 m diameter) typically have a natural frequency of oscillation that is too fast for the incident waves of interest to a WEC developer.
- Real wave trains are not of a single frequency but constantly vary.

For a WEC the resonant frequency in heave is given by [18]:

$$\omega = \sqrt{\frac{\rho g S + K}{m + A(\omega)'}}$$

Equation 25

where S is the cross-sectional area of the body at the unperturbed free surface, and K is the stiffness of the PTO. If the natural frequency is too high it can be lowered by having negative values of K i.e. reactive control (putting energy back in to the ocean through the PTO) or with a negative spring [75]. Reactive control of a WEC can increase its energy absorption [28] if the power can be cycled efficiently through the PTO. There can be problems with too much energy lost in supplying the reactive power to achieve phase-control to be of benefit. Alternatively, the technique of latching can be used which approximates phase control [16]. Theoretically it is sub-optimal but it can be almost as efficient for a single body converter, but this is difficult to achieve in real irregular seas with limited advanced information of approaching waves [18].

For an axisymmetric device, in sinusoidal waves, optimum power is reached by having the energy transferred to the PTO as equal to the energy contained in the generated outgoing wave (which is the radiation resistance). For wind-generated waves which are not sinusoidal the PTO loading should be larger than the radiation resistance [91].

Arrays

In order to generate at utility scale, point absorber WECs must be deployed in arrays of multiple devices. Although two thirds of the planet is covered by ocean, it is more cost effective to reduce infrastructure and array footprint by having devices in close proximity to

one another. As a result of this proximity there will be hydrodynamic interactions between devices that will affect power absorption. A theory for power absorption from an array of N interacting devices was first derived by Budal before being generalised independently by Evans [100] and Falnes [101]. McIver [102] extended the heaving theory of Evans and Falnes to include surging and combined heaving and surging devices. Calculation of the absorbed power requires knowledge of the device motions, exciting forces and radiation-damping matrix coefficients. By using the ‘point absorber approximation’ (neglecting diffraction effects) for an array of heaving devices they were able to derive simple expressions, the results of which showed that there were significant hydrodynamic interactions. These interactions were constructive for some frequencies and destructive for others. Constructive interference leads to an increase in the amount of power produced by the array as a whole compared to the equivalent number of isolated devices. Conversely destructive interference lowers the power output. It is therefore vital for point absorber devices that are intended to be deployed in arrays to have their array behaviour assessed and incorporated from an early stage in the design process.

Justino & Clément [103] modelled arrays of five submerged spheres in 3 different array configurations (attenuator, terminator and cross, see Figure 22) and looked at the three translational modes heave, surge and sway, separately and together (multi-axis) to examine the effects array shape has on power absorption. They used linear frequency domain modelling to calculate the maximum power available from an array of bodies, using BEM AQUADYN software to calculate the hydrodynamic coefficients. The spheres modelled were 20 m in diameter with their centre points 20 m below the sea surface. A range of separation distances were modelled. For the terminator and attenuator arrays it was from 30 m to 150 m or 1.5 to 7.5 diameters. For the cross array, separation was 50 m to 150 m. Optimum and sub-

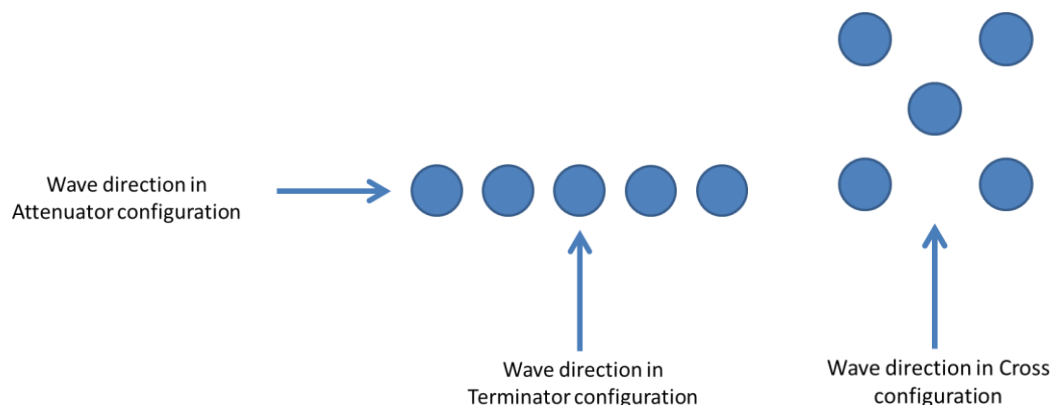


Figure 22: Submerged sphere array configurations.

optimum load impedance was used with the sub-optimum regime being created by multiplying the optimum impedance matrix by a diagonal matrix of coefficients (0.8 to 1.2). Eight-second waves in water of infinite depth were used for most of it although 7, 9, 10, 11 and 12 second waves were also calculated for the terminator configuration under sub-optimum load impedance. The off-diagonal elements of the load impedance matrix did not have a significant impact as performance was not significantly different when these were set to zero [103]. The velocities calculated for the optimum condition were rather higher for some configurations than the validity limits of linear theory allows and thus the conclusions should be treated with caution. The terminator configuration had the lowest velocities and so highest confidence in the results. Constructive interference was more pronounced across the range of periods (7-12 s) for the heave response, achieving a high of 1.8 times that of a single device compared to a high of 1.4 for the XYZ device [103]. Thus in terms of possible array interference this could suggest that heaving devices could be better. However, an XYZ sphere will have a wider capture width than a heaving sphere and so will suffer proportionally more when spacing is reduced below this. Forcing each sphere to have the same PTO characteristics rather than the optimum for each did not make a significant difference to the results for the terminator array under XYZ motion [103].

When modelling arrays, if the number of devices is large then the interactions become extremely complex and approximate methods need to be used such as the ‘multiple scattering method’, ‘the plane-wave method’ and the ‘point absorber approximation’ [18].

2.2.5 Geometry

The exciting forces and added mass on a PAWEC are dependent on its geometry [87]. Usually the geometrical parameters are fixed once the device has been built, although this is not strictly true for some devices as they have the ability to alter their form during operation. For example Quoceant [104] have patented an idea to use inflatable body parts to alter a WEC’s shape. Large devices tend to have wide resonance bandwidths while small devices tend to have narrow resonance bandwidths. However, large devices experience much higher loading due to their size than a smaller WEC and so for survival, smaller may be better.

Wave climate is an important factor in determining the performance of a given device. Most obviously the size of the device will influence performance within a given wave climate. A device may not be suitable for two different wave climates. This has been illustrated by McCabe et al. [64] where a genetic algorithm was used to optimise geometry based on performance in two different wave climates. The resulting geometries exhibited significant differences in their shape demonstrating that one device will not necessarily suit all climates.

The point absorber device SEAREV also underwent a geometry optimisation process and the results are perhaps evidence that Stephen Salter had it right from the beginning. After an extensive hydrodynamic optimisation process the SEAREV device evolved from a symmetric point absorber shape to an asymmetric quasi-point absorber that resembles the Salter Duck shown in Figure 23 [105].

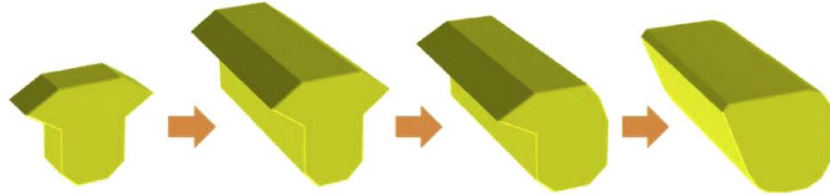


Figure 23: Evolution of the SEAREV concept, taken from [105].

Columbia Power Technologies [106], spun out from a research programme at Oregon State University also evolved their device from a simple heaving float to a more sophisticated point absorber with a surging and heaving element. Although highly dependent on the modelling design parameters, results of these optimisation processes suggest that neither heave nor axisymmetric WECs are the way forward.

2.2.6 Power Take Off Methods

A major challenge for WECs is to meet the stringent power quality standards demanded by the grid. The PTO problem is about converting the variable energy flux of the waves in to a regular and stable energy flux for the grid. The energy varies on several time scales:

- Wave-to-wave (order of seconds)
- Sea states (hours – days)
- Seasonal variations (months)

The PTO (along with the rest of the WEC) must also be able to survive in extreme storm seas. One way to mitigate the energy quality problems is to change the energy vector. Using the electricity to generate hydrogen offshore [107] would remove some power quality demands and avoid the cost of expensive undersea cables. Other energy vectors can remove the need for electricity conversion entirely. Desalination of sea water can be achieved using vapour compression or reverse osmosis with the WEC providing the hydraulic pressure [108] [20] [77]. This is particularly suitable for arid climates or island communities where fresh water is in short supply and thus expensive.

The different PTO technologies are shown in Figure 24. The general method of electrical generation is conventional high speed rotational generators but developments in slower rotating generators for wind turbines may be able to be applied to the wave energy industry.

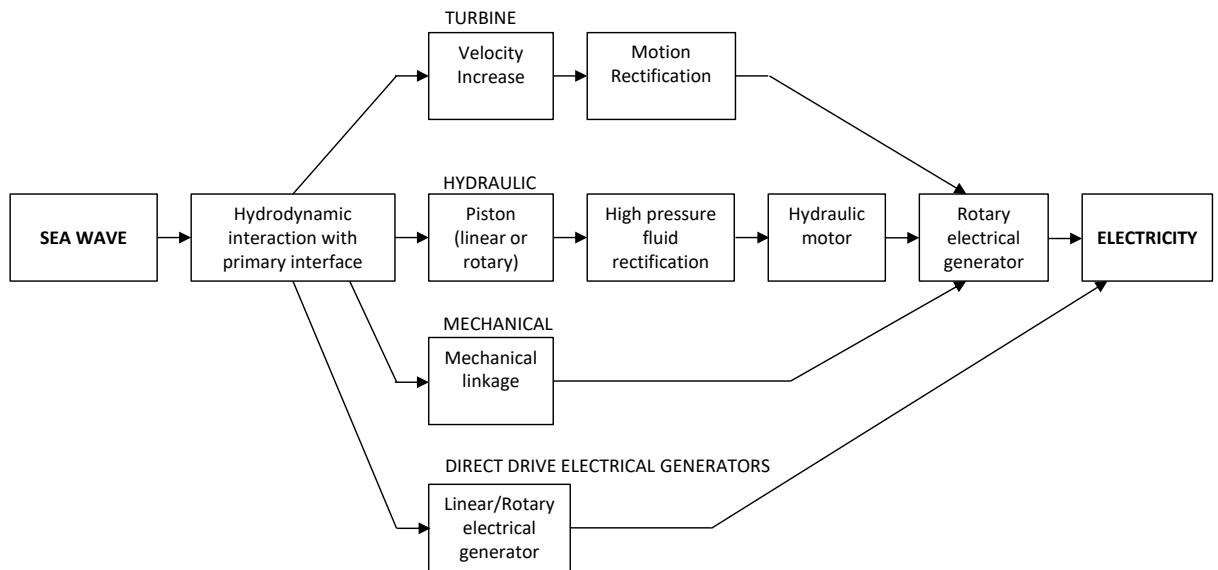


Figure 24: PTO process from wave to grid with different technologies. Adapted from [28] to include mechanical path.

Hydraulic systems are well suited to absorbing energy from high force, low speed motion [28] [56]. This makes them an attractive option for WECs as the forces created by hydraulics are considerably higher than from electrical machines of similar size. However, losses in hydraulic primary systems can be of the order of 20% over a wide operating range [55]. The efficiency of a hydraulic system drops at part loading and as a WEC hydraulic system will spend significant time operating below rated capacity it must have high part load efficiency [109]. Both linear and rotary hydraulics can be a good fit for WECs. Ceramic coatings such as Ceramax by Bosch RexRoth can protect hydraulic rams from sea water to extend their life/maintenance periods. Digital displacement pumps/motors can also be a good fit for WECs, particularly as they remove the end stop problem (up to a limit). The end stop problem is due to the limited stroke length of many PTOs. In large waves the WEC may move further than the stroke limits and so a system needs to be in place to prevent damage by overextending the PTO.

Direct drive generators (linear or rotational) typically have higher efficiencies than hydraulics but typically apply lower forces. A hydraulic system can exert significantly more force than a direct drive system of the same size [28] [110]. Direct drive generators are characterised by a large number of poles in order to create the necessary magnetic flux to generate useful damping at the slow oscillations of the WEC [111].

The variable nature of the waves means that some form of energy storage is required in order to produce a smooth output. This could be achieved using a hydraulic accumulator or kinetic energy devices, among others. There will also be limits to the power production capability of the PTO. For economic reasons a WEC should work close to its design limit for a large fraction of time [81]. Limiting the maximum power of the PTO to 20 times the mean absorbed power did not significantly decrease output [98].

As real PTOs normally have strong non-linear characteristics it is necessary to take a time domain approach when modelling devices with specific PTOs [18]. Time domain models are computationally expensive but allow these non-linearities to be included. An alternative approach is stochastic modelling which uses less computing power and produces a probability density function distribution (but is limited to linear or near-linear PTO).

Reaction Force

In order to do work, the force applied to the WEC by the wave must be resisted by an opposing reaction force through the PTO system. There are several options for providing this reaction force [112]:

1. A large floating/submerged structure that experiences multiple wave forces of different phases to provide a reaction to each other. An effective structure size should be of the order of a wavelength or greater.
2. The seabed.
3. An inertial mass which is part of the WEC.
4. Reaction against the sea (using drag forces).

2.2.7 Mooring

The primary function of a mooring system is to keep the device on station. It will need to be able to do this during the most severe storms yet not detrimentally affect power absorption of the device during calmer seas. As wave energy devices are inherently designed for unsheltered areas the mooring system must be designed to withstand the fatigue and abrasion that these high energy environments induce. As well as the wave induced loads there may be constant or slowly varying loads from currents and tidal flows. The whole system must be reliable and cost-effective as maintenance windows offshore may be limited.

A secondary function of the mooring system may be to provide part or all of the reaction force for the PTO. This function is best stated by Salter [20] who has said that “It is wrong to pay to

resist large horizontal forces and then not get any power from them ...”. Even without being directly part of the PTO, mooring connections may significantly affect the energy absorption properties through interaction with the oscillation [18]. These interaction effects are non-linear and complex resulting from the:

- Catenary affect (of slack moored lines).
- Inertia of mooring lines.
- Hydrodynamic drag forces on mooring lines.

Catenary moorings are inherently non-linear. The non-linearity stems from their changing geometry, static restoring forces, viscous damping and friction with the seabed [113]. Viscous damping and repetitive laying down of the chain on the seabed results in energy loss from the system.

Mooring cables add additional mass, stiffness and damping to a device which can be detrimental or advantageous. Cerveira et al. [114] conducted a numerical investigation into the mooring effects on power absorption of a heaving and surging cylindrical point absorber. A three line slack line catenary mooring configuration was shown to have at most a 1% reduction in annual energy absorption at an offshore Portuguese site. The numerical model was based on idealised linear PTO on the heave and surge axes against a fixed reference frame. Linear approximations were used to model the device and moorings in both regular and irregular waves.

A linear numerical analysis under optimum PTO damping with linearised mooring effects was carried out by Fitzgerald and Bergdahl [113] for five different mooring configurations on the surge, heave and pitch response of a cylindrical point absorber (see Figure 25). Their work suggested that mooring design can be used to improve energy absorption in surge and pitch by acting in phase with the device motion. Conversely, heave will probably always suffer from the restoring forces of the mooring system [113].

In offshore locations wave direction can be highly variable and if the device has a directional dependency the mooring system may have to be designed to orient the device appropriately. Nearshore waves have more consistent directions due to refraction and limited fetch on one side (coast) and so may require a simpler mooring system. When doing a mooring systems analysis the DNV (an accredited classification company for offshore technology) recommends using several sea states with a return period of 100 years [114]. However, extreme mooring loads are more likely to occur at wave conditions not along the 100 year envelope of the H_s/T_p scatter diagram [115].

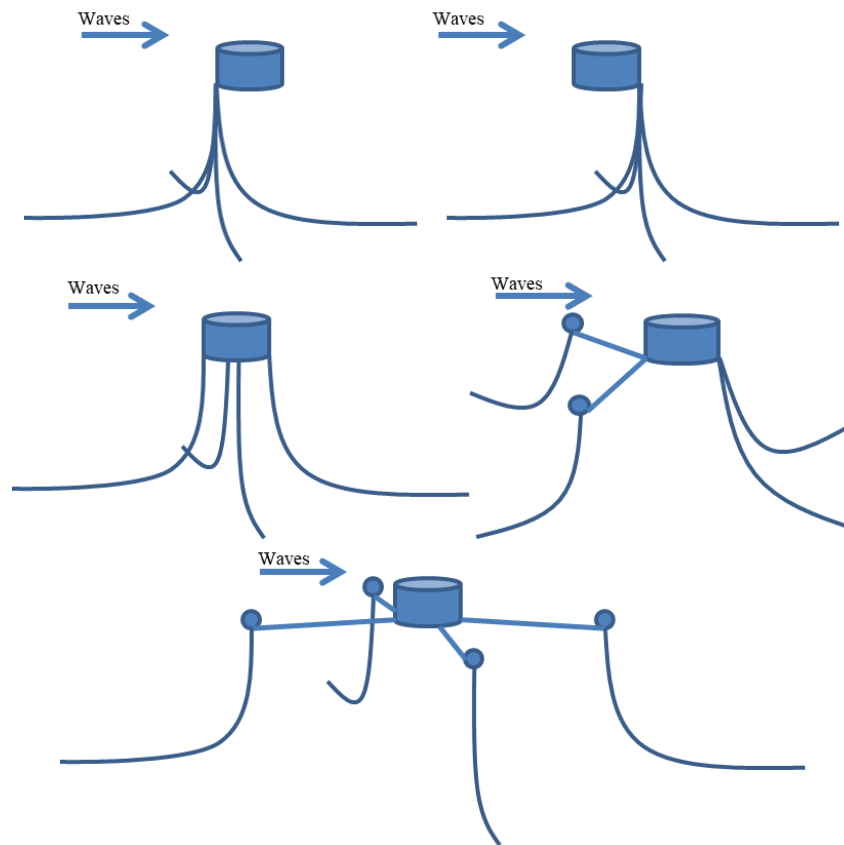


Figure 25: Mooring configurations investigated by Fitzgerald and Bergdahl [113].

2.3 Conclusions

There is evidently a significant amount of energy available from ocean waves but its variable nature over time, direction and location make it a challenging resource to exploit. Though more predictable than wind or solar it presents significant engineering challenges to exploit it due to the periodic and random nature of the large forces involved. Different mathematical modelling approaches have also been developed. Linear modelling provides good accuracy for small motions and low waves in deep water and thus is useful for estimating energy generation under normal operating conditions which will be the operating regime of interest in this research, and thus it is the chosen modelling method used throughout this work.

Many different types of device have been developed so far but none have yet managed to move in to large scale commercial viability. Within the point absorber subset of devices the majority have PTO on a single axis, but there has been research carried out on multi-axis configurations that confirm theoretically they can absorb more energy than a single axis. What can be concluded from this literature review is that the tantalising evidence that MA-PAWECs can generate more energy than existing device configurations should be extended to try and

more definitively quantify what benefits this could lead to. It is this current lack of knowledge of how much better, or worse, MA-PAWECs could be for lowering the cost of wave energy compared to existing devices that is the motivation for this research.

3 Initial Multi-Axis Considerations

This chapter is an initial discussion of some of the factors associated with MA-PAWECs and how they affect the design decisions when embarking on investigating multi-axis PTO on a point absorber. It begins with a discussion on the prevalence of single axis devices before moving on to the decision of which modes and axes to select for a MA-PAWEC. Associated factors to this decision are then discussed.

3.1 The Prevalence of the Single Axis Device

The random diversity of the wave resource suggests the reason why there are so many different ideas relating to wave energy conversion; a resource that presents itself in such a diverse way leads to diverse solutions to capture it. This variety of configurations is indicative of the challenge related to capturing wave energy. Most devices though still use a single PTO axis.

It is interesting to consider why most research and development in the last 40 years has focussed on single-axis PTO PAWECs. It is well established that a PAWEC absorbing energy from more than one mode of motion generates more energy than from a single mode under certain conditions. There are however many good reasons why most developers have so far made the decision to absorb energy from only one mode. Complexity and cost are two. Multi-axis PTO is more complicated and expensive to execute than single axis so it is logical to try and get the simpler solution working first.

Heave is the most popular mode of operation for PAWECs and there are good reasons for this:

- Point absorbers are by definition small bodies relative to the wavelength and so can be said to experience mostly long waves, in which the heave mode is considered better at absorbing power under the motion constraints that exist in the real world [62] [57].
- Coupling between modes can allow energy to be absorbed from multiple modes using a single axis [96] e.g. a taught moored heaving buoy will experience forces on its tether due to the surge motion of the buoy, so a heaving axis will normally be able to absorb some energy from other axes.

- For floating WECs the hydrostatic stiffness acts as a restoring force which allows resonant behaviour (albeit normally at a frequency that is too high for the incident wave field).
- For a heaving point absorber the energy absorption is not dependent on the direction of the incident waves. This removes the need to orient itself appropriately for changing sea states.
- A reaction force for the PTO to do work against can be provided by the seabed or water column beneath the device (via a heave damping plate).
- It is also the most obvious mode to extract energy from; to observers, floating objects bob up and down in waves.

As heaving point absorbers are the most common type of PAWEC one way of looking for the answer to the question of whether MA-PAWECs are a route to competitively priced wave energy is to compare MA-PAWECs with the incumbent heaving configuration. Currently energy from heaving point absorbers is still considered expensive and so a MA-PAWEC must produce a cost of energy lower than the heaving equivalent for it to be considered a viable route to competitively priced wave energy. This decision on adding additional PTO axes to create a MA-PAWEC depends on whether the additional energy absorbed sufficiently compensates for the additional complexity and hence cost of device. The generating side of this question is therefore how much more energy can be expected from a WEC if multi-axis PTO is applied vs. single axis? Before this question can be addressed, there is an obvious initial question that must first be looked at.

3.2 Which Modes and PTO Axes?

The most fundamental question associated with a MA-PAWEC is which modes and axes to choose. This is not a straightforward question. The answer can depend on a myriad of other factors associated with the WEC such as body geometry, PTO type, position in water column, wave climate and the metrics against which these options are measured:

- The geometry of the body will have a significant impact on whether multiple axes offer any benefit. Cam shaped WECs are already extremely effective with only a single axis.
- The choice of PTO system. Different axes make different requirements on the PTO. Heave, roll and pitch offer hydrostatic spring (on the surface). Surge and sway will

require spring to be built in to the PTO. Different types of PTO are better suited to meeting certain requirements.

- Floating or submerged? Floating devices can make use of hydrostatic spring in heave, pitch and roll. Submerged devices have no natural reciprocal spring (except that afforded by changing volumes of gas due to pressure) but are protected from some of the extremes of the waves.
- The wave climate can shift the multi-axis equation significantly. Long waves favour the heave response, short waves favour the pitch and surge (or roll and sway) response. Some sites have very little directional spread perhaps negating the need of additional PTO to capture waves from many directions. Other sites will be the opposite.
- The metrics used to measure the devices against will obviously have an effect. The end metric may be Levelised Cost of Energy (LCOE), but other subordinate metrics may also be important such as generation, capital cost, operation cost, ease of installation, component availability (whether off-the-shelf or bespoke) etc.

As an optimisation problem this is basically unsolvable given the number of possible variables. To make this question tractable, it is necessary to use some common sense. Forty years of work on wave energy has not delivered an optimum design so it is reasonably futile to attempt such an objective. A more tractable question is how adding multi-axis PTO to the most prevalent incumbent designs would affect the balance of energy vs. cost.

3.2.1 Modes and Axes

To make sense of this problem it is convenient to begin by considering the axes in their most general terms. Although there are an infinite number of DOF variations upon which a PTO can act, we obviously need no more than six (three translational, three rotational) to completely capture all modes of motion. Multi-axis devices can come in different configurations which by the definition proposed in Section 1.2 can use any combination of one or more arbitrarily defined axes with the intent to absorb energy from more than one mode of body motion. For an initial consideration of MA-PAWECs it is therefore more convenient to start by considering only the six standard axes that are used to describe the motion of a body. These are surge, sway, heave, roll, pitch and yaw. Each of these is considered below.

Surge

Surge is the name given to the horizontal component of the wave and the horizontal motion of the body in the direction of wave travel. WECs that absorb power from this horizontal motion of their bodies are therefore termed surging WECs. As was mentioned in Chapter 2, the radiation pattern of the surge mode for an axisymmetric PAWEC is of an anti-symmetrical, or dipole, nature. The surge mode does not displace volume, but rather sweeps a volume. As the draft of the WEC does not change during an oscillation, there are no hydrostatic restoring forces acting on the WEC. In order to achieve resonance behaviour in the surge mode, spring must be applied by the WEC (through the PTO or some other means). For a small body point absorber with unlimited excursion, the maximum capture width under linear theory is independent of body size and twice that of heave. Under more realistic motion constraints surge performs better in short waves.

Sway

Sway is the name given to the horizontal motion of a body that is orthogonal to the surge direction (i.e. parallel with the wave crests). There is no sway motion of water molecules in a single wave, therefore a WEC will experience no sway forces in a unidirectional wave field. Real wave climates will have some directional spread to a greater or lesser extent and so will excite a WEC in the sway mode to a greater or lesser extent. Just like in surge, the radiation pattern for sway of an axisymmetric PAWEC is of an anti-symmetrical, or dipole, nature, and there are no hydrostatic restoring forces. Spring must be applied in order to achieve resonant behaviour. As for surge, for a small body point absorber with unlimited excursion, the maximum capture width under linear theory is independent of body size and twice that of heave, and under more realistic motion constraints sway performs better in short waves.

Heave

Heave is the name given to the vertical component of the wave and the vertical motion of the body. WECs that absorb power from this vertical motion of their bodies are therefore termed heaving WECs. As was mentioned in Chapter 2, the radiation pattern of the heave mode for an axisymmetric PAWEC is of a symmetrical, or monopole, nature. For floating WECs, due to the change in draft during heave oscillations, there is a hydrostatic restoring force which gives the WEC a natural frequency. For point absorbers however, this natural frequency is often higher than the desired wave frequency. For a small body point absorber with unlimited excursion the maximum capture width under linear theory is independent of body size and

half that of surge. Under more realistic motion constraints heave performs better in long waves than the horizontal translational modes.

Roll

Roll is the rotation of the WEC about the surge axis (roll is side-to-side tipping motion). The radiation pattern of the roll mode for an axisymmetric PAWEC is of an anti-symmetrical, or dipole, nature. For a floating WEC, as it rolls in and out of the water on either side, there are hydrostatic restoring forces that allow the WEC to have a natural frequency of oscillation. For a small body point absorber with unlimited excursion the maximum capture width under linear theory is independent of body size and twice that of heave, but motion and displaced volume constraints will reduce this [57]. For a monochromatic unidirectional wave field there will be no rolling motion for an axisymmetric PAWEC as there is no sideways force component from the waves. Real wave climates will have some directional spread to a greater or lesser extent and so will excite a WEC in the roll mode to a greater or lesser extent. Non-axisymmetric geometries can be used to excite a roll motion from a head-on wave such as for the Wello Penguin PAWEC [76].

Pitch

Pitch is the rotation of the WEC about the sway axis (pitching fore and aft motion). As was mentioned in Chapter 2, the radiation pattern of the pitch mode for an axisymmetric PAWEC is of an anti-symmetrical, or dipole, nature. Just as with the roll mode, for a floating WEC, there are hydrostatic restoring forces from the pitching motion that allow the WEC to have a natural frequency of oscillation. For a small body point absorber with unlimited excursion the maximum capture width under linear theory is independent of body size and twice that of heave. In reality, motion and/or displaced volume constraints will reduce this capture width [57].

Yaw

Yaw is the rotation of the WEC about the heave axis. In order to yaw a WEC needs unbalanced horizontal forces to create a torque about its centre of rotation. With the correct geometry and/or the right wave field this torque can be created. The Pelamis [116] line absorbing WEC could absorb energy from the relative yawing of its sections but no known PAWECs are designed to use the yaw response and there is very little discussion in any literature of using the yaw response for a PAWEC.

As per the definition of a MA-PAWEC in section 1.2, there is no constraint on using any of these specific six axes, but as any arbitrary axis can be described in terms of these six it is convenient to restrict consideration to start with to these modes. The exact configuration of PTO axes can come later.

3.2.2 Geometry

Before settling on the modes and axes it is necessary to consider geometry. The geometry of the device will obviously affect the response of a PAWEC in each of the six modes via added mass, damping and spring terms. The question of geometry is an important one in that it can affect which mode of oscillation it is preferable to absorb energy from. For example, the Salter Duck and the Bristol Cylinder are both devices that have excellent absorption capabilities; under 2D conditions they can both absorb 100% of the energy of the incoming wave [20]. However the Bristol Cylinder motion is orbital because of its shape and requires two PTO axes to achieve this motion. The Salter Duck in contrast can achieve the same capture level with a single axis pitching motion.

There are some fundamental design principles to consider when choosing geometry [20]:

- The swept volume by the displacer compared to its own volume (and any idle support structure) should be maximised.
- While a large swept volume is desirable, the associated spring and inertia of such devices needs to be minimised.
- Floating devices should have low freeboards that allow large waves to wash over them to reduce loading on the mooring system.
- Sharp edges waste energy through vortex shedding so a WEC should be a bluff body.

A MA-PAWEC will face these same design challenges and has the advantage that with PTO on multiple axes it can sweep a larger volume compared to its own volume than the same size device with a single axis and so likely generate a higher MWh/ton ratio. Geometrically the best solution for energy absorption for a single axis is likely to be close to a cam shape like the Salter Duck. The optimisation procedure on the SEAREV device which evolved in to a cam shape is evidence for this [105]. The cam may also be a favourable geometry for a MA-PAWEC by choosing another axis/axes that has a different resonant frequency to the pitch mode, or different directional dependence, thus increasing the available wave energy to the device. However, the majority of the incumbent point absorbers are heaving axisymmetric devices. For the heave mode an axisymmetric shape is preferable as it does not have a directional preference, is a bluff body, and maximises the volume/structure ratio. It is likely

that the heave response will be incorporated in to a MA-PAWEC and so for a comparison between heaving PAWECs and MA-PAWECs it is appropriate to use an axisymmetric device. This will also make any results more applicable to the existing heaving point absorbers regarding the addition of PTO axes. Further development of geometry dedicated to multi-axis may be desirable but for the purposes of this work it is more appropriate to let geometry force axis choice rather than vice versa.

The shape and size of a WEC will normally not change during operation so it must be carefully selected to satisfy the environments in to which it will be placed. Recently there have been developments in creating devices that can change their shape depending on the wave environment; larger in low energy seas and smaller in higher energy seas [104]. By presenting a smaller surface in high energy seas the loading on the WEC will be lower and hence should increase survivability. The same principle could be applied to MA-PAWECs where there could potentially be more scope to change geometry to favour certain axes in different wave conditions.

3.2.3 Axis Selection

The choice of axisymmetric geometry now simplifies axis selection. For an axisymmetric point absorber it is convenient to only consider two translational modes and one rotational mode, recognising that there will be an angular dependence of the rotational and horizontal translational modes on the incident wave direction. For an incident wave heading of zero degrees (head on) the applicable modes are surge, heave and pitch. Yaw can be neglected for an axisymmetric body. Of these three modes, heave generates a symmetrical wave pattern and pitch and surge generate an anti-symmetrical wave pattern. Point absorber theory states that optimum power absorption from a wave can be obtained for an axisymmetric body with two axes combining a source mode (symmetrical) and dipole (anti-symmetrical) mode radiation pattern. It is therefore logical to begin by considering the two axes case and selecting the combinations for which maximum absorption is possible. These are heave+surge and heave+pitch. For the two anti-symmetrical modes existing research [57] has indicated that surge is more efficient at absorbing power for a given volume stroke than pitch and so heave+surge has been selected as the axis combination used to begin investigation in to the relative performance of MA-PAWECs covered in the following chapters.

Directionality

A MA-PAWEC has two sources of directional dependency that must be considered, one arising from geometry and the other from the axes configuration. For axisymmetric point absorbers there is no directional dependency on the geometry. In contrast to an axisymmetric heaving device the heave+surge and heave+pitch combinations are sensitive to wave direction due to the surge and pitch modes. Whether it is worth a device having the sway or roll axes added to be able to absorb energy from all directions in the dipole modes will depend on the wave climate at the site where it will operate. If the site receives much of its energy from significantly different wave directions simultaneously it may be cost effective to be able to absorb energy from multiple directions. However a site may experience significantly different wave directions but rarely at the same time which means a heave+surge or heave+pitch device could orient itself appropriately for the different directions and still absorb much of the available energy. The rose diagrams in Section 2.1.5 showing an example of the directionality of the wave climate at that particular site (the Wavehub [33] site 16 km from the Cornish coast in the south-west of the UK on the eastern coast of the Atlantic) shows there is clearly a dominant wave direction to the west with some significant energy from WSW too. At this particular site it would be unlikely to be cost effective to have a directionally independent MA-PAWEC.

Due to the more consistent directionality of the waves at nearshore sites (i.e. they are always heading towards the shore) compared to deep water offshore sites, multi-axis will provide less of an advantage in absorbing waves from multiple directions at near-shore sites. Therefore multi-axis devices that are intended to maximise absorption from multiple directions should be designed for deep water. An exception to this could be near-shore locations where bathymetry and coastal features create reflection, refraction or diffraction of waves on to the device in different directions. For MA-PAWECs that use a dipole mode the \cos^2 factor in Equation 24 that moderates energy available to that mode from any given direction suggests a severe penalty for these modes when the waves are not aligned with the PTO axis. However, many sites have a dominant wave direction and it is likely that a 2-axis PTO MA-PAWEC, correctly aligned, can achieve similar performance but with a lower PTO cost than a directionally independent 3-axis device. Sites that experience multi-directional spectra for a significant period of time should use a directionally independent configuration of either three axes, or heave alone depending on PTO cost. Coupling can also occur between different modes [96] such that energy from one direction can be absorbed by an axis along another direction. This reduces the need for multiple axes to make the device directionally independent.

3.3 Resonance

One of the potential advantages of MA-PAWECs is the fact they can have the ability to resonate in multiple modes. Appropriate design of the geometry and/or PTO axes can select the resonant frequencies to create a device with a wider bandwidth i.e. able to absorb energy more consistently in a wider variety of seas states. For example, a small cam shaped point absorber may be sized to pitch in short waves and heave in long waves. Alternatively a body could be configured to heave, pitch and surge, each mode at a different resonant frequency. Existing devices can change their resonant frequency by adjusting spring and mass, and the same methods would be available for a MA-PAWEC to extend each of its resonant frequencies. Cross-coupling of axes could also enhance wave power absorption across a wider bandwidth. This would involve varying the stiffness on each axis to produce the desired motion and frequency response.

3.4 PTO Considerations

The challenging aspect of a MA-PAWEC is to create a machine that can incorporate multi-axis technology without making the electricity exorbitantly expensive. The choice of PTO system is very important as it affects what control can be accomplished, the efficiency of the device, and a substantial portion of the cost; the PTO will generally be the most sophisticated part of any device. Intuitively multi-axis lends itself to PTO where there is limited additional cost for the additional axes. Hydraulic systems therefore fit this nicely as the electricity and energy storage infrastructure can be shared by axes. In contrast, direct drive generators can only be associated with a single axis so the only infrastructure they can share is the downstream power electronics.

Providing the reaction force for a MA-PAWEC is potentially complicated by the need to provide it in different directions. The same methods existing devices use to supply a reaction force may interfere with each other when combined. For example, a heave plate may inhibit surging motion. Using an inertial mass is complicated by the need to provide it with multiple degrees of freedom. Two separate inertial masses could be used but this is structurally inefficient and would decrease the advantage of combining multi-axis PTO within the same device. The seabed could provide the necessary reaction forces if the tethers/moorings are appropriately designed. For example, a surge reaction force could be provided by an angled

tether to the seabed. Rotational modes could also use the seabed if the tethers are at either end of the device.

In surge/sway there are no hydrostatic restoring forces and so to achieve resonant behaviour the PTO/mooring system should provide spring to the system. It may be challenging for a MA-PAWEC to provide the necessary horizontal spring at reasonable cost and any energy stored in springs or masses must be efficiently returned to the body motion. The requirement to provide spring in these modes can be of benefit as a load shedding mechanism. If the grid connection fails the device can become non-resonant by disabling the supplied spring (if mechanically possible in the WEC of course). While spring needs to be added for surge or sway, the heave, pitch and roll responses are likely to need a reduction in spring (i.e. adding negative spring to the system) in order to be resonant at a useful part of the spectrum. Small point absorbers typically have natural frequencies higher than the most energy dense part of the wave spectrum.

One of the intentions behind the use of multi-axis PTO is to make use of all the body motions rather than having to pay to resist them with a mooring system. A mooring system's primary function is to keep a device on station but as it is such an expensive part of a device a more cost effective strategy could be to use it as part of the PTO.

One promising aspect of a MA-PAWEC is the potential smoothing benefit associated with the different phase of each mode of motion. The difference between peak and average power can be extreme (over 20 times higher in some cases [98]) and managing this fluctuating level of power is a big challenge. PTO axes that are out of phase should mitigate this problem by reducing the peak to average ratio. The phase difference between the PTO axes will depend on the hydrodynamics of the device. It could also potentially increase the efficiency of reactive power control by reducing the need to store energy over a wave period. Energy could instead be transferred from one axis to the other as required.

3.5 Arrays

Unless being used for isolated island or coastal communities, point absorbers will be deployed in arrays. It is therefore logical to commence investigations with arrays firmly in mind. Considering a single device allows for quicker calculation but the operation of the device in an array should be a fundamental design principle included from the start of the design process. This is particularly relevant for single axis vs. multi-axis arrays. Array interactions

can have a significant effect on absorption [117] [103] and multi-axis PTO allows control of more axes, which can alter the radiation patterns from devices and thus change interaction patterns. This could be a source of greater array control for MA-PAWECs and array control strategies developed for single axis devices that are already in operation could be adapted for use within the same MA-PAWEC. These could take advantage of the increased bandwidth of the device and deliver a higher capacity factor for the array.

For arrays of equal capacity, the number of MA-PAWECs required should be less than the number of single axis PAWECs due to the improved energy capture. A single row of two axes axisymmetric MA-PAWECs (source and dipole radiation patterns) can theoretically absorb all of the incident energy whereas a single row of single axis axisymmetric point absorbers can in theory only absorb 50% of the energy [17].

It is normal practice to design a WEC with a target range of wave climates in mind and in isolation as a single absorber. An alternative approach for small point absorbers could be to design them as a modular array, the size and configuration of which varies depending on the wave climate the array will be situated in. Using this approach with the additional control of interactions between devices afforded by multi-axis PTO could yield better energy absorption than designing MA-PAWECs to operate in isolation.

3.6 Conclusions

In this chapter the following design considerations and possible benefits of multi-axis PTO for point absorbers have been identified:

- Increased energy capture per ton making the electricity potentially cheaper.
- Out of phase PTO axes could deliver a smoother power output and reduce the difference between the average power and peak power. This may reduce the size of the required storage for an equivalent power rating and increase the ratio of delivered power to power rating.
- Two axes MA-PAWEC is likely to be a preferable choice combining a source mode and dipole mode.
- With multiple axes there are more control variables to play with which could allow novel control strategies, particularly in arrays.
- With well-chosen geometry and axes a wide bandwidth can be achieved by using axes with different natural frequencies.

Similarly, there are some negative aspects that may follow from multi-axis PTO:

- More complexity so they are more expensive to make and crucially to maintain – there's more to go wrong.
- Much is still unknown about how to best configure a MA-PAWEC and the problem has many variables.
- A MA-PAWEC has additional directional dependencies from the additional axes.

Based on these geometry and axes considerations the investigation in to the performance of a MA-PAWEC against heave devices covered in the following chapters will use an axisymmetric bluff body with PTO on the heave and surge axes.

4 Relative Energy Output under Motion Constraints

It is well known that a multi-axis PTO approach can absorb a greater amount of energy than a single axis PTO under certain conditions (numerically and experimentally). The decision of whether to invest in the additional complexity and cost of multi-axis PTO depends however on the amount of extra energy (and therefore revenue) generated. To establish an idea of what additional energy could be expected during operation this chapter conducts a motion constraint analysis on a semi-submerged spherical PAWEC (i.e. wetted hemispherical surface) with PTO configurations of heave only, surge only, and heave+surge. This axisymmetric body with a heave+surge configuration for the MA-PAWEC has been selected based on the considerations discussed in Chapter 3. The energy generated in each of the three configurations is calculated for a selection of wavelengths and heights to allow comparisons between them. The nature of the motion constraint prevents the principle of superposition being applied directly in this case so the waves considered are monochromatic. This may seem to limit the applicability of this model, but it is not the absolute energy generation values that are of interest in this case, but the relative performance of multi-axis compared to single axis PTO.

Linear theory is used for the motion constraint analysis which is only applicable for small wave heights. However, in order to sufficiently leverage its expensive power structure, a WEC should operate efficiently in small waves, and can afford to operate non-optimally in higher waves where energy is abundant. Cost of power systems increases in proportion to the amount of power carried. Therefore, for cost efficiency, a WEC should try to deliver a high proportion of the rated capacity for a large proportion of the time. Due to the varying sea states this means that a WEC must be efficient in small waves, yet be able to shed power in energetic seas. In energetic seas there is abundant energy and the WEC can operate non-optimally at rated power capacity. Thus a linear analysis is suitable for absorbed energy performance analysis. However, the results become less reliable in increasingly energetic sea states and a higher order analysis is required for extreme conditions.

4.1 Generic Device

Figure 26 shows the generic point absorber devices to be considered in this chapter. The body is a semi-submerged sphere which can be considered an approximation for many existing

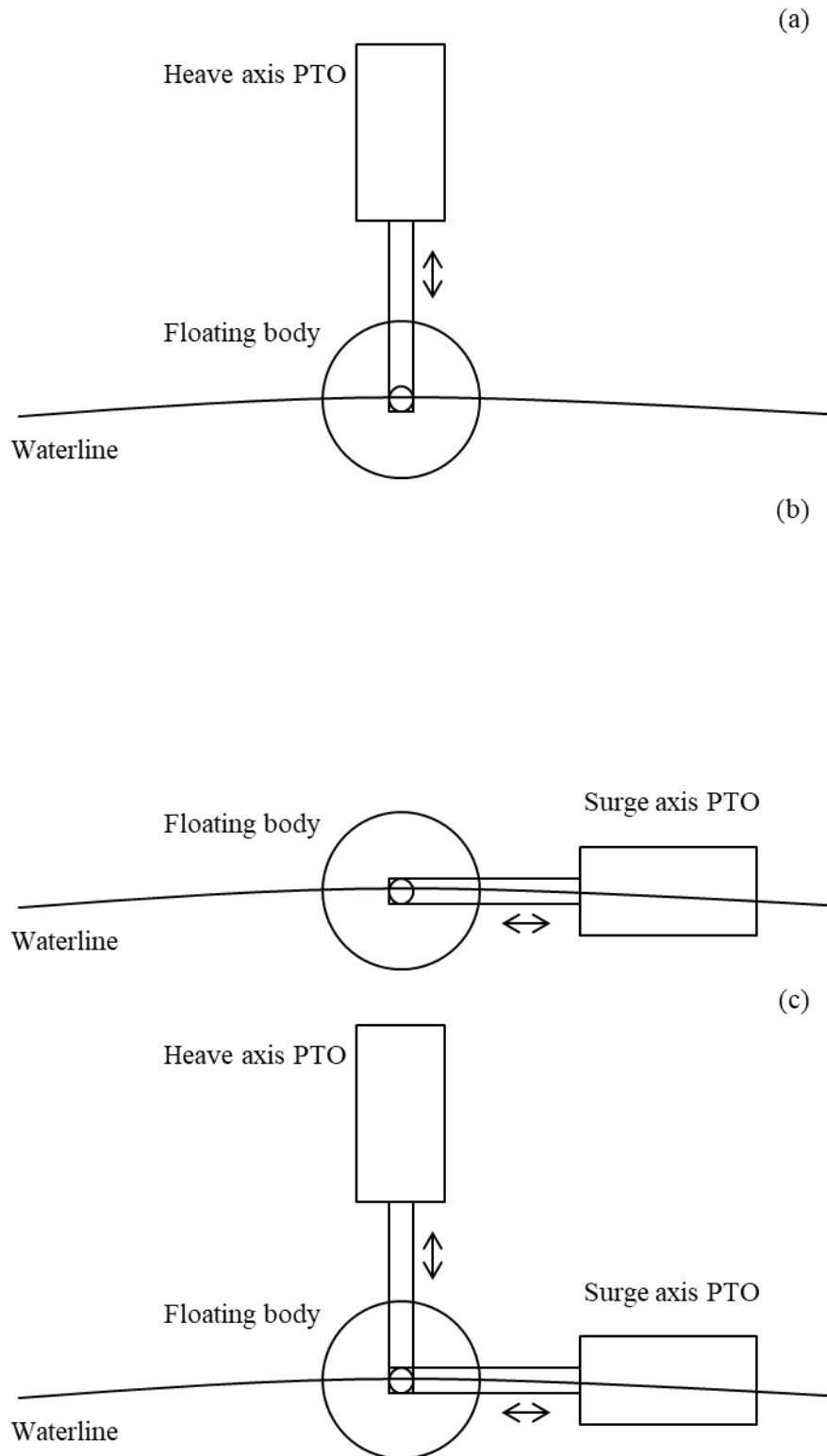


Figure 26: Generic device configurations. (a) Heave PAWEC. (b) Surge PAWEC. (c) Multi-Axis PAWEC (MA-PAWEC).

heaving point absorbers that use an axisymmetric float typically close to an ellipsoidal, cylindrical or spherical/hemispherical geometry. In Figure 26 (a) the device shows a heave only PTO configuration which for illustrative purposes is shown as a rigid connector above

the waterline, which could be a hydraulic ram or linear generator and applies a certain spring and damping to the float. Figure 26 (b) shows the surge configuration and Figure 26 (c) shows the multi-axis PTO configuration which in this case is simply the two translational modes surge and heave. Other configurations are possible, such as rotating the PTO assembly 45 degrees to remove it from the water. This would simply change the loading on each PTO. The two degrees of freedom of Figure 26 (c) allow the float to move anywhere within the area described by the PTO extension limits and thus can account for horizontal and vertical motions. An additional PTO axis for sway could be added orthogonal to the heave and surge PTOs to give the device three degrees of freedom and thus capture horizontal motions in any direction. Obviously this would have an associated increase in complexity and cost which must be balanced against the benefit and may depend on whether there is a predominant wave direction or if the device can weathervane. The PTO axes can be arranged in any configuration that allows absorption of both horizontal and vertical motions. Due to the spherical shape of the float there will be no rotational forces (roll, pitch, yaw). This may not be true of other devices and there is no reason why a device cannot be designed to include a rolling/pitching/yawing PTO. The fore-aft PTO configuration on the Solo Duck is an example of a pitching, heaving and surging point absorber [62].

The following assumptions are made for the PTO system in the modelling:

1. No account is taken at this stage of any problems associated with these PTO layouts such as the end-stop problem and buckling of rigid connectors.
2. The spring and damping of these generic device PTO units are assumed to operate in a linear fashion to simplify response characteristics.
3. No consideration is given to PTO efficiency at this stage. It is the hydrodynamic absorbed power that is of interest.

Linear modelling using potential flow theory is used to determine the response of the device. Potential flow theory is based on the assumptions of irrotational, inviscid and incompressible fluid [118]. For linear modelling the wave height and body responses are assumed to be small relative to the wave length. This naturally limits the validity of the model to small displacements in low waves where the waveform is close to sinusoidal.

Only the hydrodynamic performance is examined, without reference to the efficiency of the PTO system to convert the absorbed power to useful electricity. This is based on the assumption that all devices will have similar power conversion efficiencies as they use similar PTO technology. Therefore hydrodynamic energy absorption alone is sufficient for a performance comparison, with the respective PTOs treated as black boxes.

4.2 Unconstrained Optimum Performance

The capture width (L) of a device is the width of wave front equivalent to the energy absorbed by the device, $L = P/P_w$, where P_w is the power per unit width of wave front and P is the power absorbed by the device. The optimum capture width of an axisymmetric point absorber with arbitrary geometry operating in heave (vertical translation) was given by Equation 23 and for surge or sway (horizontal translation) by Equation 24.

Both Equation 23 and Equation 24 show the remarkable result that the optimum capture width depends only on wavelength. These results are shown graphically in Figure 27. The relative capture width (RCW) on the y-axis of Figure 27 is the ratio of the capture width (L) of a device to its key dimension (in the case of this spherical device $RCW = L/2a$ where a is the device radius). This ratio is useful for comparing WECs as it normalises the capture width by making it independent from the device size, thereby allowing different sized devices to be compared on their energy absorbing effectiveness. A value greater than one indicates the WEC is absorbing more energy than is incident across its width.

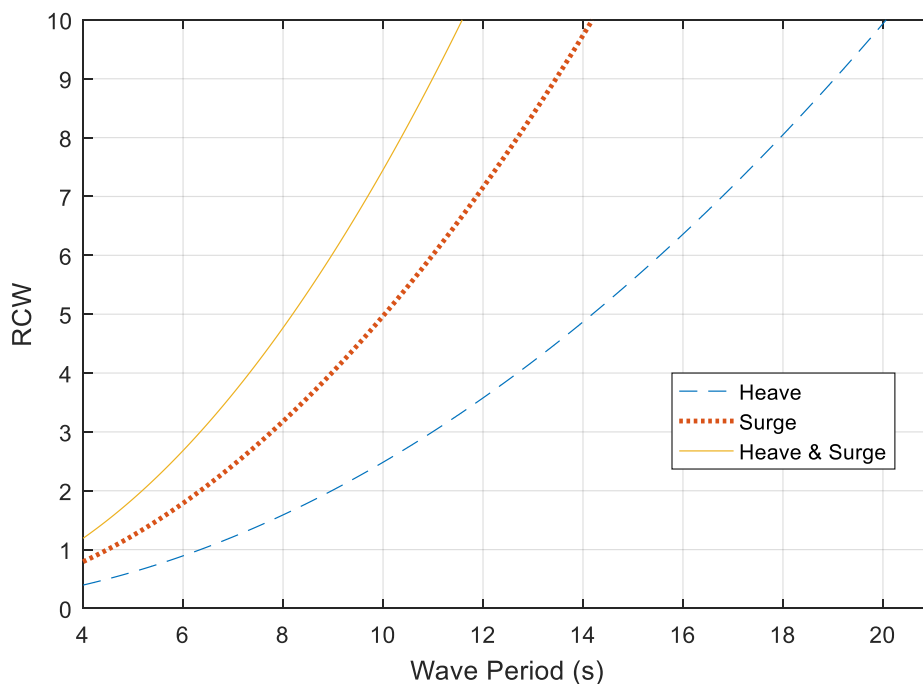


Figure 27: Plot of maximum RCW for an axisymmetric device oscillating in heave, surge, and combined heave and surge.

Note that the optimum absorbed power from the surge motion can be twice that from heave. If the point absorber operates in both heave and (uncoupled) surge then the optimum capture width is the sum of Equation 23 and Equation 24. If the MA-PAWEC has two PTO axes, one

horizontal, one vertical, and the waves are aligned with the horizontal PTO then the optimum capture width of the MA-PAWEC is three times that of the heave-PAWEC. The maximum energy captured drops as the angle of incidence of waves on the device shifts towards beam seas where the horizontal component is therefore zero from Equation 24. A 3DOF device with orthogonal axes can make the device directionally independent but at the cost of an additional PTO. Any designer of a MA-PAWEC must choose the PTO axes carefully, based on the directionality of the deployment site wave resource and any radiated waves from adjacent devices in an array.

These optimum capture widths are the theoretical upper limits of energy absorption and are not realistic as for a typical deep water ocean wave a small body point absorber (e.g. <10 m diameter) would have to undergo large oscillations. This will violate the small displacement assumption of linearity, result in large viscous losses and encounter the end-stop problem where the PTO is over-extended.

The PTO characteristics are assumed to be linear whereas in reality the PTO system may be highly non-linear. Thus these optimum capture widths are not realistic in terms of calculating energy output, but do offer insight into the potential *relative* performance of a MA-PAWEC as being significantly higher than heave alone.

Using Figure 27 to compare the relative energy production at any given site it is obvious that in head seas, the heave and surge configuration has an upper limit of three times that of heave, and one and half times that of surge.

4.3 Global Weighted Constraint - Optimum Performance

Due to the small displacement assumption of a linear model, viscous losses associated with high body velocities and practical engineering limits of the PTO, it is preferable to analyse the energy production of a device with some form of motion constraint. Imposing a constraint regime represents more realistic PTO and increases the validity of the linear model by preventing large displacements. The constraints do not however prevent viscous losses. A study combining a boundary element method (BEM) model with viscous losses for a 15 m diameter heaving cylinder at an offshore site found that viscous losses reduced the annual energy production by less than 4% [119]. The relative viscous loss increases with a smaller body so the linear model validity also decreases with body size. The bluff spherical shape of

the devices studied here will present less viscous loss than a cylinder but will still result in decreasing validity with decreasing device size.

Here the performance of the heave-PAWEC, surge-PAWEC and MA-PAWEC are modelled assuming optimum linear PTO control but with constraints on the excursions. This adds a greater measure of reality to the comparison than simply comparing Equation 23 and Equation 24 as was done in section 4.2. By restricting the device motions the linear assumptions are still fairly accurate and it takes account of the limits of real PTOs which cannot undertake large excursions at reasonable cost. Although it is very difficult to achieve optimum power absorption with a real device this simplification can be used comfortably in this case by only looking at the relative performance between the single-axis and multi-axis PAWECs rather than the absolute values.

The mean power absorption for a device in N degrees of freedom was given by Equation 21 with the optimal power absorption (i.e. moving at optimum velocity) given by Equation 22. To constrain the device to move within certain extension limits a velocity constraint can be formulated which can take the form [62]:

$$\mathbf{U}^* \mathbf{\Gamma}^{-2} \mathbf{U} \leq 1,$$

Equation 26

where \mathbf{U} is the complex N -vector describing the velocity of the body, $\mathbf{\Gamma}$ is an $N \times N$ diagonal matrix with elements γ_i representing the velocity constraint in each degree of freedom i , and $*$ denotes the conjugate transpose. The velocity constraint restricts motion of the body within an ellipsoid, the principal axes of which are given by the respective translational axes constraints. The form of Equation 26 makes it a global constraint as the sum of all constraints within the matrices must satisfy the single scalar condition of totalling less than or equal to the value of the right hand term. The global constraint can be weighted for each degree of freedom by adjusting the appropriate diagonal element (γ_i) within the diagonal constraint matrix. This allows different limits to be placed on different axes (degrees of freedom) which is equivalent to stretching or compressing the ellipsoid within which the body can move. While the individual limits restrict motion along their respective axes the actual motion required for optimum power absorption may not be distributed evenly among the axes. Any combination of motion along the axes that satisfies the limit of Equation 26 will be valid and the body will only reach the maximum motion constraint along any one axis if motion along all others is zero. This is the nature of a global constraint. For the heave and surge axes considered here the velocity constraint (γ_i) on these translational axes can be specified as a proportion (α) of the device radius (a) multiplied by the angular frequency: $\gamma_i = \alpha a \omega$.

As long as Equation 26 is satisfied the constraint has no effect and the maximum power absorption is given by the unconstrained equations - Equation 23 and Equation 24. In matrix form the unconstrained optimum power absorbed is given by Equation 22. The optimum velocity in order to achieve this optimum power is given by [87]:

$$\mathbf{U}_{opt} = \frac{A}{2} \mathbf{B}^{-1} \hat{\mathbf{X}},$$

Equation 27

where $\hat{\mathbf{X}}$ is the complex exciting N -vector for a unit amplitude wave, \mathbf{B} is the $N \times N$ symmetric radiation damping matrix and A is the incident wave amplitude. If the constraint is exceeded ($\mathbf{U}^* \Gamma^{-2} \mathbf{U} > 1$) then power (P) must be maximised subject to Equation 28 [62]:

$$\mathbf{U}^* \Gamma^{-2} \mathbf{U} = 1$$

Equation 28

The maximum power is found by introducing a Lagrange multiplier μ which can be used to solve constrained optimisation problems such as this. The Lagrange multiplier is simply a function ($f(\mu)$) that will take a certain value at \mathbf{U}_{opt} . When $\mathbf{U}^* \Gamma^{-2} \mathbf{U} > 1$ the optimum velocity is given by [96]:

$$\mathbf{U}_{opt} = \frac{A}{2} (\mathbf{B} + \mu \Gamma^{-2})^{-1} \hat{\mathbf{X}}$$

Equation 29

Here the unconstrained optimum velocity equation (Equation 27) has been modified by adding in a constraint term to the damping bracket ($\mathbf{B} + \mu \Gamma^{-2}$) consisting of the velocity constraint matrix multiplied by the scalar quantity of the Lagrange multiplier. This constraint term has the effect of artificially changing the damping and thus the velocity of the body. The Lagrange multiplier is determined from a scalar equation derived from Equation 29 [62]:

$$f(\mu) = \hat{\mathbf{X}}^* \Gamma (\Gamma \mathbf{B} \Gamma + \mu \mathbf{I})^{-2} \Gamma \hat{\mathbf{X}} = \frac{4}{A^2}$$

Equation 30

In solving Equation 30 it is found there are a maximum of $2N$ roots with one positive and a minimum of one negative root. The root that yields the maximum power absorption is the positive root [62]. The equation can be solved to find the roots numerically and for this Matlab [120] was used. Once the positive root has been found it can be substituted in to a modified form of Equation 21 where the velocity vectors have been replaced with the

constrained optimum form of Equation 29. This modified form of Equation 21 thus gives the maximum power (P_{opt}) that can be absorbed under a weighted global constraint in N degrees of freedom [62]:

$$P_{opt} = \frac{A^2}{8} \widehat{\mathbf{X}}^* \mathbf{B}^{-1} \widehat{\mathbf{X}} - \frac{A^2}{8} \mu^2 \widehat{\mathbf{X}}^* \Gamma [(\Gamma \mathbf{B} \Gamma + \mu \mathbf{I}) \Gamma \mathbf{B} \Gamma (\Gamma \mathbf{B} \Gamma + \mu \mathbf{I})]^{-1} \Gamma \widehat{\mathbf{X}},$$

Equation 31

The exciting ($\widehat{\mathbf{X}}$) and damping (\mathbf{B}) matrices were obtained using WAMIT [89], a boundary element method (BEM) computer programme used for analysing surface wave interactions with bodies. It is based on linear potential theory using Green's theorem to determine the velocity potentials on a body's wetted surface. Appendix A.1 contains details of the software package WAMIT and how it was used. For this analysis the waves are assumed to be in deep water and come head-on to the body, or alternatively the MA-PAWEC is assumed as having three PTO axes: heave, surge and sway. Either assumption results in the MA-PAWEC being directionally independent and therefore does not require additional directional wave data.

4.3.1 Relative Capture Widths under a Global Weighted Constraint

Figure 28, Figure 29 and Figure 30 show the RCWs for the semi-submerged sphere devices with different wave amplitude ratios (A/a) across a non-dimensional frequency spectrum (denoted by the non-dimensional wavenumber ka , where k is the wavenumber in rad/m and a is the body radius in metres). Due to the motion constraints the frequency response curves change depending on the wave height as the device may not be allowed to oscillate at the optimum amplitude required for higher waves. The wave height has been normalised by dividing the wave amplitude by the device radius to give an 'amplitude ratio'. For the frequency response curves in Figure 28, Figure 29 and Figure 30 a constraint of a maximum excursion of one half of the radius was used ($0.5a$) for each axis. The motions of a cylinder with a hemispherical end for power absorption have been found to be linear up to its radius [82] but unlike a cylinder a sphere's water plane area will change with heaving motions. Therefore the linear approximations will be less accurate in this mode at larger constraints and so motions are limited here in both modes to no more than half the radius in order to keep the responses closer to the linear regime.

The plots show RCWs for the device operating in heave mode, surge mode, and heave+surge modes. It is clear from all three plots that under a motion constraint the performance drops away from the unconstrained optimum as the frequency decreases. RCWs also drop with increasing wave amplitude ratio. Both of these reductions are due to the body being unable

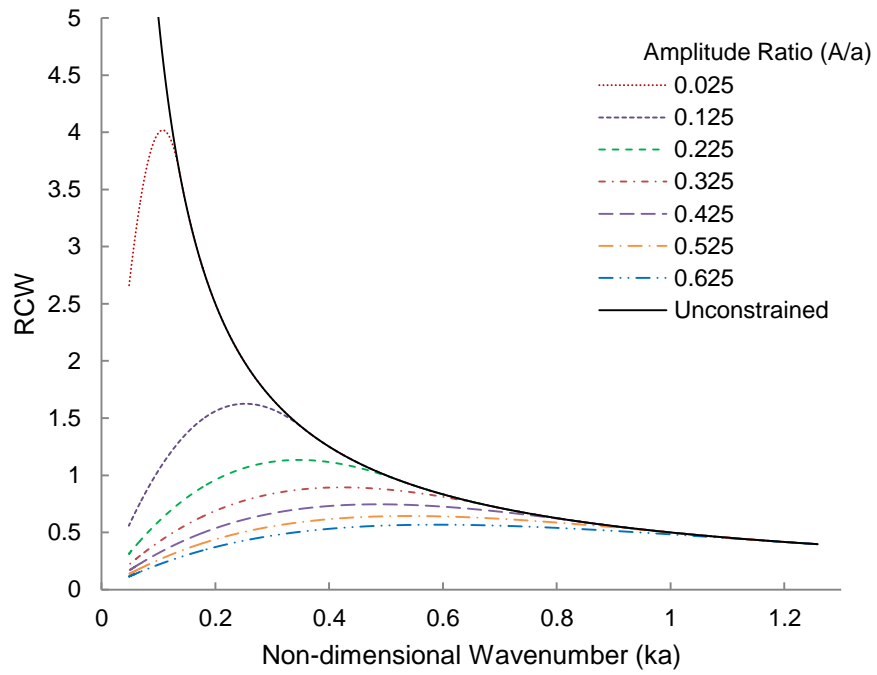


Figure 28: Relative Capture Widths (RCW) of a heaving PAWEC with a $0.5a$ motion constraint.

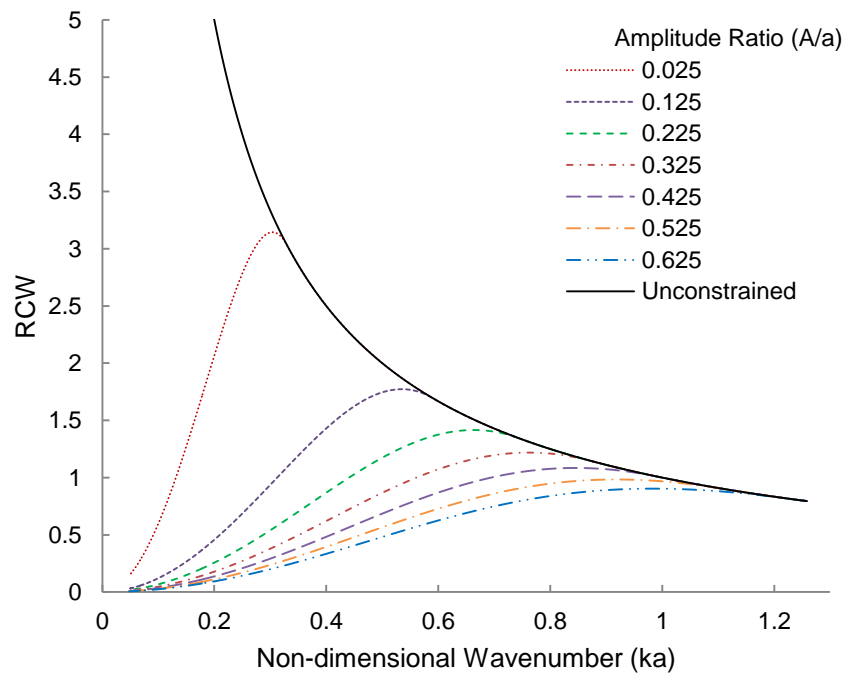


Figure 29: Relative Capture Widths (RCW) of a surging PAWEC with a $0.5a$ motion constraint.

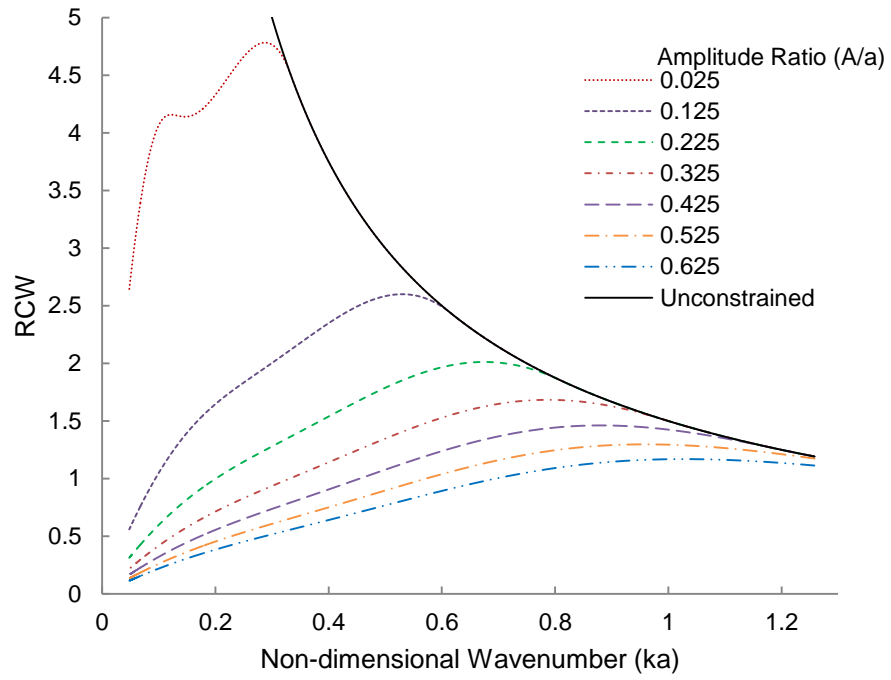


Figure 30: Relative Capture Widths (RCWs) of a heaving and surging MA-PAWEC under a global motion constraint with a constraint of $0.5a$ on each axis.

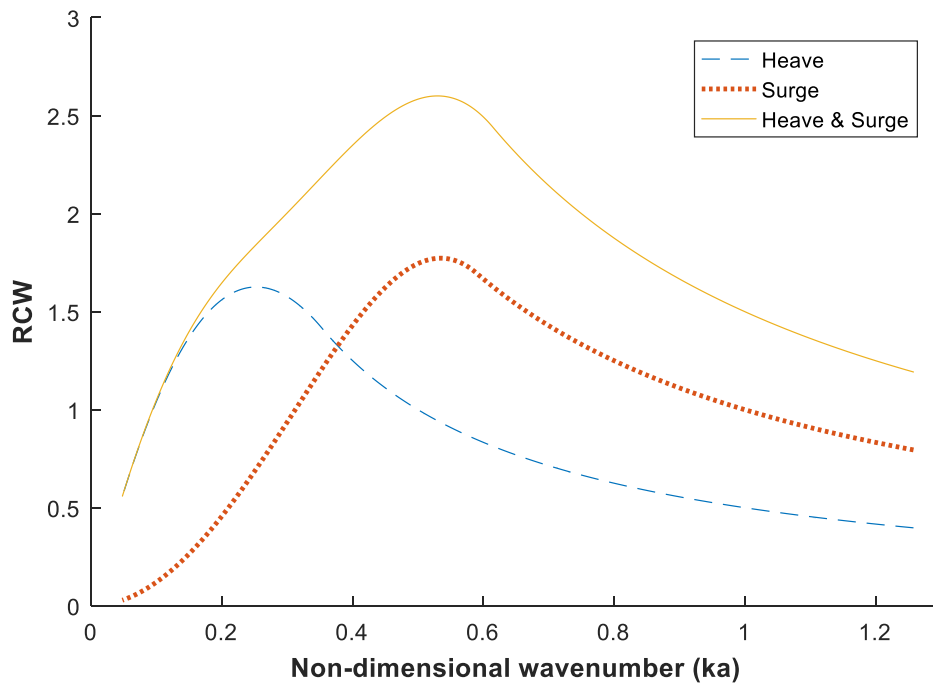


Figure 31: RCW for an amplitude ratio (A/a) of 0.125 at a motion constraint of $0.5a$ in the three configurations heave only, surge only, and heave+surge.

to oscillate at the larger amplitudes required for the optimum absorption of long, high waves.

Comparing Figure 28 and Figure 29, the heaving device is better at absorbing power at low frequencies (long waves), while surge has a better RCW at higher frequencies (short waves). To better visualise this comparison Figure 31 shows the RCWs for a single amplitude ratio at the 0.5a constraint with all configurations plotted on the same graph. Additional plots containing the curves for motion constraints 0.1a to 0.5a for each wave amplitude ratio can be found in Appendix A.2. By using heave and surge together the MA-PAWEC performs well in both long and short waves resulting in the broader peaks seen in Figure 30. This is most clearly seen with two separate peaks on the $A/a=0.025$ curve corresponding to the respective peaks on the heave and surge plots. The MA-PAWEC outperforms both single axis devices across the entire frequency range for all cases where there are equal motion constraints between 0-0.5 radii.

4.3.2 Comparative Energy Production under a Global Weighted Constraint

The number of interest for a comparison between devices at a particular site is the Annual Energy Production (AEP). This is found by integrating the power generated over the course of a year in a particular wave climate.

$$AEP = \int_0^t P dt = \sum_j f_j P_j,$$

Equation 32

where f_j is the frequency of occurrence (in units of time) over a year of sea state j . P_j is the converted useful power for sea state j . The method used here of applying motion constraints in the frequency domain to determine absorbed power restricts the model to single frequency wave trains and so sea states cannot be modelled as a superimposed spectrum of linear waves. To get a comparison of energy production the device is instead modelled for regular waves across a range of frequencies and wave heights to obtain a maximum power absorption matrix for regular waves. This can then be multiplied by a weighting matrix that assigns a particular frequency of occurrence to each combination of wave frequency and height. This weighting matrix can obviously be varied to represent short or long wavelength environments. This method renders the numerical results unsuitable for estimating actual production of devices at a site, but its intention is to be used for comparing the performance of devices *relative* to each other. A modified version of Equation 32 to represent this method of energy comparison is shown in Equation 33 where it is simply termed Energy Production (EP) rather than Annual Energy Production because the time period is no longer relevant for the comparison.

$$EP = \sum_i \sum_j f_{ij} P_{ij}$$

Equation 33

Here, f_{ij} is the frequency of occurrence weighting for a wave of period i and height j . Similarly P_{ij} is the absorbed power from a wave of period i and height j . To create the weighting distribution matrix for the occurrence of particular wave heights and frequencies the wave climate for the Wavehub [33] test site off the coast of Cornwall in the UK (Table 2) was used which has an average resource of 17 kW/m [121]. The wave climate is represented by a frequency table recording the frequency of occurrence of sea states of significant wave height H_s and zero crossing period T_z . The zero crossing period is the measured time between successive crossings of the mean water level by the free surface (either between two up-crossings or two down-crossings). It is the shape of the height and period distribution from Table 2 that is of use here rather than the sea state parameters. For the EP calculation in Equation 33 in regular waves the wave periods i and heights j will be taken as T_z and H_s .

T_z (s)	4.5	5.5	6.5	7.5	8.5	9.5	10.5	11.5	12.5	Total
H_s (m)										
0.25	3	9	5	2	0	0	0	0	0	19
0.75	57	95	56	16	2	0	0	0	0	226
1.25	21	120	69	35	8	3	1	0	0	257
1.75	0	67	80	38	17	6	3	0	1	212
2.25	0	11	61	29	14	5	1	0	0	121
2.75	0	0	27	26	12	3	1	1	0	70
3.25	0	0	3	20	14	5	1	0	0	43
3.75	0	0	0	9	11	4	2	0	0	26
4.25	0	0	0	1	5	3	1	1	0	11
4.75	0	0	0	0	3	2	1	0	0	6
5.25	0	0	0	0	2	3	1	0	0	6
5.75	0	0	0	0	0	2	1	0	0	3
6.25	0	0	0	0	0	1	0	0	0	1
Total	81	302	301	176	88	37	13	2	1	1001

Table 2: Frequency table for the Wavehub test site plotting frequency of sea state occurrence in bins of significant wave height (H_s) and zero crossing period (T_z) [121].

respectively from Table 2. This is not an accurate representation of what would be generated at the site but provides a quantitative scale for comparison between configurations.

While Figure 28 to Figure 31 were snapshots of the frequency response of the body under a single motion constraint (0.5a on each axis), Figure 32 maps out the performance of all three devices under a range of motion constraints using the proxy of the EP value as calculated by Equation 33. Whereas the RCW plots are non-dimensional and are applicable for any size device, the EP calculations are necessarily for the specific case of a 10 m diameter body in a selection of monochromatic waves based on the Wavehub test site (Table 2). The frequency specific performance information is lost with the EP but instead it provides an overall measure of device performance in terms of energy produced. The energy produced from a device determines how much income it generates and is therefore crucial in deciding on its viability.

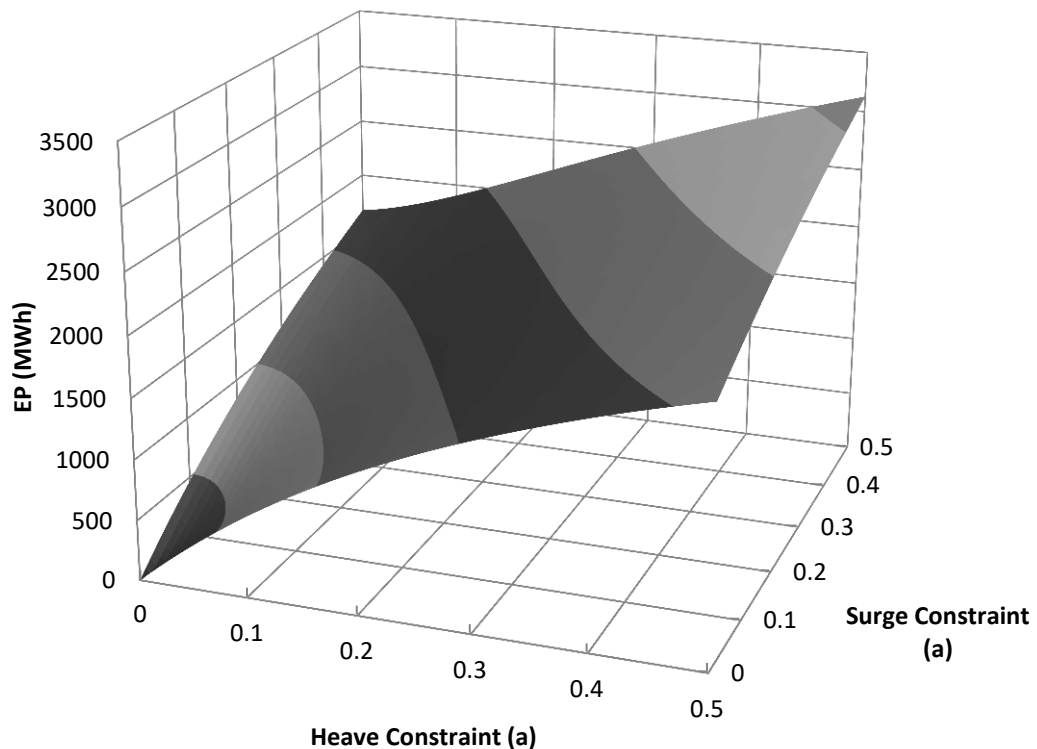


Figure 32: Energy Production (EP) of the three devices in a set of waves based on Table 2 with each axis at different motion constraints. The single mode device outputs are shown by the extreme edges of the surface. Contour shading to help show 3D curvature.

The single mode device outputs are shown by the extreme edges of the surface in Figure 32 where one or the other of the constraints is zero. The intermediate surface points represent the multi-axis 2DOF device with varying constraints on the axes. For clarity, the single axis edges and the diagonal slice from the origin (representing equal constraints for heave and surge axes) are shown in a separate plot in Figure 33.

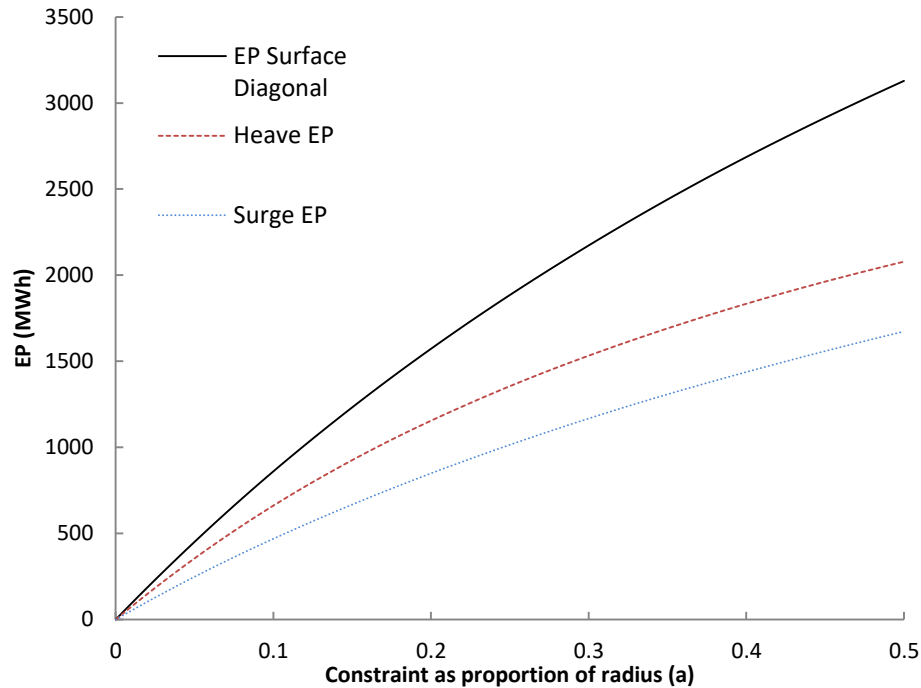


Figure 33: Energy Production (EP) of the single axis devices (extreme edges of surfaces in Figure 32) and an equal axis constraint configuration i.e. the diagonal slice from the origin of Figure 32.

Reflecting on Figure 32 and Figure 33 it can be seen that for a 10 m device under a 0-0.5 radius motion constraint a heaving device performs better than a surging device, with the difference becoming proportionally smaller as the motion constraint is relaxed. This is in contrast to what the RCWs for each mode suggest in Figure 28 to Figure 31 with surge showing higher RCWs over most of the frequency range. The higher power of the long waves where heave has higher RCWs than surge result in a higher EP for this sample wave distribution. This illustrates how important it is to focus on energy output with specific wave distributions rather than simply at each frequency. The MA-PAWEC performs better than both the single axis devices. In general, the skewed dome shape of Figure 32 suggests a MA-PAWEC of any constraint combination generates more energy under linear assumptions than either single axis alone with the equivalent component constraints. For cases of equal constraints the higher performance of the MA-PAWEC across the entire wave frequency and amplitude range that was seen in Figure 30 manifests as a significantly higher Energy Production value in Figure 33. At the constraint used in Figure 30 of $0.5a$, the MA-PAWEC output is 50% higher than heave and 87% higher than surge.

For cases of non-equal constraints the advantage of multi-axis PTO varies. Close to the x and y axes (i.e. at small constraints on one axis, large on the other axis) there is little benefit in a MA-PAWEC as most of the energy is absorbed by the axis with the larger constraint. In these cases it is unlikely to be economical to add the additional axis due to the large additional cost

for the PTO. This may not be true if a different PTO technology is used for each axis: a small extension PTO system of low cost on the additional axis may produce a net decrease in cost of energy from the device. At these very small PTO extensions the surge axis offers a steeper marginal improvement in energy production than the heave axis. This can be seen in the different curve of the contour lines close to each axis. Thus the combination of heave as the predominant axis with small extension on the surge is a more favourable configuration than vice versa.

In general, the reducing gradient of the surface with larger constraints in Figure 32 suggests decreasing marginal returns for greater PTO extension. This has implications for selecting a suitable PTO system where PTO extension limits must be balanced with cost. Ultimately, the question of whether to have multi-axis PTO depends on the value of the additional energy absorbed exceeding the additional cost of the PTO axis.

Scaling and Indexing to Heave

Figure 34 displays the EP figures relative to heave for the range of motion constraints $0-0.5a$ for surge and heave+surge devices of different sizes for the sample wave distribution based on Table 2. By indexing the EPs to the heave device it provides an indication of the performance of MA-PAWECs relative to the most common point absorber design today.

What is immediately clear in comparing the relative EPs in Figure 34 is that the improvement of the MA-PAWEC over heave decreases as size decreases. This reduction in relative EP can also be seen for the surge device and explains the poorer performance of the MA-PAWEC; as was seen in Figure 29, power from surge drops off rapidly with increasing wavelength under a motion constraint. As the radius of the device reduces, the same wave is perceived as longer relative to the body dimensions. This suggests multi-axis with heave and surge is more appropriate for larger point absorbers, or quasi-point absorbers, rather than very small buoys. The implication of this is that sizing the MA-PAWEC to the wave climate is important for multi-axis to be viable. Therefore multi-axis devices employing heave and surge would be well suited to short wave environments. The fact that MA-PAWEC devices, and by extension surge devices in general, should not be very small relative to the wavelength implies that reasonable PTO extension is likely to be a small fraction of the device radius and remain within the constraint boundaries investigated here.

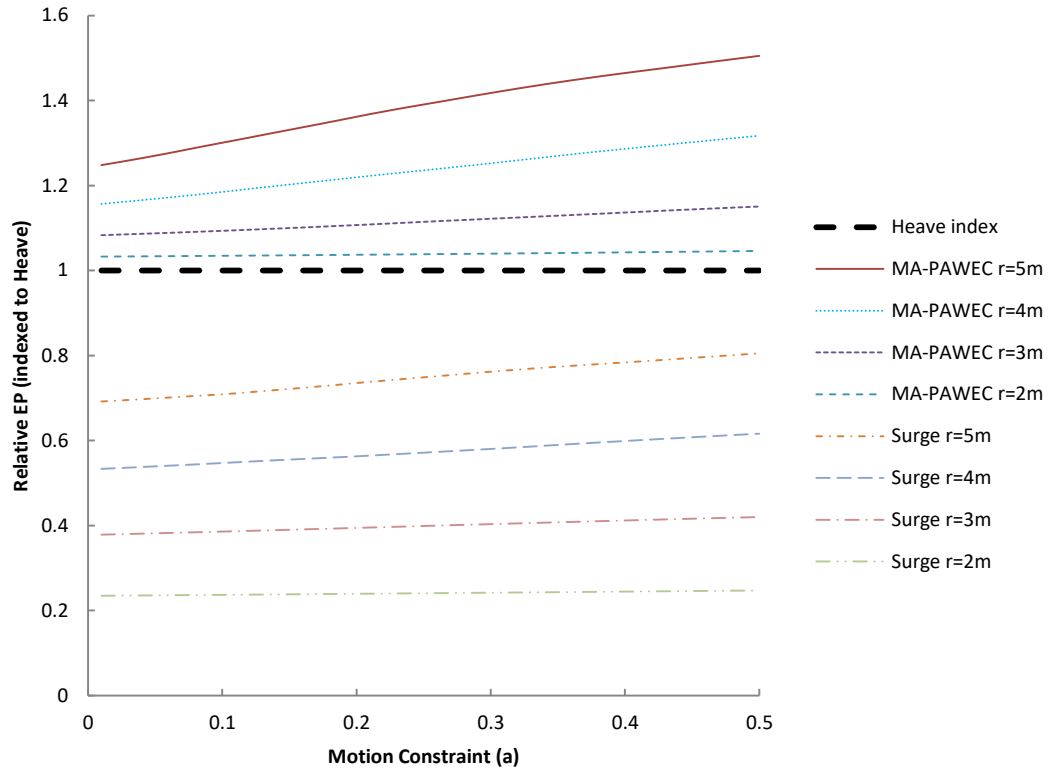


Figure 34: Relative Energy Production (EP), indexed to the heave device EP value, of four different sizes of device with the radius ranging from 2m to 5m.

4.4 Independent Constraints – Optimum Performance

Rather than having a global weighted constraint in which no axis limit can be reached without the other axis motions being zero, a more realistic engineering constraint is to have independent constraints on each axis. In the linear model this would mean that an excursion along one axis would have no effect on the maximum allowable excursion on a second axis. Thus, unlike the global constraint, both axes can reach the limits of the motion constraint at the same time. Conveniently heave and surge for a spherical body are not coupled in the linear domain with the damping matrix being diagonal [97]. Therefore the matrix optimisation of Equation 31 can be rearranged in to a sum of algebraic equations where the optimum velocity for each mode is determined independently of the others. This independent constraint equation takes the form shown in Equation 34. The coefficients represent the same quantities as in Equation 31 but in scalar form for a single mode. The Lagrange multiplier μ_i is now for a specific mode i . Each value is found using Equation 30 as before but this time for a single

degree of freedom. The maximum power is therefore found from the sum of the power absorbed through each uncoupled degree of freedom.

$$P_{opt} = \sum_{i=1}^N \frac{A^2 \hat{X}_i^* \hat{X}_i}{8 B_i} - \frac{A^2}{8} \frac{\mu_i^2 \hat{X}_i^* \hat{X}_i \Gamma_i^2}{(\Gamma_i^2 B_i + \mu_i)^2 \Gamma_i^2 B_i}$$

Equation 34

As before for the global weighted constraint, the independent velocity constraint on each translational axis (γ_i) can be specified as a proportion (α) of the device radius (a) multiplied by the angular frequency: $\gamma_i = \alpha a \omega$.

4.4.1 Relative Capture Widths under Independent Constraints

Figure 35 shows the RCWs for the heave+surge semi-submerged sphere device with different wave amplitude ratios (A/a) across the non-dimensional frequency spectrum for a constraint of 0.5a. The plots for single axis heave and surge are omitted here as they are the same as Figure 28 and Figure 29 respectively in Section 4.3.1. Similar to the global constraint scenario, under independent motion constraints the RCWs drop away from the unconstrained optimum given by Equation 23 and Equation 24 as the frequency decreases and wave amplitude increases. Figure 36 shows the RCWs for the device operating in heave mode, surge mode, independent constraint heave+surge mode, and global constraint heave+surge mode for the single wave amplitude ratio of 0.125 under the 0.5a constraint. Additional plots containing the curves for motion constraints 0.1a to 0.5a for each wave amplitude ratio can be found in Appendix A.2.

The difference between the global weighted constraint and independent constraints can be seen in the two curves in Figure 36 where the independent constraint curve is shown to be higher than the global weighted constraint curve. This is to be expected as the independent constraint formulation allows for greater combined translational motion for a given combination of motion constraints. The advantage of a MA-PAWEC is therefore increased under this independent constraint model over the single axis configurations. Necessarily, the MA-PAWEC outperforms both single axis devices across the entire range of frequencies and motion constraints for both independent and global constraints.

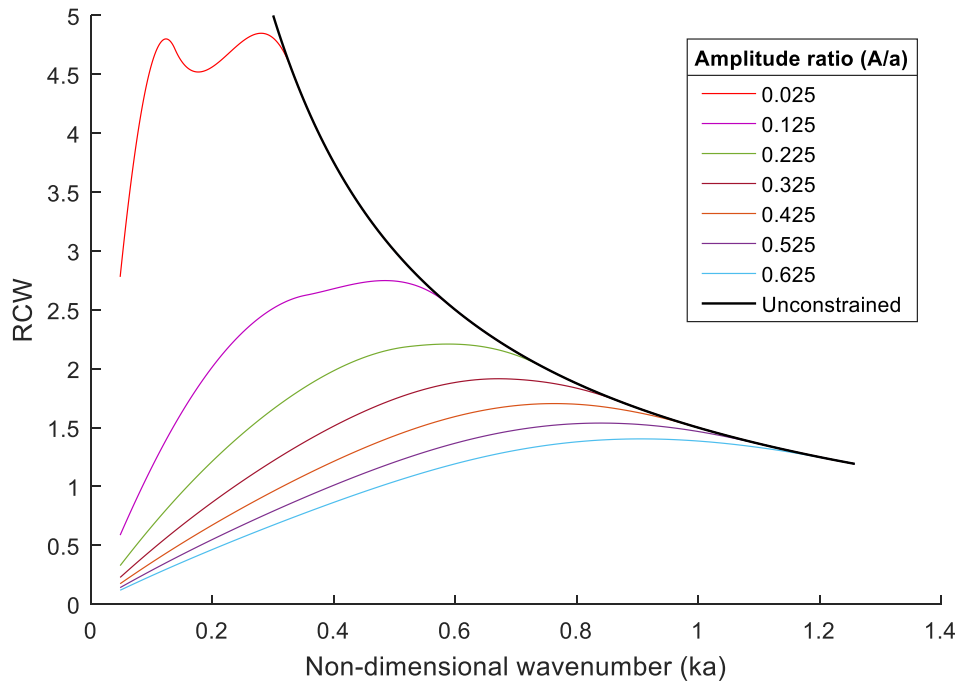


Figure 35: RCW of a heave+surge MA-PAWEC with independent constraints of $0.5a$ on each axis.

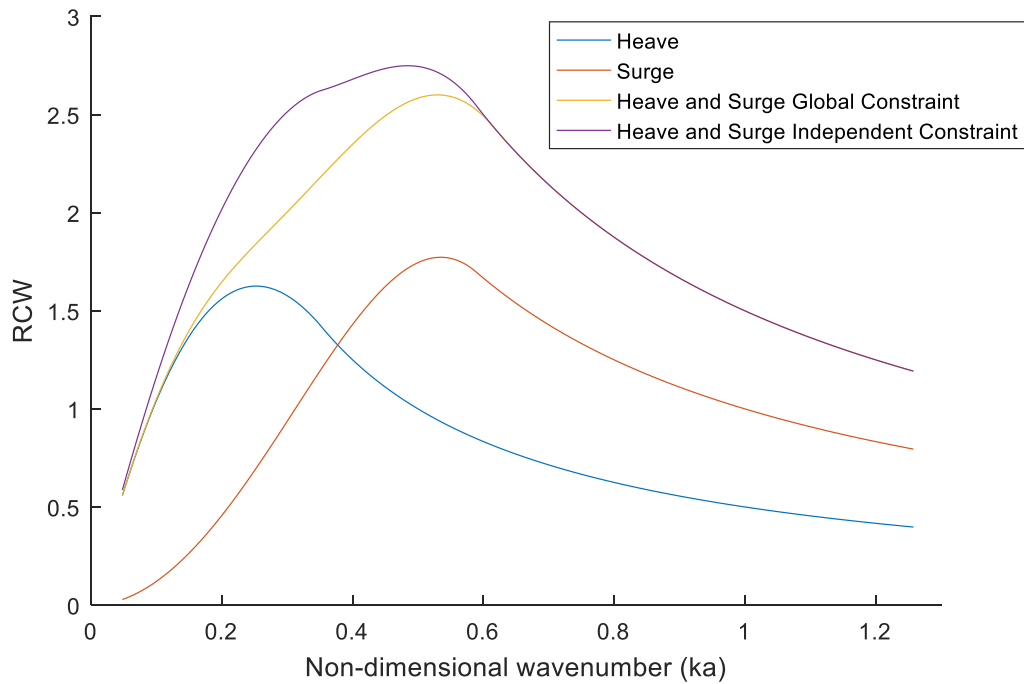


Figure 36: RCW for an amplitude ratio (A/a) of 0.125 at a motion constraint of $0.5a$ in the three configurations heave only, surge only, and heave+surge (both global and independent constraint curves shown).

4.4.2 Comparative Energy Production under Independent Constraints

The Energy Production (EP) for any particular distribution of monochromatic waves can be found by summing the power absorbed (P_{ij}) from a wave of given period (i) and height (j) multiplied by its frequency of occurrence f_{ij} (in units of time) as given by Equation 33 in Section 4.3.2. Following the same approach the EP can be calculated for a MA-PAWEC under independent motion constraints. The results are shown in Figure 37 which maps out the performance of all three device configurations across the different constraint levels for each axis. The same parameters of a 10 m device in a selection of monochromatic waves based on Table 2 are used. The single mode device outputs are shown by the extreme edges of the surface in Figure 37 where one or the other of the constraints is zero and the intermediate surface points represent the multi-axis 2DOF device with varying constraints on the axes. For clarity, the single axis edges and the diagonal slice from the origin (representing equal constraints for heave and surge axes) are shown in a separate plot in Figure 38. The global constraint EP surface diagonal is also plotted on Figure 38 for comparison.

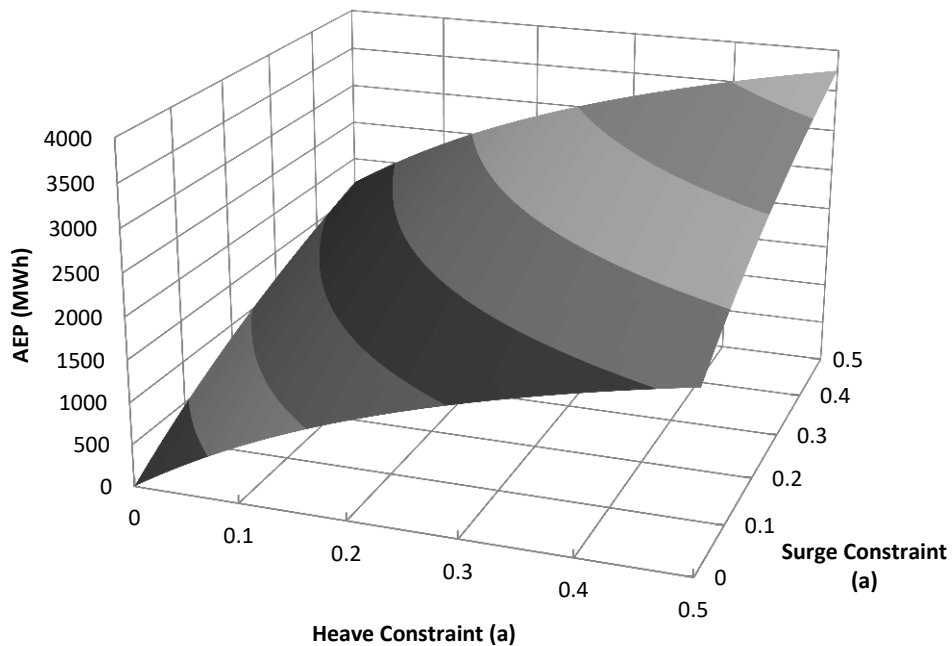


Figure 37: Energy Production (EP) of the three devices in a wave climate based on Table 2 with each axis at different independent motion constraints. The single mode device outputs are shown by the extreme edges of the surface. Contour shading to help show 3D curvature.

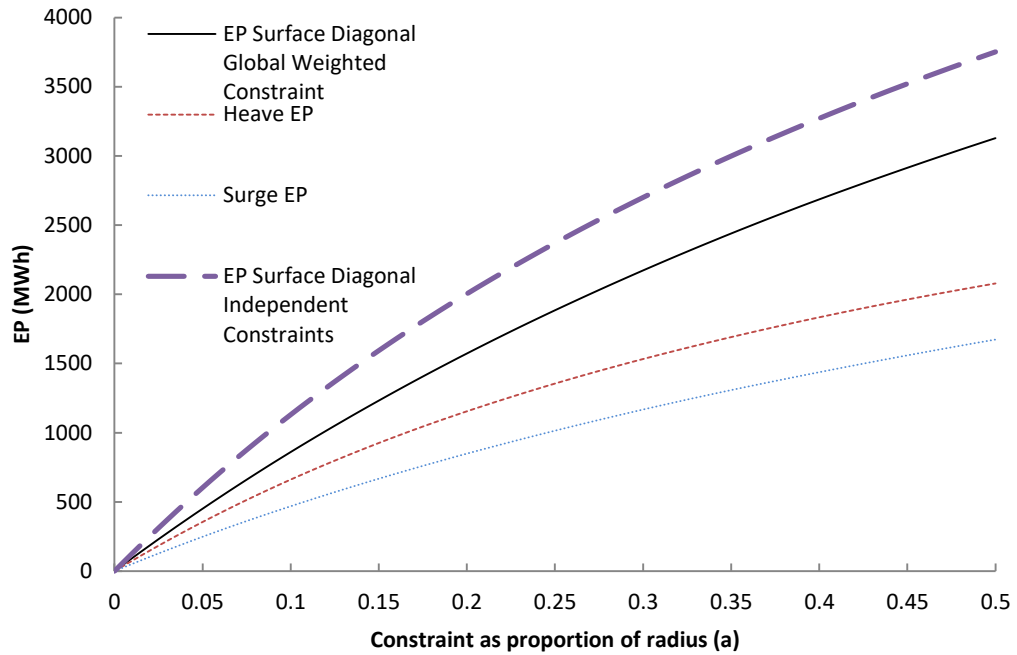


Figure 38: Energy production at different motion constraints for the heave, surge and heave+surge configurations. Motion constraints are equal for each axis. Both independent and global weighted constraint curves are shown.

The domed shape of Figure 37 along with Figure 32 (for global constraints) shows a MA-PAWEC of any constraint combination generates more energy under linear assumptions than either single axis alone with the equivalent single axis constraint. For cases of equal constraints shown in Figure 38 the higher performance of the MA-PAWEC across the entire wave frequency and amplitude range that was seen in the RCWs manifests as a significantly higher Energy Production value. At the constraint used of $0.5a$, the independent constraints MA-PAWEC output is 80% higher than heave and 124% higher than surge. The percentage increase in EP of the independent constraint MA-PAWEC vs. the other curves for the full range of equal motion constraints is shown in Figure 39. The proportional advantage of a MA-PAWEC over heave increases as the motion constraint increases while for surge the MA-PAWEC advantage decreases with increasing motion constraints. This suggests that a MA-PAWEC is most attractive relative to a heave device with PTO that allows large excursions.

Figure 38 and Figure 39 also show the MA-PAWEC under the independent motion constraints performs significantly better than the heave+surge MA-PAWEC with a global weighted constraint. This is to be expected as there is a greater combined total stroke length available for the PTO under the independent constraints. From Figure 39 this difference over the motion constraint range $0-0.5$ radii is 20-35%, with the difference decreasing as the motion constraint is relaxed. The percentage discrepancy over all motion constraint combinations (up to $0-0.5$ radii on each axis) is shown in the surface plot of Figure 40. The peak discrepancy near the

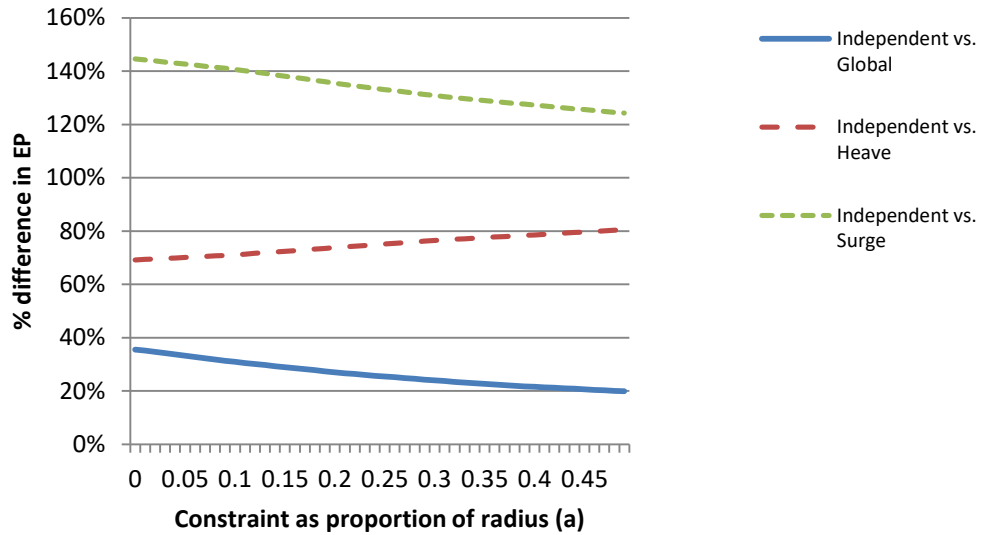


Figure 39: Percentage difference in energy production of the independent motion constraint heave+surge configurations vs. the global weighted heave+surge constraint, heave only and surge only. Equal motion constraints on each axis.

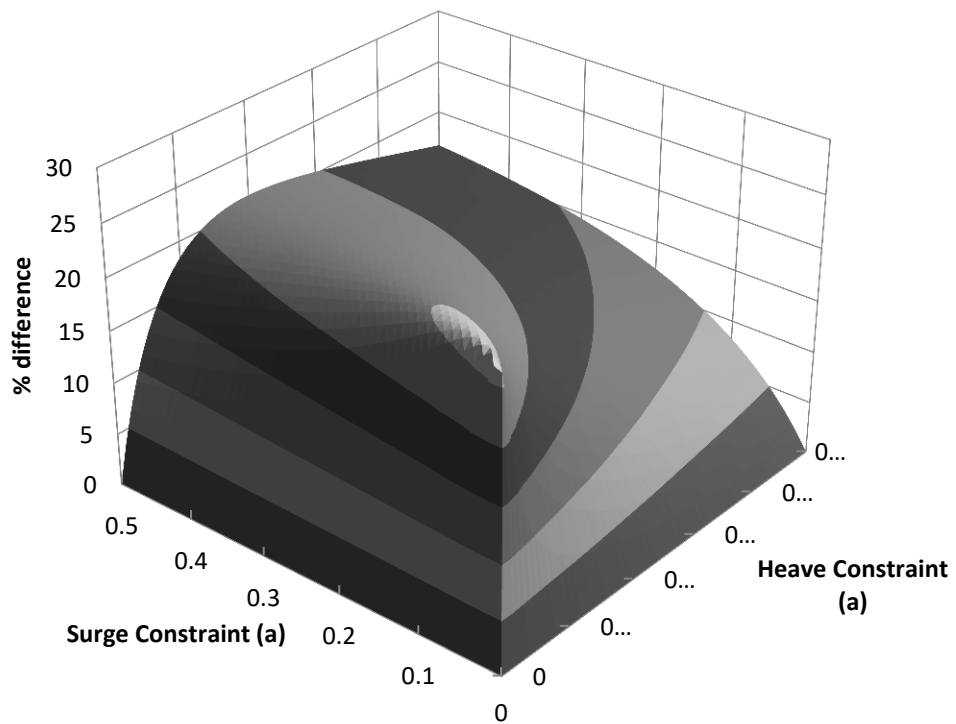


Figure 40: Percentage difference between the energy production under independent motion constraints and global weighted constraints.

origin (motion constraint of 0.01 – the origin discrepancy is obviously zero) can be clearly seen along with the reducing difference moving away from the origin in all directions as the motion constraints increase and are therefore not reached as often. This reduction is steeper on

the heave side and shallower on the surge side as heave performs better than surge under small motion constraints.

4.5 Conclusions

This chapter has focussed on the question of the magnitude of additional energy that can be expected to be generated by a MA-PAWEC relative to single axis equivalents in order to better judge how advantageous a MA-PAWEC architecture can be. A semi-submerged spherical device with PTO on the heave and surge axes was compared on an energy absorption basis with equivalent single axis heaving and surging devices using linear potential theory. Motion constraints of 0-0.5 radii of the device were applied on a global weighted and independent basis to simulate PTO extension limits and increase the validity of the small displacement assumption associated with linear theory. By using both PTO axes the MA-PAWEC performed well in both long and short waves and thus had a higher bandwidth than the single axis equivalents. The magnitude of this benefit was dependent on motion constraints and the wave (height and period). MA-PAWEC devices should be sized appropriately to the site resource and the advantages of adding surge to a heaving device are most apparent in relatively short wave environments.

An Energy Production (EP) figure was calculated analogous to the Annual Energy Production used to assess WEC performance but using a discrete set of monochromatic waves of specified height and period. The heights and periods were chosen from an example distribution of waves. The Energy Production figure takes no account of PTO losses and is particular for the given geometry in question (10 m wetted hemispherical surface in this case). For the EP of a device with a motion constraint 0-0.5 times the radius of the device the heave response absorbed more energy than surge, and a heave+surge MA-PAWEC absorbed more energy than either single axis. Under a global weighted motion constraint of 0.5a the MA-PAWEC output was 50% higher than heave and 87% higher than surge. Under independent motion constraints of 0.5a the output of the MA-PAWEC was 80% higher than heave and 124% higher than surge. This improvement over the heave device decreases as the body size decreases due to the surge motion performing poorly in long waves. Larger point absorbers (relative to the incident wave field) may be the best candidates for multi-axis PTO. The independent constraint formulation produced higher EP figures due to the higher RCWs it allows the MA-PAWEC to achieve with the longer translation stroke available to each axis. Based on the results of this motion constraint analysis a combination of heave as the

predominant axis with a smaller excursion surge axis would be the most favourable combination to maximise energy generated per unit length of PTO.

5 Relative Energy Output under Power Constraints

The motion constraints applied in the previous chapter represent an approximation of the real world where motions will be limited by engineering constraints on the excursion of the PTO. The power conversion capability of the PTO is another constraint on the energy absorption of a device. Applying a damping force over a stroke length to absorb power has a capital cost associated with it (generally expected to be higher with increasing force and stroke length) whereas the energy in the wave is supplied free. Therefore in order for a WEC to be financially viable it is expected that it must be operating at maximum capacity for a large fraction of the time i.e. it is not worth the investment to optimally capture energy at levels seen only rarely [91]. This is therefore another important perspective from which to assess the potential impact of adding additional PTO axes to create a MA-PAWEC.

In this chapter the energy absorbed by a semi-submerged spherical PAWEC in heave, surge and heave+surge configurations is calculated assuming a limit on the maximum mean power of the PTO. The energy absorbed is calculated for a range of monochromatic waves based on the wave climate of the Wavehub test site (Table 2).

5.1 Power Absorbed under Optimum Motion Control

The power absorbed under optimum motion control can be calculated by rearranging the maximum capture width equations (Equation 23 and Equation 24) used to calculate the RCWs in Chapter 4. The capture width (L) is $L = P/P_w$, where P_w is the power per unit width of wave front and P is the mean power absorbed by the device [87]. Substituting this in to Equation 23 and Equation 24 and setting P to the optimum power P_{opt} , gives equations for the unconstrained optimum power absorbed by a point absorber for a particular wave:

$$P_{opt} = P_w \frac{\lambda}{2\pi}$$

Equation 35

$$P_{opt} = P_w \frac{\lambda}{\pi} \cos^2 \beta$$

Equation 36

The incident wave power (P_w) for a unit length of crest of a linear wave can be calculated using the equation [17]:

$$P_w = \frac{\rho g^2 H^2 T}{32\pi}$$

Equation 37

Note that power is proportional to the wave period and the square of the wave height. Therefore power levels increase dramatically with increasing wave height and period. The surface plots below in Figure 41, Figure 42 and Figure 43 show the absorbed average power of an axisymmetric point absorber for the different configurations (heave, surge, heave+surge) with optimum unconstrained motion across the different combinations of wave height and period. The relationship between power absorption and the mode of PTO is obviously the same as was seen with the optimum RCW plots with surge absorbing twice as much as heave and multi-axis absorbing three times as much as heave. What is not as evident in the RCW plots but can be seen clearly from these power plots is the dramatic difference in absorbed power as the waves get higher and longer. As these plots are showing unconstrained motion the surge plot could also be representing pitch and the heave+surge plot could also be representing heave+pitch of an axisymmetric PAWEC. The increase in gradient from heave, to surge/pitch, to heave+surge/pitch towards increasing period and height is evident too. This means that if a power limit exists (as it will in real devices) it will have a significant modifying effect on energy production from higher power waves.

Comparing the plots of absorbed power under unconstrained motion to an example wave climate such as that at Wavehub in Figure 44 shows that the device will indeed spend most of its life in the lower energy area of these power matrices (note that the perspective of Figure 44 is opposite that of Figure 41, Figure 42 and Figure 43 for clearer viewing of the distribution shape).

Absorbed Average Power in Heave Unconstrained Optimum Motion

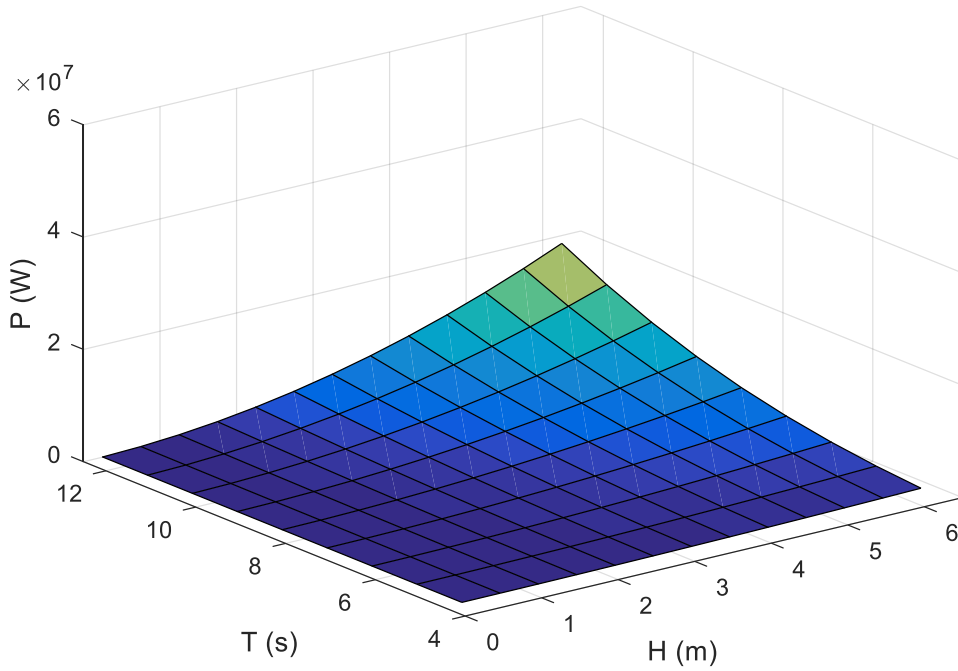


Figure 41: Average absorbed power in Heave with unconstrained motion for an axisymmetric point absorber with optimal motion.

Absorbed Average Power in Surge Unconstrained Optimum Motion

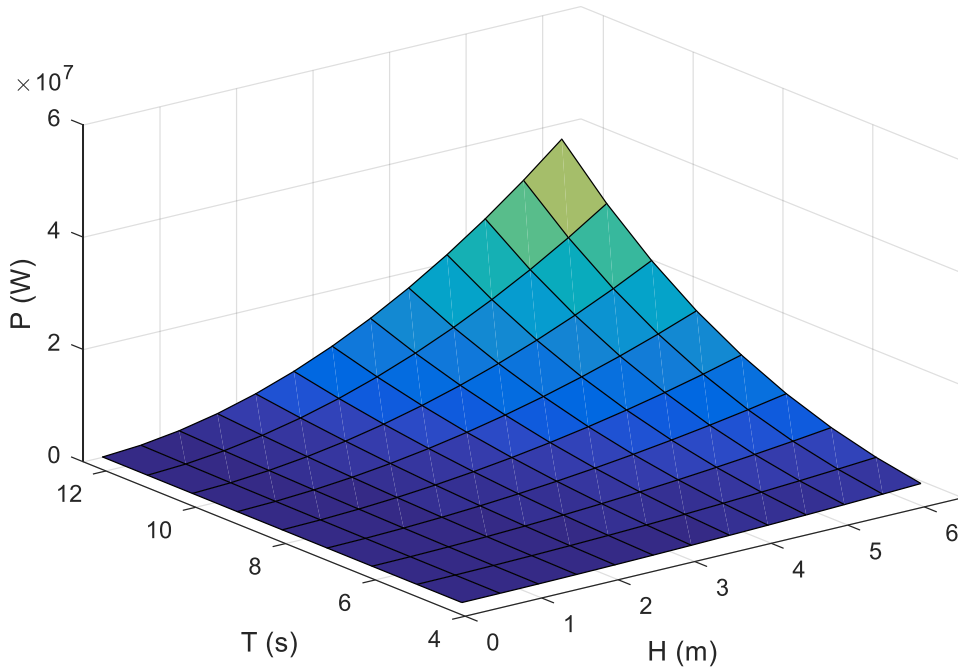


Figure 42: Average absorbed power in Surge with unconstrained motion for an axisymmetric point absorber with optimal motion.

Absorbed Average Power in Heave&Surge Unconstrained Optimum Motion

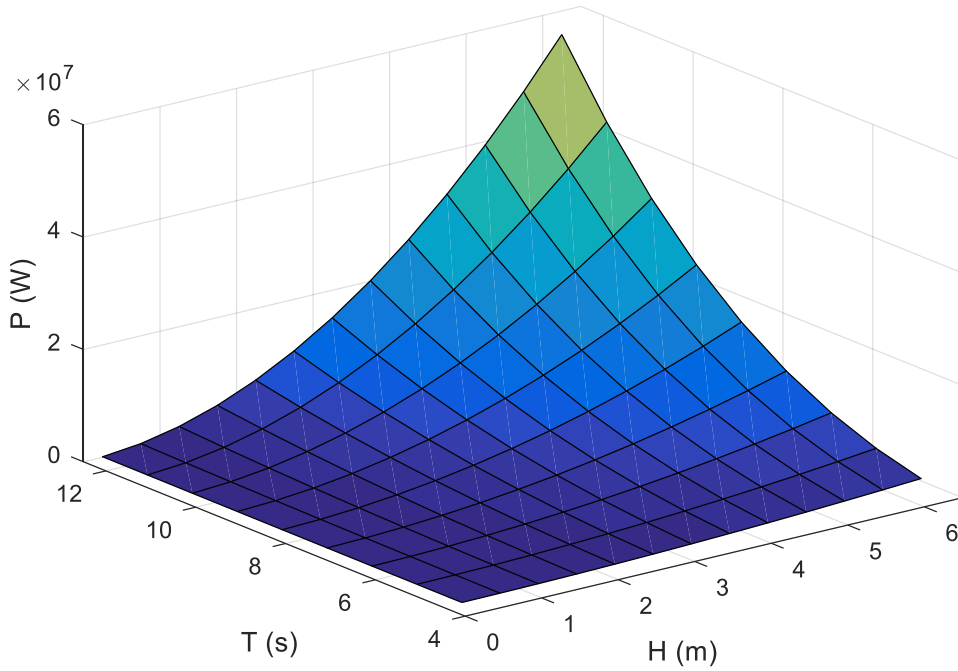


Figure 43: Average absorbed power in Heave+Surge with unconstrained motion for an axisymmetric point absorber with optimal motion.

Wavehub Seastate Frequency of Occurrence

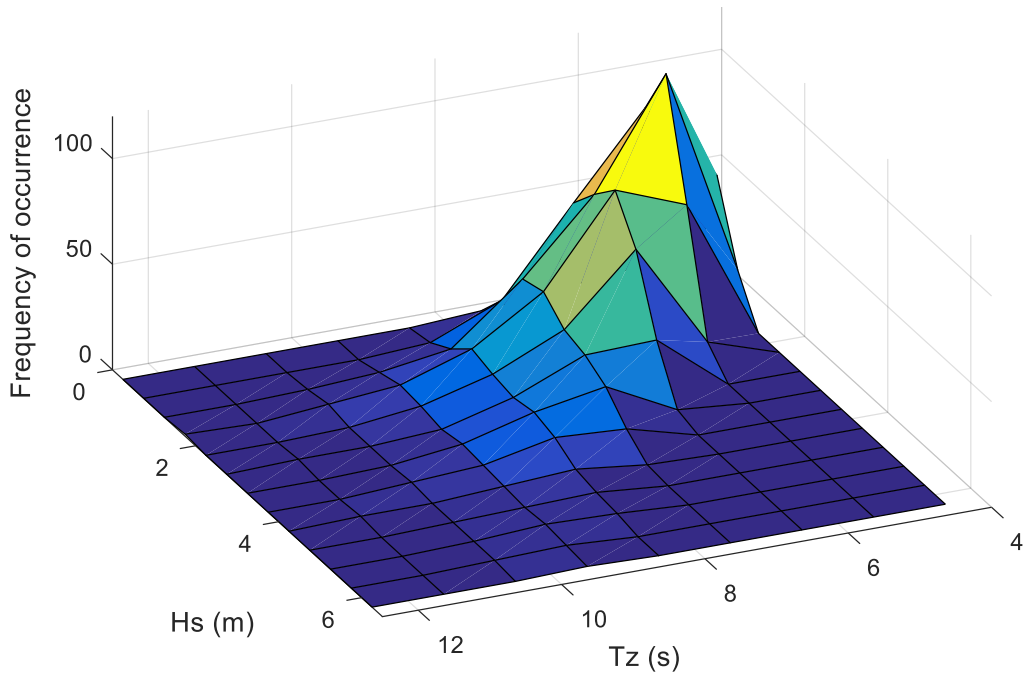


Figure 44: Wavehub seastate frequency of occurrence. Sea states represented by significant wave heights and zero crossing periods.

5.2 Optimum Power Absorption under Power Constraints

Applying a power constraint to the average absorbed power creates a plateau on the absorbed power plots at the specified limit. Figure 45, Figure 46 and Figure 47 show these modified power absorption plots (representing power absorption matrices for a device) with a 340 kW global power constraint on the device in the heave, surge and heave+surge configurations of an axisymmetric point absorber with optimal motion. Similar to the global motion constraint of Chapter 4 the global power constraint applies to the whole device, meaning that in a MA-PAWEC the sum of the power output of all the axes must be no more than the global limit, but each can go up to that limit. The figure of 340 kW is arbitrary at this stage and represents twice the average power (17 kW/m [40]) of the example wave climate in Table 2 that would be incident on a 10 m diameter device. This level of power is in the region of what may be expected from an individual point absorber. It is obvious that the power limit in this case is reached in the majority of cases for all three configurations, as shown by the yellow plateau covering most of the plot area. The fact that the power limit is reached for the majority of the waves means that the advantage of the surge (or pitch) mode over heave is drastically reduced for most waves. Whereas in the unlimited power case surge (or pitch) mode could be expected to absorb twice the power of heave with optimal motion, under this particular power constraint surge mode can only absorb more power than heave on the smaller waves, as visible by the slightly larger yellow power limit plateau on the surge power matrix. Correspondingly the heave+surge configuration of Figure 47 with a global constraint can only absorb more power than the single axes in the smaller waves.

Figure 48 instead shows the power absorption matrix for a device with a 340 kW power limit on each axis rather than on the whole device as was the case for the global limit. As with the motion constraint this condition will be termed ‘independent’ power constraints. The plateau under this independent condition is obviously twice as high as the global constraint (680 kW maximum device output in this example for a two-axis device) and it is reached less than under the global constraint for heave+surge. Under this independent condition the MA-PAWEC absorbs twice as much power as the single axes across a large portion of the matrix.

The power constraints considered in this chapter are for the power absorbed at the hydrodynamic interface rather than the PTO or device output. An equivalent PTO output power limit can easily be calculated if necessary by using the PTO efficiency. For the example of a 340 kW hydrodynamic interface limit, the equivalent PTO output limit for an 80% conversion efficiency would be 272 kW.

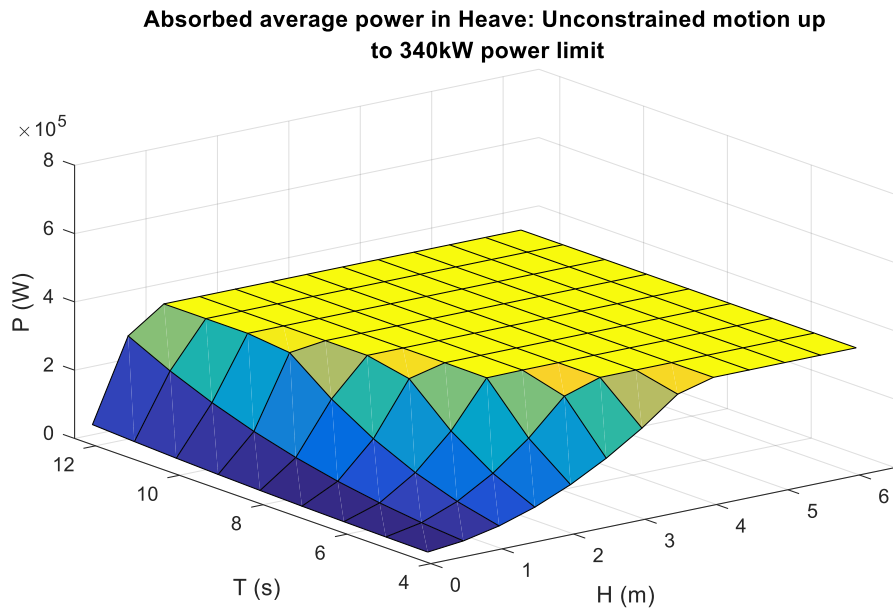


Figure 45: Absorbed average power for an unconstrained axisymmetric point absorber with optimal motion in heave with a 340 kW power constraint.

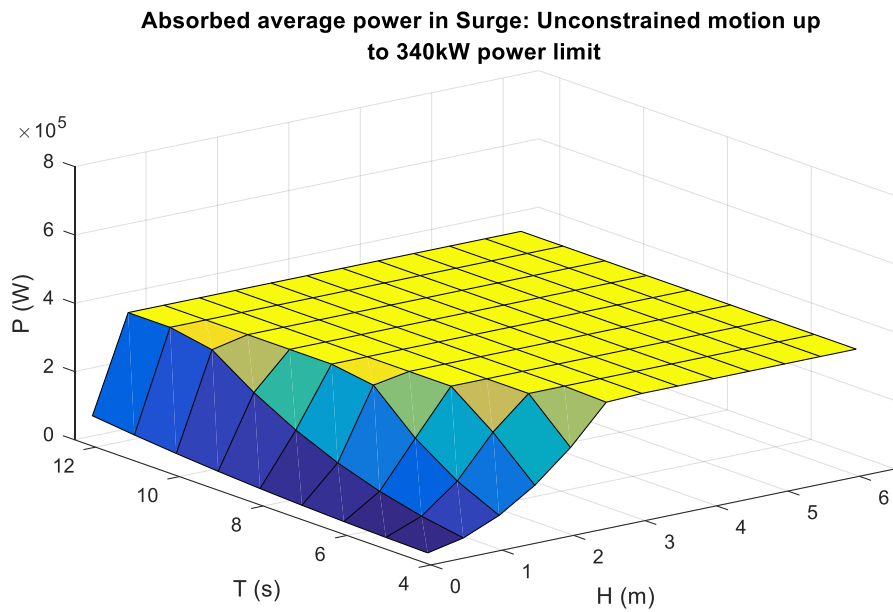


Figure 46: Absorbed average power for an unconstrained axisymmetric point absorber with optimal motion in surge with a 340 kW power constraint.

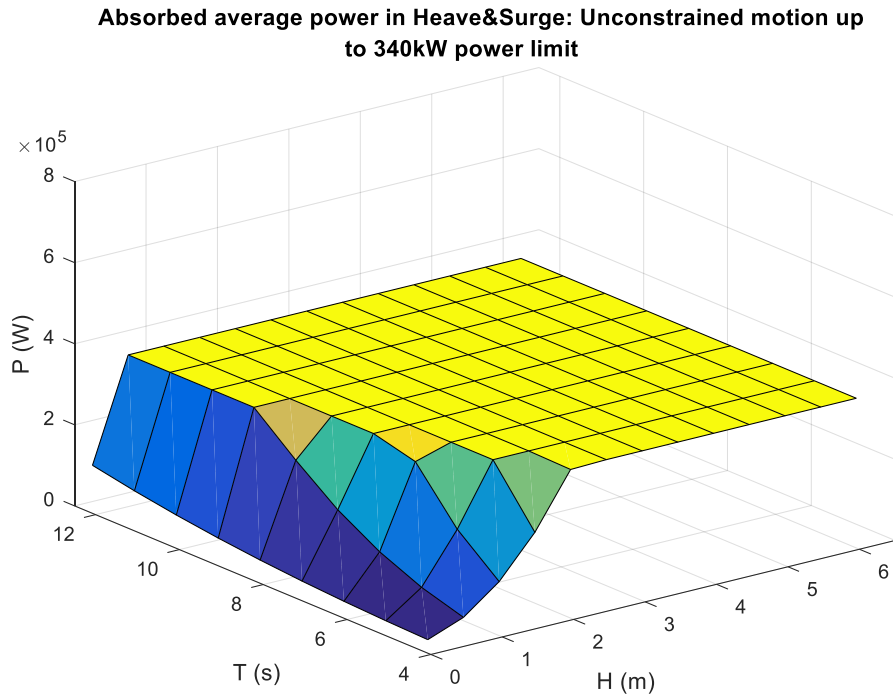


Figure 47: Absorbed average power for an unconstrained axisymmetric point absorber with optimal motion in heave+surge with a combined 340 kW global power constraint.

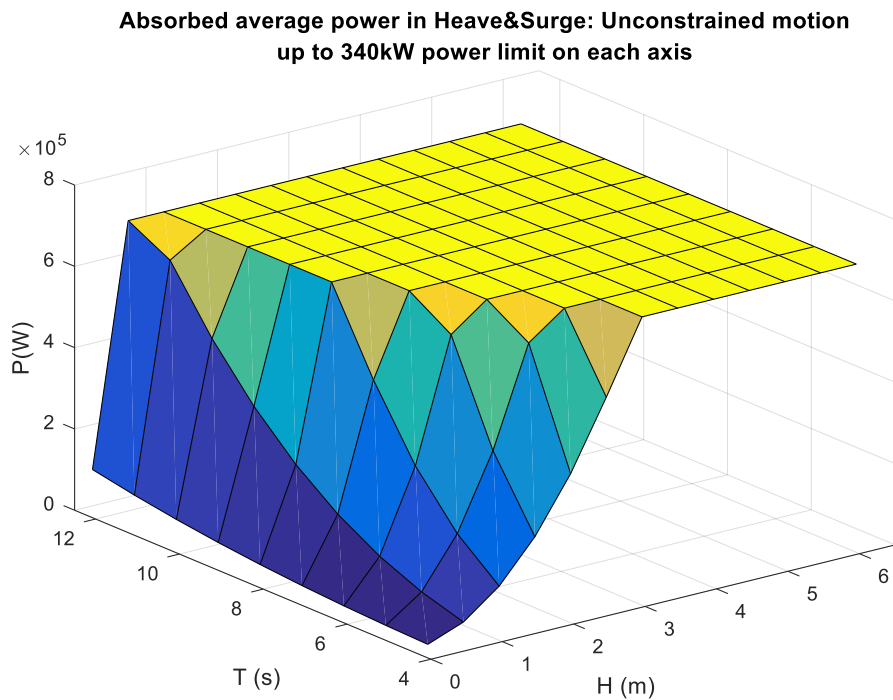


Figure 48: Absorbed average power for an unconstrained axisymmetric point absorber with optimal motion in heave+surge with a 340 kW independent power constraint on each axis (680 kW combined power constraint).

5.3 Optimum Power Absorption under Motion and Power Constraints

Combining a motion and a power constraint is a more severe condition than either constraint alone and is a closer representation of reality where both stroke length and power output both have an associated capital cost and are therefore limited. Returning to the semi-submerged spherical PAWEC of Chapter 4, the power absorption matrices for each configuration under a 0.5 radii of device (a) motion constraint and a 340 kW power constraint are shown in Figure 49 to Figure 56. These are derived from the RCWs calculated in Section 4.4. For visualisation of the effect the power constraint has on the motion constrained power matrix, both the un-power-constrained and power-constrained plots are presented sequentially in Figure 49 to Figure 56.

The motion constraint type chosen here is the independent constraint model formulated in Section 4.4 as it better represents the real world where each PTO usually has an independent extension limit (e.g. a hydraulic ram). Using the global weighted constraint would reduce the power matrices accordingly in proportion to the differences in the RCW curves. For the example plots shown here the motion constraint is 0.5 times the radius of the device.

The power constraint is again 340 kW but for the MA-PAWEC configuration it has been applied in three different ways. There are two global power constraints of 340 kW and 680 kW that represent the total power absorbed by the MA-PAWEC. The 340 kW figure represents a MA-PAWEC with the same total device output limit as a single axis equivalent. The 680 kW obviously represents a doubling of this to keep the power limit per axis ratio for the MA-PAWEC device equal to the single axis equivalent. This formulation of the constraint does not specify limits to the proportion of the total power absorbed in each axis. The limit on each axis is therefore effectively the total power limit of the device, although in order to deliver this the power absorbed on the other axis would have to be zero. This is basically an impossible situation in real life due to the fact that if there is a wave to induce motion in one axis, that same wave is available to induce motion in the other axis. The more common situation would be where the power contributions from each axis are unequal, but of the same order of magnitude. The global power constraint can be considered to represent the constraint of the grid connection or any other system that acts as a constraint on the entire MA-PAWEC. For example, it could also be the maximum power of the generator in a hydraulic system. The third formulation of the power constraint is to apply an individual power constraint to each axis. The power limits of each axis are therefore independent from one another. For the case shown here it would be 340 kW on each axis. This is analogous to the power limits that affect

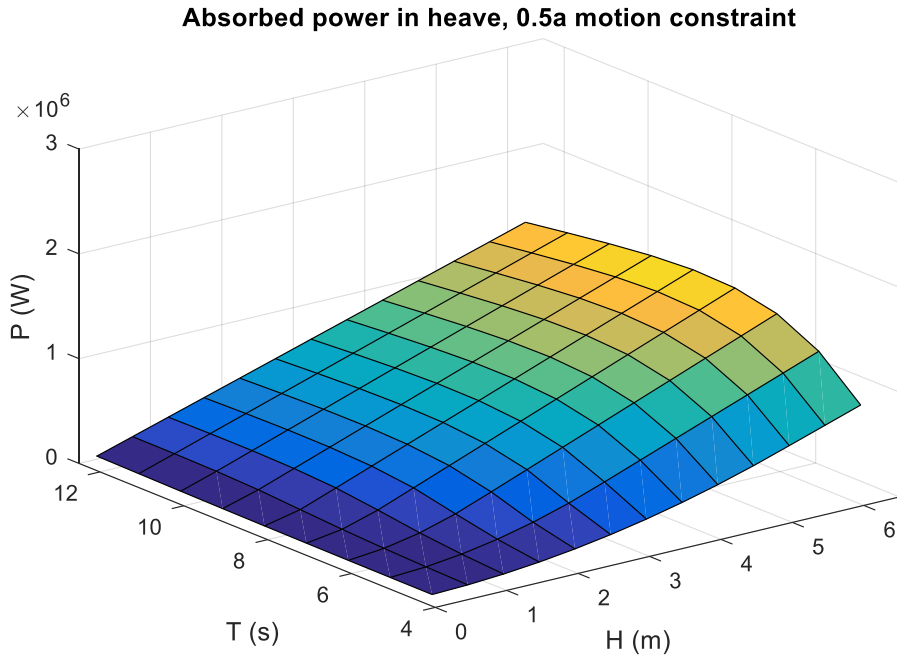


Figure 49: Power absorption matrix of the semi-submerged spherical PAWEC in heave with 0.5a motion constraint.

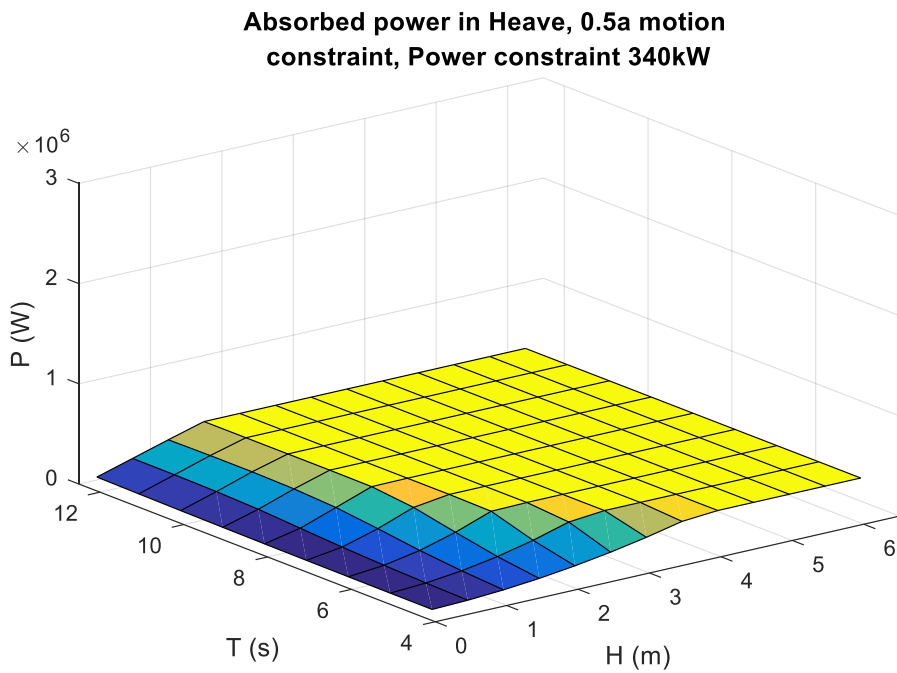


Figure 50: Power absorption matrix of the semi-submerged spherical PAWEC in heave with 0.5a motion constraint and a 340 kW power constraint.

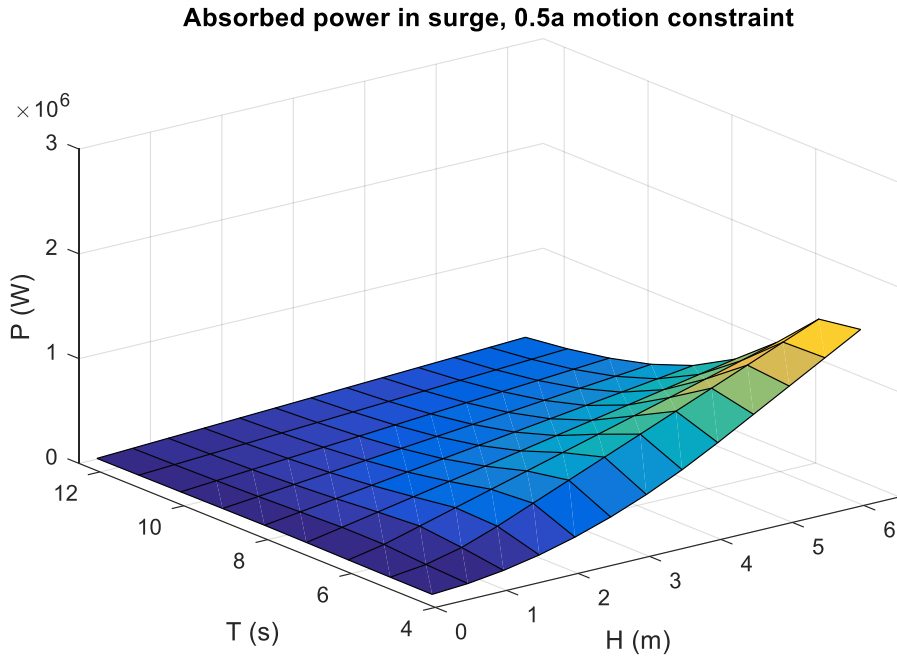


Figure 51: Power absorption matrix of the semi-submerged spherical PAWEC in surge with 0.5a motion constraint.

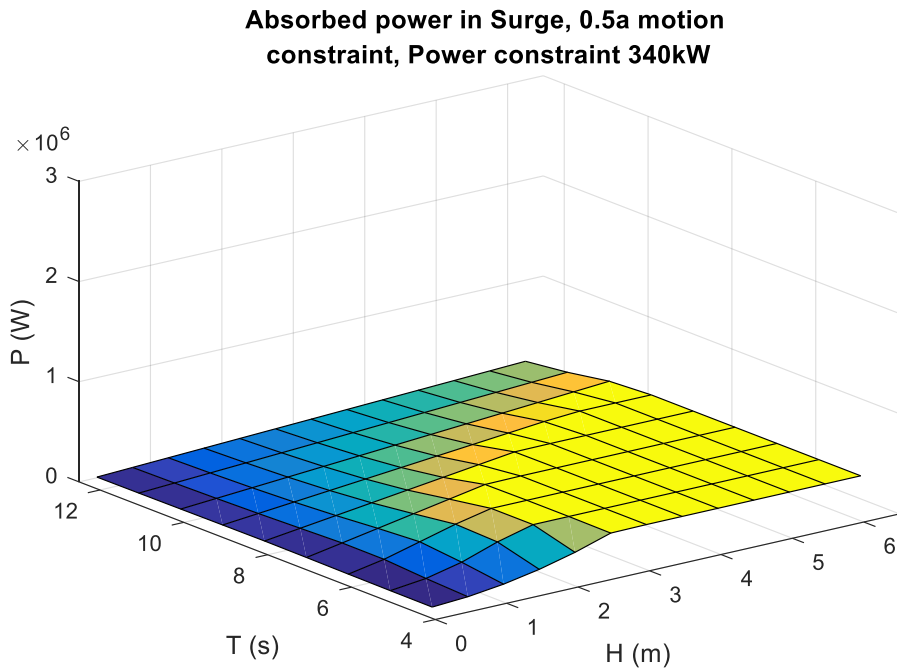


Figure 52: Power absorption matrix of the semi-submerged spherical PAWEC in surge with 0.5a motion constraint and a 340 kW power constraint.

Absorbed power in heave&surge, Independent 0.5a motion constraints

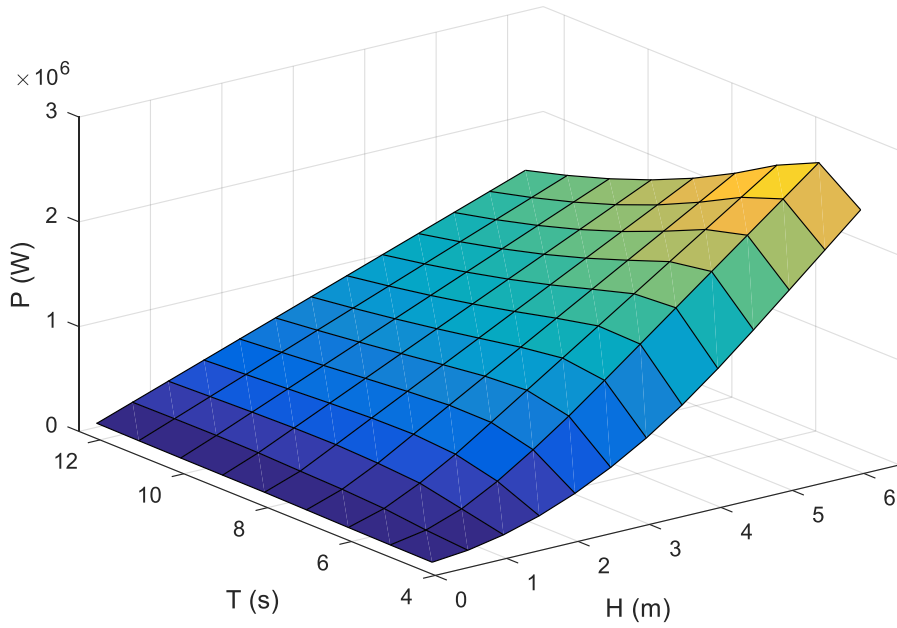


Figure 53: Power absorption matrix of the semi-submerged spherical PAWEC in heave+surge with independent 0.5a motion constraints.

Absorbed power in Heave and Surge, Independent motion constraint 0.5a, Global power constraint of 340kW

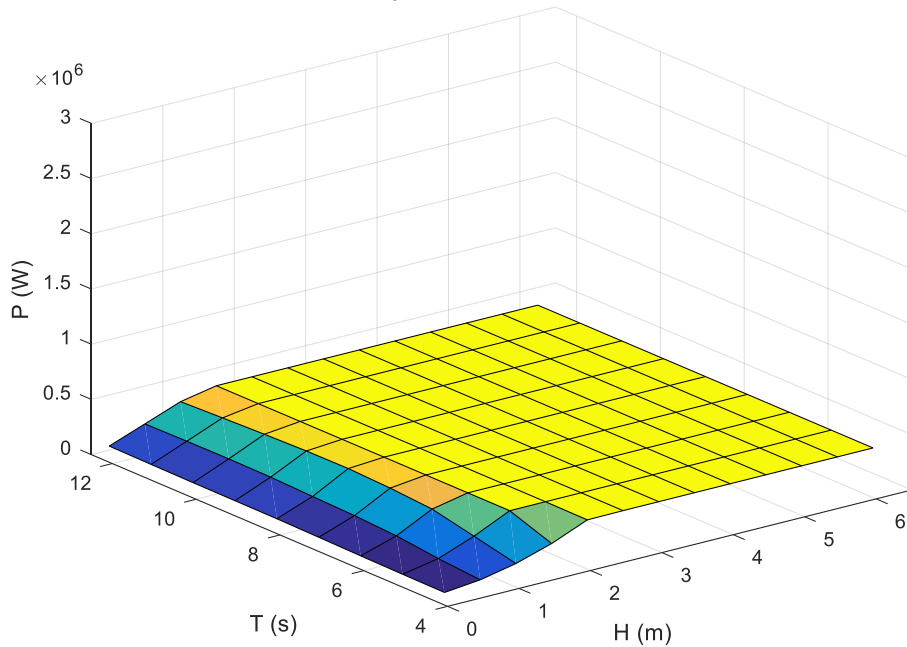


Figure 54: Power absorption matrix of the semi-submerged spherical PAWEC in heave+surge with independent 0.5a motion constraints and a global power constraint of 340 kW.

**Absorbed power in Heave and Surge, Independent motion constraint 0.5a,
Global power constraint of 680kW**

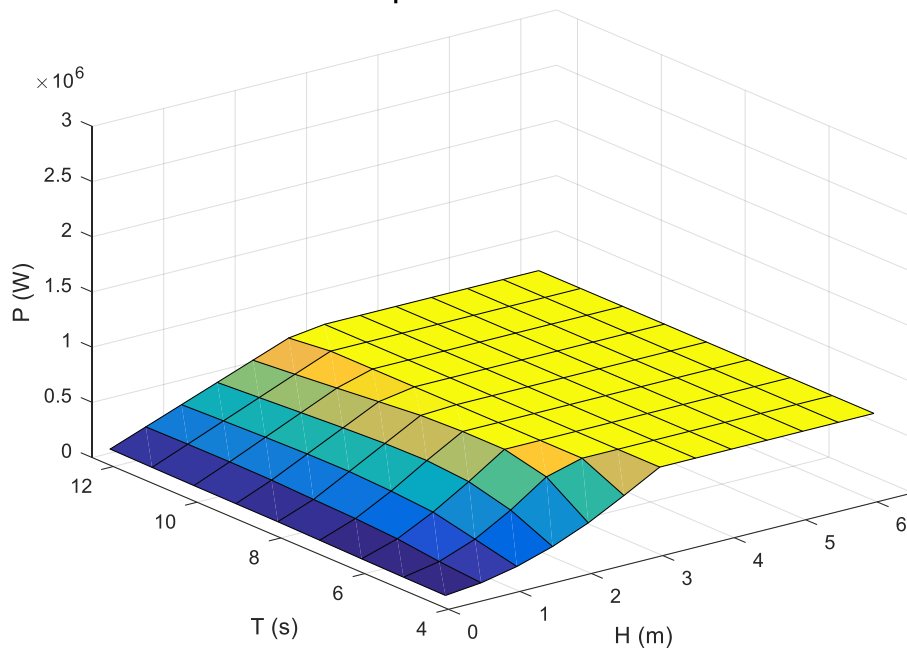


Figure 55: Power absorption matrix of the semi-submerged spherical PAWEC in heave+surge with independent 0.5a motion constraints and a global power constraint of 680 kW.

**Absorbed power in Heave and Surge, Independent motion
constraint 0.5a, Independent power constraints of 340kW on each axis**

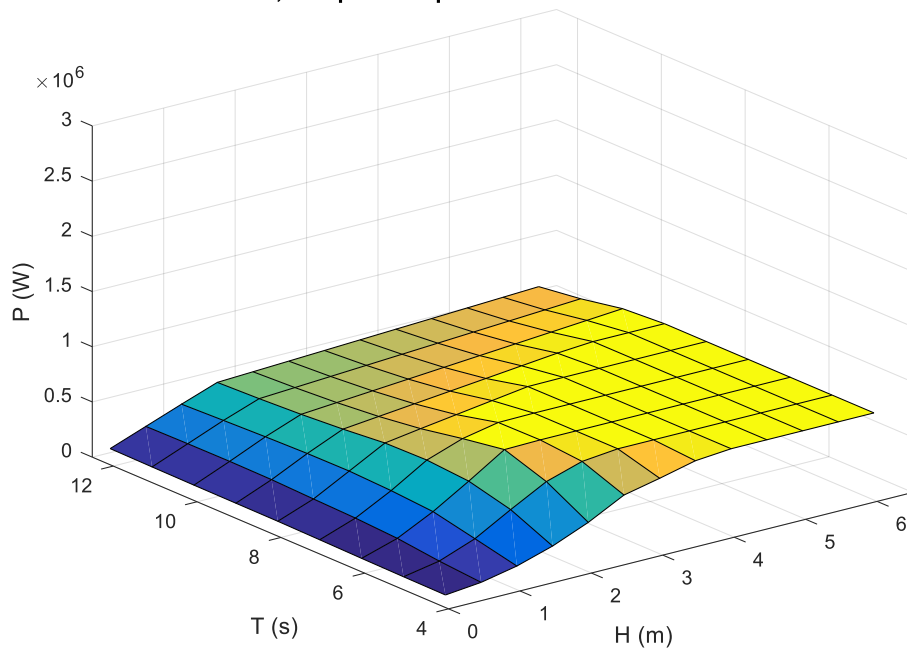


Figure 56: Power absorption matrix of the semi-submerged spherical PAWEC in heave+surge with independent 0.5a motion constraints and independent power constraints of 340 kW on each axis.

the PTO system only on a specific axis. For example, a linear generator for one axis has a maximum power capacity that is specific to a single axis of motion.

The higher RCWs of heave in longer waves and surge in shorter waves that was seen in Sections 4.3 and 4.4 are evident in the position of the power limit plateaus in relation to wave period of Figure 50 and Figure 52 respectively. The much larger power limit plateau of heave compared to surge also shows heave absorbing more power than surge over a larger wave range under this 0.5a motion constraint.

The difference between the power limit plateaus of the 680 kW global power constraint (Figure 55) and 2x 340 kW independent power constraint (Figure 56) show that the independent power constraint is the more severe condition. It also raises the question of what equipment power ratings for individual axes vs. total output should be chosen. For a MA-PAWEC the decision of what power rating to size each PTO axis and the downstream equipment is evidently more complicated than for a single axis.

5.4 Energy Production under Motion and Power Constraints

The power matrices of section 5.3 show the effect of the power constraint on the devices' ability to absorb energy from particular waves and suggests a reduction in the advantage of MA-PAWECs over single axis equivalents. It is a very limited picture however as it gives no weighting to the frequency of occurrence of each wave type. The energy production at any particular site will be dependent on the distribution of the wave heights and periods in the wave climate. For the example here it is a monochromatic wave distribution based on Table 2. Equation 33 can then be used but in this case the power absorbed (P_{ij}) for each wave of period i and height j will be subject to the limits:

$$P_{ij} > P_c : P_{ij} = P_c$$

$$P_{ij} \leq P_c : P_{ij} = P_{ij}$$

Equation 38

These limits effectively cap the maximum power output to a certain level given by the power constraint P_c . If the power output is below this constraint these limits have no effect. The weighting given to each wave type (of different height and period) is specified by f_{ij} . Using the average power of the wave climate in Table 2 (17 kW/m) as a normalising value the power constraint (P_c) can be described as a non-dimensional ratio by dividing by the average

incident power across the diameter of the point absorber device in the particular wave climate (P_{wc}):

$$\text{Power constraint ratio} = P_c/P_{wc}$$

The power constraint ratio for the 340 kW example would therefore be 2. When using this power constraint ratio to compare energy production between different wave distributions the spread of waves in each wave climate distribution should be proportionally similar.

Figure 57 to Figure 60 show the energy production for the semi-submerged spherical PAWEC in heave, surge and heave+surge across the motion constraint range of 0-0.5 times the radius of the device with the heave+surge under both independent and global power constraints. For the heave+surge configuration the motion constraint is independent on each axis and equal in magnitude. This is analogous to a diagonal slice across a surface plot of EP such as seen in Figure 38. The unconstrained (no power limit) curves are the same as those in Figure 38. The plots have been scaled equally to allow easier comparison between the configurations. Note that there is an additional curve for the power ratio $0.25P_{wc}$ on the heave+surge global power plot. This is equivalent to the $0.5P_{wc}$ power constraint ratio curve on the single axis plots as the power constraints are scaled per number of axes.

The unconstrained curves represent the boundary curve from which the other curves deviate when the power constraint begins to have an effect. As was noted from Figure 38, surge has the lowest unconstrained EP curve with heave slightly above and heave+surge significantly above them both. What is apparent on all the plots is a decreasing spacing between successive curves. This represents decreasing marginal returns for additional power capability. Heave curves deviate from the unconstrained boundary at lower motion constraints than surge curves, consistent with heave having a higher energy production figure than surge for the same motion constraint.

Although it is not immediately obvious, there is a difference between the curves under global and independent power constraints. The energy production figures under the global power constraint regime are slightly higher than under the independent power constraint regime. This is most clearly seen by the closer bunching of curves at the top right of the global power constraint plot and the earlier separation of the global power constraint curves from the optimum boundary. This difference in energy production is the manifestation of the slightly different power matrices for the global and independent power constraint configurations seen in Figure 55 and Figure 56. Under the global power limit regime it is possible for axes to generate more than half the limit and so as absorbed energy through one axis drops off, so the other axis has the capability to make up the difference and keep the device at full power.

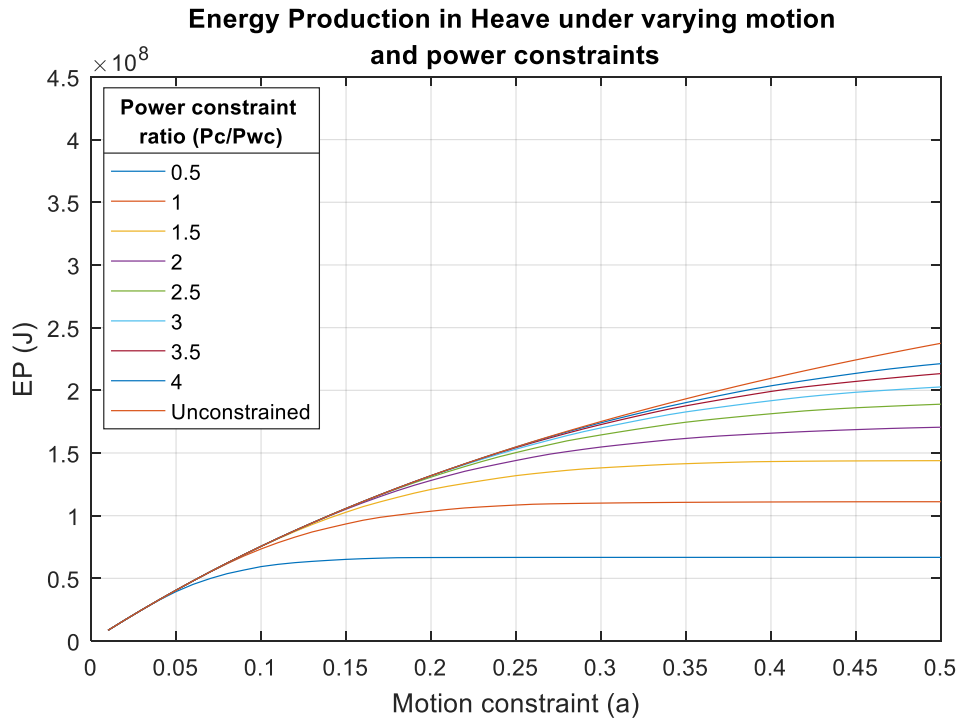


Figure 57: Energy production in Heave under motion and power constraints. Power constraints are represented by the power constraint ratio (P_c/P_{wc}) and are scaled per number of axes.

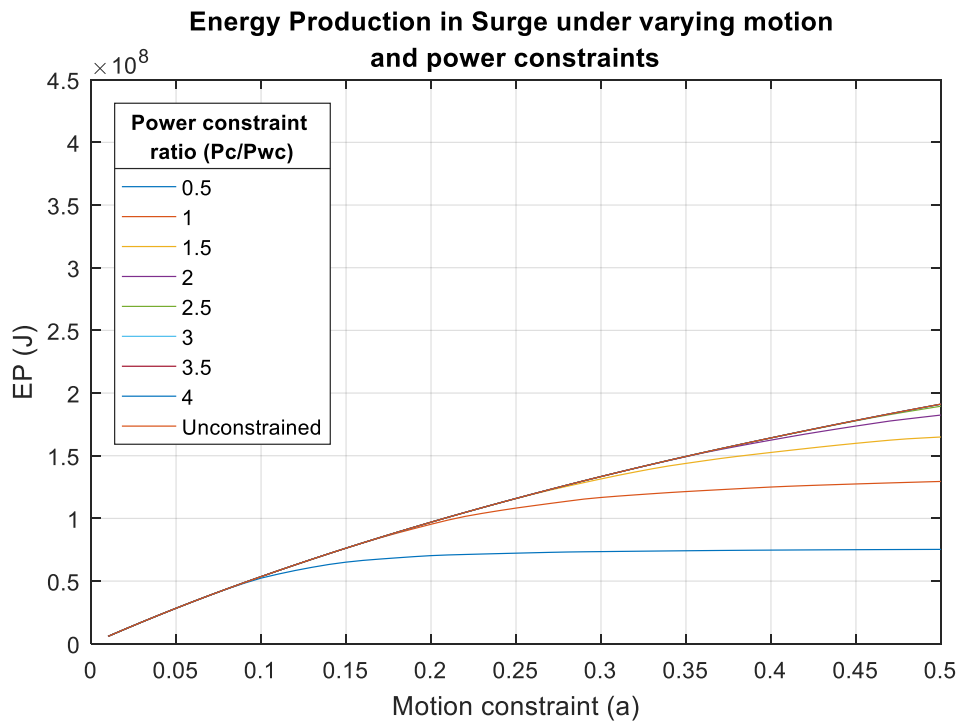


Figure 58: Energy production in Surge under motion and power constraints. Power constraints are represented by the power constraint ratio (P_c/P_{wc}) and are scaled per number of axes.

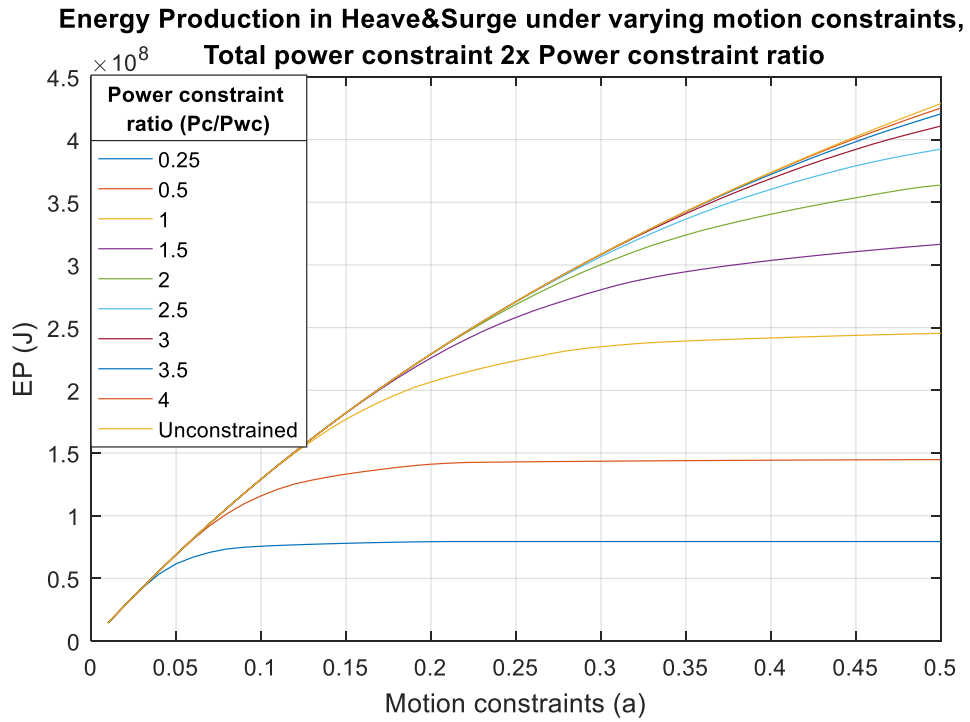


Figure 59: Energy production in Heave+Surge under motion and global power constraints. Power constraints are represented by the power constraint ratio (P_c/P_{wc}) and are scaled per number of axes.

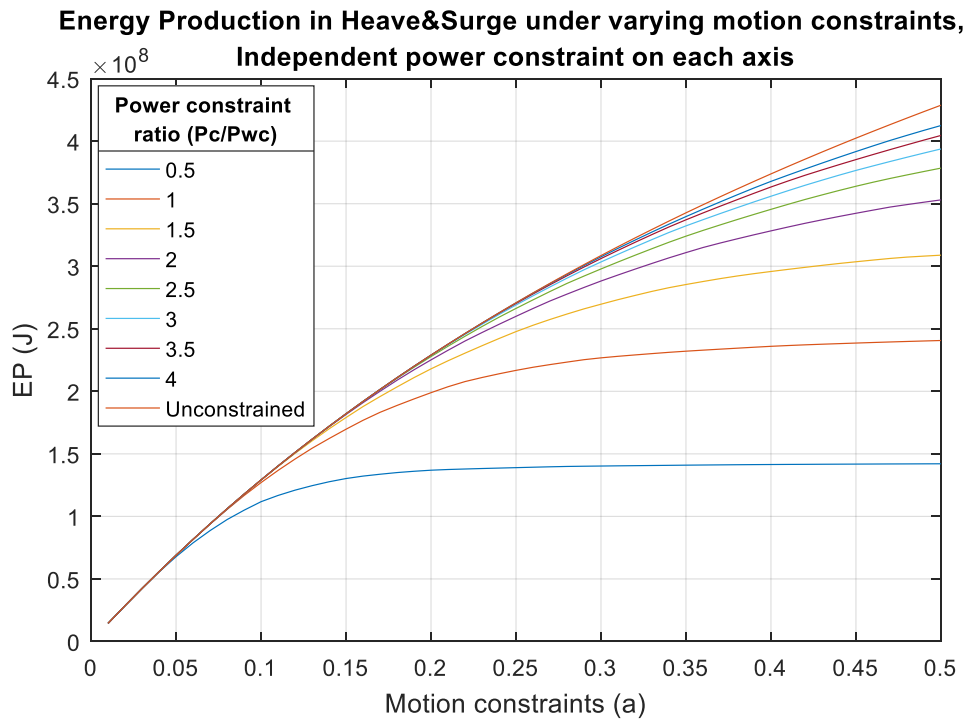


Figure 60: Energy production in Heave+Surge under motion and independent power constraints. Power constraints are represented by the power constraint ratio (P_c/P_{wc}) and are scaled per number of axes.

To compare the different configurations directly the EP curves from Figure 57 to Figure 60 are plotted on graphs arranged by power constraint in Figure 61 to Figure 68. Each plot is for a fixed power constraint ratio. Note that the blue, red and yellow curves (heave, surge, heave+surge) all have the same device power output limit. The purple and green curves (both heave+surge) have double the device power output limit of the other three curves but are global and independent power limits respectively. The higher global limit is denoted as '2x global' as it is double the lower global limit. The optimum curves without power constraint are also shown for comparison purposes in Figure 69.

Looking at the heave and surge curves of Figure 61 to Figure 68 we can see that under the lower power constraints (0.5 to $2.5P_{wc}$) the surge mode produces slightly more than heave across the upper part of the range of motion constraints. This contrasts with the unconstrained power scenario where heave outperforms surge across the entire range of motion constraints. The intercept between the two curves moves further away from the origin with higher power constraints until the plot of $3P_{wc}$ where heave remains above surge for the entire graph. The implications of this are interesting. Basing a decision of what single PTO axis of a PAWEC to develop on the results of the motion constraints alone would have favoured heave as it generated more energy for a given motion constraint than surge. The power constraint instead tips the favour towards surge in this wave distribution under certain conditions. Under lower power constraints and higher motion constraints surge may be a better choice for a single axis point absorber.

The cause of this change is due to the wave type in which each axis absorbs most of its energy. As was seen in Chapter 4 surge performs better in short waves which, as they contain less energy, do not cause the PTO to reach its power limit. Heave absorbs more of its energy from long waves which are more powerful and so will reach the limit. Under a MA-PAWEC configuration the implications of this are that it may in fact be better to have a large motion constraint on surge and small motion constraint in heave. Making the assumption that a unit of PTO extension for either axis has the same cost and can be linearly added to either, the most cost effective method of allocation would be to begin with the heave axis and then switch to extending the surge axis. The transition point would be where the gradient of the heave curve on graphs such as in Figure 61 to Figure 68 dropped below that of the surge curve at the origin. Thus the optimal use of PTO units would be a large surge excursion absorbing most of the WEC power and a small heave excursion absorbing a smaller portion.

Comparing the independent and 2x global curves in Figure 61 to Figure 68 the generation difference between the two approaches becomes clearer. This difference does not remain

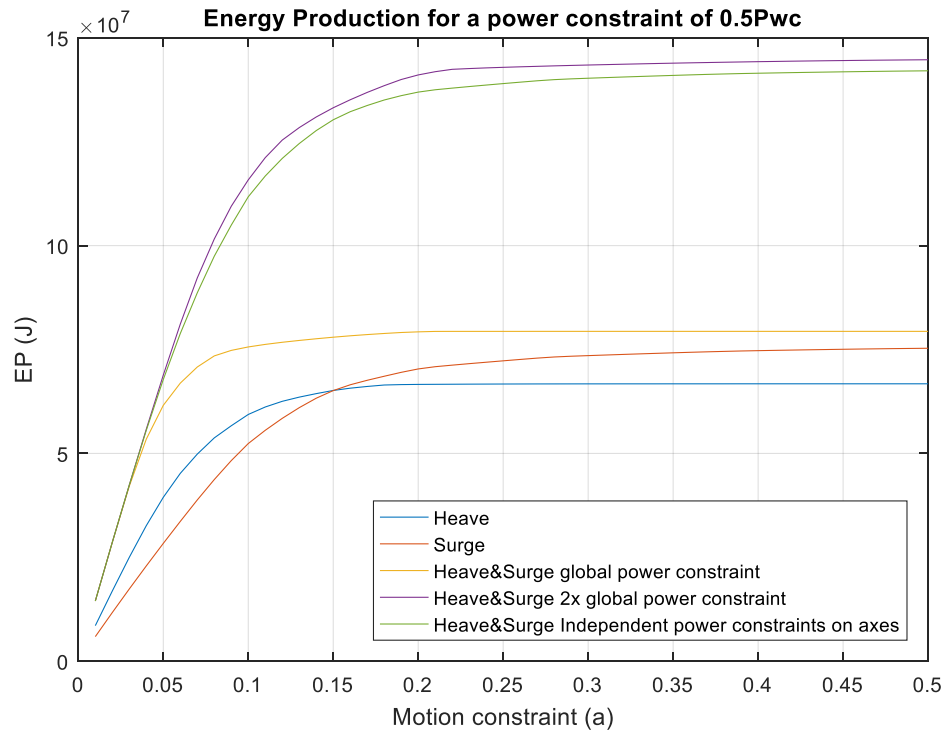


Figure 61: Energy production under power and motion constraints with a power constraint $0.5P_{wc}$.

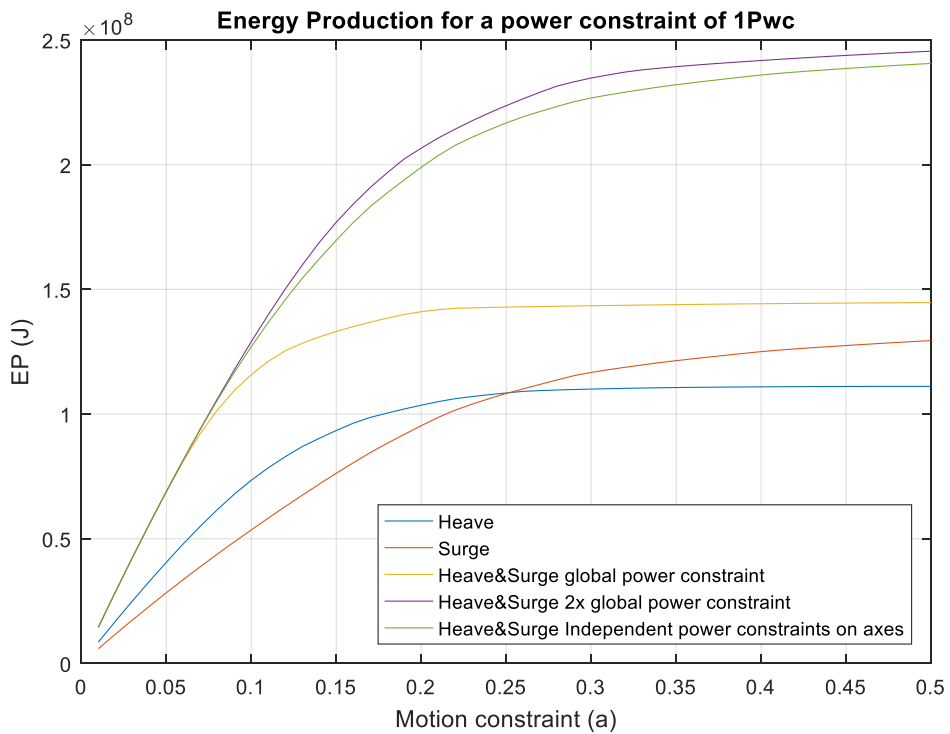


Figure 62: Energy production under power and motion constraints with a power constraint $1P_{wc}$.

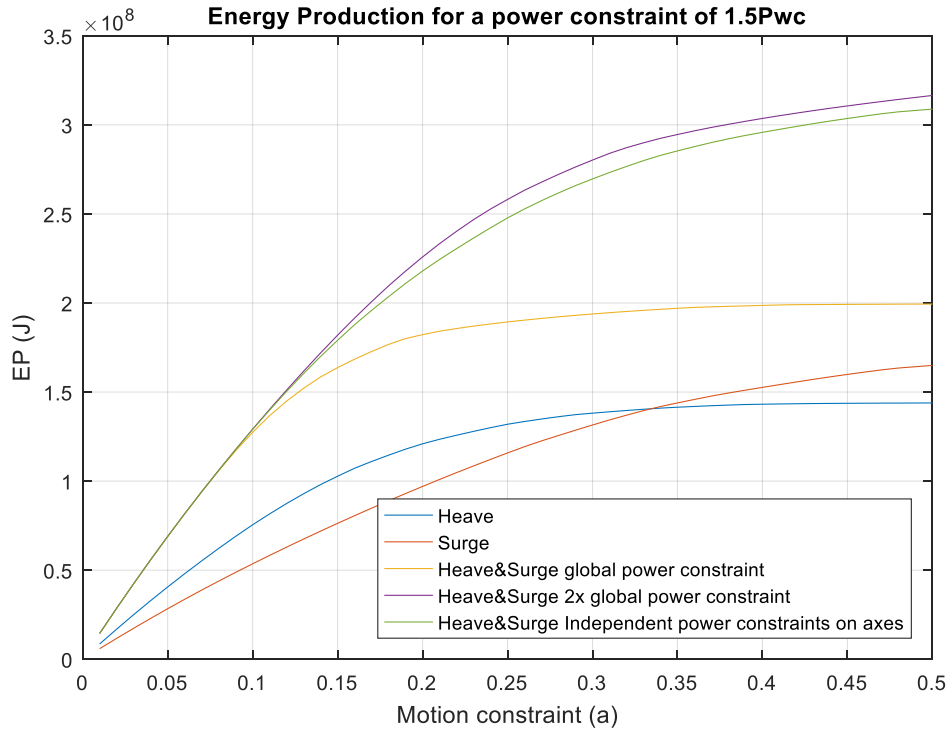


Figure 63: Energy production under power and motion constraints with a power constraint 1.5P_{wc}.

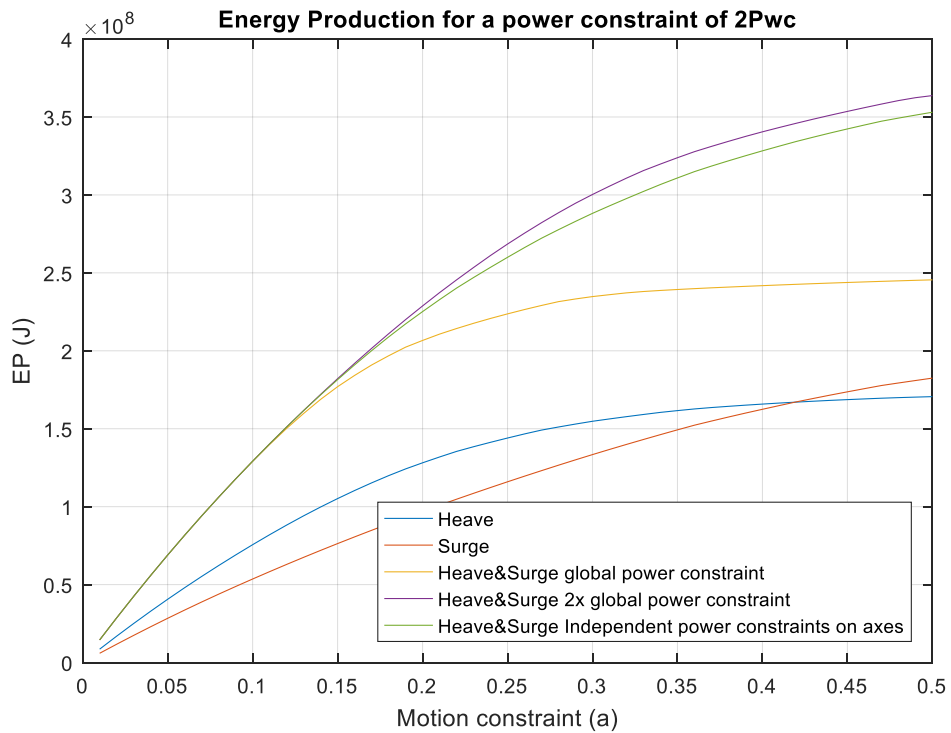


Figure 64: Energy production under power and motion constraints with a power constraint 2P_{wc}.

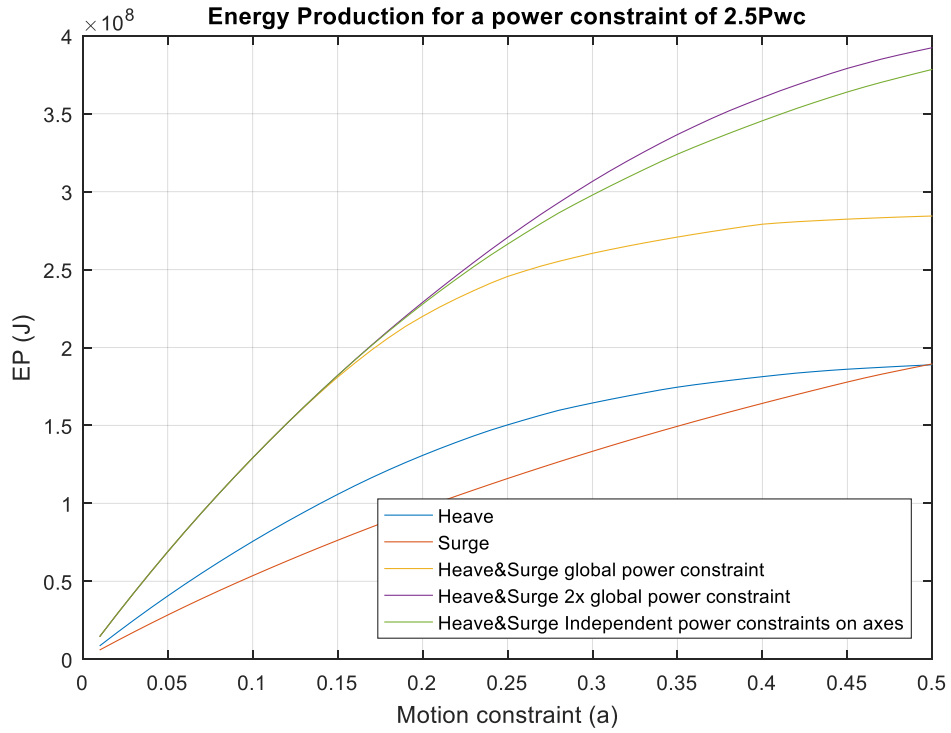


Figure 65: Energy production under power and motion constraints with a power constraint 2.5P_{wc}.

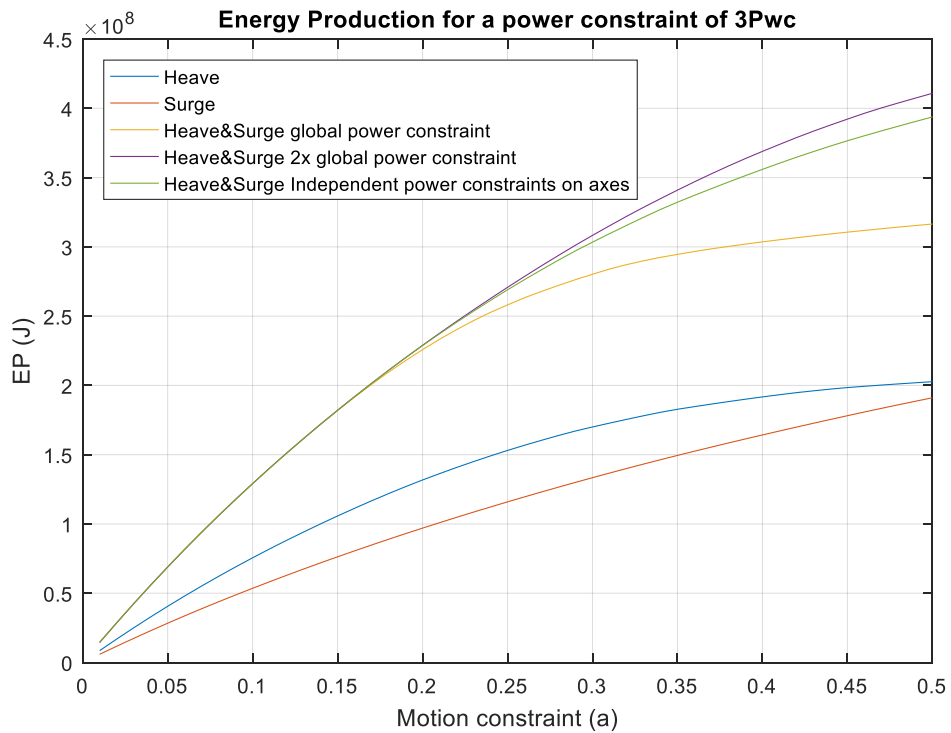


Figure 66: Energy production under power and motion constraints with a power constraint 3P_{wc}.

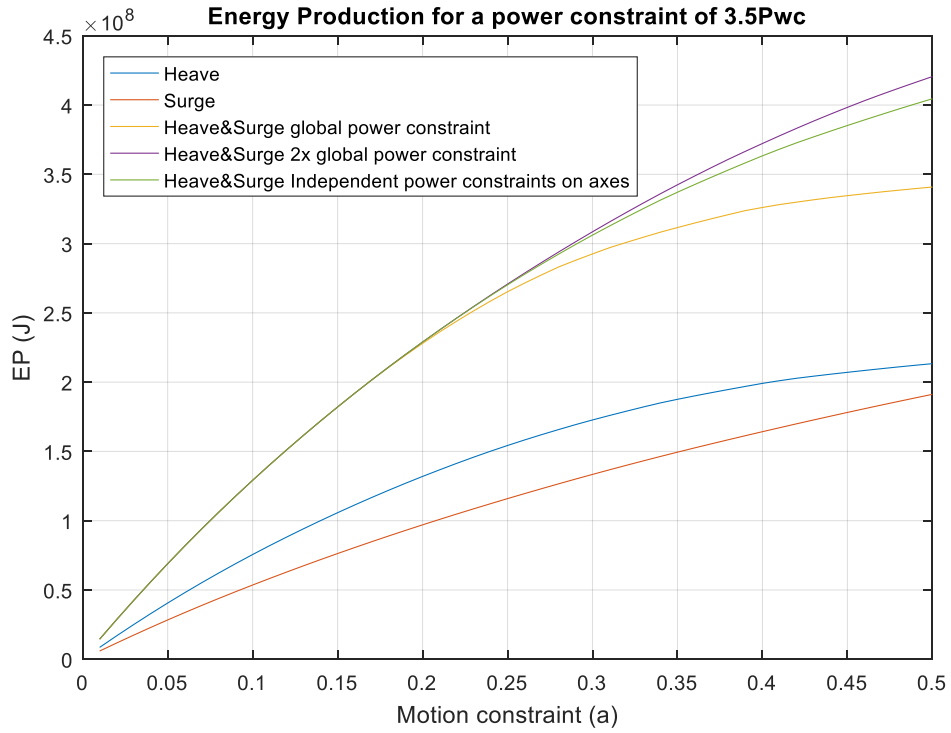


Figure 67: Energy production under power and motion constraints with a power constraint 3.5P_{wc}.

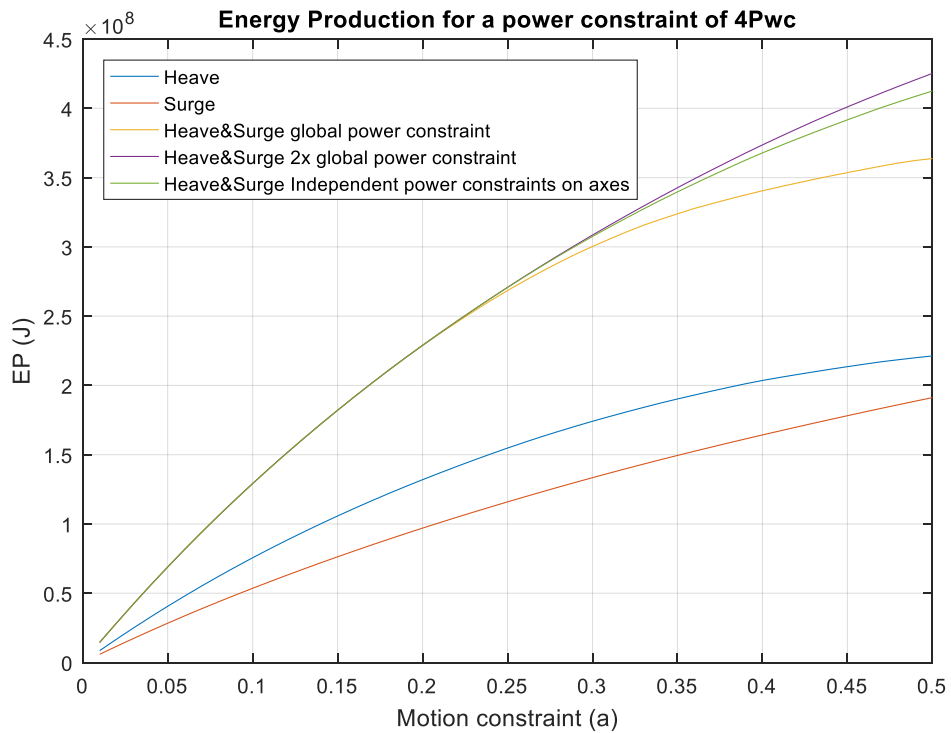


Figure 68: Energy production under power and motion constraints with a power constraint 4P_{wc}.

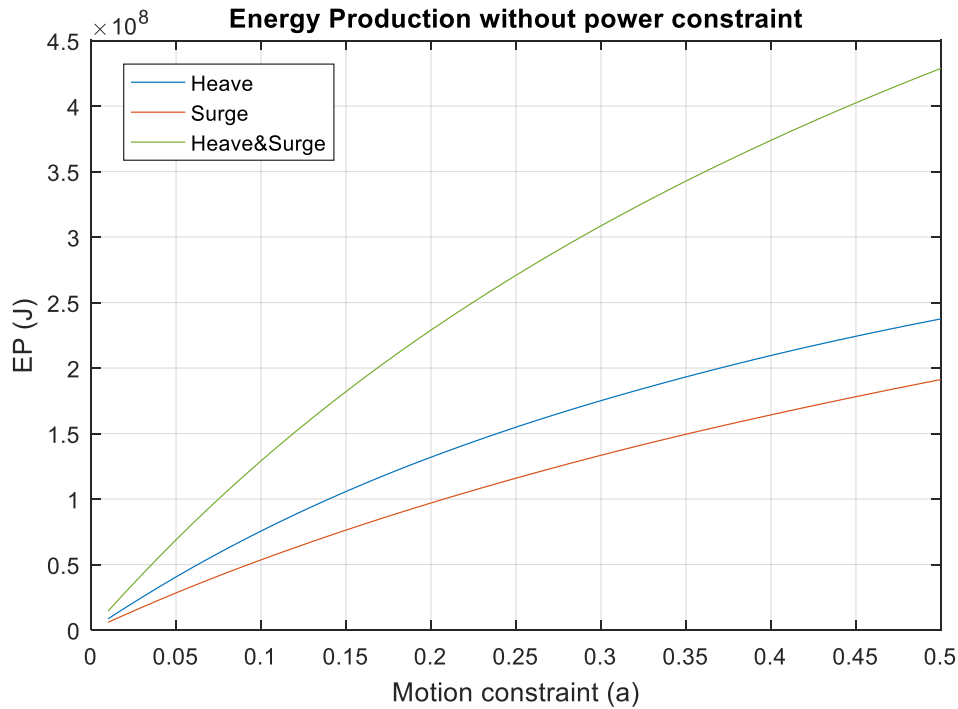


Figure 69: Energy production under motion constraints for the three configurations heave, surge and heave+surge. No Power constraints.

constant over the range of motion constraints or power constraints. In all cases the difference is very small near the origin at small motion constraints. The difference increases with motion constraint but at lower power constraints the difference begins to narrow again as motion constraint increases. The cause of this variation in difference is of course due to the variation in power absorption of the underlying independent axes mentioned earlier.

To more clearly see the effect the power constraint has on relative energy production between configurations, plots of EP against power constraint ratios for the point absorbers under motion constraints from 0.1a to 0.5a are shown in Figure 70 to Figure 74. All curves tend towards their maximum as the power limit is increased as would be expected. The small difference between the independent and 2x global curves can be seen once again, the maximum difference shifting with both motion and power constraints. The heave and surge curves once again exhibit an intercept which shifts. In this case it shifts due to motion constraints with heave becoming successfully better than surge over a larger range of the power constraints as motion constraints are tightened. This suggests that heave will be the better choice under power limits and small motion constraints. Surge remains the better choice when longer excursions are an option and the power limits are low.

The MA-PAWEC global power constraint curves reveal an interesting advantage to this configuration of PTO. This MA-PAWEC has the same total rated output as the single axis

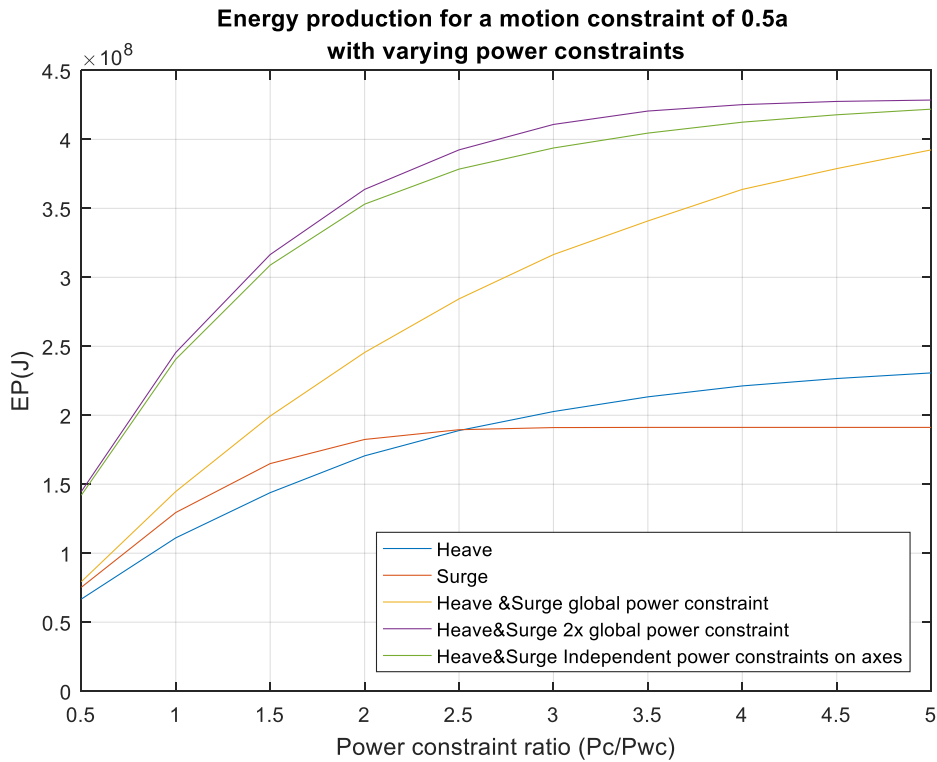


Figure 70: The effect of the power constraint on energy production for heave, surge and heave+surge configurations under motion constraints 0.5a.

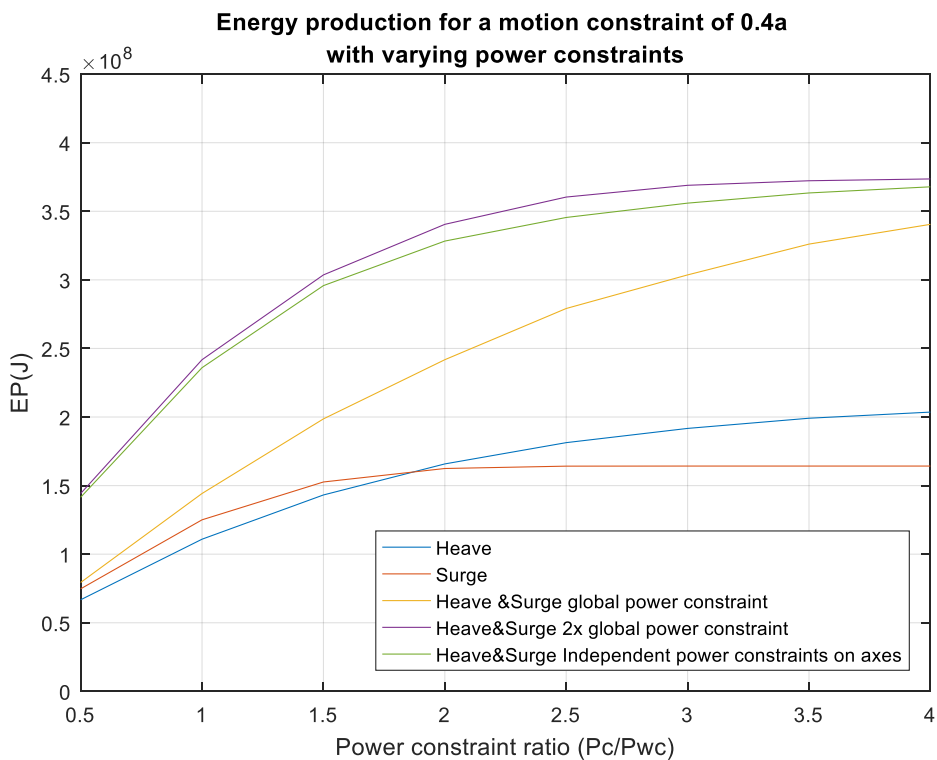


Figure 71: The effect of the power constraint on energy production for heave, surge and heave+surge configurations under motion constraints 0.4a.

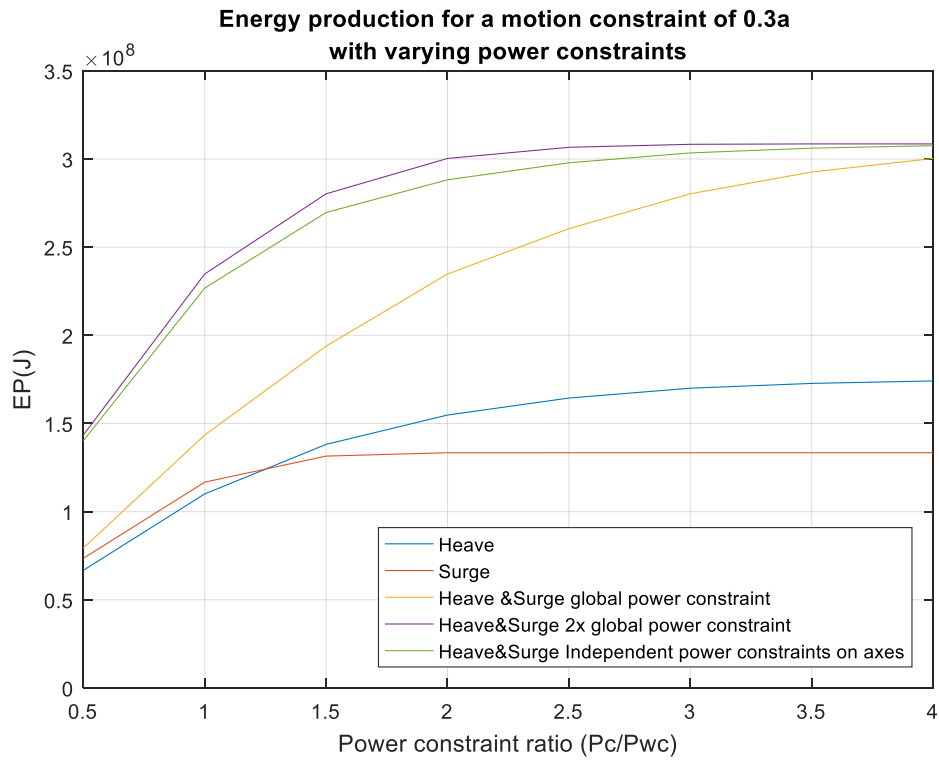


Figure 72: The effect of the power constraint on energy production for heave, surge and heave+surge configurations under motion constraints 0.3a.

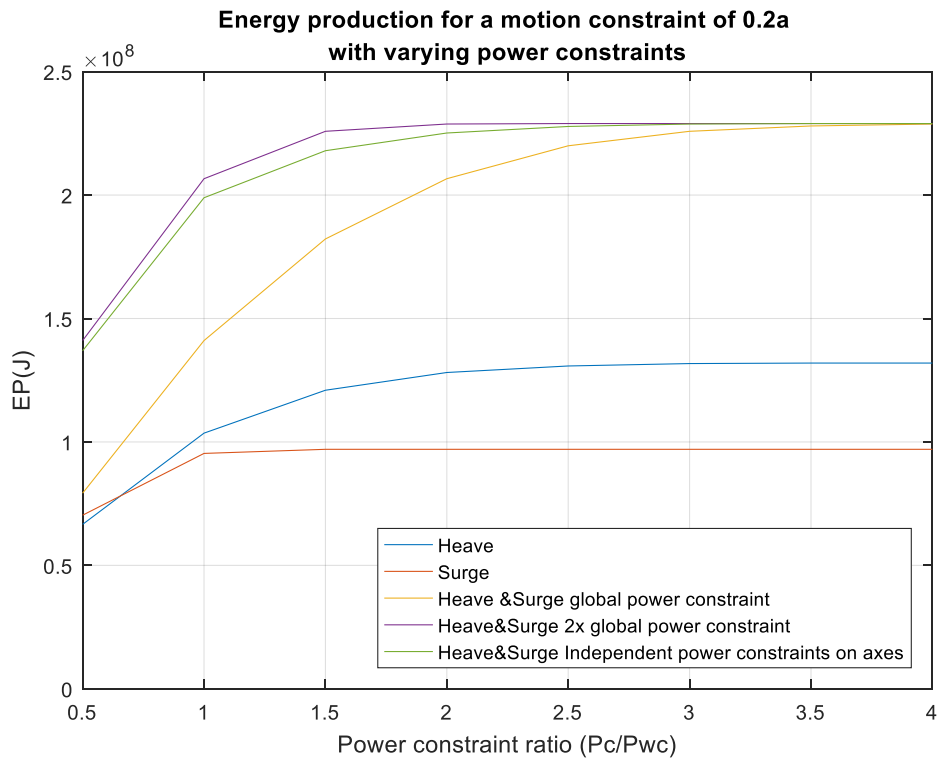


Figure 73: The effect of the power constraint on energy production for heave, surge and heave+surge configurations under motion constraints 0.2a.

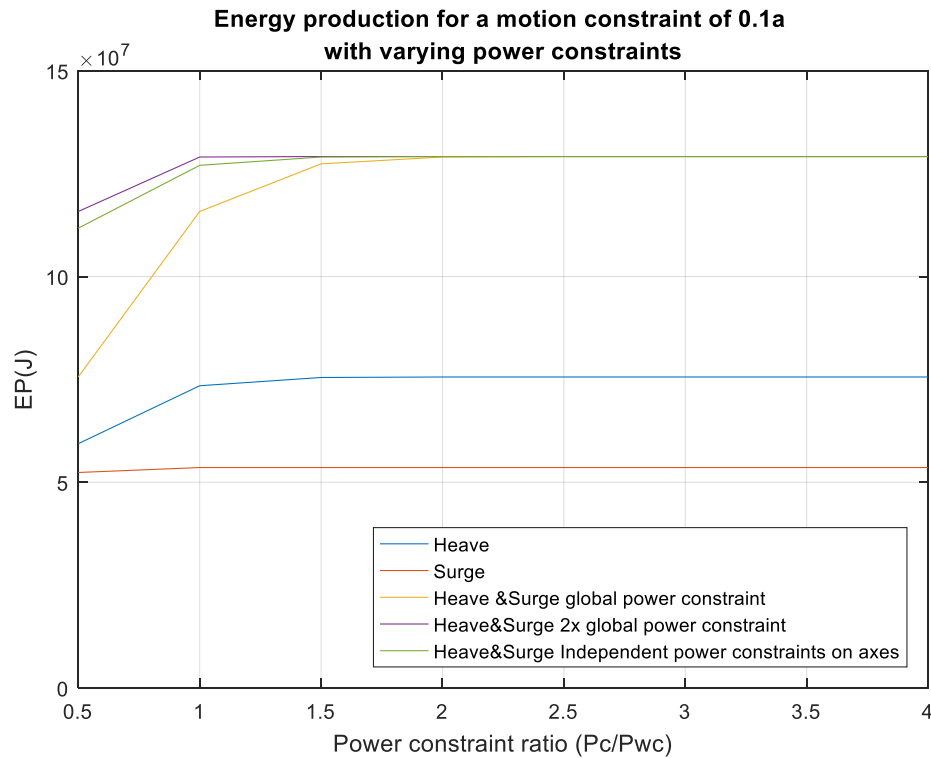


Figure 74: The effect of the power constraint on energy production for heave, surge and heave+surge configurations under motion constraints 0.1a.

PAWECs but achieves significantly higher energy production, particularly at small constraints. This increases as the power limit is increased until it reaches the independent and 2x global limits for the motion constraints 0.1a and 0.2a. For 0.3a, 0.4a and 0.5a motion constraints the curve approaches but does not reach the independent and 2x global curves although the trend at the graph limit is closing the gap. This trend reflects the fact that as motion constraints are tightened, so the maximum energy produced is lower and thus the power limit is reached less often. The lower power constraint of the global constraint vs. the 2x global and independent constraints has less of an impact on production. The difference between the global and 2x global and independent curves varies in magnitude with power constraint. The point where the magnitude of the difference is largest shifts to lower power constraints as motion constraints decreases.

In reality this effect would mean a higher energy delivered by the global constraint device for a given rating of energy infrastructure compared to the independent and 2x global devices that have double the rated capacity. Note that within the WEC the rating of each PTO axis remains the same as for the single axis devices and the independent double capacity devices. It is the downstream equipment from the PTO axes that benefit from this effect. In a real WEC a PTO system such as hydraulics would be able to benefit from this effect by having an accumulator and generator set at a lower rated capacity than simply doubling the rating of a single axis

machine. This would give a higher usage factor for the hydraulic system which in turn would reduce part load inefficiency losses. For direct drive or mechanical PTO the advantages may be less pronounced but any downstream equipment such as power electronics and grid connection would be better leveraged.

Plots showing the percentage of time each configuration is at maximum power are shown in Figure 75 to Figure 78. The uneven nature of the curves is due to the discrete nature of the wave periods and heights used. They are all plotted on the same scale for easier comparison. All plots show that time at maximum power decreases as the power limit increases as expected. Heave (Figure 75) reaches its maximum power limit for 60% of the time at a power constraint of $0.5P_{wc}$ over a large range of motion constraints from 0.19a to 0.5a. Surge (Figure 76) achieves a higher maximum percentage (73%) but only at the upper end of the motion constraints. The time at max power for surge decreases much more rapidly than heave as the power constraint is relaxed with the limit not being reached at all for power limits above $2.5P_{wc}$. For the MA-PAWEC under a global power constraint the time at max power reaches a peak of 82% which is the highest of the four configurations. This maximum occurs at the higher motion constraints as would be expected but it remains high over the majority of the range of motion constraints. Contrast this with the relatively low time spent at maximum power of the independent power limit MA-PAWEC (Figure 78). It reaches a maximum of 61% at the higher motion constraints but this drops off almost as rapidly as the surge. Comparing the two power configurations of the MA-PAWEC we can see that the global limit configuration (Figure 77) spends significantly more time at max power for a given power limit than the independent case. Therefore if a WEC developer wants to maximise time at the rated capacity of the WEC then the sum of the PTO axes ratings should be larger than the total rated capacity of the WEC.

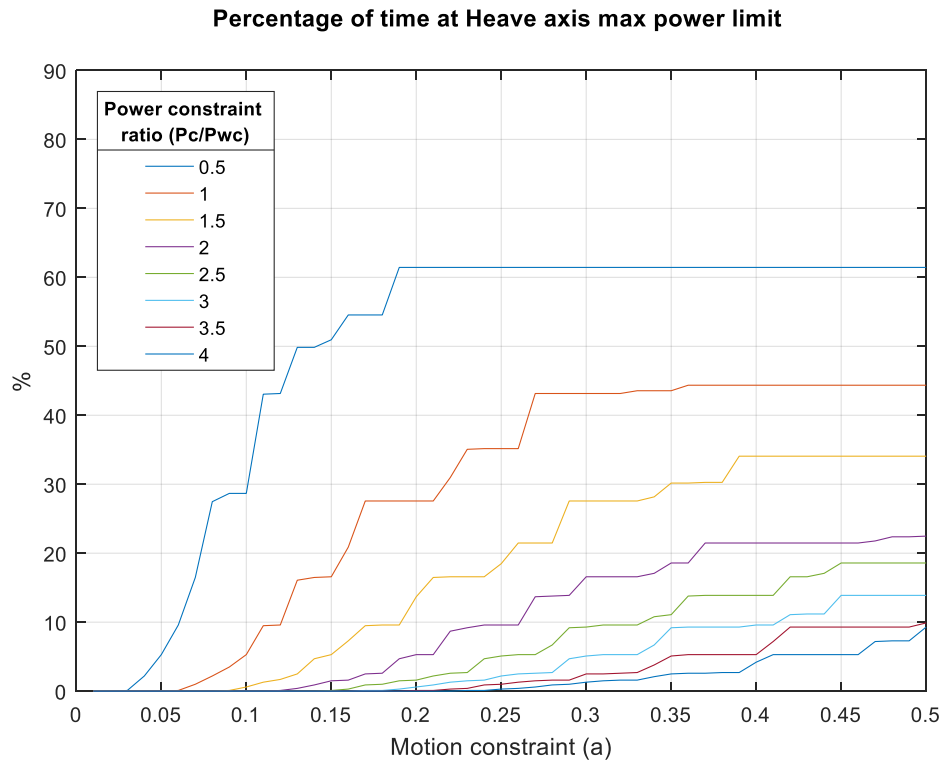


Figure 75: Percentage of time heave configuration was operating at maximum power capacity.

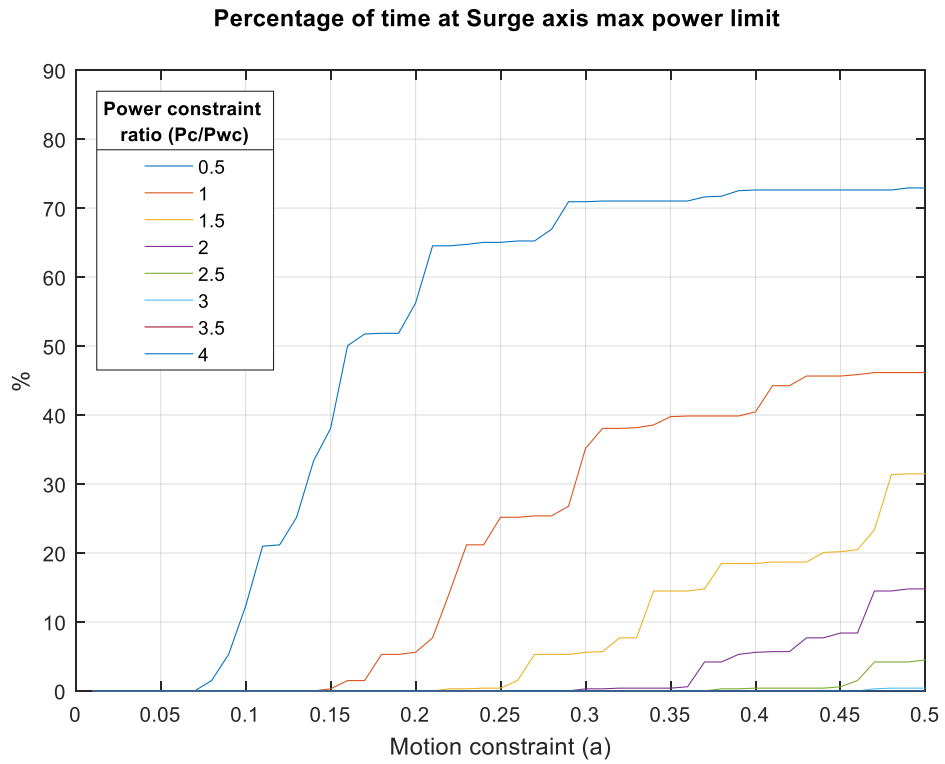


Figure 76: Percentage of time surge configuration was operating at maximum power capacity.

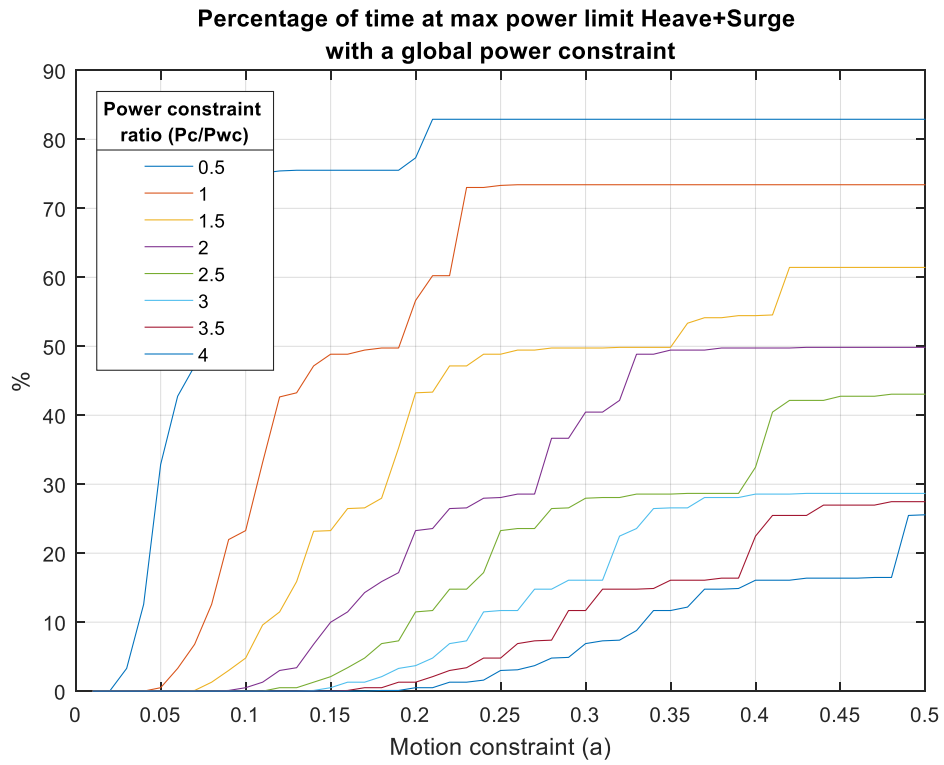


Figure 77: Percentage of time heave+surge configuration was operating at maximum power capacity with a global power constraint.

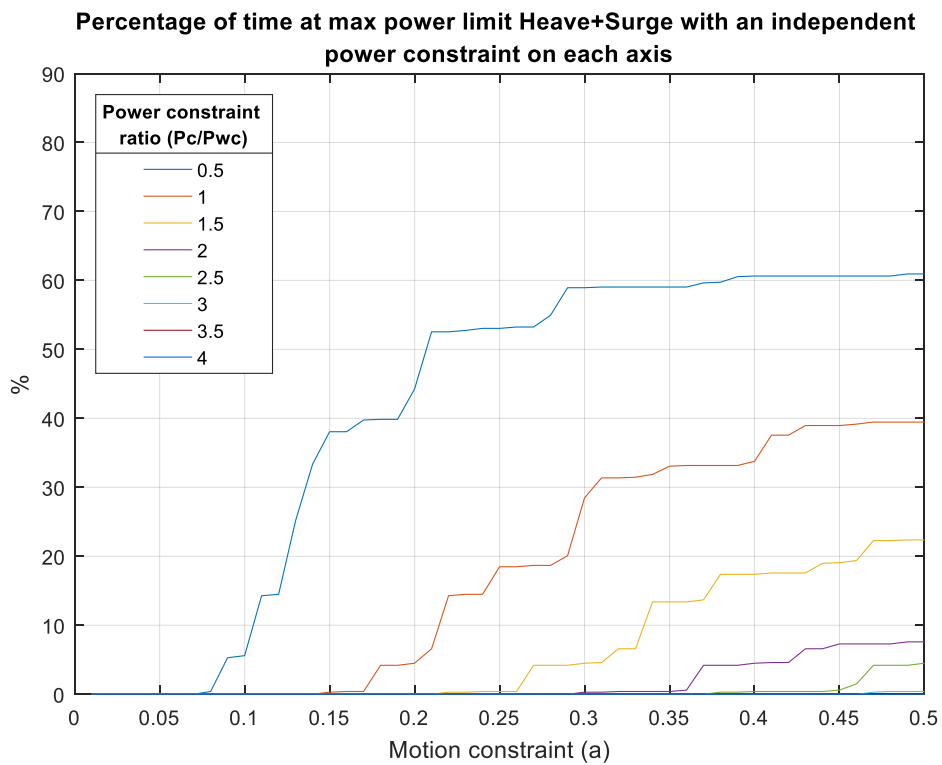


Figure 78: Percentage of time heave+surge configuration was operating at maximum power capacity with independent power constraints.

5.5 Conclusions

This chapter looked at the effect on energy production of mean power limits on the PTO under optimal and constrained motion. Under optimal unconstrained motion a power limitation will reduce any advantage surge or pitch has over heave. Relaxing the power constraints obviously increases absorbed power but there are decreasing marginal returns for additional power capacity.

Two types of power constraint were analysed, an independent form and a global form. With independent constraints the axes are limited to a defined fraction of the WEC rated capacity, the sum of which fractions equal the total rated capacity of the WEC. Under the global form each axis has an effective capacity up to the limit of the WEC. Independent power constraints on PTO axes is the more severe condition and the magnitude of the difference between the two forms for a given WEC capacity is dependent on motion constraints and hydrodynamic absorption characteristics. By selecting axes such as surge and heave that are each suited to short and long waves respectively, the WEC can absorb energy more consistently. Therefore a MA-PAWEC with the same rated capacity as a single axis equivalent can deliver significantly more energy than the single axis devices when operating under a global form of power constraint. A heave+surge MA-PAWEC should have its PTO system sized such that the sum of the individual limits of the PTO axes is higher than the rated output of the device. This would maximise time at the rated power for the MA-PAWEC and increase usage of downstream equipment thus better leveraging grid connection infrastructure.

Whereas the analysis with motion constraints in Chapter 4 concluded that the likely best combination for maximising energy absorbed per unit PTO length was to have heave as the dominant axis and surge as a minority axis, the conclusion under power and motion constraints is quite the opposite for certain scenarios. Under a low power constraint and larger motion constraint the surge mode outperforms heave. For financial viability a WEC should be operating at its power limit for a significant portion of the time implying a low power constraint relative to the wave climate. This suggests that for single axis devices surge may be the optimum choice if directionality and reaction force allows. For heave+surge MA-PAWECs the implications are that the optimum configuration to maximise energy per unit of PTO length may be to have most of the energy absorbed through the surge mode with long extension, coupled with a small extension heave mode.

The interplay between motion constraints (stroke length), power limit and hydrodynamic absorption characteristics makes deciding on the power rating and configuration of MA-

PAWECs a more complicated task than for a single axis device. But there is the potential for significant performance improvement from the correct selection of these parameters on a MA-PAWEC as well as relative cost savings on downstream power infrastructure.

6 Economics of MA-PAWECs

Parts of this chapter are derived from the OMAE 2013 conference paper ‘The Economics of Multi-Axis Point Absorber Wave Energy Converters’ [122].

In this chapter the economic factors for a WEC are identified and used to compare the generic heave and multi-axis concepts. For a performance comparison the generic body PAWEC results from Chapter 4 and Chapter 5 are used. Figure 26 (Section 4.1) shows the floating semi-submerged sphere generic point absorber devices to be considered, which are an approximation to existing heaving axisymmetric point absorbers which usually have an ellipsoidal, cylindrical or spherical/hemispherical geometry. The difference in costs between heave-PAWECs and MA-PAWECs are estimated and given economic scaling factor ranges. Using these scaling factors the performance and cost are compared to estimate the relative difference in levelised cost of electricity between heave-PAWECs and MA-PAWECs.

6.1 WEC Economics

In 2016 the state of the art was a structural efficiency of 1-1.5 MWh/ton for wave energy whereas wind is closer to 10 MWh/ton. Using tonnage as a proxy for cost, wave energy needs an order of 10 step change in structural efficiency. Wave energy has the potential to make a significant contribution to the global energy supply if this gap can be narrowed.

A chapter has been devoted to the economics of wave energy conversion because it should be a fundamental consideration in any wave energy device. The ultimate goal for the wave energy industry is an economically, environmentally and socially acceptable WEC, however rigorous assessment of environmental and social acceptability is beyond the scope of this work. The economics of WECs is concerned with the goal of reducing the cost of energy from the WECs and this can be achieved by either lowering the costs (capital and operational) or raising performance (increasing energy output). These options are shown in the matrix of Figure 79. Ideally wave energy developers want to end up in the lower right quadrant. Unfortunately (perhaps inevitably) new WECs start life in the upper left quadrant and developers must try and find a route to the lower right. Currently most WECs are in the OK or Poor quadrants rather than the Excellent (which can be interpreted as generating competitively priced energy). The difficulty in reaching Excellent over the past forty years could mean that wave energy may never be destined to become competitive with the more common wind and

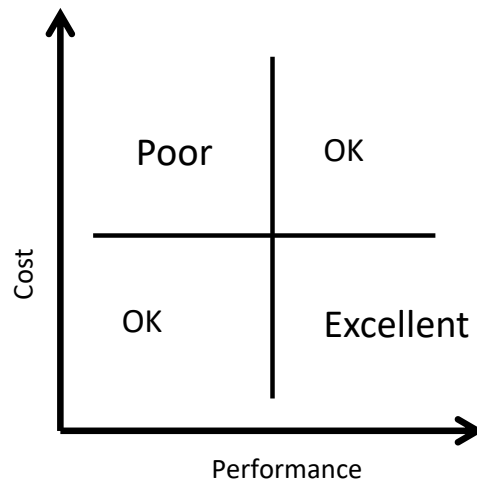


Figure 79: Economic matrix for a WEC

solar technologies, and forever remain a niche. Alternatively it could be taken as an incentive to find novel WEC topologies.

Given the necessary increase in complexity of a MA-PAWEC over a single axis equivalent device it is likely that the MA-PAWEC will reside in the upper quadrants of Figure 79 above single axis equivalents. As has been seen in earlier chapters though, the performance of a MA-PAWEC is expected to be significantly higher than an equivalent single axis device, with better leverage of power infrastructure. Therefore a multi-axis PTO approach could offer improved performance with the penalty of increased complexity and cost of the device. The aim of this chapter is to estimate if the improved performance of a MA-PAWEC outweighs this additional cost, giving a lower cost of electricity.

6.2 Cost Estimation

The cost estimation methodology used in this work follows that laid out by the Carbon Trust [123]. The key factors that determine the cost of energy are capital costs, operating and maintenance costs (O&M) and the performance of the device. These key factors can be broken down into sub-categories.

- Performance (Annual Energy Production)
 - Device characteristics
 - Resource
 - Losses
 - Availability
- Capital Cost
 - Structural
 - Mechanical and Electrical (PTO)
 - Mooring
 - Installation
 - Grid connection
 - Project management
- Operating Costs
 - Planned maintenance
 - Unplanned maintenance

The performance of the device represents the income over the lifetime of the installation. A higher performance device generates more income, but Capital and O&M costs must be weighed against this. A high performance device (high energy capture) can afford to be more expensive and yet provide a lower cost of energy than a cheap, poor performing device, equivalent to being in the top right and bottom left quadrants of Figure 79 respectively.

Each item of cost will be considered to estimate the relative difference between the heave and multi-axis approach. By assigning a relative cost for the MA-PAWEC, indexed to the heave device, the uncertainty associated with material, labour costs, technological advancement etc. can be removed. This method of assessment is designed to assist in choosing a cost-effective device rather than a certain technology.

6.2.1 Performance Characteristics

‘Performance Characteristics’ is a characterisation of the device performance in terms of wave loading. To describe the MA-PAWEC performance relative to the heaving device the upper and lower bounds of the energy production figures calculated in Chapter 4 and Chapter 5 are used. These are listed below in Table 3:

Modelling Condition	Lower Bound scaling factor	Upper Bound scaling factor
Unconstrained optimum motion	3	3
Independent motion constraints (0-0.5 times radius of device) with optimum motion	1.69	1.81
Power and motion constraints (0-0.5 times radius of device) with optimum motion	1.19	2.21

Table 3: Upper and lower bounds of the scaling factors relating the performance of the MA-PAWEC with that of the heave device.

The range of performance scaling factor is 1.19 to 3. The unconstrained upper bound of three is unrealistic due to linearity assumptions and engineering constraints therefore the range will be taken using the lowest and highest bounds of the constrained models. Both the lowest and highest bounds are from the ‘power and motion constrained model’ range from 1.19 to 2.21, or 19% and 121% higher. The lower boundary of 1.19 occurs at the maximum motion constraint with the lowest power constraint. The upper boundary of 2.21 occurs at the maximum motion constraint but with the second lowest power constraint.

Resource

The resource describes the energy available to a WEC, typically using the parameters of wave height and period. A heaving point absorber can absorb energy from waves incident upon it from any direction due to its vertical motion. In contrast, a MA-PAWEC may have a directional dependency arising from the choice of axes on which the multiple PTOs are applied. Thus, for MA-PAWECs the direction of the incident energy at the site is important. Directional data is more difficult to obtain than wave height and period as it requires special methods of measurement [124] which may complicate site selection for MA-PAWECs. The performance results used here are dependent on the distribution of waves by height and period so these performance factors are only representative for similar wave distributions to that of Table 2.

Losses and Availability

In this case, losses refer to the various energy losses that take place between the PTO system and the point at which the energy enters the grid on shore [123]. The losses are usually expressed as a reduction factor that can be applied to the output of the PTO. For the heave-PAWEC and the MA-PAWEC the reduction factor will be similar as it is assumed the same acceptable loss limits are used when sizing the electrical infrastructure in both cases.

The availability of a device is a measure of how much time it is running without fault [123]. Equal availability is assumed based on the premise that each device is using the same technology. In reality the additional components associated with multiple PTO axes means there is more to go wrong with a MA-APWEC that could mean increased maintenance. Conversely, a MA-PAWEC may be able to continue to operate with a single axis if one fails and so reduce the urgency of maintenance visits whilst maintaining a higher average availability.

6.2.2 Capital Costs (CAPEX)

The breakdown of capital costs for each wave energy project will be unique to the WEC in question and may be widely different depending on the technologies. Some examples for average cost breakdowns are shown in Figure 80. The PTO & Control sections are the areas most impacted by multi-axis PTO which in these breakdowns represent 23% of the capital cost.

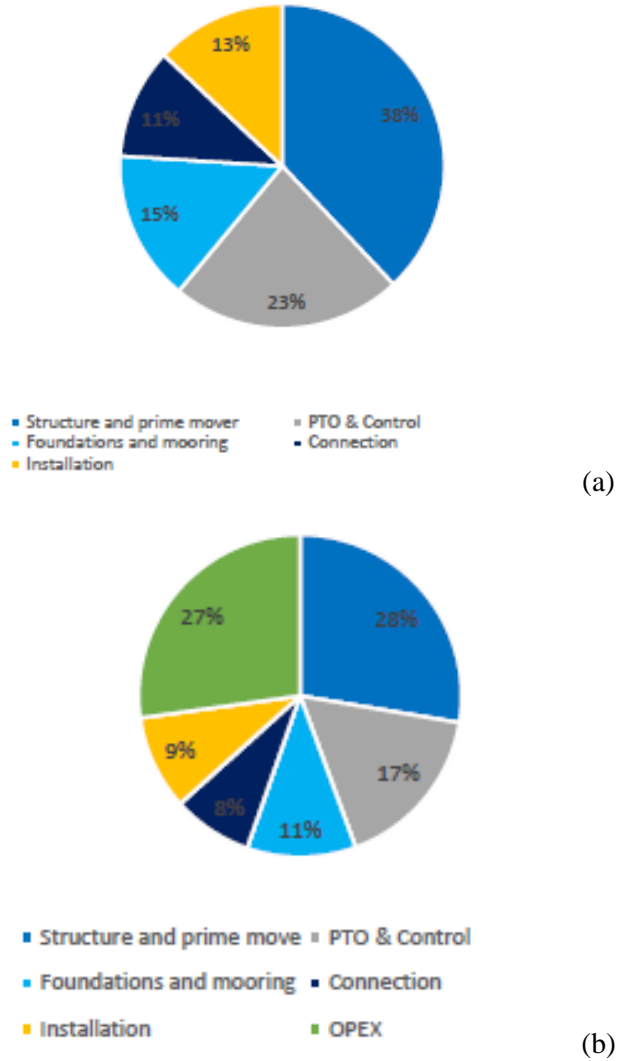


Figure 80: Example cost breakdowns for WECs. (a) Capital cost breakdown. (b) Project cost breakdown. [22]

Structural

The structure must interact with the waves and support the power conversion equipment. It can be the largest cost of a WEC in some cases [123] [35], although this depends heavily on the WEC design. The cost of the structure will be a function of the amount of material and the complexity of fabrication.

A MA-PAWEC may have a more complex structure than a similar heave-PAWEC as there needs to be support for additional PTO equipment. The additional structure and space for the PTO will depend heavily on the type of PTO, its configuration and the design of the WEC. A floating WEC with PTO units attached to mooring lines will not require a significantly more complicated or larger structure than a single PTO unit WEC. If the WEC has its reaction force

provided by an external superstructure then there may be additional cost for providing reaction against multi-directional forces. However, heave devices are already subjected to multi-directional forces due to incident waves and these must be dealt with by the superstructure in some way.

Much of the cost of a WEC is driven by the need for survivability [39], although this may not always be the case. Individual device configurations and future technological advances may significantly alter what drives the cost of a WEC. In order to survive, the WEC structure must withstand extreme loading caused by storms. Under such conditions the structural loading of a MA-PAWEC and a heave-PAWEC of similar design has little to do with PTO characteristics and will be assumed to be the same. This translates into an equal cost assumption for survivability structural requirements.

Comparing like-for-like, the additional structural cost required for a MA-PAWEC should be predominantly driven by the increased complexity of the internal structure rather than an increase in material volume or structural reinforcements. At the lower bound of the range the structural cost could be the same (a factor of 1) for a MA-PAWEC. For an upper bound a conservative factor could be 1.5.

Structural economic scaling factor range = 1 - 1.5

Mechanical and Electrical (PTO)

The PTO mechanism can be of any configuration and could be hydraulically or mechanically connected to a rotary generator, or have a direct drive with linear or rotary generators [110] [109]. A hydraulic system could be advantageous for a multiple axis system as all PTO axes can utilise the same accumulator and hydraulic motor. In scaling up from a single axis PTO, any additional PTO axes require only an additional actuator and the subsequent scaling up of the accumulator and motor. A multi-axis hydraulic system was already in use with the Pelamis device [125]. Hydraulic systems - although more easily extended to multi-axis - are not as efficient as direct-drive generators, achieving a maximum efficiency of 75-80% compared to a direct drive generator maximum efficiency of 90% [126]. However they are better able to benefit from the effect seen in Chapter 5 which has shown that MA-PAWECs can yield significant benefits in increasing energy output for a given rated PTO capacity.

With a direct drive system there is no mechanical interface coupling the floating body to the generator. Thus there are fewer moving parts and this therefore has the potential to provide a

simpler system. This could offer lower maintenance requirements and higher efficiencies. A problem with direct drive generators is the requirement to react to large forces at a velocity typically in the range 0.5-2 m/s. This is necessary if the generator is to provide a useful amount of power. To produce these forces direct drive generators must be very large to provide the necessary airgap surface area [126]. For multi-axis devices that must have multiple actuators, the additional cost of direct drive generators may be prohibitive.

The cost of the additional PTO units will be a critical factor in determining if a MA-PAWEC device is viable. It is reasonable to assume that due to synergies between PTO units within an individual device, such as those described for hydraulics above, the additional cost of the PTO units will not be a simple product of the number of PTO axes. The cost may be less per PTO than for a single PTO device and so the lower bound for the PTO scaling factor is taken as 1.6 (equivalent to a 20% reduction in the per PTO unit cost). Conversely, the additional complexity may increase the cost per PTO and so the upper bound scaling factor is taken as 2.4 (20% more expensive per PTO).

PTO Economic Scaling Factor range = 1.6 – 2.4

It is assumed that any differences between the PTO units for each axis such as greater excursion or power limit in one axis such as that discussed in Chapter 5 is accounted for in this scaling factor.

Mooring

The primary purpose of a mooring is to keep the device on station. It must also be sufficiently cost effective to make the device viable [127]. There are many guidelines and regulations adapted from the offshore industry that can be adapted for WECs (e.g. from DNV [128]). Point absorber WECs are typically floating or neutrally buoyant structures and as such the most suitable mooring configuration (in terms of station-keeping and cost) are either spread moorings (catenary or multi-catenary) or single point mooring either to a taught or catenary moored buoy [129]. The PTO in Figure 26 could be a representation of a PAWEC attached to a floating structure such as an offshore wind turbine, but the PTO could equally be reversed and be attached to mooring lines. The role of the mooring system is to resist both the horizontal and vertical forces of the waves. With a heave device the vertical forces are damped by the PTO but the horizontal forces must be resisted by the mooring. By incorporating a horizontal PTO the surge/sway reciprocal forces acting on the mooring will generate power and lower the fatigue loading through the damping.

Mooring costs are driven largely by depth and the extreme loading requirement [129] [127] [123] [130]. As the deployment site and extreme loading is assumed to be the same for these two similar devices there should be little difference in cost per mooring line. Whereas a heave device can operate with a single mooring, a MA-PAWEC may need multi-directional mooring to provide the necessary reaction forces along the different axes. The additional cost of this multi-directional mooring will be heavily dependent on the design of the WEC and whether it is fixed to another floating structure such as an offshore wind turbine. If an inertial mass is used for the reaction force then the mooring system may be the same as for the heaving device. The lower bound therefore can be taken as 1. The upper bound can be taken as 3 to represent an additional two mooring lines/connections to potentially provide multi-axis reaction forces.

Mooring Economic Scaling Factor range = 1 - 3

Co-location of WECs and Wind Turbines

It can make economic sense to deploy wave energy converters at offshore wind turbine sites. The turbines and WECs can share grid infrastructure and port facilities, and environmental planning costs are shared. The water between turbines is usually dead space unsuitable for commercial navigation and so WECs would not increase the amount of restricted area at sea. Access to both devices will need to be managed which will affect layout. The stable nature of the turbine mount may be able to be used for power-take-off while damping any motions of a floating turbine. However the amount of energy generated will likely be small compared to the turbine.

Installation and Project Management

Installation costs are assumed to be equal for the two devices as they are of the same size and should therefore present similar difficulty for installation. Any additional costs due to a more complicated mooring configuration are assumed to be incorporated into the mooring scaling factor.

Project management covers the costs associated with managing the installation and operation of the devices. Although a MA-PAWEC is a more complicated device to engineer than a heave-PAWEC, the difference in project management costs should be small or non-existent.

Grid Connection

The electrical infrastructure for the MA-PAWEC may need to be capable of carrying more power than a heave PAWEC. However, as was shown in Chapter 5 a MA-PAWEC can deliver almost twice the amount of energy over a given period of time with the same rating grid connection as a heaving PAWEC under certain wave distributions. The lower bound can therefore be taken as 1. Cost for electrical infrastructure typically increases in proportion to power delivered [131] [132]. The upper bound can be taken as 2, representing the doubling of rated power that was used for the MA-PAWEC in Chapter 5.

Grid Connection Economic Scaling Factor range = 1 - 2

6.2.3 Operating Costs (OPEX)

The operating costs are those incurred over the lifetime of the device to keep it in working order. The costs can be incurred through monitoring, refit, insurance, licences and maintenance, both planned and unplanned. As an approximate measure operating costs can be taken as 4.5% of the capital costs per year [130] or alternatively as a proportion of the total project cost such as the 27% in Figure 80. The largest proportion of this is usually maintenance [123]. As the heave and multi-axis devices are assumed to employ the same technology, it can be assumed that their maintenance schedule will be broadly the same but there is more to maintain with the additional PTOs of the MA-PAWEC so there is an additional cost incurred. If however the 4.5% a year approximation is used then the increase in OPEX costs are automatically increased in line with the capital cost and no separate scaling factor is required.

6.3 Levelised Cost of Energy

The levelised cost of energy (LCOE) of a WEC is the price at which the WEC must sell electricity to cover the capital costs and all future cash outflows. It is this ratio between the total cost (capital, maintenance, operation, etc.) and the energy produced that should be minimised [91]. It is given by Equation 39 (adapted from [123]) in which n is the economic lifespan of the WEC, t is a unit of time (in years if using AEP) and r is a discount rate per unit time to be applied to future cash flows.

$$LCOE = \frac{CAPEX + \sum_{t=1}^n \frac{OPEX_t}{(1+r)^t}}{\sum_{t=1}^n \frac{AEP_t}{(1+r)^t}}$$

Equation 39

It is not the LCOE that is of interest here but the relative LCOE between the MA-PAWEC and the heave PAWEC. The assumptions used to calculate the energy performance make it unsuitable for providing a reliable estimate of LCOE directly. Assuming a discount rate that maintains the 4.5% relationship between OPEX and CAPEX the ratio of LCOE for a MA-PAWEC vs. a heave PAWEC can be written as:

$$LCOE_{REL} = \frac{1.045C_{SF}}{P_{SF}},$$

Equation 40

where C_{SF} is the total CAPEX scaling factor and P_{SF} is the performance scaling factor.

Table 4 summarises the capital cost scale factors for the MA-PAWEC device relative to the heave-PAWEC device with example weightings for each category taken from the Carbon Trust [123]. Multiplying the scale factors by the weightings gives weighted scaling factors that are summed to provide the total CAPEX scaling factor C_{SF} .

CAPEX component	Scale factor range		% Weighting of CAPEX Carbon Trust CAPEX breakdown	Weighted MA-PAWEC scale factors	
	Lower Bound	Upper Bound		Lower Bound	Upper Bound
Structural	1	1.5	27%	27%	41%
PTO	1.6	2.4	49%	78%	118%
Mooring	1	3	5%	5%	15%
Installation	1	1	13%	13%	13%
Grid Connection	1	2	4%	4%	8%
Project Management	1	1	2%	2%	2%
Total			100%	129%	196%

Table 4: CAPEX scale factors for a MA-PAWEC device relative to a heave device.

The scale factors of 129% and 196% represent the capital cost of the MA-PAWEC relative to the heave device i.e. 29% and 96% more expensive for the lower and upper bounds respectively. The most significant contributor to this cost is the mechanical and electrical (PTO) aspects which represents the largest single weighted cost in the CAPEX breakdown of Table 4 and is also subject to a high scaling factor.

These upper and lower cost factors can now be paired up with the upper and lower bounds of the performance scaling factor in the relative LCOE equation to give a 4x4 results matrix shown in Table 5.

Relative LCOE		P _{sf}	
		Upper	Lower
C _{sf}	Upper	93%	172%
	Lower	61%	114%

Table 5: Relative LCOE matrix for the upper and lower bounds of the performance and CAPEX scaling factors.

From the numbers in Table 5 it is clear that MA-PAWECs have the potential to both dramatically lower the LCOE and also raise it. The performance improvement of the MA-PAWEC over the heave is sufficiently large as to lower the LCOE even with the upper CAPEX bound. Well-designed MA-PAWECs could approach a 40% reduction in LCOE under the CAPEX breakdown of Table 4, although this is the optimistic view.

The relative LCOE figures will be sensitive to shifts in the weightings of the CAPEX breakdown. The two largest CAPEX items in Table 4 are the structural and PTO expenditure which combined represent 76% of the total CAPEX cost and also have widely different scaling factors. The relative LCOE figures will therefore be most sensitive in this case to shifts in the weightings of these. Using a cost breakdown such as that of the Sloped IPS Buoy, where Structure represents 58% [35] of the capital cost, would give a lower total Capital Cost scaling factor and hence lower relative cost of energy. The effect of changing the weightings can be seen in Table 6 and Table 7 which are for variations of the weightings of structure and PTO between 10% and 66%.

Relative LCOE		P _{sf}	
		Upper	Lower
C _{sf}	Upper	100%	186%
	Lower	66%	123%

Table 6: Relative LCOE matrix for Structure weighting of 10%, PTO of 66%

Relative LCOE		P _{sf}	
		Upper	Lower
C _{sf}	Upper	76%	141%
	Lower	50%	93%

Table 7: Relative LCOE matrix for PTO weighting of 10%, Structure of 66%

Increasing PTO weighting increases the relative LCOE from the values in Table 5 but still manages a significant reduction under the optimistic scenario of low cost/high performance with only a 5 percentage point difference. Conversely reducing the PTO weighting reduces the relative LCOE. This linear trend is plotted in Figure 81 using the average of the two performance scaling factor bounds to produce a relative LCOE envelope.

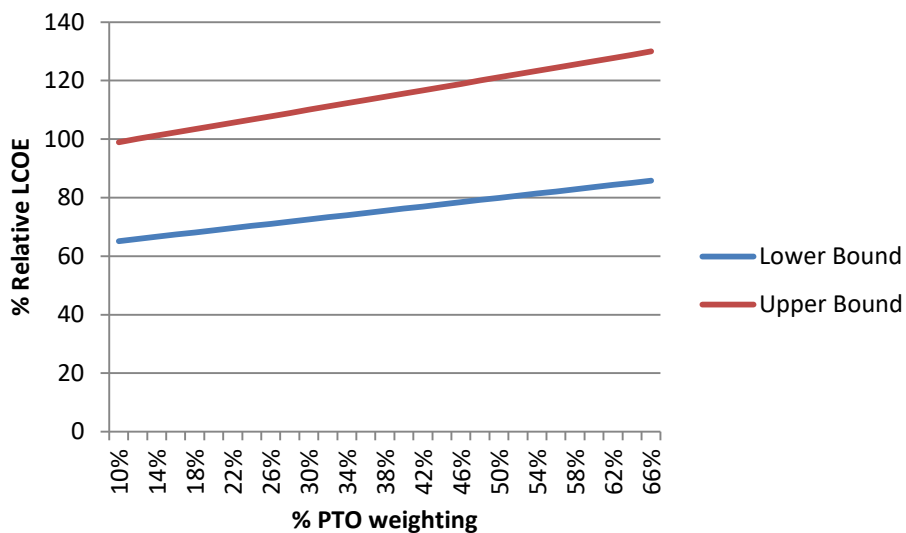


Figure 81: Relationship between PTO weighting and relative LCOE.

The potential for reducing LCOE is suggested by these results with a maximum reduction under the most optimistic scenario presented as 50%. This is still short of the 80-90% decrease that would make it competitive with wind but it is a promising result and would represent a significant improvement on structural efficiency over existing devices. This would only be achieved though for MA-PAWECs that managed to incorporate additional axes at the lower cost boundary while still achieving high performance. At the lower end of performance the cost of energy is higher from a MA-PAWEC unless the PTO is a particularly small proportion

of the CAPEX. MA-PAWECs are therefore not a panacea and it will not necessarily provide a lower LCOE, quite the opposite when considering the pessimistic scenarios of +80-90% above heave.

The validity of these results are limited by the fact that the performance data is obtained from a particular distribution of waves. Changing this distribution may change the performance scaling factor and hence the relative LCOE by the proportional amount. The directional nature of the site resource is also key for the economics if the MA-PAWEC has a directional dependency. However, many sites have a dominant wave direction and it is likely that a 2-axis PTO MA-PAWEC, correctly aligned, can achieve similar performance to a directionally independent 3 axis device but with a lower PTO cost. The directional characteristics will be site specific and so a MA-PAWEC deployment will require wave direction data as well as the traditional height and period data.

6.4 Conclusions

This economic analysis has used the Carbon Trust cost estimation methodology to compare a generic heave-PAWEC with a generic two axis heave+surge MA-PAWEC based on relative economic scaling factors indexed to the heave device. Both devices were assumed to have the same floating semi-submerged spherical body under motion and power constraints. The cost of a MA-PAWEC is estimated to be between 29% and 96% higher than an equivalent heaving device but it could compensate for this with improved performance. The MA-PAWEC and the heave PAWEC were compared on a levelised cost of energy (LCOE) basis relative to the heave device with upper and lower bounds to the cost and performance scaling factors. Under pessimistic scenarios with the PTO making up a large portion of the CAPEX (~60%) along with the upper estimate of cost and lower estimate of performance, the relative LCOE was 80-90% higher than heave. Under optimistic scenarios with the PTO making up a small portion of the CAPEX (10-20%) along with the lower estimate of cost and upper estimate of performance, the relative LCOE showed reductions of 35-50%. Therefore even under these best case scenarios the maximum reduction in LCOE of 50% still falls short of the 90% reduction required for wind power structural efficiency parity. It is however a promising indication that MA-PAWECs could deliver lower LCOE than existing WECs. As the relative LCOE is most sensitive to the PTO cost, it suggests that multi-axis is most appropriate in those devices where PTO costs make up a small proportion of the total CAPEX, or the marginal cost of adding additional axes is low.

7 Conclusions

This concluding chapter presents the overall conclusions from this thesis which was intended to be a step along the path towards competitively priced wave energy by exploring the concept of a multi-axis point absorber and assessing it against a heaving point absorber, historically the most common design of point absorber.

From an initial assessment of the factors that affect the choice of axes for a MA-PAWEC there were several potential problems and benefits identified which make developing MA-PAWECs both appealing and daunting. A significant problem for designing MA-PAWECs is the interdependency and number of variables that affect the decision of how to configure the device, something the wave energy industry has been grappling with for 40 years on mostly single axis devices. Adding in additional axes complicates the choices further and progress can only be made by making assumptions. Yet the benefits may outweigh the challenges. MA-PAWECs should have a greater structural efficiency (MWh/ton) than single axis devices thus providing the potential for more energy from the same size device than a single axis equivalent. Out of phase oscillation modes can reduce the average to peak loading ratio of a multi-axis PTO system and with multiple PTO axes there are more control variables to play with which could allow novel control strategies, particularly in arrays. With well-chosen geometry and axes a wider bandwidth of absorption can be achieved by virtue of the different oscillation frequencies in different modes. When choosing axes for a MA-PAWEC two axes is likely to be a preferable choice combining a source mode and dipole mode.

The heaving (source mode) and surging (dipole mode) generic MA-PAWEC device investigated here performed well in both long and short waves and thus had a wider bandwidth than the single axis equivalents. The magnitude of this benefit was dependent on motion constraints and the wave (height and period). The advantage of this wider bandwidth becomes more evident with energy production values. Under the specific modelling conditions the heave response absorbed more energy than surge, and a heave+surge MA-PAWEC absorbed more energy than either single axis. Under a global weighted motion constraint of $0.5a$ the MA-PAWEC output was 50% higher than heave and 87% higher than surge. Under independent motion constraints of $0.5a$ the outputs were higher with the MA-PAWEC producing 80% more than heave and 124% more than surge. This improvement over the heave device decreases as the size of the body decreases due to the surge motion performing poorly in long waves. This highlights the importance of sizing MA-PAWEC devices appropriately to the site and selecting modes to favour different waves. Larger point

absorbers (relative to the incident wave field) may be the best candidates for adding dipole multi-axis PTO because of this effect. The results of this motion constraint analysis suggests a combination of heave as the predominant axis and a smaller excursion surge axis would be the most favourable combination to maximise energy generated per unit length of PTO.

Motion constraints limit the excursion of the device which is necessary for many types of PTO but PTO systems are also subject to power limits, both on individual axes and on the whole device. By selecting axes such as surge and heave that are each suited to absorb power in short and long waves respectively, the WEC can absorb energy more consistently. Therefore a MA-PAWEC with the same rated capacity as a single axis equivalent can deliver significantly more energy but without the additional cost of increasing the rating of the grid connection. Based on these results a heave+surge MA-PAWEC should have its PTO system sized such that the sum of the individual limits of the PTO axes is higher than the rated output of the device. This would maximise time at the rated power for the MA-PAWEC and increase usage of downstream equipment thus better leveraging grid connection infrastructure.

The analysis with motion constraints concluded that the likely best combination for maximising energy absorbed per unit PTO length was to have heave as the primary axis and surge as a secondary axis. Interestingly the conclusion under power and motion constraints is quite the opposite for certain scenarios. Under a low power constraint and larger motion constraint the surge mode outperforms heave. This is significant as for financial viability a WEC should be operating at its power limit for a significant portion of the time implying a low power constraint relative to the wave climate. This suggests that for single axis devices surge may be the optimum choice under these conditions if directionality and reaction force allows. For heave+surge MA-PAWECs the implications are that for low power constraints (relative to wave climate) and large available excursions then investing in the surge mode as the primary absorbing axis with heave as a secondary axis may be the most cost effective option. If the power constraint is large (relative to wave climate) and/or excursions are tightly limited the heave mode should be the primary absorbing axis with surge as a secondary axis.

This interplay between motion constraints (stroke length), power limits and hydrodynamic absorption characteristics makes designing a PTO system for a MA-PAWEC significantly more complicated than for a single axis device. But there is the potential for significant performance improvement from the correct selection of these parameters on a MA-PAWEC as well as relative cost savings on downstream power infrastructure. When comparing the relative cost of equivalent MA-PAWEC and heaving devices the additional cost of a MA-PAWEC is estimated to be between 29% and 96% higher but the improved energy generation can compensate for this. Under pessimistic scenarios of a higher CAPEX and low

performance improvement, the MA-PAWEC produced a relative LCOE 80-90% higher for the heave device. Under optimistic scenarios of a lower CAPEX and high performance improvement, the MA-PAWEC produced a relative LCOE 35-50% lower than for the heave device. These reduction figures are a promising indication that MA-PAWECs can deliver lower LCOE than existing WECs, but the higher figures in excess of the heave LCOE serve as a warning that it will not automatically be so. As the relative LCOE of a MA-PAWEC is most sensitive to the PTO cost, it suggests that multi-axis is most appropriate in those devices where PTO costs make up a small proportion of the total CAPEX, or the marginal cost of adding additional axes is low. MA-PAWECs have the potential to make a significant (in the order of tens of percent) reduction in LCOE compared to the incumbent heave devices if they are designed appropriately.

As a relatively underdeveloped avenue of the wave energy industry the MA-PAWEC route offers plenty of potential advantages over existing point absorber topologies along with some significant challenges. A path to competitively priced wave energy is not yet clear for MA-PAWECs, but they offer the opportunity of a new generation of WECs that have some tantalising possibilities despite their complexity.

7.1 Recommendations for Further Work

There are innumerable directions in which work on MA-PAWECs can be extended as there is still so little explicit work. A significant drawback with the modelling formulation used in this thesis is its inability to be used with irregular waves. Extending this work in to the time domain and with non-optimal motion would allow more confidence to be placed in the results of any comparison between devices along with more reliable figures to use to assess performance of MA-PAWEC configurations in general. The effect of ratings of PTO axes vs. the total rating of the WEC should be investigated further as it promises to yield benefits for MA-PAWECs in improving time at rated capacity. There is also potential for benefits from greater array control by virtue of additional axes to apply damping and spring, thus altering the radiation pattern and energy absorption characteristics. As directionality is important for the dipole modes of operation it would be interesting to investigate under what conditions it becomes worth adding additional axes to make the device directionally independent in all modes. Whether there are enough deployment sites (close to demand, sufficient infrastructure etc.) with directional characteristics to make directional independence necessary on a MA-PAWEC would also be an interesting question to answer.

References

- [1] United Nations Framework Convention on Climate Change, “The Paris Agreement,” 2019. [Online]. Available: <https://unfccc.int/process#:a0659cbd-3b30-4c05-a4f9-268f16e5dd6b>. [Accessed 12 January 2019].
- [2] DECC, “News,” gov.co.uk, 19 April 2012. [Online]. Available: <http://www.decc.gov.uk/en/content/cms/news/climatearticle/climatearticle.aspx>. [Accessed 20 April 2012].
- [3] International Energy Agency, “World Energy Investment 2018,” IEA Publications, 2018.
- [4] IMechE, “UK 2050 Energy Plan - The Challenge Continues, Version 1-4a,” IMechE, 2011.
- [5] European Commission, “The Commission presents strategy for a climate neutral Europe by 2050 - Questions and Answers,” 28 November 2018. [Online]. Available: http://europa.eu/rapid/press-release_MEMO-18-6545_en.htm. [Accessed 12 January 2019].
- [6] European Commission, “2030 Climate and Energy Framework,” [Online]. Available: https://ec.europa.eu/clima/policies/strategies/2030_en. [Accessed 12 January 2019].
- [7] Committee on Climate Change, “How the UK is progressing,” [Online]. Available: <https://www.theccc.org.uk/tackling-climate-change/reducing-carbon-emissions/how-the-uk-is-progressing/>. [Accessed 12 January 2019].
- [8] K. Gunn and C. Stock-Williams, “Quantifying the Global Wave Power Resource,” *Renewable Energy*, vol. 44, pp. 296-304, 2012.
- [9] BBC News, “Wave power firm Pelamis calls in administrators,” 21 November 2014. [Online]. Available: <https://www.bbc.co.uk/news/uk-scotland-scotland-business-30151276>. [Accessed 21 February 2019].
- [10] BBC News, “Jobs lost as wave energy firm Aquamarine Power folds,” 23 November 2015. [Online]. Available: <https://www.bbc.co.uk/news/uk-scotland-scotland-business-34901133>. [Accessed 21 February 2019].
- [11] DECC, “Wave and Tidal Energy: Part of the UK's energy mix,” 22 January 2013. [Online]. Available: <https://www.gov.uk/wave-and-tidal-energy-part-of-the-uks-energy-mix>. [Accessed 13 November 2014].
- [12] Ocean Energy Europe, “Ocean Energy Europe: Key trends and statistics 2018,” Ocean Energy Europe, 2019.

References

- [13] National Statistics, “UK Energy in brief 2018,” Department for Business, Energy and Industrial Strategy, 2018.
- [14] Wind Energy, “Wind Energy in Europe 2018: Trends and Statistics,” Wind Energy, 2019.
- [15] The Carbon Trust, “TINA - Marine Energy,” The Carbon Trust, 2012.
- [16] J. Falnes and J. Hals, “Heaving buoys, point absorbers and arrays,” *Philosophical Transactions of the Royal Society A*, vol. 370, pp. 246-277, 2012.
- [17] M. E. McCormick, *Ocean Wave Energy Conversion*, Mineola, N.Y.: Dover Publications Inc., 2007.
- [18] A. Falcao, “Wave Energy Utilization: A Review of the Technologies,” *Renewable and Sustainable Energy Reviews*, vol. 14, pp. 899-918, 2010.
- [19] S. Salter, “Wave Power,” *Nature*, vol. 249, pp. 720-724, 1974.
- [20] S. Salter, “Looking Back,” in *Ocean Wave Energy; Current Status and Future Perspectives*, J. Cruz, Ed., Springer, 2008.
- [21] International Energy Agency, “Annual Report 2010: Implementing Agreement on Ocean Energy Systems (OES-IA),” OES-IA, 2010.
- [22] Wave Energy Scotland, “Wave Energy Scotland,” 2017. [Online]. Available: <http://www.waveenergyscotland.co.uk/>. [Accessed Jan 2017].
- [23] Supergen UKCMER, “Supergen UKCMER,” [Online]. Available: <https://www.supergen-marine.org.uk/>. [Accessed 21 January 2019].
- [24] US Department of Energy, “Marine and Hydrokinetic Technology Database,” [Online]. Available: <http://www1.eere.energy.gov/water/hydrokinetic/default.aspx>. [Accessed February 2012].
- [25] J. Cruz, Ed., *Ocean Wave Energy: Current status and future perspectives*, Leipzig: Springer, 2008.
- [26] International Energy Agency: Ocean Energy Systems, “Annual Report 2011,” IEA-OES, 2011.
- [27] Marine Power Systems, “WaveSub - The future of energy,” [Online]. Available: <http://marinepowersystems.co.uk/>. [Accessed 21 February 2019].
- [28] B. Drew, A. R. Plummer and M. N. Sahinkaya, “A Review of Wave Energy Converter Technology,” *Proc. IMechE Part A: J. Power and Energy*, vol. 223, pp. 887-902, 2009.
- [29] J. Newman, *Marine Hydrodynamics*, MIT Press, 1977.

- [30] M. E. McCormick, *Ocean Engineering Mechanics*, Cambridge University Press, 2010.
- [31] The COMET Program, “Nearshore wave modelling Print Version,” [Online]. Available: http://stream1.cmatc.cn/pub/comet/MarineMeteorologyOceans/NearshoreWaveModeling/comet/oceans/nearshore_wave_models/print.htm. [Accessed 4 February 2019].
- [32] Flow-3D, “Flow3D - Waves,” [Online]. Available: <https://www.flow3d.com/modeling-capabilities/waves/>. [Accessed 12 November 2017].
- [33] Wavehub, “Wavehub,” [Online]. Available: <https://www.wavehub.co.uk/>. [Accessed 3 March 2018].
- [34] Channel Coastal Observatory, “WaveHub statistics,” [Online]. Available: http://www.channelcoast.org/data_management/real_time_data/charts/?chart=116&tab=stats&disp_option=. [Accessed Feb 2018].
- [35] T. W. Thorpe, “A brief review of wave energy, Report no. R120,” UK Department of Trade and Industry, 1999.
- [36] A. Cornett, “A global wave energy resource assessment,” in *Sea Technology*, 2008.
- [37] L. Duckers, “Wave Energy,” in *Renewable Energy*, G. Boyle, Ed., 2004.
- [38] H. Polinder and M. Scuotto, “Wave energy converters and their impact on power systems’,” in *Proceedings of the International Conference on Future Power Systems*, 2005.
- [39] M. Leijon et al., “An electrical approach to wave energy conversion,” *Renewable Energy*, vol. 31, pp. 1309-1319, 2006.
- [40] M. Pontes et al., “An atlas of the wave-energy resource in Europe,” *J Offshore Mechanical Arctic Engineering*, vol. 118, pp. 307-309, 1996.
- [41] Climate Change in Wales, “Other Marine Energy,” [Online]. Available: <http://resources.hwb.wales.gov.uk/VTC/2012-13/20032013/climate/eng/cc-reducing-climate-change/cc-renewable-energy2/cc-other-marine-energy.htm>. [Accessed 12 February 2019].
- [42] T. Pontes, R. Aguiar and H. Pies, “A nearshore wave energy atlas for Portugal,” *J Offshore Mechanics and Arctic Engineering*, vol. 127, no. 3, pp. 249-255, 2005.
- [43] A. Clement et al., “Wave energy in Europe: Current status and perspectives,” *Renewable and Sustainable Energy Reviews*, vol. 6, no. 5, pp. 405-431, 2002.
- [44] J. Falnes, “A review of wave energy extraction,” *Marine Structures*, vol. 20, no. 4, pp. 185-201, 2007.

References

- [45] A. F. O. Falcao, "Design and construction of the Pico OWC wave power plant," in *Proc. of the 3rd European Wave Energy Conference*, 1998.
- [46] Y. Torre-Enciso, I. Ortubia, L. I. Lopez de Aquileta and J. Marques, "Mutriku Wave Power Plant; from the thinking out to the reality," in *Proc. of the 8th European Wave and Tidal Energy Conference*, Uppsala, 2009.
- [47] Hydrocap, "Seacap," [Online]. Available: http://www.hydrocap.com/index.php?l_nr=index.php&l_nr_c=aeb764a6a854dd20beb97ec048c4ac14&l_idpa=17&langue_id=1. [Accessed 4 February 2014].
- [48] V. Baudry and A. Babarit, "Assessment of the annual energy production of a heaving wave energy converter sliding on the mast of a fixed offshore wind turbine," in *Proc. of the World Renewable Energy Congress XI*, Abu Dhabi, 2010.
- [49] Renewable-Technology.com, "Green Ocean Energy Wave Treader, United Kingdom," [Online]. Available: <http://www.renewable-technology.com/projects/green-ocean-wave-treader/>. [Accessed 5 August 2013].
- [50] M. Folley and T. J. T. Whittaker, "Analysis of the nearshore wave energy resource," *Renewable Energy*, vol. 34, pp. 1709-1715, 2009.
- [51] T. Whittaker and M. Folley, "Nearshore oscillating wave surge converters and the development of Oyster," *Philosophical Transactions of the Royal Society A*, vol. 370, no. 1959, pp. 345-364, 2012.
- [52] Aquamarine Power, "How Oyster Wave Power Works," [Online]. Available: <http://www.aquamarinepower.com/technology/how-oyster-wave-power-works.aspx>. [Accessed 12 December 2014].
- [53] U. Korde, "Control system applications in wave energy conversion," in *Proceedings of OCEANS 2000 MTS/IEEE*, 2000.
- [54] B. M. Count, "Wave Power - A problem searching for a solution," in *Power from Sea Waves*, B. M. Count, Ed., London, Academic Press, 1980, pp. 11-27.
- [55] R. Yemm, D. Pizer, C. Retzler and R. Henderson, "Pelamis: experience from concept to connection," *Philosophical Transactions of the Royal Society A*, vol. 370, pp. 365-380, 2012.
- [56] R. Henderson, "Design, simulation and testing of a novel hydraulic power take-off system for the Pelamis wave energy converter," *Renewable Energy*, vol. 31, pp. 271-283, 2006.
- [57] J. H. Todalshaug, "Practical limits to the power that can be captured from ocean waves by oscillating bodies," *International Journal of Marine Energy*, Vols. 3-4, pp. e70-e81, 2013.

- [58] Jumanji Solar, “Pelamis,” 26 June 2004. [Online]. Available: <https://www.flickr.com/photos/jumanjisolar/4377442735/in/photostream/>. [Accessed 19 May 2019].
- [59] Buch der Synergie, “Teil C,” [Online]. Available: http://www.buch-der-synergie.de/c_neu_html/c_06_08_wasser_wellenenergie_d_bis_norwegen.htm. [Accessed July 2014].
- [60] D. Evans, D. Jeffery, S. Salter and J. Taylor, “Submerged Cylinder Wave Energy Device: Theory and Experiment,” *Applied Ocean Research*, vol. 1, pp. 3-12, 1979.
- [61] H. Heikkinen, M. J. Lampinen and J. Boling, “Analytical Study of the interaction between wave and cylindrical wave energy converters oscillating in two modes,” *Renewable Energy*, vol. 50, pp. 150-160, 2013.
- [62] D. Pizer, “Maximum wave-power absorption of point absorbers under motion constraints,” *Applied Ocean Research*, vol. 15, pp. 227-234, 1993.
- [63] Ocean Power Technologies, “PowerBuoy Technology,” [Online]. Available: <https://www.oceanpowertechnologies.com/powerbuoy>. [Accessed Nov 2017].
- [64] A. McCabe, “Constrained optimisation of the shape of a wave energy collector by genetic algorithm,” *Renewable Energy*, vol. 51, p. 271, 2013.
- [65] Ocean Power Technologies, “Media Resources,” [Online]. Available: <https://www.oceanpowertechnologies.com/resources>. [Accessed 19 May 2019].
- [66] Marine Power Systems, “Marine renewable milestone hit as UK 'WaveSub' unveiled for sea-based testing,” [Online]. Available: <http://marinepowersystems.co.uk/marine-renewable-milestone-hit-as-uk-wavesub-unveiled-for-sea-based-testing/>. [Accessed 21 February 2019].
- [67] D. Bull, D. S. Jenne, C. S. Smith, A. E. Copping and G. Copeland, “Levelised cost of energy for a backward bent duct buoy,” *International Journal of Marine Energy*, vol. 16, pp. 220-234, 2016.
- [68] M. D. House, “Oscillating Water Column,” [Online]. Available: <https://wiki.uiowa.edu/display/greenergy/Oscillating+Water+Column>. [Accessed February 2017].
- [69] WaveDragon, “Wave Dragon Home Page,” [Online]. Available: <http://www.wavedragon.net/>. [Accessed Nov 2017].
- [70] Global Greenhouse Warming, “WaveDragon,” [Online]. Available: <http://www.global-greenhouse-warming.com/wave-dragon.html>. [Accessed Nov 2017].
- [71] AWS Ocean Energy Ltd, “Archimedes Wave Swing,” [Online]. Available: <http://www.awsocan.com/>. [Accessed Nov 2017].

References

- [72] Bombora Wave Power, “Bombora Wave Power,” [Online]. Available: <http://www.bomborawave.com/>. [Accessed 17th January 2018].
- [73] OpenEI, “MHK Technologies/Archimedes Wave Swing,” [Online]. Available: https://openei.org/wiki/MHK_Technologies/Archimedes_Wave_Swing. [Accessed 15 January 2019].
- [74] The Switch Report, “Bombora Wave Power heads for the sea floor,” [Online]. Available: <http://www.theswitchreport.com.au/business/bombora-wave-power/>. [Accessed Nov 2017].
- [75] Corpower Ocean, “Corpower Wave Energy Converter,” [Online]. Available: <http://www.corpowerocean.com/corpower-technology/corpower-wave-energy-converter/>. [Accessed Nov 2017].
- [76] Wello, “Wello Wave energy,” [Online]. Available: <https://wello.eu/>. [Accessed November 2017].
- [77] Carnegie Wave, “Perth Project,” [Online]. Available: <http://www.carnegiwave.com/projects/perth-project.html>. [Accessed 25 March 2015].
- [78] 40SouthEnergy Ltd, “The Technology,” [Online]. Available: <http://www.40southenergy.com/wave-energy-converters/the-technology/>. [Accessed 19 June 2014].
- [79] Carnegie Wave Energy Limited, “CETO-unit,” [Online]. Available: <https://commons.wikimedia.org/wiki/File:CETO-unit.jpg>. [Accessed 19 May 2019].
- [80] Scottish Government, “Aquamarine Power's first full scale Oyster 1 wave energy device (Library pic),” 11 April 2010. [Online]. Available: <https://www.flickr.com/photos/scottishgovernment/5229163394>. [Accessed 19 May 2019].
- [81] J. Falnes, “Principles for capture of energy from ocean waves. Phase control and optimal oscillation,” 1997. [Online]. Available: http://folk.ntnu.no/falnes/web_arkiv/InstFysikk/phcontrl.pdf. [Accessed 8 August 2013].
- [82] K. Budal, A. Falnes, M. Kyllingstad and G. Olstedal, “Experiments with point absorbers in regular waves,” in *1st Symposium Ocean Wave Energy Utilization*, Gothenberg, 1979.
- [83] D. V. Evans, “A theory for wave-power absorption by oscillating bodies,” *J. Fluid Mech*, vol. 77, pp. 1-25, 1976.
- [84] J. N. Newman, “The interaction of stationary vessels with regular waves,” in *Proceedings of 11th symposium on Naval Hydrodynamics*, 1976.

References

- [85] C. C. Mei, "Power extraction from water waves," *J Ship Research*, vol. 20, pp. 63-6, 1976.
- [86] K. Budal and J. Falnes, "A resonant point absorber of ocean-wave power," *Nature*, vol. 257, pp. 478-9, 1975.
- [87] G. Thomas, "The theory behind the conversion of ocean wave energy: a review," in *Ocean Wave Energy: Current status and future perspectives*, J. Cruz, Ed., Springer, 2008, pp. 41-91.
- [88] D. Mollison, "The prediction of device performance," in *Power from sea waves*, B. Count, Ed., 1980, pp. 135-172.
- [89] WAMIT Inc, "WAMIT," WAMIT Inc, [Online]. Available: <http://www.wamit.com/>. [Accessed November 2012].
- [90] ANSYS Inc., "Aqwa," [Online]. Available: <https://www.ansys.com/products/structures/ansys-aqwa>. [Accessed 27 February 2019].
- [91] J. Falnes, *Ocean Waves and Oscillating Systems*, Cambridge University Press, 2002.
- [92] Y. Li and Y. Yu, "A synthesis of numerical methods for modelling wave energy converter-point absorbers," *Renewable and Sustainable Energy Reviews*, vol. 16, pp. 4352-4363, 2012.
- [93] D. Evans, "Power from water waves," *Annual Review of Fluid Mechanics*, vol. 13, pp. 157-187, 1981.
- [94] J. N. Newman, "The exciting forces on fixed bodies in waves," *J Ship Res*, vol. 6, pp. 10-17, 1962.
- [95] D. V. Evans, "Maximum wave-power absorption under motion constraints," *Appl. Ocean Res.*, vol. 3, no. 4, pp. 200-203, 1981.
- [96] D. Pizer, "Numerical Modelling of Wave Energy Absorbers," University of Edinburgh, 1994.
- [97] T. Bódai and N. Srinil, "Performance analysis and optimization of a box-hull wave energy converter concept," *Renewable Energy*, vol. 81, pp. 551-565, 2015.
- [98] A. Babarit, "A database of capture width ratios of wave energy converters," *Renewable Energy*, vol. 80, pp. 610-628, 2015.
- [99] A. Babarit and A. Clement, "Optimal latching control of a wave energy device in regular and irregular waves," *Applied Ocean Research*, vol. 28, no. 2, pp. 77-91, 2006.
- [100] D. V. Evans, "Some analytic results for two- and three-dimensional wave-energy absorbers," in *Power from Sea Waves*, B. M. Count, Ed., Academic Press, 1980, pp.

213-49.

- [101] J. Falnes, "Radiation impedance matrix and optimum power absorption for interacting oscillators in surface waves," *Applied Ocean Research*, vol. 2, pp. 75-80, 1980.
- [102] P. McIver, "Some hydrodynamic aspects of arrays of wave-energy devices," *Applied Ocean Research*, vol. 16, pp. 61-69, 1994.
- [103] P. Justino and A. Clément, "Hydrodynamic performance for small arrays of submerged spheres," in *Proc. Fifth European Wave Energy Conference*, Cork, 2003.
- [104] Quoceant, "Quoceant," [Online]. Available: <https://www.quoceant.com/>. [Accessed Nov 2017].
- [105] J. Cordonnier, F. Gorintin, A. De Cagny, A. Clément and A. Babarit, "SEAREV: Case study of the development of a wave energy converter," *Renewable Energy*, vol. 80, pp. 40-52, 2015.
- [106] Columbia Power Technologies Inc., "C·POWER: Power from the next wave," [Online]. Available: <https://columbiapwr.com/>. [Accessed 14 March 2019].
- [107] A. Serna and F. Tadeo, "Offshore hydrogen production from wave energy," *International Journal of Hydrogen Energy*, vol. 39, pp. 1549-1557, 2014.
- [108] P. Davies, "Wave-powered desalination: resource assessment and review of technology," *Desalination*, vol. 186, pp. 97-109, 2005.
- [109] J. Taylor, "Hydraulics," in *Ocean Wave Energy: Current Status and Future Perspectives*, J. Cruz, Ed., Springer, 2008, pp. 241-260.
- [110] O. Danielsson, K. Thorburn and M. Leijon, "Direct Drive - Linear Generators," in *Ocean Wave Energy: Current Status and Future Perspectives*, J. Cruz, Ed., Springer, 2008, pp. 220-240.
- [111] D. G. Dorrell, S. S. Ngu and C. Cossar, "Outline Design of a Direct-Drive Low-Speed Brushless Permanent-Magnet Generator for an Ocean-Going Bristol-Cylinder Type Device," in *Proc. IEEE International Symposium on Industrial Electronics*, Hangzhou, 2012.
- [112] M. French, "On the difficulty of inventing an economical sea wave energy converter: A personal view," *Proceedings of the Institution of Mechanical Engineers, Part M: Journal of Engineering for the Maritime Environment*, vol. 220, pp. 149-155, 2006.
- [113] J. Fitzgerald and L. Bergdahl, "Including moorings in the assessment of a generic offshore wave energy converter: A frequency domain approach," *Marine Structures*, vol. 21, pp. 23-46, 2008.
- [114] F. Cerveira, N. Fonseca and R. Pascoal, "Mooring System Influence on the Efficiency of Wave Energy Converters," *International Journal of Marine Energy*, Vols. 3-4, pp.

65-81, December 2013.

- [115] V. Harnois, L. Johanning and P. R. Thies, “Wave conditions inducing extreme mooring loads on a dynamically responding moored structure,” in *10th European Wave and Tidal Energy Conference*, Aalborg, 2013.
- [116] Pelamis Wave Power, “Technology,” [Online]. Available: <http://www.pelamiswave.com/pelamis-technology>. [Accessed 8 December 2011].
- [117] C. Fitzgerald and G. Thomas, “A preliminary study on the optimal formation of an array of wave power devices,” in *Proceedings of the 7th European Wave and Tidal Energy Conference*, Porto, 2007.
- [118] R. Standing, “Use of potential flow theory in evaluating wave forces on offshore structures,” in *Power from sea waves*, B. Count, Ed., Academic Press Inc., 1981, pp. 177-212.
- [119] M. A. Bhinder, A. Babarit, L. Gentaz and P. Ferrant, “Assessment of viscous damping via 3D-CFD modelling of a floating wave energy device,” in *EWTEC*, Southampton, 2011.
- [120] Mathworks, “Matlab - Overview,” [Online]. Available: <https://uk.mathworks.com/products/matlab.html>. [Accessed 15 March 2019].
- [121] K. Nielson and T. Pontes, “ANNEX II Task 1.1 Generic and site related wave data; Final technical report,” IEA-OES, 2010.
- [122] D. Richardson and G. Aggidis, “The Economics of Multi-Axis Point Absorber Wave Energy Converters,” in *Proceedings of the ASME 2013 32nd International Conference on Ocean, Offshore and Arctic Engineering*, Nantes, 2013.
- [123] Entec UK Ltd, commissioned by Carbon Trust, “Cost Estimation Methodology,” 2006.
- [124] M. J. Tucker and E. G. Pitt, *Waves in Ocean Engineering*, Elsevier, 2001.
- [125] Pelamis Wave Power, “Pelamis Wave Power,” [Online]. Available: <http://www.pelamiswave.com/>. [Accessed December 2012].
- [126] M. A. Mueller, H. Polinder and N. Baker, “Current and Novel Electrical Generator Technology for Wave Energy Converters,” in *IEEE Electric Machines and Drives Conference*, 2007.
- [127] H. Ming and G. A. Aggidis, “Developments, Expectations of Wave Energy Converters and Mooring Anchors in the UK,” *J. Ocean Univ. Chin. (Oceanic and Coastal Sea Research)*, vol. 7, no. 1, pp. 10-16, 2008.
- [128] Det Norske Veritas, “Offshore Standards DNV_OS 301, Position Mooring,” Norway, 2001.

References

- [129] R. E. Harris, L. Johanning and J. Wolfram, “Mooring systems for wave energy converters: A review of design issues and choices,” in *Proceedings of the 3rd International Conference on Marine Renewable Energy*, London, 2004.
- [130] Amec for the Carbon Trust, “UK Wave Energy Resource,” Carbon Trust, 2012.
- [131] M. Dicorato, G. Forte, M. Pisani and M. Travato, “Guidelines for assessment of investment cost for offshore wind generation,” *Renewable Energy*, vol. 36, no. 8, pp. 2043-2051, 2011.
- [132] S. Lundberg, “Performance comparison of wind park configuration,” Chalmers University of Technology, Goteborg, 2003.
- [133] WAMIT Inc, *WAMIT User Manual Versions 6.1, 6.1PC, 6.1S, 6.1S-PC*, Chestnut Hill, MA, 2002.

Appendices

A.1 Appendix 1 – WAMIT

This Appendix describes the software package WAMIT and how it was used to calculate the hydrodynamic coefficients for section 4.3. For the calculation of maximum absorbed power for a device using the method described in section 4.3 the hydrodynamic coefficients for the exciting force (X_i) and damping force (B_{ij}) are required. These can be determined either by experiment, numerically, or in limited circumstances with analytic solutions. For this work the hydrodynamic coefficients were determined numerically using the software package WAMIT V6.1 [89].

WAMIT is a program widely used to analyse the linear interactions between surface waves and offshore structures [133]. It does this by numerically solving the radiation and diffraction problems for the body/bodies which can be either on the free surface, submerged or mounted on the seabed/bottom [133]. As it is based on a linear analysis the program is suited to small amplitudes and waves with low steepness. It does not take account of viscous effects or slamming as these are non-linear effects.

The program assumes the flow to be harmonic and the fluid inviscid, irrotational and incompressible, which allows velocity potentials to be calculated for the wetted body surface. The body geometry can be represented either with discrete panels or with continuous B-splines. B-splines allow a continuous representation of the velocity potentials. These velocity potentials for the radiation and diffraction problems are calculated from the solution of an integral equation obtained using Green's theorem. The free-surface source-potential is used as the Green function [133].

The WAMIT program consists of two sub-programs named POTEN and FORCE:

1. POTEN solves the radiation and diffraction velocity potentials on the body surface and is the main computational burden.
2. FORCE computes global quantities such as hydrodynamic coefficients, body motions and forces (first and second order).

These sub-programs are run sequentially by executing the single command 'WAMIT'. On a PC the program is run from the command prompt. There is the option to store the output of

POTEN in a binary file so that the FORCE program can be run with varying parameters without having to re-run the more computationally intensive POTEN.

Using WAMIT

The steps to using WAMIT are:

1. Prepare input files.
2. Run WAMIT.
3. Process output files.

The user interface of WAMIT V6.1 isn't the most user friendly as inputted and outputted data is in the form of text files (ASCII) and so pre- and post-processing of the files is required. The WAMIT process with the input and output files is shown in Figure 82.

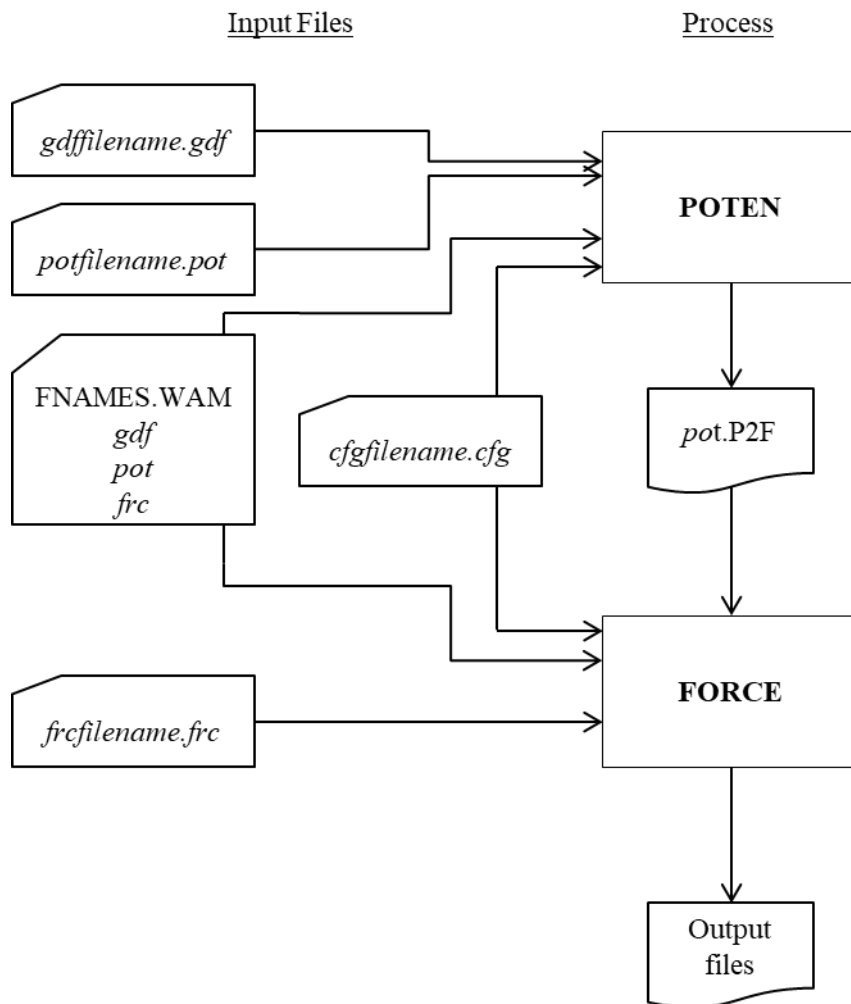


Figure 82: Flow diagram showing the process of running WAMIT with input and output files (adapted from [133]).

The input files required to run WAMIT are:

- *FNAMES.WAM*: Specifies which input files (.gdf, .pot, .frc) are used (this file is optional).
- *cfgfilename.cfg*: Configuration file used to specify options and parameters. The filename can be specified by the user.
- *frcfilename.frc*: Force control file used to input parameters to FORCE.
- *gdffilename.gdf*: Geometric data file used to specify body geometry.
- *potfilename.pot*: Potential control file used to input parameters to POTEN.

These input files can be edited in a text editor to modify the parameters of each run.

The output files contain the values evaluated by WAMIT. WAMIT can evaluate many quantities (see [89] or [133] for a full list) but for the method in section 4.3 only the exciting force (X_i) and damping (B_{ij}) coefficients are required.

The hydrodynamic coefficients are outputted in non-dimensional form, denoted here with an overbar on the coefficient. Values are evaluated for each selected wave period and wave heading specified in the input files. For the damping coefficient the non-dimensional output form is [133]:

$$\bar{B}_{ij} = \frac{B_{ij}}{\rho L^k \omega},$$

Equation 41

where L is a length scale specified in the input files and normally set to 1. The i and j are mode indices (modes 1 to 6; heave, surge, sway, roll, pitch, yaw respectively). The exponent k takes different values depending on the modes of i and j as set out in Table 8 but with L set to 1 they do not have any effect on the coefficient value.

Value of k	i, j modes
3	$i, j = 1, 2, 3,$
4	$i = 1, 2, 3, j = 4, 5, 6,$ or $i = 4, 5, 6, j = 1, 2, 3$
5	$i, j = 4, 5, 6$

Table 8: Values of the exponent k for the non-dimensional damping coefficient.

The exciting force coefficient in the non-dimensional output form is [133]:

$$\bar{X}_i = \frac{X_i}{\rho g A L^m}$$

Equation 42

Just as for the damping coefficient, L is a length scale specified in the input files and normally set to 1. The coefficient A is the incident wave amplitude (in metres) and the exponent m takes different values depending on mode index i : $m = 2$ for $i = 1,2,3$ and $m = 3$ for $i = 4,5,6$. As with Equation 41 the value of m does not affect the value of the coefficient if the length scale L is set to 1.

For use within the method of section 4.3 the non-dimensional values in the output files must be converted to the dimensional form. This can be achieved by rearranging Equation 41 and Equation 42 and processing the data accordingly. With the length scale L set to 1 the dimensional forms of the coefficients can be calculated using Equation 43 and Equation 44. For post-processing of the hydrodynamic coefficients the density of the fluid was taken as 1026kg/m^3 for that of seawater [17].

$$B_{ij} = \rho \omega \bar{B}_{ij}$$

Equation 43

$$X_i = \rho g A \bar{X}_i$$

Equation 44

The exciting force coefficients used in section 4.3 are for a unit amplitude wave which can be found by setting the wave amplitude in Equation 44 to 1 m. The exciting force coefficient for a unit amplitude wave is therefore found from Equation 45.

$$\hat{X}_i = \rho g \bar{X}_i$$

Equation 45

The output text files contain a value of each coefficient for each wave period, wave heading and mode (or combination of modes for damping) specified in the input files.

Hemisphere

For the semi-submerged spherical devices considered in section 4.3 the wetted body surface is hemispherical (see Figure 26). It is only the wetted surface that is relevant for WAMIT. A hemisphere is included in the WAMIT library of standard geometries and so no additional geometric definition was required other than to specify the radius. For the analysis of different

sized devices, coefficients were calculated for hemispheres of radius 2 m to 5 m in 1 m increments. The main input parameters are shown in Table 9.

Parameter	Value (s)
Gravity	9.80665 kg/m ³
Water depth	Infinite – deep water assumption
Wave period(s)	4 s to 20 s in 0.01steps – this resolution produces smooth curves as well as covering all of the periods in Table 2.
Wave heading(s)	0 degrees (head on)
Geometry	Hemisphere
Geometry characterisation	B-splines – this allows for a continuous representation of the velocity potentials.
Radius	2 m to 5 m in 1 m steps
Buoyancy	Neutral
Centre of gravity	At the free surface in the centre
Free modes	1,2,3,4,5,6 (no fixed modes)

Table 9: Input parameters for hemisphere WAMIT run.

The format of the output files containing the non-dimensional damping coefficients and exciting force coefficients are shown below. The format of the output files containing the damping coefficient can be seen in the example of Figure 83 of data for one wave period (5.5 s). The columns are (from left to right) the wave period (s), *i* mode, *j* mode, non-dimensional added mass and non-dimensional damping.

```

0.550000E+01    1    1  1.728247E+02  4.950449E+01
0.550000E+01    1    5  2.851014E-06  3.975448E-07
0.550000E+01    2    2  1.728249E+02  4.950457E+01
0.550000E+01    2    4 -2.857125E-06  2.995617E-08
0.550000E+01    3    3  1.340615E+02  8.277256E+01
0.550000E+01    4    2  1.037218E-06  3.191505E-07
0.550000E+01    4    4 -6.077582E-14  3.451772E-16
0.550000E+01    5    1  9.926940E-07  2.195053E-07
0.550000E+01    5    5 -5.019283E-14  1.642036E-15
0.550000E+01    6    6 -2.562930E-14 -2.034684E-18
    
```

Figure 83: Format of output file for added mass and damping coefficients.

The format of the output files containing the exciting force coefficient can be seen in the example of Figure 84 of data for one wave period (5.5 s). The columns are (from left to right) the wave period (s), wave heading (degrees), *i* mode, modulus of \bar{X}_i , phase of \bar{X}_i (degrees), real part of \bar{X}_i , imaginary part of \bar{X}_i . The exciting force/moment is given in polar complex form and in complex Cartesian coordinates.

0.550000E+01	0.000000E+00	1	6.239294E+01	8.042712E+01	1.037608E+01	6.152411E+01
0.550000E+01	0.000000E+00	2	0.000000E+00	9.000000E+01	0.000000E+00	0.000000E+00
0.550000E+01	0.000000E+00	3	2.447352E+01	1.714643E+01	2.338578E+01	7.215156E+00
0.550000E+01	0.000000E+00	4	0.000000E+00	9.000000E+01	0.000000E+00	0.000000E+00
0.550000E+01	0.000000E+00	5	9.912907E+01	-9.957293E+01	-1.648545E+01	-9.774867E+01
0.550000E+01	0.000000E+00	6	0.000000E+00	9.000000E+01	0.000000E+00	0.000000E+00

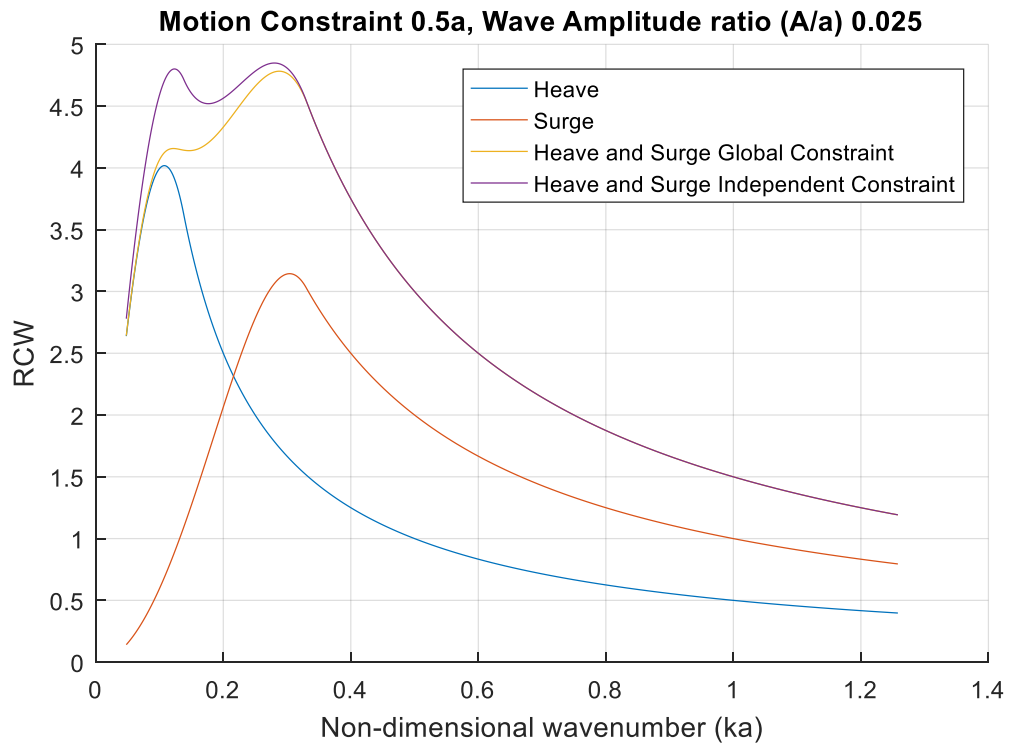
Figure 84: Format of output file for exciting force coefficients.

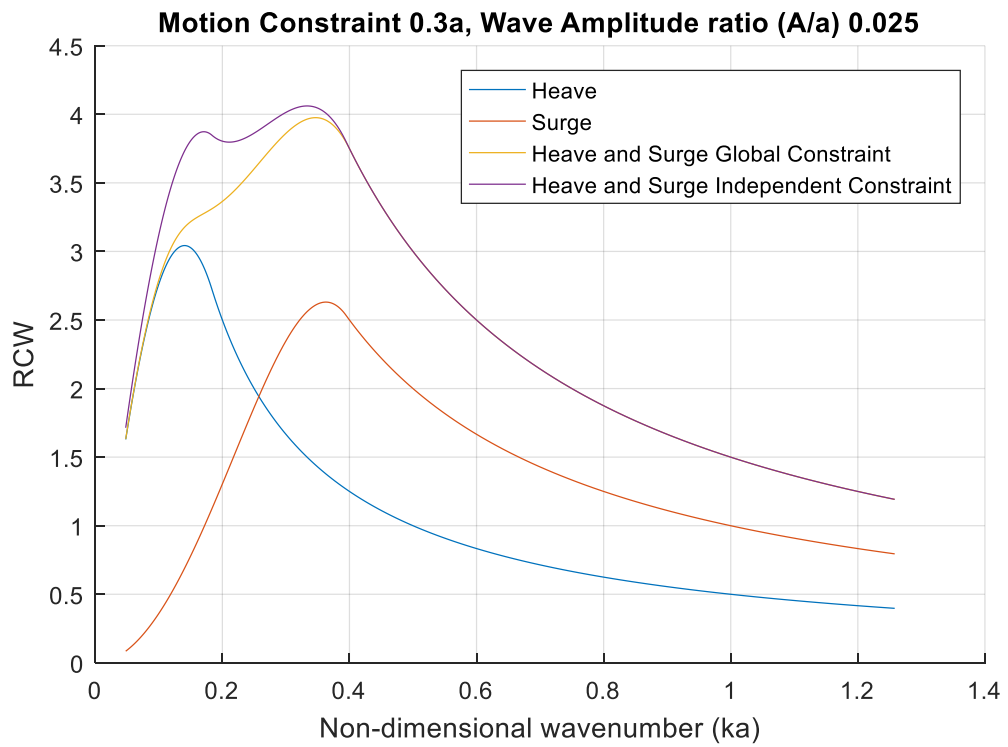
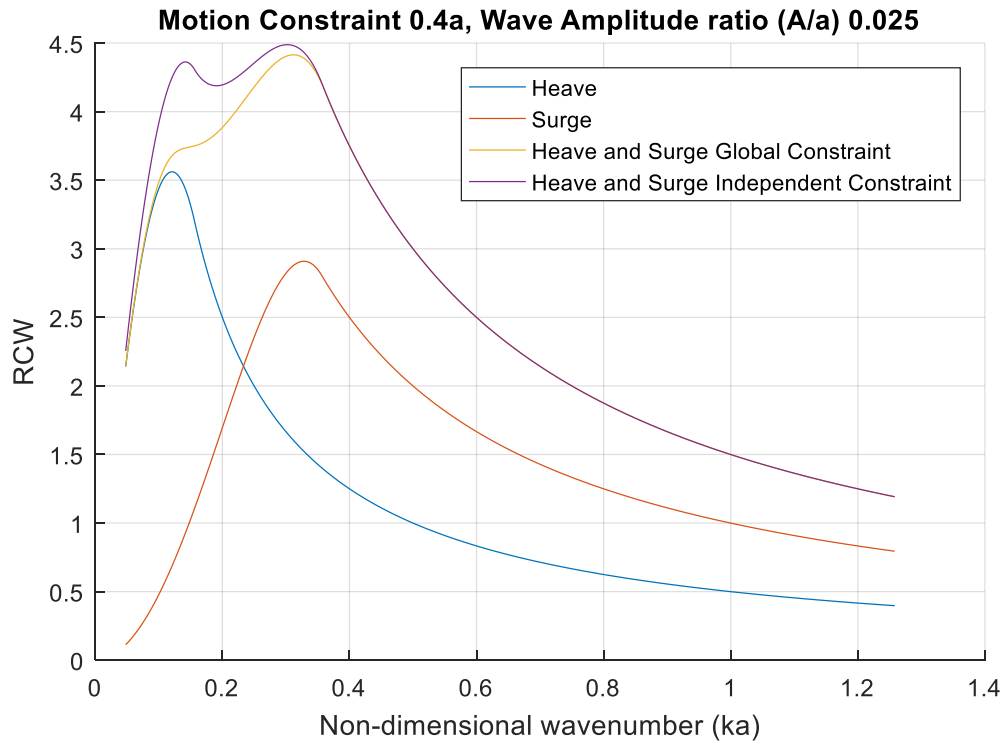
The processing of this data was carried out using Matlab [120] to extract the data and filter out the coefficients of interest. These non-dimensional coefficients could then be dimensionalised and packaged in arrays suitable for use with the equations in section 4.3 which were also processed using Matlab. This was accomplished by writing bespoke Matlab scripts that could carry out these functions.

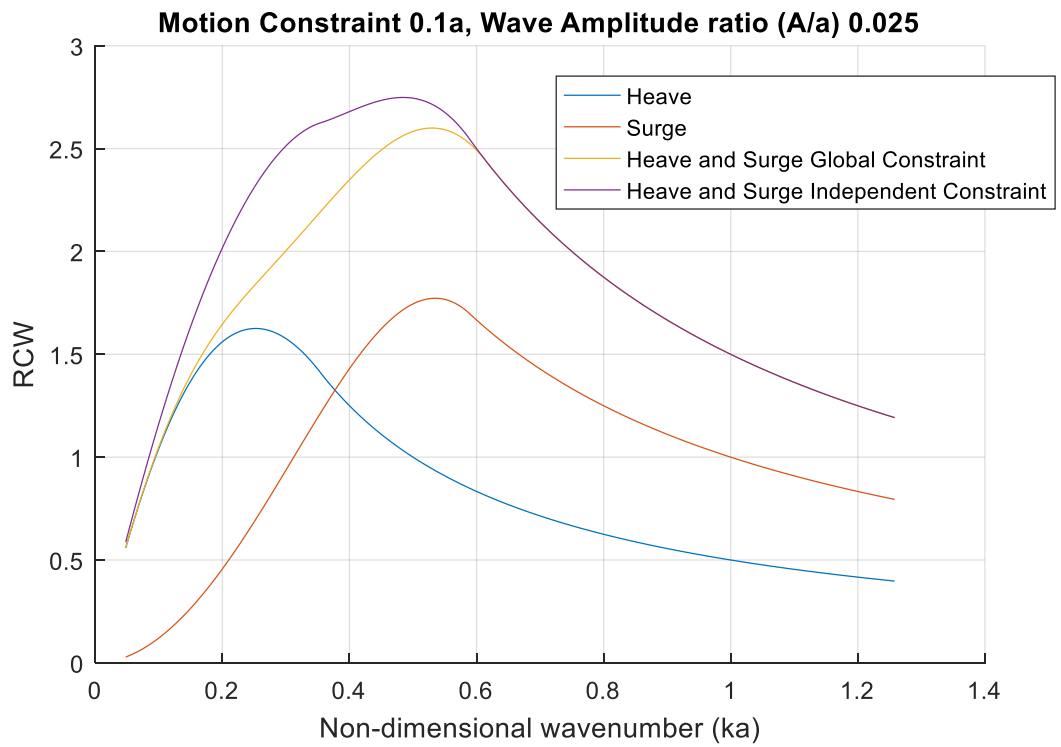
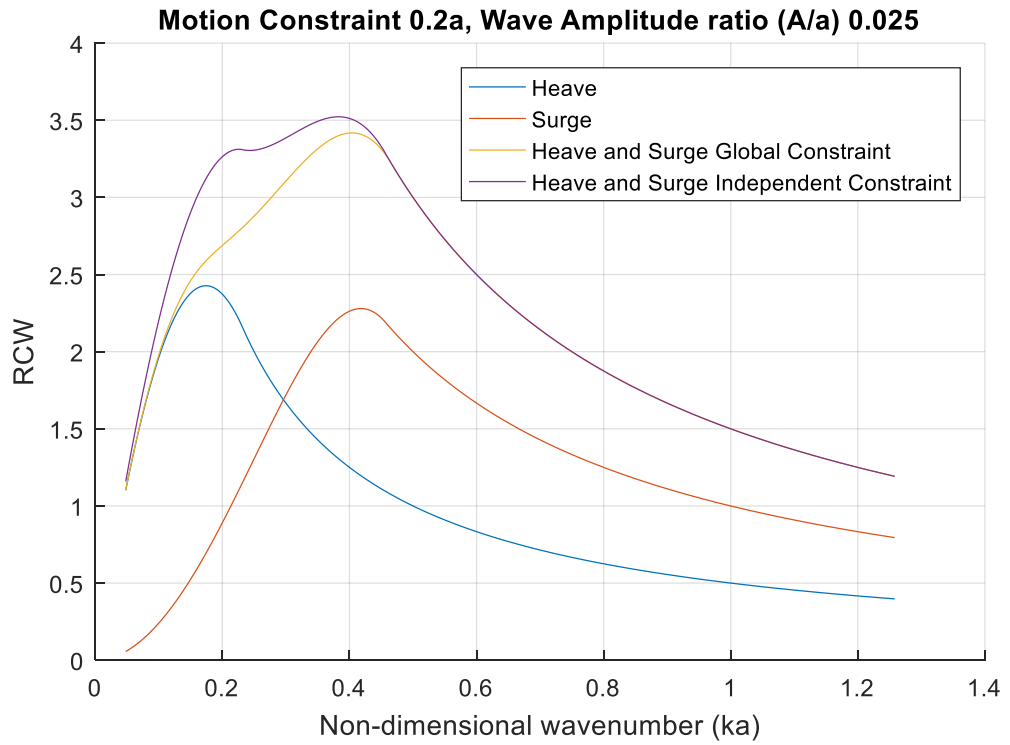
A.2 Appendix 2 – Relative Capture Widths under Global Weighted Motion Constraints and Independent Motion Constraints

This Appendix relates to Section 4.3.1 and 4.4.1. It contains additional plots that show the comparison between RCWs for a semi-submerged sphere under motion constraints in the four configurations; heave only, surge only, heave+surge global weighted constraint, and heave+surge independent constraints. Each plot shows the RCW under a particular motion constraint and wave amplitude ratio. The range of motion constraints is from 0.1 to 0.5 of the device radius (a) in intervals of 0.1a, and the wave amplitude ratios of 0.025 to 0.625 of the device radius in intervals of 0.1.

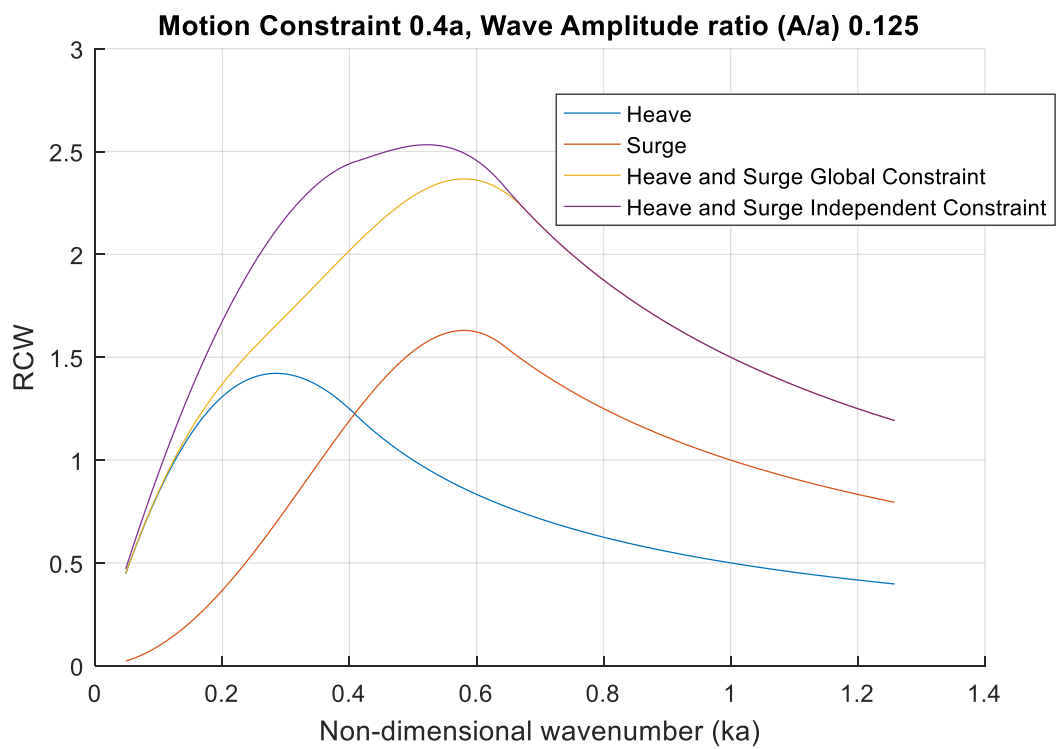
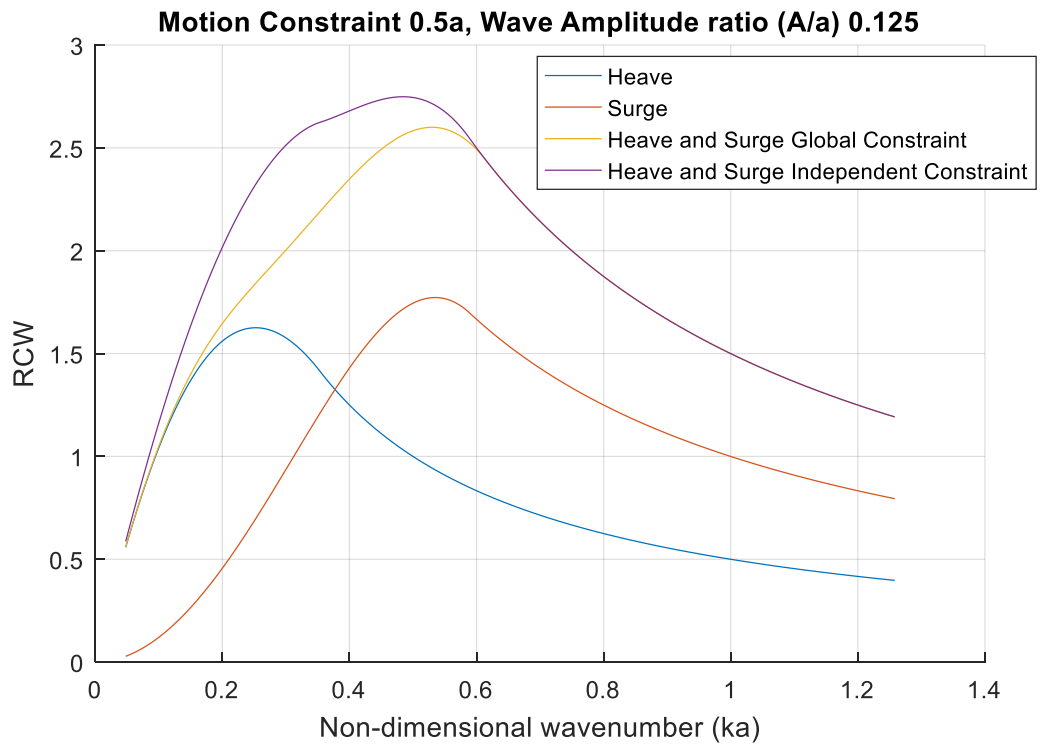
A.2.1 Wave Amplitude Ratio (A/a) 0.025 radii of device

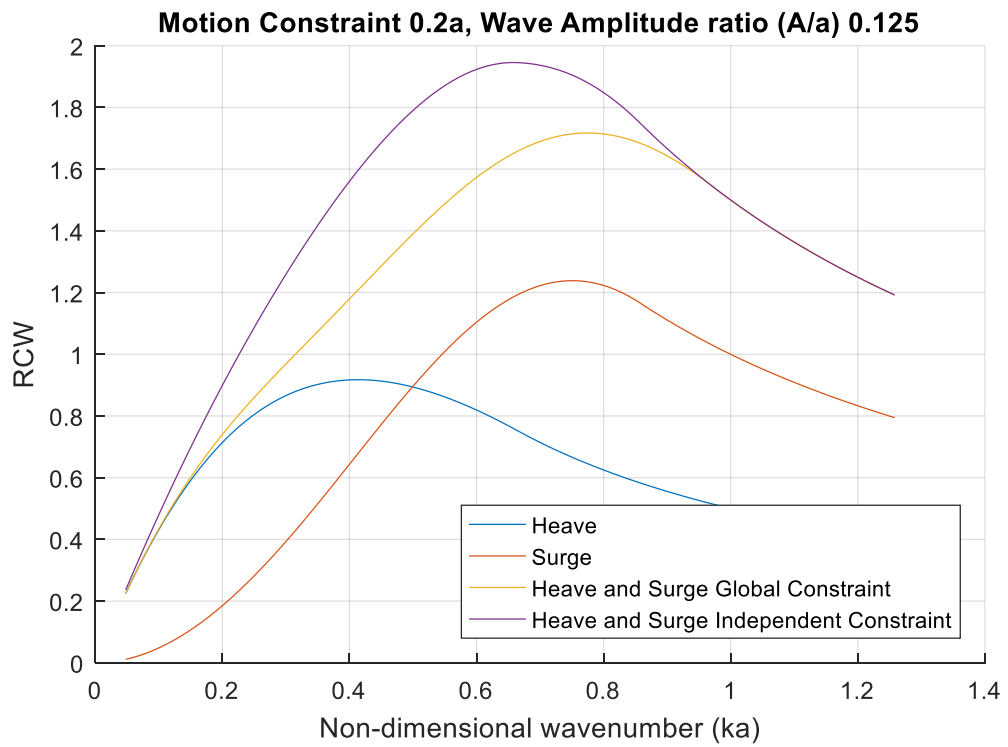
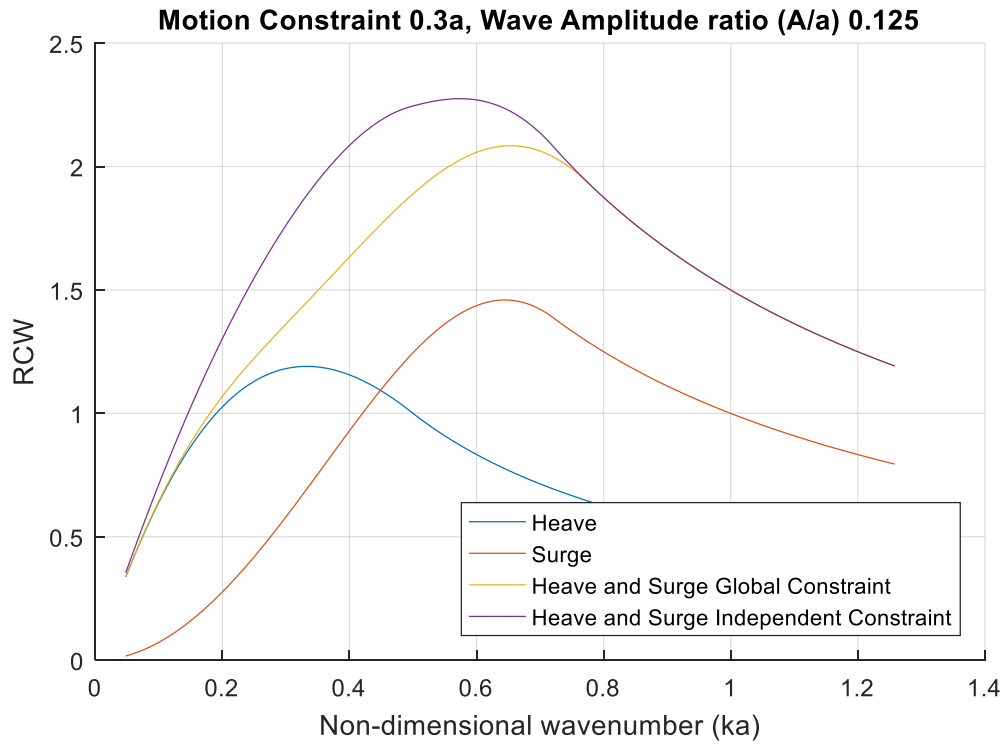


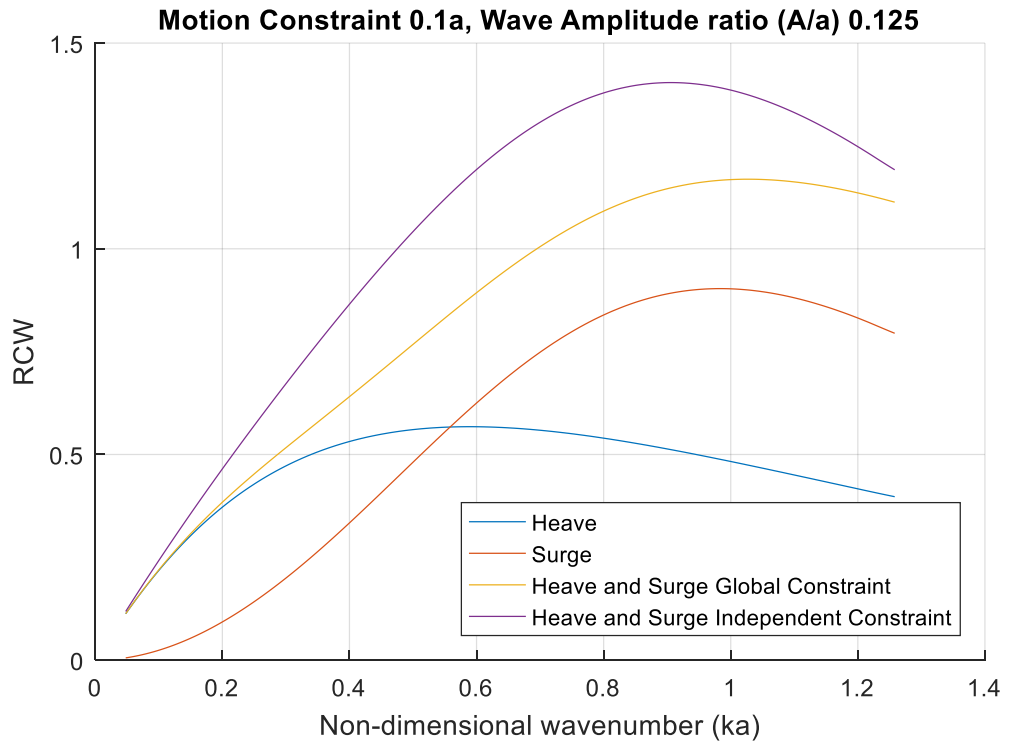




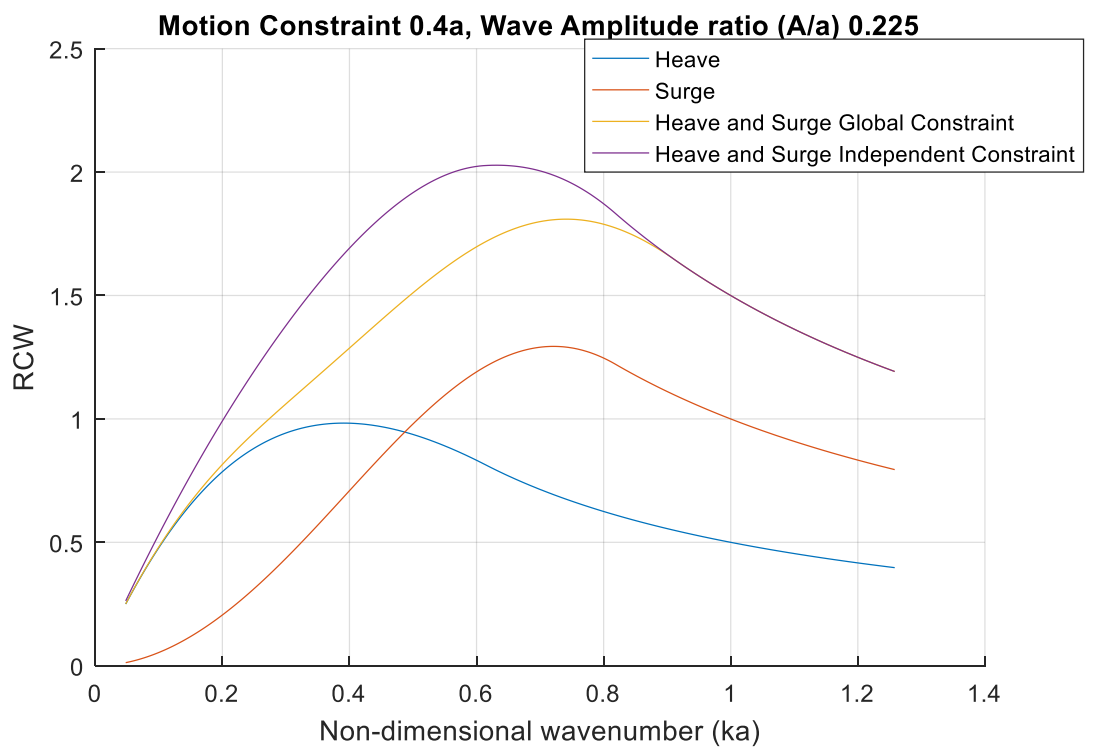
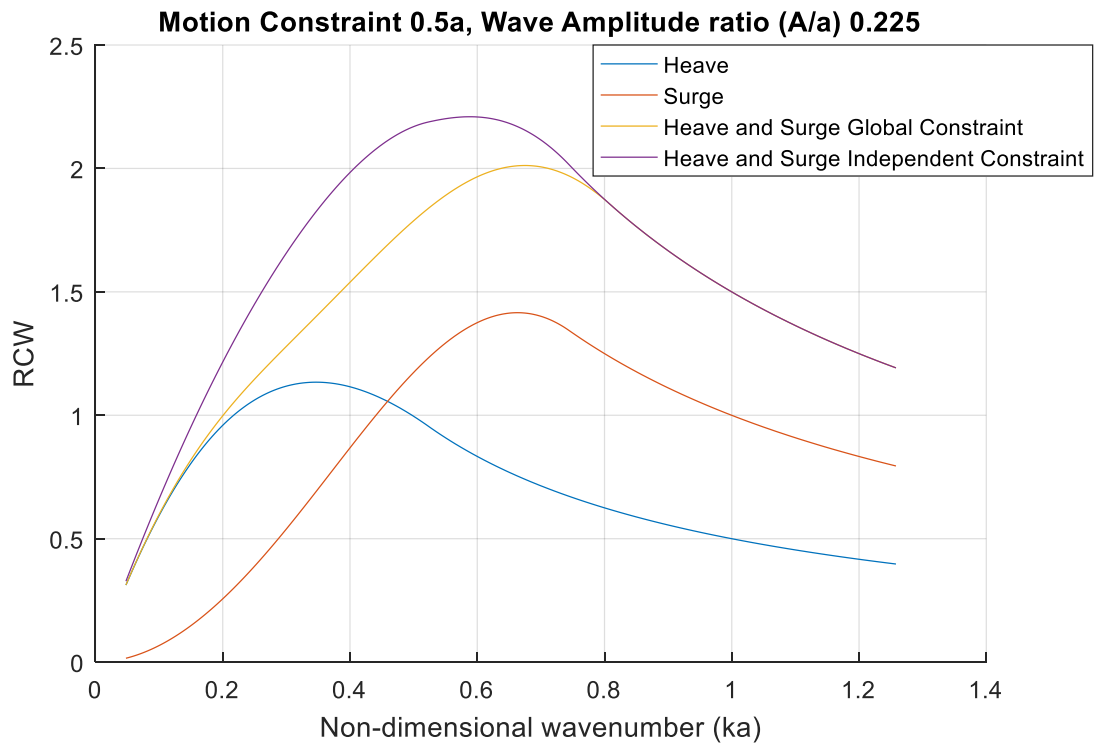
A.2.2 Wave Amplitude Ratio (A/a) 0.125 radii of device

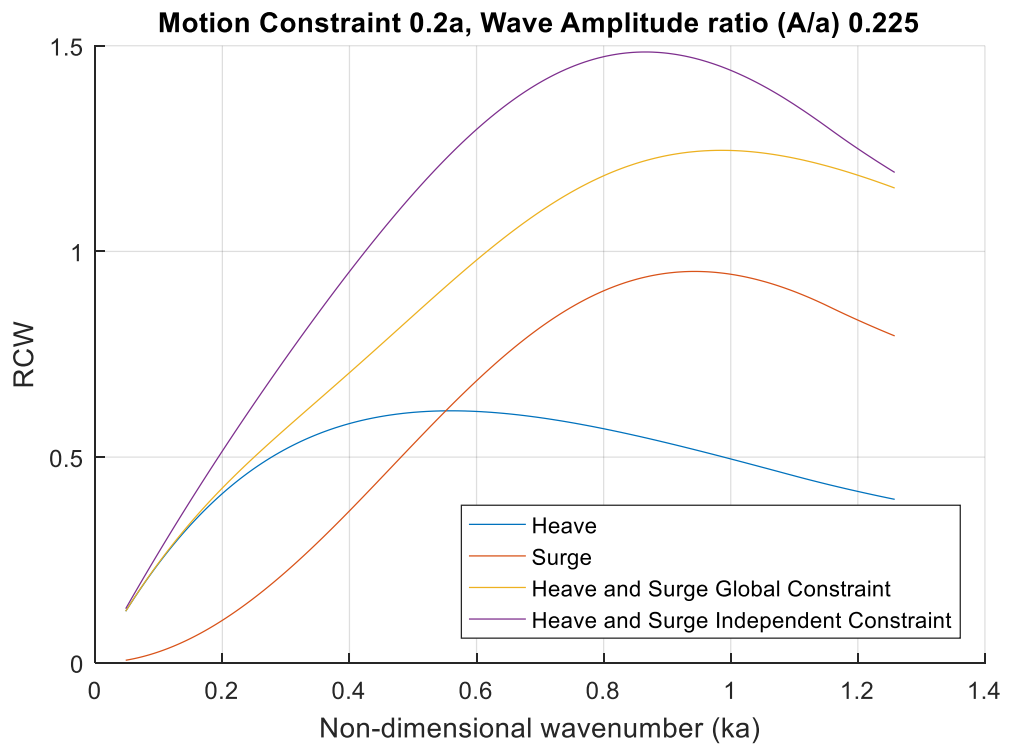
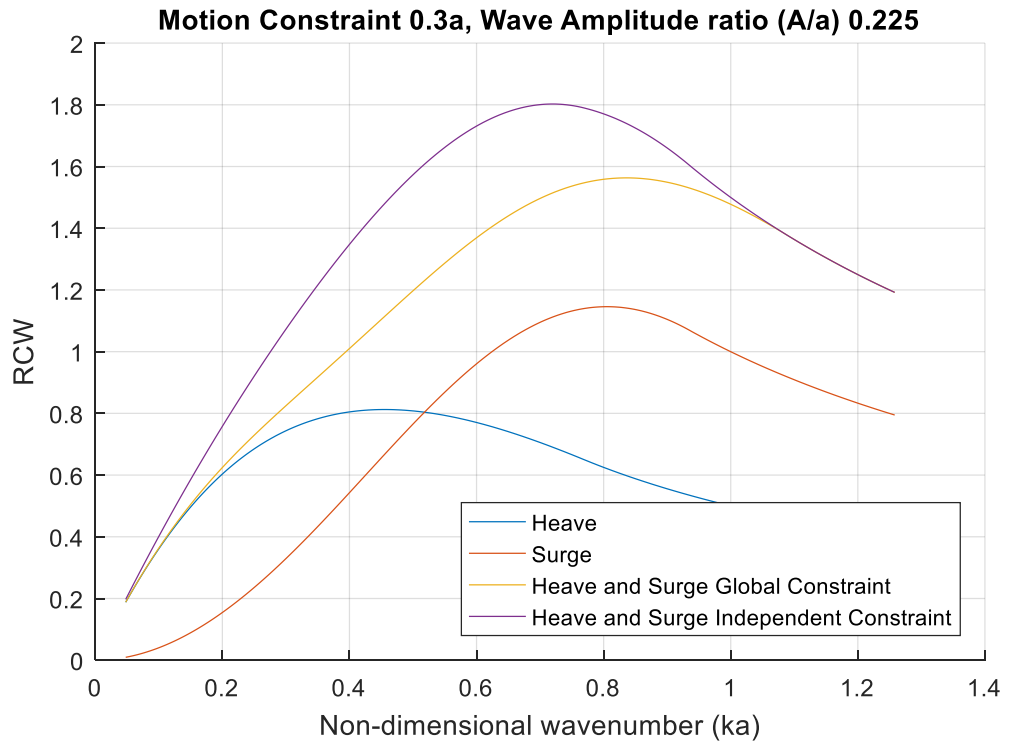


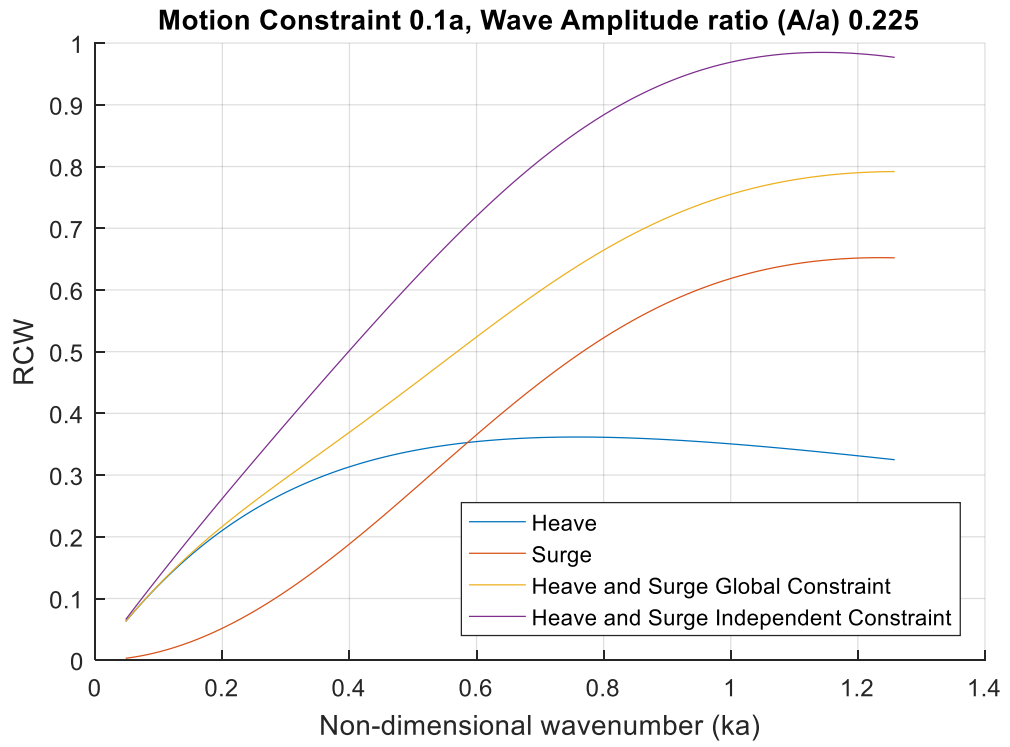




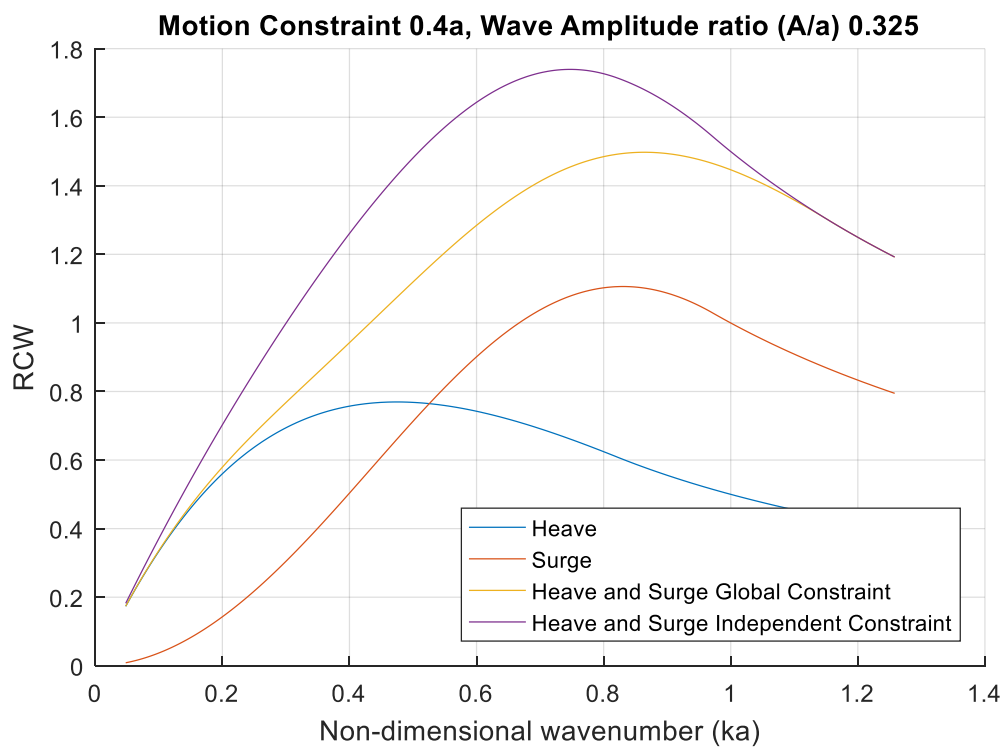
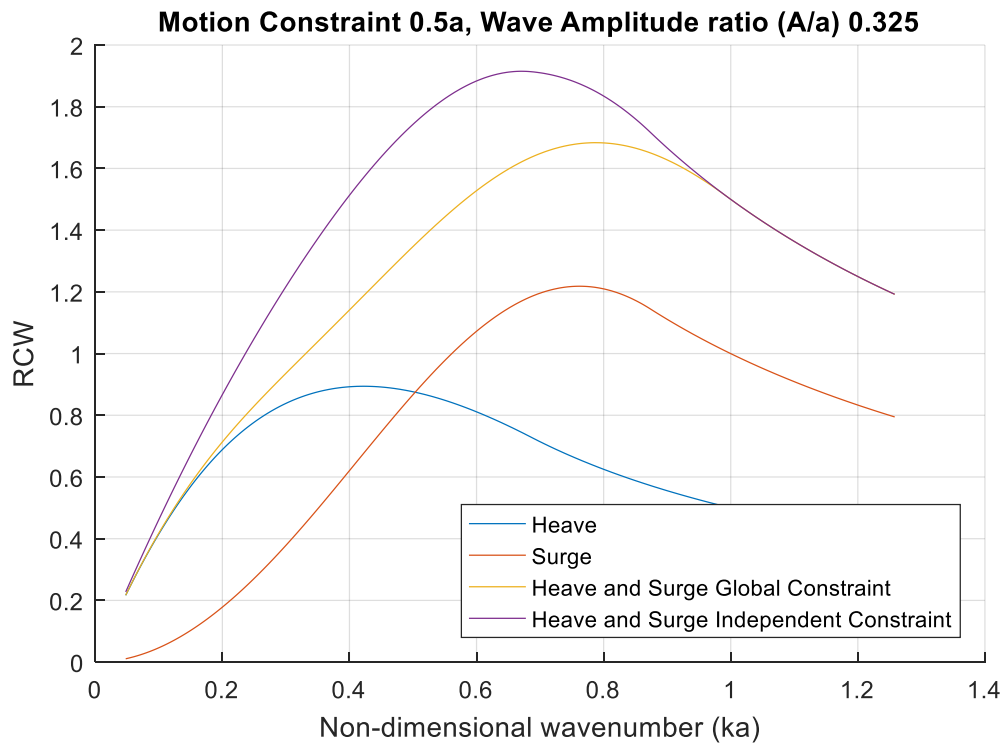
A.2.3 Wave Amplitude Ratio (A/a) 0.225 radii of device

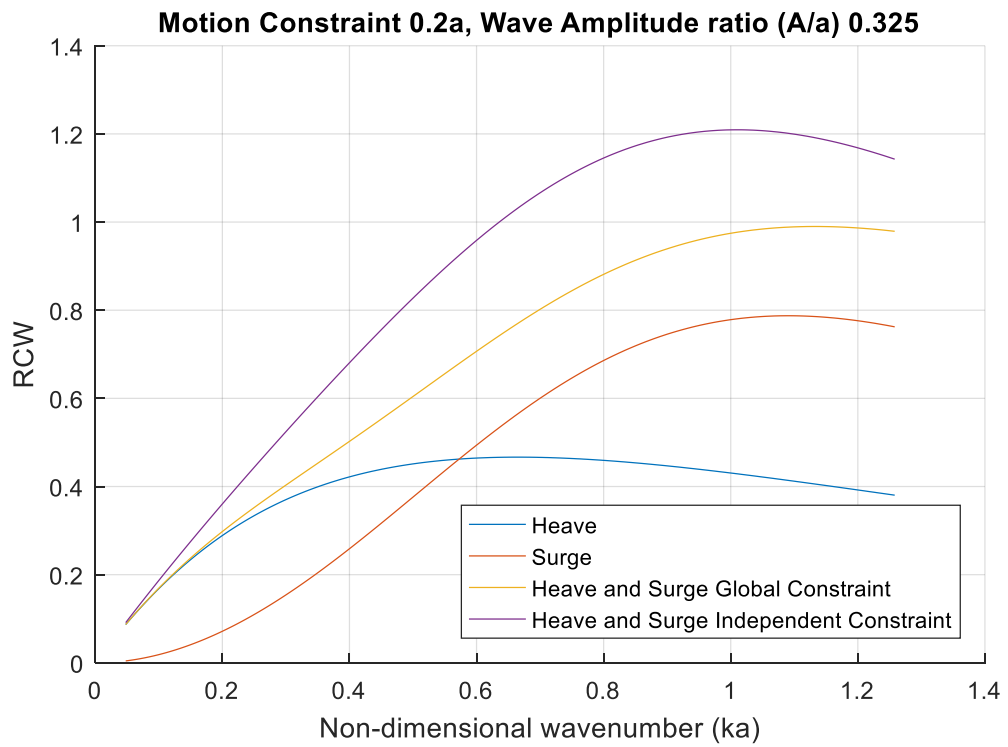
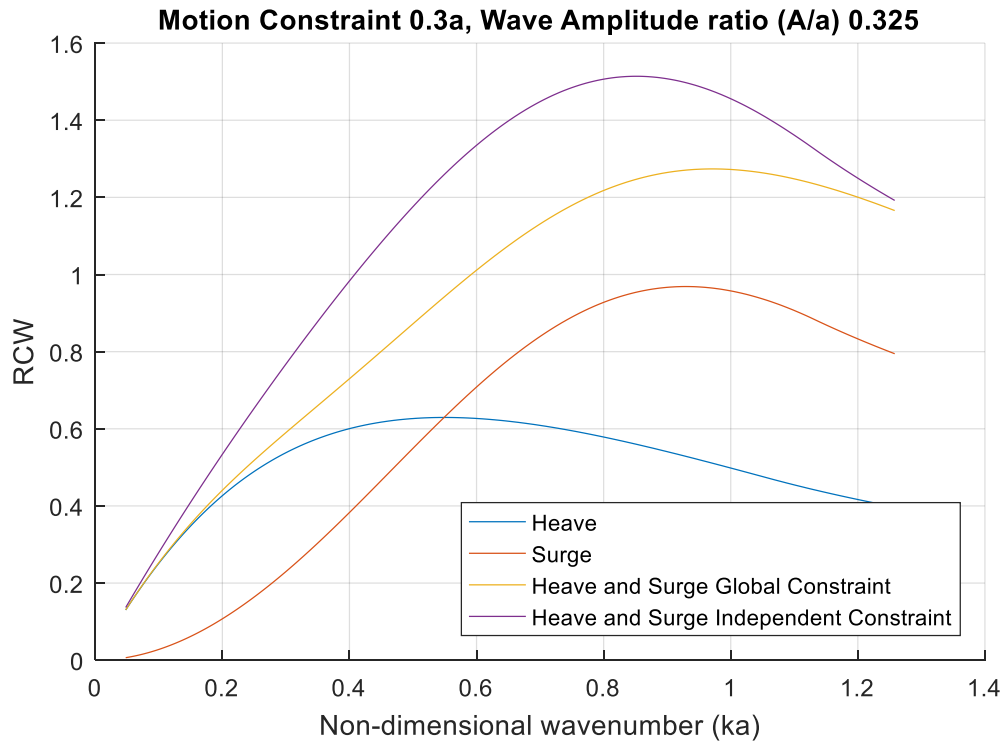


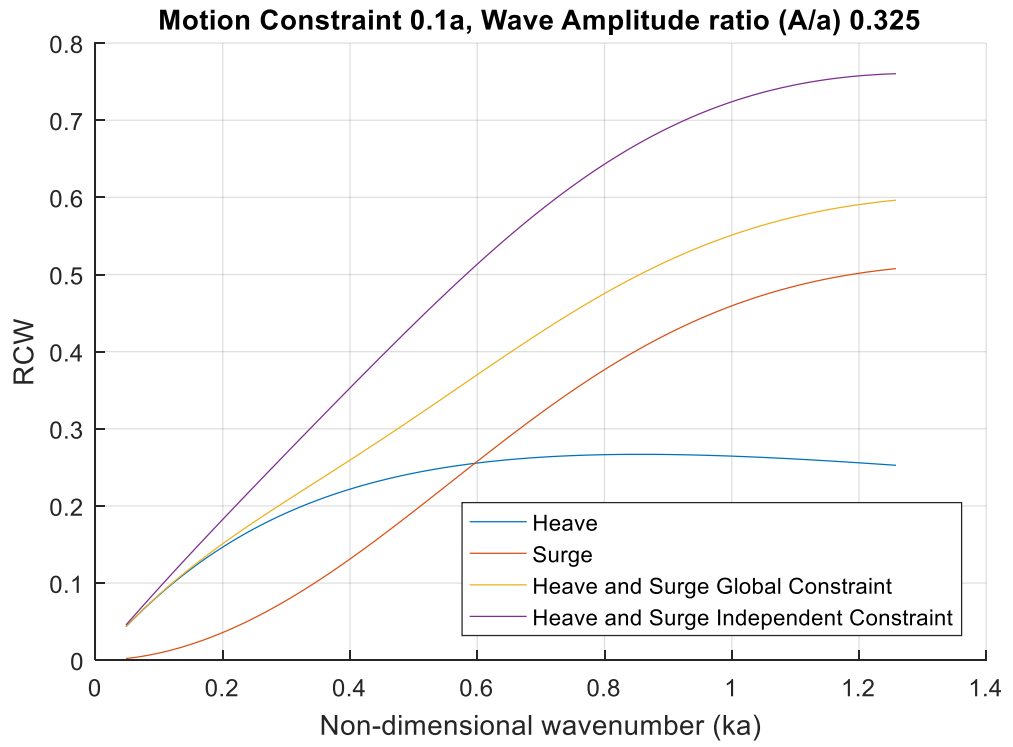




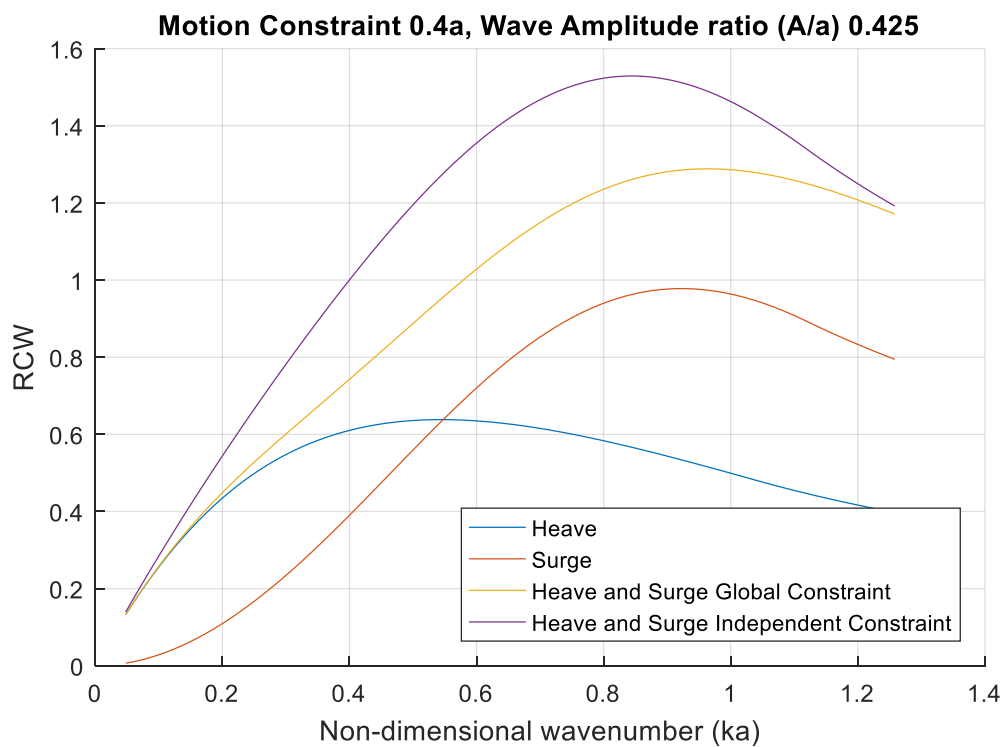
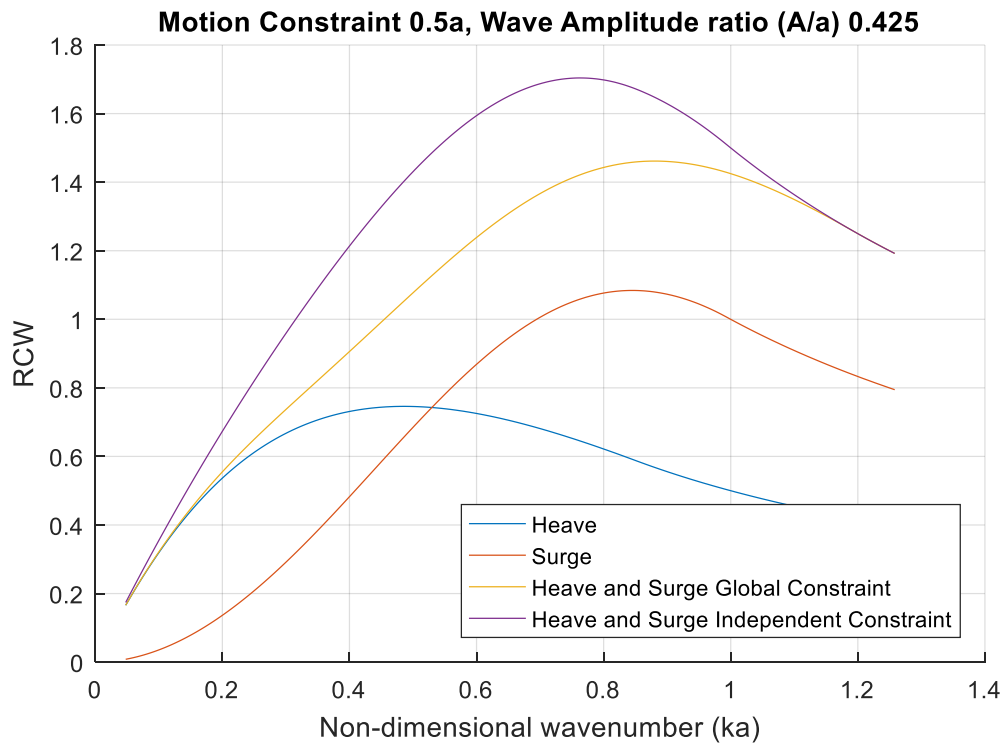
A.2.4 Wave Amplitude Ratio (A/a) 0.325 radii of device

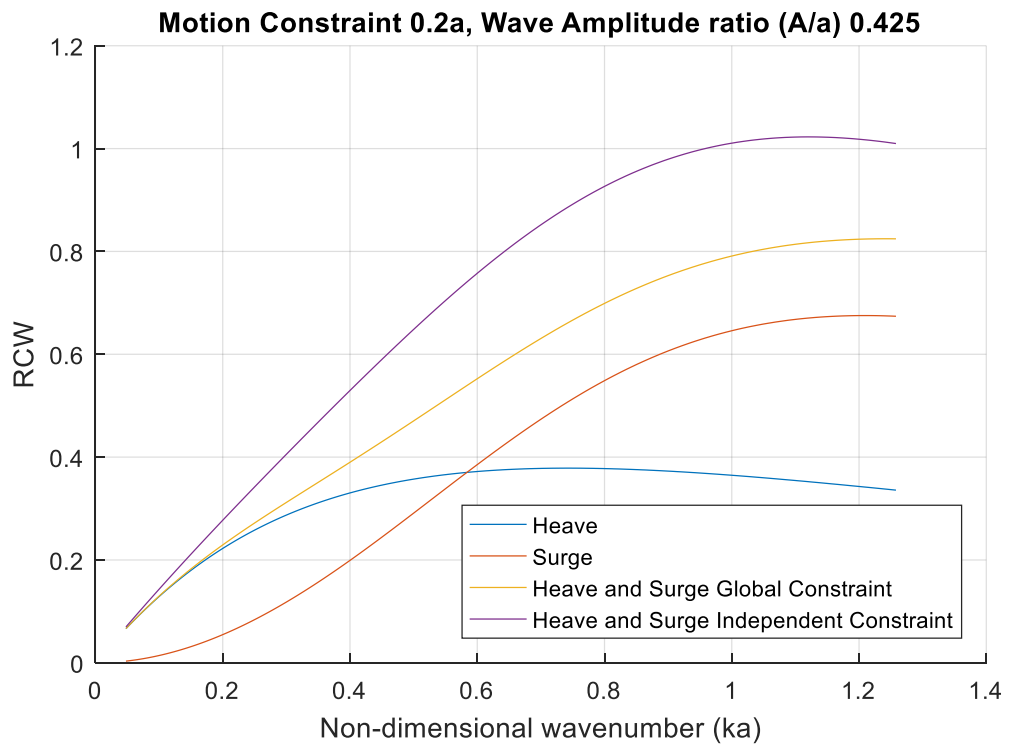
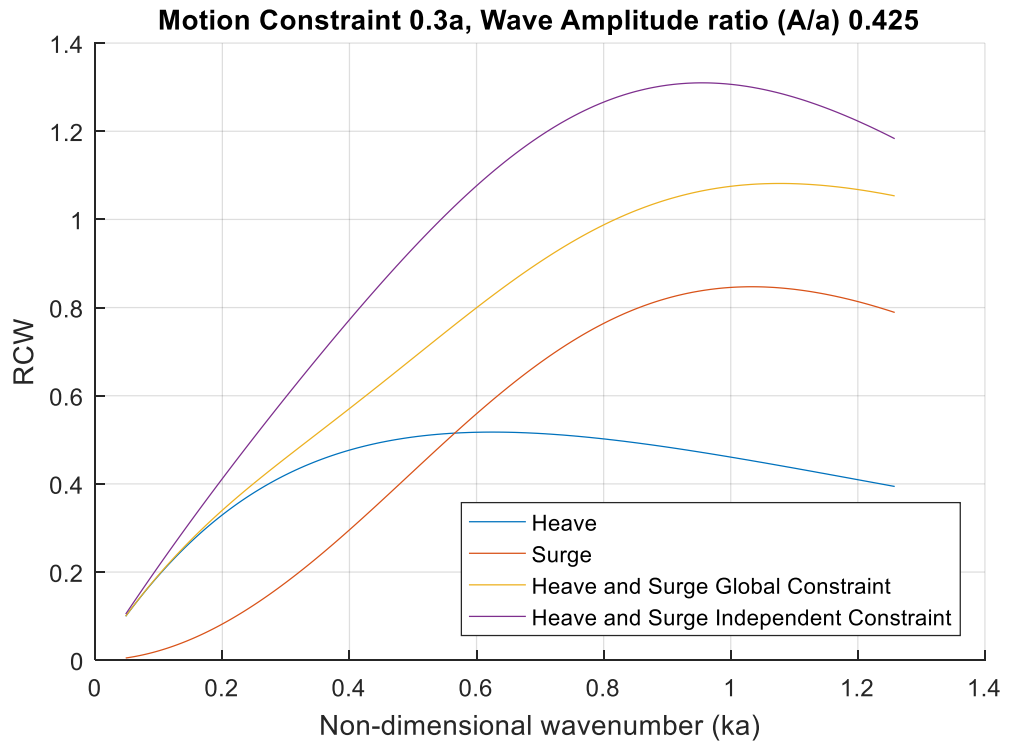


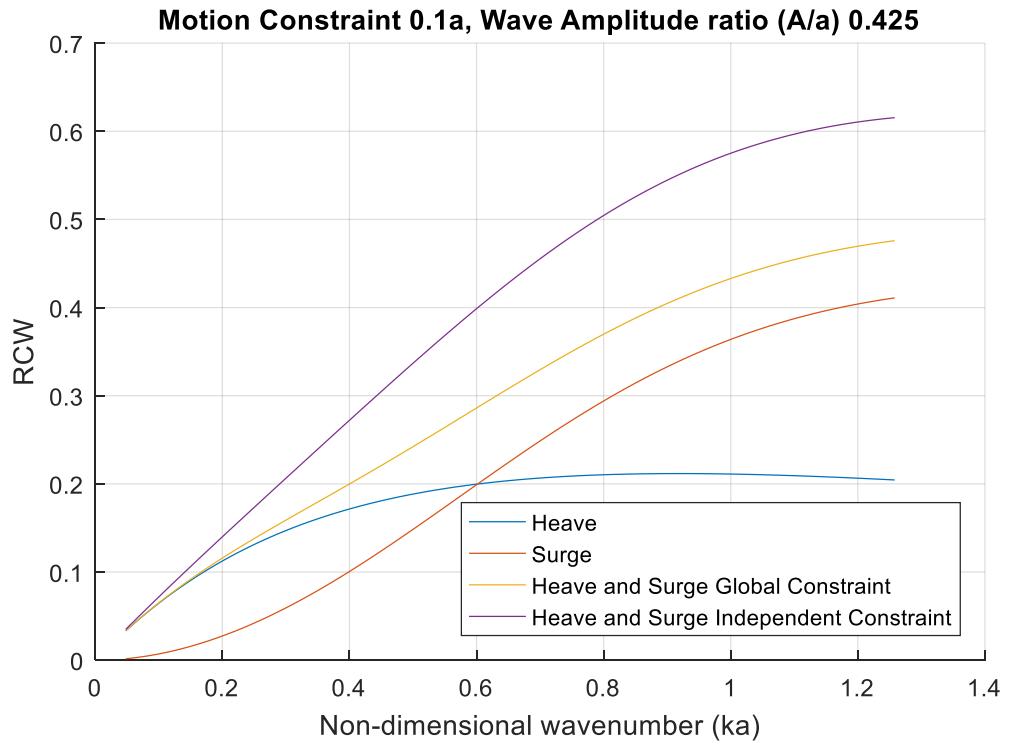




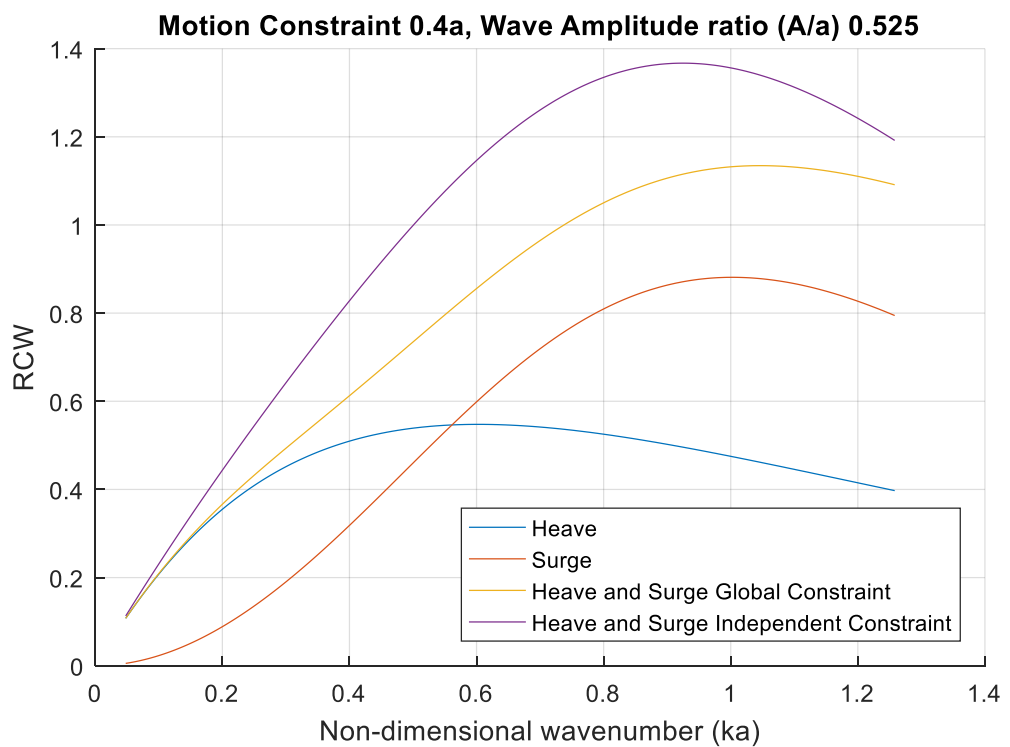
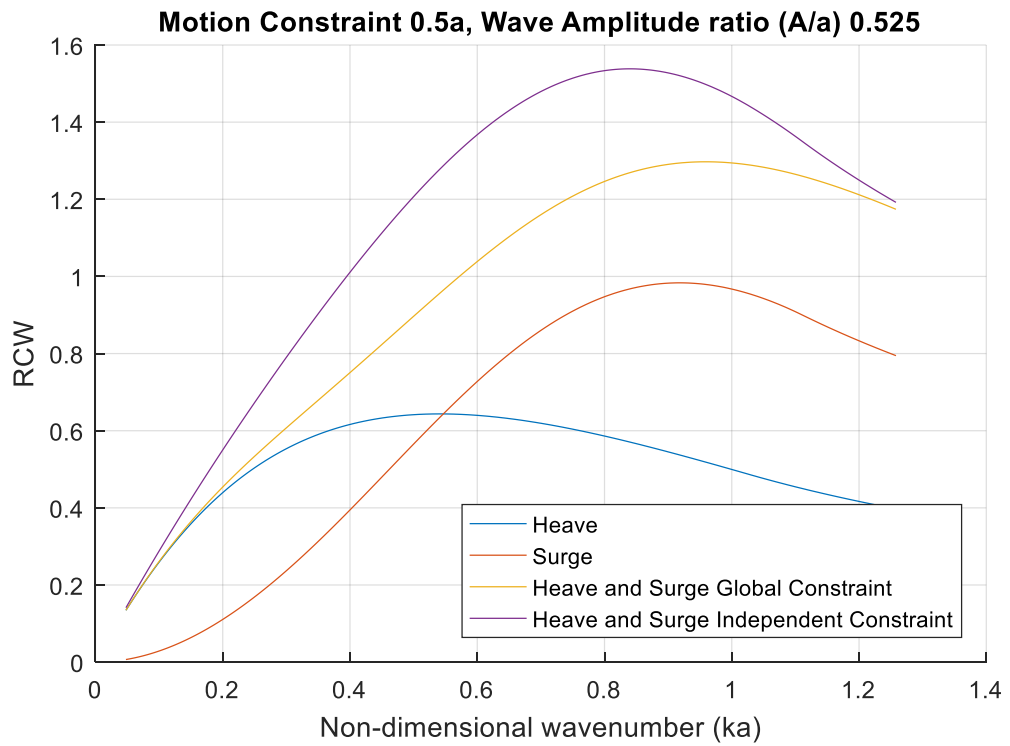
A.2.5 Wave Amplitude Ratio (A/a) 0.425 radii of device

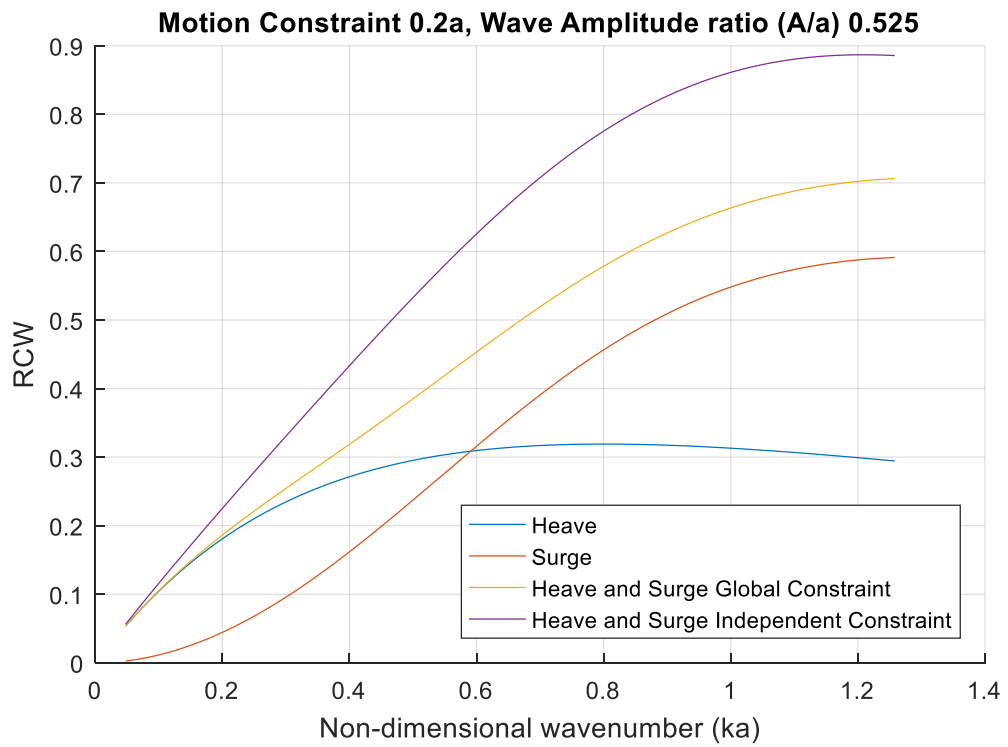
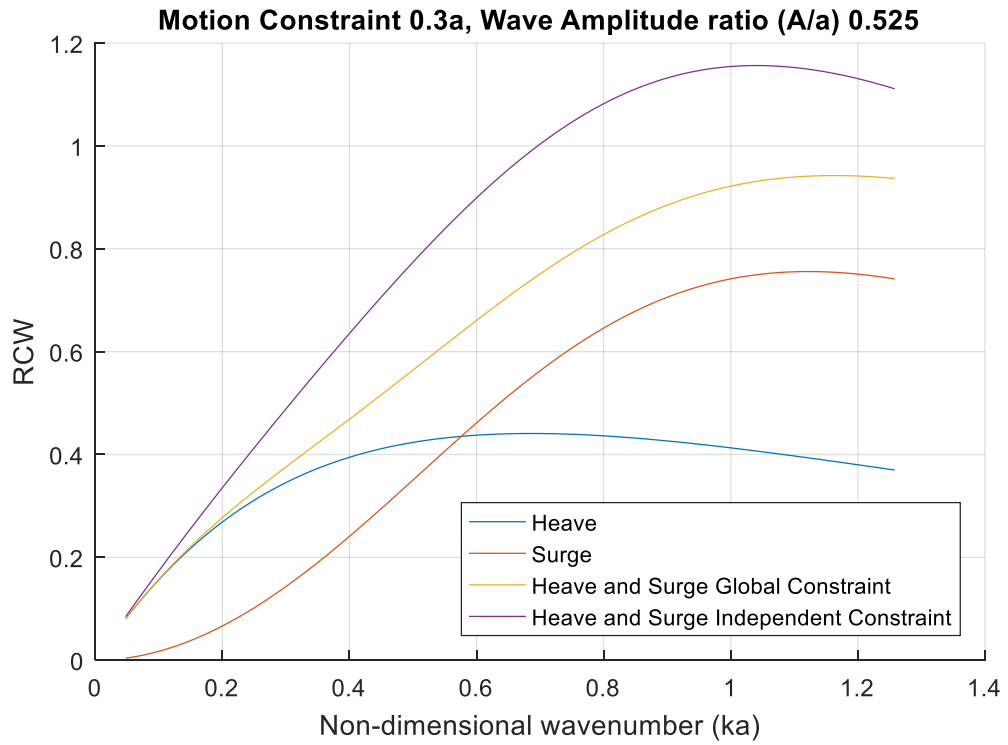


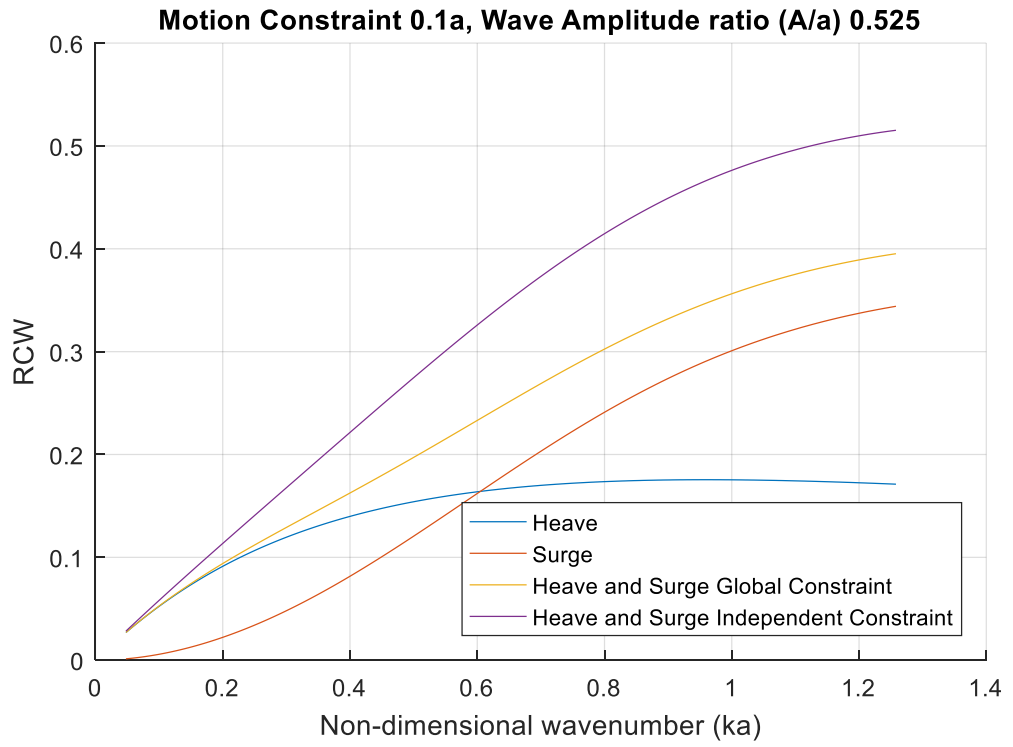




A.2.6 Wave Amplitude Ratio (A/a) 0.525 radii of device







A.2.7 Wave Amplitude Ratio (A/a) 0.625 radii of device

